I. STUDIES IN THE CHEMISTRY OF SODIUM DITHIONITE

II. A PRELIMINARY STUDY OF THE CATALYZED ADDITION OF HYDROGEN CHLORIDE TO VINYL CHLORIDE IN A STIRRED REACTOR

Thesis by

Robert Gene Rinker

In Partial Fulfillment of the Requirements

For the Degree of

Doctor of Philosophy

California Institute of Technology

Pasadena, California

1959

ACKNOWLEDGEMENTS

The work presented in this thesis represents the combined efforts of many people. I wish first to express my appreciation to Professor William H. Corcoran. The direction and success of the research program were a direct result of his valuable suggestions and periodic discussions. My colleagues and I have been impressed very favorably by his general policy of allowing maximum student freedom. His interest in students is shown by his friendly cooperation, his patience, and his understanding of their problems.

My thanks and appreciation also go to Professors Lacey and Sage for their constant interest in the work and for their helpful suggestions.

The first section of the thesis is submitted jointly with Thomas P. Gordon. His clear thinking and careful experimental techniques contributed greatly to the success of this work. Our association in the laboratory has been beneficial and enjoyable to me.

Two of my colleagues, Roy R. Sakaida and Yui Loong Wang, deserve special recognition. Roy devoted a large amount of time and effort to the study of sodium dithionite. Much of the data and the experimental techniques presented here are the results of his work. He also contributed significantly in the initial construction and testing of the chromatography unit. Wang was most helpful by voluntarily assisting in part

of the experimental work. During the preparation of the thesis, his valuable assistance in many ways, especially in correlating the data by means of the Datatron, is greatly appreciated.

From a third colleague, John J. Kalvinskas, I obtained helpful suggestions and useful information regarding high-speed digital computations.

Henry H. Dearman is to be credited with the successful experimentation and for the valuable information obtained in the EPR studies.

Throughout the course of the dithionite work, the advice and comments of Professors Norman Davidson, Don Yost, Edward King, Harden McConnell, Fred Anson, Carl Niemann and Ernest Swift were extremely helpful. Useful suggestions and assistance were also obtained from Professor S. G. Bankoff and Dr. Richard A. McKay.

Willard DeWitt, George Griffith and Seichi Nakawatase of the Chemical Engineering machine shop aided in the construction of equipment for the stirred-reactor experiments.

The manuscript was typed in rough-draft form by Evelyn Anderson, and the final draft was typed by Alethea Miller. Their superb workmanship under the pressure of a demanding time-schedule deserves much credit.

I am also grateful to Ethel Reger, the librarian of the Chemical Engineering Department, for her able assistance

in obtaining reference material used during the course of this study.

To the California Institute, I am indebted financially for Institute Scholarships and Teaching Assistantships. Also, the assistance obtained from a Monsanto Fellowship and a Union Carbide Fellowship is greatly appreciated.

Finally, I owe an immeasurable debt of gratitude to my wife, Peggy, who died during the progress of this work. As a small token of remembrance, I dedicate this thesis to her.

ABSTRACT

I. Rate studies of the air oxidation and thermal decomposition of aqueous sodium dithionite, $Na_2S_2O_4$, were conducted. These experiments were supplemented by studies of the electron-paramagnetic-resonance properties and the electrolytic formation of dithionite.

In the air-oxidation experiments, the overall rate was observed to have half-order dependence on the dithionite concentration and a first-order dependence on molecular oxygen concentration. This could be explained mechanistically on the basis of an instantaneous equilibrium reaction between dithionite and the SO_2^- radical ion.

The results of the EPR studies confirmed the presence of SO_2^- and established the existence of equilibrium between the free radical and dithionite.

The electrolytic production of dithionite from a bisulfite solution gave current efficiencies of 75% but did not show conclusively that the reduction was either a one- or two-electron transfer process.

In the thermal decomposition studies, the overall rate showed a 3/2-order dependence on dithionite concentration and a half-order dependence on hydrogen ion concentration. A mechanism involving SO_2^- or a protonated form of the radical in a reaction with the dimer appeared to fit the observed facts.

II. A preliminary rate study of the catalyzed addition-reaction between HCl and vinyl chloride was conducted in a continuous-flow stirred reactor. Gas-phase chromatography was used in the analysis of the chemical constituents.

The rate data for the primary reaction appeared to fit, at least empirically, a second-order rate law with respect to the forward reaction.

In addition to the primary reaction, fouling of the catalyst, $ZnCl_2$, was also observed, but the decreasing conversion as a function of catalyst-exposure time reached an asymptotic value greater than zero. This indicated that the catalyst fouling was an irreversible dual-site mechanism.

The fact that 1,1 dichloroethane was formed exclusively in the primary reaction eliminated the possibility of a free-radical reaction. Because of the relatively low rate of reaction, even in the presence of a catalyst, the addition probably occurred by a four-center-type mechanism.

TABLE OF CONTENTS

SECTION PAGE

SECTION I

STUDIES IN THE CHEMISTRY OF SODIUM DITHIONITE

GENERAL INTRODUCTION

CHEMISTRY OF SODIUM DITHIONITE

Sodium dithionite, $Na_2S_2O_4$, is a powerful reducing agent that has considerable usage in vat dyeing, bleaching, and in the manufacture of various chemicals. The first step in the process most generally used in the United States for the production of dithionite involves the reduction of liquid sulfur dioxide with zinc dust slurried in water. A continuous reactor is used. The reaction mixture is circulated through a tubular cooler at 35°C and zinc is continually removed. The filtered liquor is converted to the sodium salt by addition of caustic soda at 25°C. Filtration of the slurry removes the zinc hydroxide. To the filtrate is added sodium sulfide for removal of heavy metals. The final solution, containing 20% by weight of sodium dithionite, is then salted out with sodium chloride and alcohol. Partial dehydration of the dithionite crystals is accomplished with direct steam at 65°C, and final drying is done under vacuum at 85°C.

As early as 1850, dithionite (also called hydrosulfite or hyposulfite) was prepared by Schonbein (1) from the action of zinc dust on an aqueous solution of sodium bisulfite. In 1869, Schutzenberger (2) crystallized sodium dithionite and found its composition to be $Na_2S_2O_4$.

An important contribution to the knowledge of the properties and reactions of dithionite was made by Jellinek (3) in

1911. He prepared pure anhydrous sodium dithionite by heating a saturated solution of the impure salt to 60°C and then salting it out with NaCl and a small amount of NaOH. At a lower temperature, the hydrate, $Na_2S_2O_4 \cdot 2H_2O$, was salted out but was much less stable. Also, he found that the solubility of sodium dithionite dihydrate in water at 20°C was 21.8 gm/100 gm of water and that the temperature-solubility curve between 1°C and 20°C was a straight line. Freezing-point and conductance measurements gave good evidence in favor of the doubled formula $Na_2S_2O_4$. From careful measurements of the equivalent conductance of $Na_2S_2O_4$ solutions, Jellinek (4) determined the degrees of ionization in a 0.125 molar solution to be 0.697, 0.698 and 0.700 at 0, 18.3 and 25°C, respectively. A comparison with freezing point data showed that the value of the degree of ionization calculated from the freezing point was always greater for the sodium salts than that derived from the conductivity data. For the potassium salts, however, the degree of ionization was the same whether calculated from freezing-point or conductivity data. Jellinek explained the peculiarity by concluding that intermediate ions such as $NaS_2O_4^-$ were present in the sodium dithionite solutions but not in the potassium dithionite solutions. From conductance data for dithionous acid and the acid salt, the first and second ionization constants were calculated to give $K_1 = 0.45$ and $K_2 = 0.0035$ in a 0.1 molar solution of dithionite.

PART 1. AIR OXIDATION STUDIES

INTRODUCTION

Probably the earliest air-oxidation study of dithionite was conducted by Meyer (5) in 1903. He studied the oxidation of sodium dithionite by observing the oxygen uptake in shaken flasks containing aqueous dithionite solution. His results showed that the products of reaction were sulfite and sulfate. He proposed the primary reaction to be:

$$H_2S_2O_4 + H_2O + O_2 = H_2SO_4 + H_2SO_3 \qquad (1)$$

Also, he found that a competing reaction was

$$2H_2S_2O_4 + 2H_2O + O_2 = 4H_2SO_3 \qquad (2)$$

From the over-all reaction rates, he computed first-order rate constants but found that they drifted over a wide range.

Bassett and Durrant (6) in 1927 studied the reaction between dithionite and molecular oxygen but without any meaningful results. Their explanation of the oxidation mechanism was based upon arguments which will be summarized in the introduction to Thermal Decomposition Studies.

Nicloux (7) in 1933 was interested in determining the over-all stoichiometry of the reaction between dithionite and oxidizing agents of varying strengths. With a comparatively weak oxidizing agent such as silver ion, the dithionite was oxidized to sulfite. With molecular oxygen, an equimolar

mixture of sulfite and sulfate was formed. Finally, with a very strong oxidizing agent, sulfate was the only product. No experimental details were given.

The results of Lynn (8) suggested that the atmospheric oxidation of $Na_2S_2O_4$ proceeded according to a first-order mechanism with respect to dithionite and that the rate increased with temperature. He stated that the over-all stoichiometry was described by the equation:

$$Na_2S_2O_4 + O_2 + H_2O = NaHSO_4 + NaHSO_3 \qquad (3)$$

An examination of his data at 50°C showed that the oxidation rate increased with an increase in air flow. As a result, the reaction rate was dependent upon the diffusion rate of oxygen, which was not carefully controlled. Therefore, his results are only approximate. In the presence of 0.1 molar sodium bisulfite, the oxidation rate was extremely high, but in the presence of 0.1 molar sodium hydroxide the rate was inhibited, and the reaction proceeded smoothly.

SUMMARY

A study of the air-oxidation of sodium dithionite was conducted in aqueous solutions which were 0.1 molar in sodium hydroxide. The concentration of the dithionite was measured as a function of time at 30, 40, 50 and 60°C. Initial concentrations varied from 5×10^{-3} to 20×10^{-3} molar.

Air was bubbled into the reacting mixture through a glass frit at a rate of 2500 to 3000 cc/min, and the volume ratio of air flow per minute to reactor contents ranged from five to six. With stirring at a rate of 1100 rpm, the mixture was homogeneous and sufficiently turbulent to allow good contact between the air and liquid so that diffusion from gas to liquid and within the liquid was not a rate-determining factor.

Analyses of the end products showed the presence of sulfite, sulfate and thiosulfate. The sulfite and sulfate, usually found in a molar ratio of three to one, were the principal products and were considered to be the end products of the primary oxidation. The thiosulfate, however, was found only in relatively small quantities and was considered to be a product of a secondary reaction, namely, the thermal decomposition of dithionite. This reaction accounted for about 10% of the overall dithionite decomposition at 30°C.

An analysis of the rate data showed that the oxidation was one-half order with respect to dithionite and first order with respect to molecular oxygen. The specific rate constant

k_c was determined by integrating the rate expression at constant oxygen concentration for a half-order reaction to give:

$$k_c = \frac{2}{\theta} [C_o^{1/2} - C^{1/2}] \qquad (4)$$

For each initial concentration, C_o, the rate constant was calculated as a function of time θ from the unsmoothed oxidation data. Since it was found that k_c drifted slightly with time, its value at zero time was determined by extrapolation. Most of the drift was attributed to the effects of thermal decomposition since analysis showed the presence of thermal decomposition products, thiosulfate and sulfite, at the end of the reaction. Experiments involving increases in ionic strength by factors of three and five showed no effect on the rate of the reaction.

At each temperature, the average value of k_c at zero time was divided by the saturation concentration of oxygen in the solution to give k_c°. The rate expression is given as follows:

$$r_{observed} = k_c^{\circ}[S_2O_4^{=}]^{1/2} [O_2] \qquad (5)$$

k_c° at 30°C was found to be 0.151 $(moles/liter)^{-1/2}sec^{-1}$. A plot of log k_c° vs 1/T °K was used to obtain the Arrhenius activation energy of 9.3 kcal/mole. The frequency factor, A, was found to be 7×10^5 $(moles/liter)^{-1/2}sec^{-1}$. The observed half-order dependence on dithionite concentration and first

order dependence on molecular oxygen concentration suggested the following mechanism:

$$S_2O_4^{=} \rightleftharpoons 2SO_2^{-} \qquad (6)$$

$$SO_2^{-} + O_2 \rightleftharpoons \text{products} \qquad (7)$$

The equilibrium between the SO_2^{-} and $S_2O_4^{=}$ species was assumed to be the initial step in the mechanism of the oxidation. The second step was rate-determining, and consisted of an electron transfer or bimolecular combination reaction between SO_2^{-} and molecular oxygen.

APPARATUS

Reactor and Auxiliary Components

The air oxidation of the sodium dithionite was carried out in a glass reactor with a volume of approximately 600 cc (see Figure 1). Air was bubbled at a rate of 2500 to 3000 cc/min into the reaction mixture near the bottom of the reactor through a medium-coarse glass frit which could be inserted or removed through a standard-taper opening on the reactor. During the reaction, the frit was always immersed in the liquid contents.

Before the air entered the frit, it was passed first through an alundum-stone trap to remove suspended solids and aerosols; next through a molecular-sieve dryer; and finally through a temperature-conditioning coil. The air flow was measured by means of a wet-gas meter placed on the downstream side of the reactor.

Mixing was accomplished by means of a glass stirrer having two impellers. The stirrer was supported and sealed through a mercury-in-glass bearing. Stirring speeds could be varied up to 1100 revolutions per minute.

The reactor and temperature-conditioning coil were thermostated in a 28-liter water bath, which maintained the temperature within $\pm$ 0.02°C. Heaters in the water bath were energized by an electronic-relay circuit which in turn received its signal from a mercury-expansion switch immersed in the water.

Samples were taken from the reactor through an opening in the top. A syringe needle or pipette was inserted into the reacting mixture, and the sample was then removed.

Nitrogen Purification Train

Commercial-grade nitrogen was the source of supply for the oxygen-free atmosphere required in preparing the sample of fresh sodium dithionite to be charged to the reactor. The nitrogen contained approximately 0.01% oxygen by volume. That amount proved excessive. Hence, most of the oxygen was removed by passing the nitrogen through two scrubbing towers in series. Each contained 0.2 molar chromous chloride solution in 1.0 normal hydrochloric acid. Acid and water vapors were subsequently removed by passing the nitrogen through a 0.1 molar sodium hydroxide solution and then through a calcium chloride dryer.

EXPERIMENTAL PROCEDURE

Concentration of Dithionite as a Function of Time

Chemically pure sodium dithionite (Baker Chemical Company, Batch No. 3712, Lot No. JTB6113) was the starting point for the source of dithionite ions. In preparing the dithionite for a typical run, approximately 25 gm of the powder were placed in an oxygen-free flask into which a stream of oxygen-free nitrogen had been passed for several minutes. Then, approximately 100 cc of distilled water, free of oxygen and carbon dioxide, were injected into the flask through a serum-bottle cap. The mixture was heated to 60°C with constant agitation until a saturated solution was obtained. With great care to avoid contact with oxygen, a 60 cc sample of the saturated solution was withdrawn with a syringe and injected into a side-armed test-tube already filled with nitrogen. The tube with its contents was then cooled to 0°C in an ice bath while maintaining the pressure of the nitrogen constant at slightly above one atmosphere. At the lower temperature the liquid became supersaturated with sodium dithionite; and with sufficient agitation, crystals of $Na_2S_2O_4 \cdot 2H_2O$ were formed. Again, with great care, practically all the liquid was removed from the tube leaving the white crystals settled at the bottom. Approximately 4 cc of distilled water at 0°C and free of carbon dioxide and oxygen were injected into the tube to wash the crystals.

This process was repeated once again to obtain reasonably pure crystals. The final saturated solution with a volume of approximately 20 cc was used to supply the reactor with an initial concentration of dithionite.

Before injection of the dithionite, the reactor was filled with 505.0 cc of 0.1 molar sodium hydroxide solution. The reactor was then immersed in the water bath and allowed to reach steady conditions of temperature, stirring rate, and air flow. The time of initial air flow was noted in order to account for evaporation losses from the reactor. At steady conditions, 5.00 to 15.00 cc of the saturated dithionite solution, depending upon the initial concentration desired, were injected into the reactor. Since the delivery times of large syringes are of the order of several seconds the time at which half of the sample was injected was taken as the initial time of the reaction.

Without delay, 1.00 or 2.00 cc samples were removed from the reactor with a calibrated syringe and injected into 150 cc flasks containing a mixture of 50 cc of 0.1 molar potassium hydroxide and 15 cc of methyl alcohol. Also, the flasks contained a nitrogen atmosphere which was maintained during titration. The titration flasks were stirred magnetically. The time at which half of a sample from the reactor had been injected into a titration flask was recorded as the injection time.

The concentration of dithionite in the titration flasks

was determined by titration with a standardized aqueous solution of methylene blue having a concentration in the range of 9.0×10^{-4} to 9.3×10^{-4} molar.

Usually, the total time required to obtain a sample and titrate it was 40 sec. At the maximum temperature of 60°C and at the minimum initial concentration of 5×10^{-3} molar, the time of reaction was a minimum. Under these conditions, at least five titrations were accomplished before the end of the reaction.

As soon as all the dithionite had been oxidized, the air-flow was stopped, and the time was noted. The reactor was removed from the water bath, and the volume of its contents was measured. A material balance coupled with the knowledge of the air-flow rate and the assumption that the exit air was saturated with water vapor, made it possible to calculate the loss of water by evaporation prior to and during the reaction.

In the analysis of the dithionite samples, the methylene blue was reduced quantitatively on an equimolar basis from an intense blue color to an almost colorless leuco-form. It was found, in agreement with Lynn's work (8), that the leuco-form was relatively insoluble in water at room temperature; and unless it was dissolved, it apparently absorbed unreacted methylene blue during the titration. This resulted in a lowered over-all rate of reaction because of the time required for the dithionite to diffuse to the solid surface before

reaction could occur. The purpose of the addition of the methyl alcohol in the titration flasks was to dissolve the solid leuco-compound and hence speed up the titrations. When titrated quickly, any thiosulfate and sulfite present in a sample did not interfere in the reaction between dithionite and methylene blue for the temperature range 0 - 30°C. The end-point was sharp and was rapidly attained at room temperature.

Standardization of the methylene blue was done according to the method of Welcher (9) and Kolthoff (10). Briefly, the methylene blue was titrated into a standard water-solution of 0.005 molar picrolonic acid which was buffered at a pH of about 6. Periodic removal of the dark green product, methylene blue picrolonate, from the water phase was necessary in order to detect the end-point. This was accomplished by extraction of the methylene blue picrolonate with chloroform. Neither the picrolonic acid nor the methylene blue was soluble in the chloroform. Near the end-point, only 2 or 3 drops of methylene blue were titrated into the acid between successive extractions with chloroform. The end-point occurred when a blue color persisted in the water phase after addition of one drop of methylene blue, but with no color in the chloroform phase. When carefully applied, this method gave results accurate to $\pm$ 0.5% compared with the classical iodine-precipitation method (11).

Solubility of Dithionite at 0°C

A solution of sodium dithionite saturated at 0°C was prepared as described in the previous section. The saturation concentration of the dithionite, however, far exceeded the desired value for titrations with reasonable volumes of methylene blue. Therefore, 5.00 cc of the saturated solution were injected through a serum-bottle cap into a 1-liter vessel which contained 500.0 cc of 0.1 molar sodium hydroxide maintained under a nitrogen atmosphere and at a temperature of 0°C. Several 2.00 cc samples of the resulting solution were titrated with methylene blue under conditions similar to those stated in the previous section. From these results, the solubility of the dithionite at 0°C was calculated.

End-Products of the Dithionite Oxidation Reaction

A knowledge of the types and quantities of the oxidation products of dithionite was important in determining a mechanism for the reaction. For the qualitative tests, a decomposed sample of dithionite was prepared by adding 0.20 gm of the purified powder to 100 cc of 0.1 molar sodium hydroxide solution through which air was bubbled until a negative test for dithionite was obtained. A sample of the reaction mixture was acidified with hydrochloric acid to a pH of about 2, followed by addition of lead acetate. A white precipitate resulted which indicated the absence of sulfide from the mixture. Had sulfide been present in the absence of appreciable amounts of chloride ion, it would have appeared as the black

precipitate of lead sulfide. Another sample, when mixed with potassium triiodide at a pH of about 5, decolorized the iodine, indicating the presence of thiosulfate and/or sulfite. Still another sample at that pH was treated with barium chloride to remove sulfite and sulfate, if present, as barium sulfite and barium sulfate. The white precipitate was filtered, and the filtrate was titrated with potassium triiodide to give a positive test for thiosulfate. Treatment of the precipitate with strong hydrochloric acid resulted in the evolution of sulfur dioxide to give a positive test for sulfite. The fact that a portion of the precipitate was unattacked by an excess of acid showed the presence of sulfate as barium sulfate.

The procedure for the quantitative analysis was based upon the results of the qualitative findings. The principal ions of interest were sulfite, sulfate, and thiosulfate. Any complexes of these ions or the presence of other ions were considered highly unlikely or in concentrations too low to be detected.

Samples for quantitative analysis were taken from two sources, both of which were different from the source used in the qualitative analysis. The first source was contained in a flask which originally was charged with 500 cc of 0.1 molar sodium hydroxide at 30°C and with 7 cc of saturated dithionite solution. Oxygen entered the liquid bulk only by molecular diffusion through the surface of the liquid. This

mixture was checked for completion of dithionite oxidation before other components were studied. The second source was contained in the reactor following a usual run at 30°C as described previously.

In both cases, the method of analysis for end-products was the same. Four separate analyses were made on four separate samples from each source. These were as follows:

1. Iodometric titration to determine the sum of the concentration of thiosulfate and sulfite.
2. Iodometric titration to determine only the concentration of thiosulfate.
3. Barium chloride titration to determine the sum of the concentration of sulfite and sulfate.
4. Barium chloride titration to determine only the concentration of sulfate.

In the iodometric analysis for the sum of the sulfite and thiosulfate, a 10 to 25 cc sample was buffered with a solution which was 0.4 molar in sodium acetate and 0.4 molar in acetic acid. Usually, a volume of the buffer solution equal to the volume of the sample was added to give a constant pH of about 5. Using a starch end-point, the solution was titrated with a standardized solution of approximately 0.01 normal triiodide. In case of excess addition of triiodide back-titration was done with a standard thiosulfate solution which was approximately 0.01 normal in thiosulfate.

In the iodometric analysis for only the thiosulfate ion,

a 10 to 25 cc sample was buffered to a pH of about 5. To this was added a volume of 37 wt % formaldehyde in water equal to about half the volume of the the sample. The purpose of the formaldehyde was to form a complex with the bisulfite according to the reaction:

$$\begin{matrix} H \\ \diagdown \\ \quad C = O \\ \diagup \\ H \end{matrix} + HSO_3Na \longrightarrow CH_2(OH)SO_3Na \qquad (8)$$

The mixture was stirred for fifteen minutes at room temperature to allow sufficient time for the complexing to occur. The unreacted thiosulfate was then determined with the standard triiodide solution.

The use of barium chloride in a titration method to determine sulfate was suggested in the literature by Fritz and Freeland (12). This method depends upon a color change in the indicator Alizarin Red-S which acts as an adsorption indicator in the presence of a barium sulfate precipitate. In solution the alizarin anion was yellow; but on the surface of suspended barium sulfate and in the presence of excess barium ion, the alizarin complexed with the barium ion to give a red color to the suspended solid. In using the procedure outlined by Fritz and Freeland, however, the method was limited to concentrations of sulfate greater than 20×10^{-3} molar. It was necessary, then, to modify the procedure in applying it to concentrations of sulfate down to 4×10^{-3}

molar. After several tests, it was noted that the limitation in the amount of sulfate detectable was mainly due to the relative concentration of the precipitate on which the alizarin could absorb. Too small a quantity of precipitate, although colored red with complexed alizarin, could not overshadow the yellow color of the alizarin in solution. Therefore, by adding a quantity of semi-colloidal barium sulfate suspended in methyl alcohol to the titration mixture, it was possible to detect the end-point with an accuracy of 1 or 2%. A further improvement in detecting the end-point was to pass an intense light beam through the suspension during the titration. This aided in bringing out color changes more sharply.

To determine the sum of the sulfite and sulfate concentration by the above method, it was first necessary to oxidize the sulfite to sulfate by means of the triiodide ion. The amount of triiodide needed was determined by a starch end-point; but there was some uncertainty as to the effects of the starch on the subsequent sulfate titration. Therefore, it was decided to avoid using the starch by first running a blank to determine the exact triiodide requirement and then adding the same amount in the absence of starch to a fresh sample buffered at a pH of about 5 as specified above. Following the oxidation of the sulfite, the buffered solution was acidified to a pH of about 3.5 with 20% acetic acid. The volume of acetic acid required was about equal to the volume of the original sample. Then methyl alcohol containing a

semi-colloidal suspension of barium sulfate was added in an optimal amount equal to 38% by volume of the final mixture. With constant stirring, 90% of the estimated 0.1 molar barium chloride requirement was rapidly added and was followed by the addition of 3 to 5 drops of 0.020 % alizarium-red solution. The final titration was performed slowly with an interval of 3 to 5 sec between drops of barium chloride solution.

Finally, in determining the concentration of sulfate alone, the sulfite was complexed by addition of formaldehyde. The subsequent barium chloride titration was not affected adversely by the presence of the formaldehyde.

All the standard solutions used in the foregoing analyses were prepared and standardized according to the procedures outlined by Swift (13).

RESULTS

Kinetic Analysis

Tables 1-4 list the experimental and derived data for the air-oxidation of dithionite. Graphical presentations of the data are shown in Figures 2-5, in which concentrations of dithionite in moles per liter are plotted against time in seconds. Initial concentrations of dithionite ranged from 5×10^{-3} to 20×10^{-3} moles/liter. The rate of change of concentration was rapid in the initial stages but fell off continuously and rapidly as the concentration decreased.

In the determination of the order of the reaction with respect to dithionite, the oxygen concentration was held constant for a given temperature. Only for those experiments in which the order with respect to oxygen was to be determined was the oxygen concentration varied. Pure oxygen was used at atmospheric pressure instead of air to give a fivefold increase in oxygen concentration. If Henry's Law is assumed to apply, the concentration ratio in solution between oxygen dissolved from pure oxygen and oxygen dissolved from air would be 4.76. For the equipment used, this method of varying the oxygen partial pressure in the gas phase at a constant total pressure of one atmosphere was preferred to the method in which the total pressure on the system would have been increased.

It was found experimentally that the initial rate of the

reaction was increased by a factor of 5 when pure oxygen was substituted for air, all other conditions remaining the same. Hence the reaction was believed to be first order with respect to molecular oxygen. (See Table IIA and Figure IA in Appendix I.)

The first step in analyzing the data was to determine initial concentrations and the corresponding initial rates. Several procedures were available for determining the initial concentrations. Experimentally, solubility tests were performed on the dithionite to determine its concentration at 0°C in the saturated solutions which were injected into the reactor for any given decomposition run. From a knowledge of the solubility and the initial quantity of water in the reactor, the initial concentration could be calculated.

A direct extrapolation of the concentration-vs-time curves back to zero time was the second method and a fairly reasonable one since sampling from the reactor was begun 30 to 50 sec after the injection. The total time for decomposition varied from 120 to 530 sec over the temperature and initial concentration range studied.

Of the two procedures, the direct extrapolation method was used. Although the solubility of dithionite at 0°C was fairly well established by the procedure described in the experimental section, the use of this value in calculating the initial concentrations in the reactor depended upon exact reproducibility of injection samples for each run.

The initial rates were determined by plotting slopes of

concentrations vs time curves as a function of time for each initial concentration. A series of these curves is shown in Figure 6 for runs at 50°C. An extrapolation to zero time produced the initial rates. These compared satisfactorily with the values obtained by drawing tangents to the concentration vs time curves at zero time.

From a knowledge of the initial rates and concentrations, the order n of the reaction with respect to dithionite was obtained. The relationship used in this determination and applied at time zero was the following:

$$-\frac{dc}{d\theta} = k_c[C]^n \qquad (9)$$

in which C is the concentration of dithionite in moles per liter; θ is the time in seconds; and k_c is the specific reaction rate constant which includes the constant concentration of oxygen.

A plot of log $(\frac{dc}{d\theta})_o$ vs log C_o is shown in Figure 7 for runs at 30, 40, 50 and 60°C. The slopes of the best straight lines through the points at each temperature were calculated to be 0.50 ± 0.04 which was near enough to 0.5 to indicate that the reaction was one-half order with respect to dithionite. The purpose of obtaining n for conditions at zero time was to eliminate any possible effects of reaction products or side reactions in masking the true order of the reaction. More explanation of these effects is given in a later discussion on product analysis.

The integrated form of Equation 9 was used to obtain values of k_c as a function of time, and the unsmoothed data provided the numerical information to solve for k_c. Integration of Equation 9 gives:

$$k_c = \frac{2}{\theta} [C_o^{1/2} - C^{1/2}] \qquad (4)$$

It was found that k_c calculated from Equation 4 drifted slightly as a function of time when calculated over 50% completion of reaction, but the variation was smooth and linear. A typical plot for data at 30°C is shown in Figure 8. The curves for k_c, when extrapolated to time zero, seemed to converge to a range of values well within experimental accuracy. Hence greater credence was placed upon an average value of k_c at time zero than for any other time. The fact that the values for k_c varied smoothly provided a satisfactory argument in favor of using unsmoothed data in the calculations. The calculated values of k_c as a function of temperature are shown in Figures 8-11. Since these values included the concentration of oxygen, which is a function of temperature itself, the dependence of k_c on oxygen concentration was eliminated by dividing k_c by the saturation concentration of oxygen in water, and hence in the dilute solutions used here, in moles per liter at that temperature (14). The new k's, independent of concentration and designated as k_c^o, are also shown in Figures 8-11.

The overall activation energy and frequency factor were obtained from the Arrhenius Equation relating the rate constant to temperature. A form of the Arrhenius Equation was used in which the dependence of the frequency factor on temperature was omitted. The range of temperatures studied was sufficiently narrow to make this simplification justified. The form of the equation used is:

$$k = Ae^{-\frac{\Delta E}{RT}} \qquad (10)$$

A plot of log k_c° vs 1/T °K is shown in Figure 12. The slope of the best straight line through the points gave a value for the activation energy, ΔE, of 9.3 kcal/mole. The intercept, at 1/T equals zero, gave a value of 7×10^5 (moles/liter)$^{-1/2}$ sec^{-1} for the frequency factor A.

Product Analyses

Table 10 lists the experimental results for the end-product analyses. For the reactions conducted in the flasks, the molal ratio of sulfite to sulfate was found to be 2.3. In the case of the analyses of the end products in the reactor, the ratio was more nearly 3.0. Such a large difference between the two ratios was due primarily to the difference in reaction time. Whereas the flask-reactions required approximately 29 hr for completion, the reactor runs were completed in about 300 sec. During the relatively long time in the flasks, the oxidation of sulfite to sulfate was undoubtedly

significant. In comparison to the rate of dithionite oxidation, and under identical conditions, the sulfite oxidation without catalysis was shown to be quite slow (see Figure 15 and Table 9). This was also shown to be true when at the completion of a dithionite oxidation the air flow was allowed to continue for 10 to 15 minutes without a significant change in the sulfite-sulfate ratio. There was no real assurance, however, that in the presence of dithionite ions or transient intermediates the sulfite oxidation was not catalyzed. Indeed, the oxidation of sulfite to sulfate by molecular oxygen has been shown to be catalyzed by free radicals (15). The presence of appreciable amounts of sulfate in the reaction products suggests that catalysis was occurring. The observed ratio of sulfite to sulfate of 3 to 1 sets an upper limit of 25% conversion of sulfite to sulfate by catalyzed air oxidation.

As shown in Table 10, thiosulfate in small but measurable quantities was also among the products. There seemed to be no explanation of its formation unless it were assumed that a secondary reaction involving thermal decomposition was occurring simultaneously with the air oxidation. As the product of a secondary reaction, it accounted for nearly 10% of the dithionite disappearance for a temperature of 30°C. This is based upon the stoichiometry of the thermal decomposition in which the two major products are sulfite and thiosulfate. Probably the secondary reaction was the greatest single factor contributing to the drift in the rate constant k_c.

The stability of thiosulfate in the basic solution and in the presence of molecular oxygen was established by the absence of sulfide and tetrathionate in the end-products, and also by the fact that the thiosulfate concentration in the flask reactions remained constant up to 100 hours after the depletion of the dithionite. Further evidence for the very slow oxidation of thiosulfate was obtained when a 0.028 molar solution was subjected to the same conditions of temperature, stirring and air flow in the reactor that existed for dithionite oxidations. No significant oxidation was measured for times up to 15 min (see Figure 15 and Table 9).

Diffusion Effects

As stated in the experimental procedure, the rate of air or oxygen discharge through the frit into the reacting mixture was varied from 2500 to 3000 cc/min. Preliminary tests showed, however, that an air rate of only 1200 cc/min was sufficiently high to oxidize the dithionite independently of the air rate. Hence, reproducibility of tests was not affected by variable air rates greater than 1200 cc/min. The rate of stirring (approximately 1100 rpm) in the reactor was rapid enough to maintain an isothermal, homogeneous mixture. A stirring rate of only 800 rpm, coupled with an air rate of 1200 cc/min gave the same results within experimental error as a stirring rate of 1100 rpm and an air rate of 2500 cc/min, all other conditions being the same (see Figure 13 and Table 7).

Figure 13 also shows concentrations of dithionite as a function of time for the same initial concentration at 60°C and a stirring speed of 800 rpm but with different air rates. As the air rate was increased up to 1200 cc/min, the curves moved closer to an asymptotic curve which established the lower limits of operation. The fact that the curves of Figure 13 differed indicated that diffusion of oxygen to a point in the system was a controlling factor in the rate of oxidation for air rates less than the asymptotic value of 1200 cc/min. In the kinetic experiments, the greatest demand for oxygen occurred at the highest temperature, which was 60°C, and at the maximum initial concentration of dithionite, which was approximately 20 x 10^{-3} molar. The tests represented by Figure 13 were performed at nearly the extreme demand conditions, as noted above, except that the initial concentration was only 12 x 10^{-3} molar. The experimental data for the kinetic runs at concentrations higher than 12 x 10^{-3} molar were consistent with data obtained for runs below this concentration. Thus, it was assumed that for the air rates and stirring speeds used throughout the experimental work the diffusion of oxygen was not a controlling factor.

Ionic Strength Effects

Figure 14 shows that the rate of the reaction did not change upon increasing the concentration of NaOH, and hence the ionic strength, by factors of three and five. The result shown in Figure 14 for an experiment conducted in 0.01 molar

NaOH appears anomalous. It is almost certain that the different course of reaction resulted from thermal decomposition when generated hydrogen ion neutralized the added NaOH.

pH and Metal Ion Effects

The pH of the dithionite solutions changed approximately from 13 to 12.8 for the highest initial concentration of 20×10^{-3} molar. This indicated that hydrogen ion was generated as one of the products of reaction. No detailed study of the pH variation was made for the air oxidation of dithionite.

No careful study was made to determine the effects of metal ions on the oxidation of dithionite. It was observed, however, in a qualitative way, that mercury in minute quantities caused the reaction to become erratic. A reasonable suggestion is that the mercury reacted to form complexes such as $Hg(SO_3)_2^{=}$.

Solubility Studies

Table 11 lists the experimentally determined solubility of sodium dithionite in water at 0°C. The average value of 11 determinations was found to be 13.20 gms/100 gms of water with a standard deviation of 1.08 gms/100 gms of water or about 8%. Yost (16) lists a value of 12.85 gms/100 gms of water at 1°C, and Rao and Patel (17) list 11.86 gms/100 ml of solution at 0°C. These authors do not give any error limits.

DISCUSSION OF RESULTS

Reaction Mechanisms

A mechanism which satisfied the established order of reaction with respect to dithionite and oxygen and in which the initial step was dissociation of dithionite is as follows:

$$S_2O_4^{=} \rightleftharpoons 2SO_2^{-} \qquad (6)$$

$$SO_2^{-} + O_2 \longrightarrow \text{Products} \qquad (7)$$

Since the first step is a quickly-established equilibrium, the second step is rate determining. Thus, the observed reaction rate is

$$r_{observed} = k_2[SO_2^{-}][O_2] \qquad (11)$$

where

$r_{observed}$ = reaction rate in moles per liter per second.
k_2 = rate constant in moles-liters-seconds units.
$[SO_2^{-}]$ = concentration of SO_2^{-} in moles per liter.
$[O_2]$ = concentration of O_2 in moles per liter.

The equilibrium constant for the first step may be written

$$K_c = \frac{[SO_2^{-}]^2}{[S_2O_4^{=}]} \qquad (12)$$

where K_c has the units of moles per liter

A substitution of the concentration of SO_2^- from the equilibrium-constant expression into the rate expression gives

$$r_{observed} = k_2 K_c^{1/2} [S_2O_4^=]^{1/2} [O_2] \qquad (13)$$

The experimentally determined rate constant, k_c^o, is related to k_2 and K_c by

$$k_c^o = k_2 K_c^{1/2} \qquad (14)$$

The variation of k_c^o with temperature permitted the calculation of the Arrhenius activation energy of 9.3 kcal/mole and the frequency factor of 7.5×10^5 $(moles/liter)^{-1/2} sec^{-1}$. It will be shown later that the rate determining step probably involves an electron transfer to form O_2^- and SO_2. The observed activation energy of 9.3 kcal/mole seems high for such an electron transfer. Uri (18) has correlated data for a number of exothermic electron transfer reactions, and found typical activation energies to lie between 0 and 5 kcal/mole. The observed value of 9.3 kcal/mole, however, includes a contribution from the equilibrium step. Using approximate values of frequency factors from Frost and Pearson (19), order-of-magnitude calculations can be made for the limiting contributions of the equilibrium and rate-

determining steps to the observed activation energy. The calculations are as follows:

$$k_c^{\circ} = k_2 K_c^{1/2} \text{ where } K_c = \frac{k_1}{k_{-1}} \tag{14}$$

$$A_c^{\circ} e^{-\frac{\Delta E_c^{\circ}}{RT}} = A_2 e^{-\frac{\Delta E_2}{RT}} \left[\frac{A_1 e^{-\frac{\Delta E_1}{RT}}}{A_{-1} e^{-\frac{\Delta E_{-1}}{RT}}} \right]^{1/2} \tag{15}$$

$$\ln A_c^{\circ} - \frac{\Delta E_c^{\circ}}{RT} = \ln A_2 - \frac{\Delta E_2}{RT} + \frac{1}{2} \ln \frac{A_1}{A_{-1}} - \frac{1}{2} \frac{(\Delta E_1 - \Delta E_{-1})}{RT} \tag{16}$$

$$\Delta E_c^{\circ} - RT \left[\ln \frac{A_c^{\circ}}{A_2} - \frac{1}{2} \ln \frac{A_1}{A_{-1}} \right] = \Delta E_2 + \frac{1}{2} (\Delta E_1 - \Delta E_{-1}) \tag{17}$$

Frost and Pearson suggest 10^6 to 10^7 $(\text{moles/liter})^{-1/2}\text{sec}^{-1}$ for A_2, 10^{13}sec^{-1} for A_1, and 10^5 to 10^6 $(\text{moles/liter})^{-1/2}\text{sec}^{-1}$ for A_{-1}. Substituting 9.3 kcal/mole for ΔE_c° and 7×10^5 $(\text{moles/liter})^{-1/2}\text{sec}^{-1}$ for A_c° gives:

$$\Delta E_2 + \frac{1}{2} (\Delta E_1 - \Delta E_{-1}) = 15 \text{ kcal/mole} \tag{18}$$

Thus the above order-of-magnitude calculations place mathematical limits on ΔE_2 and $(\Delta E_1 - \Delta E_{-1})$ as follows:

$$0 \leqslant \Delta E_2 \leqslant 15 \text{ kcal/mole}$$

$$0 \leqslant \Delta E_1 - \Delta E_{-1} \leqslant 30 \text{ kcal/mole} \qquad (19)$$

If one goes further and assumes a value of ΔE_2 median in the range 0 - 5 kcal/mole, namely 3 kcal/mole, the equations above can be used to calculate K_c and k_2. K_c is found to be 8×10^{-11} moles/liter and k_2 is therefore 2×10^4 $(\text{moles/liter})^{-1}$ sec^{-1}. These values are, at best, order-of-magnitude estimates.

The order of reaction of the air oxidation studies with respect to dithionite and molecular oxygen determines the composition of the transition state in the rate-determining step. That is, the activated complex must consist of one molecule of SO_2^- and one molecule of O_2. Further information about the geometry of the activated complex or the products which result from its decomposition cannot be inferred with certainty from the observed data. Knowledge of the composition of the transition state and the composition of the end products does, however, place a reasonable limit on the number of mechanisms which might be proposed for the intermediate steps. Two possibilities are suggested immediately for the rate determining step:

$$SO_2^- + O_2 \xrightarrow{k_2} \text{complex A} \xrightarrow{k_3} SO_4^- \qquad (20)$$

$$SO_2^- + O_2 \xrightarrow{k_2} \text{complex B} \xrightarrow{k_3} SO_2 + O_2^- \qquad (21)$$

It is not inconceivable that both of these mechanisms could occur. Both free radical intermediates SO_4^- and O_2^- have ample precedent in the literature (18). End product analysis does, however, exclude the mechanism given in Equation 20 from being the only mechanism by which the activated complex is decomposed. Subsequent steps would almost certainly be of the type

$$SO_4^- + SO_2^- \longrightarrow SO_4^= + SO_2 \qquad (22)$$

which would lead to a sulfite-to-sulfate ratio of unity in the reaction products. The mechanism given by Equation 21 leads to a series of free-radical intermediates of hydrogen peroxide. The following series of reactions may be written as a suggestion:

$$S_2O_4^{=} \rightleftharpoons 2SO_2^{-}$$

$$SO_2^{-} + O_2 \xrightarrow{k_2} \text{complex B} \xrightarrow{k_3} SO_2 + O_2^{-}$$

$$SO_2^{-} + O_2^{-} \xrightarrow{k_4} SO_2 + O_2^{=}$$

$$O_2^{=} + H_2O \xrightarrow{k_5} HO_2^{-} + OH^{-}$$

$$HO_2^{-} + SO_3^{=} \xrightarrow{k_6} SO_4^{=} + OH^{-} \qquad (23)$$

$$HO_2^{-} + SO_2^{-} \xrightarrow{k_7} SO_3^{=} + OH$$

$$OH + SO_2^{-} \xrightarrow{k_8} SO_2 + OH^{-}$$

$$SO_2 + OH^{-} \xrightarrow{k_9} SO_3^{=} + H^{+}$$

$$\frac{1}{2} SO_3^{=} + \frac{1}{4} O_2 \xrightarrow{k_{10}} \frac{1}{2} SO_4^{=}$$

Certainly there is nothing unique about this suggested series of reactions. It does lead to the observed overall stoichiometry and by suitable choice of kinetic constants could be shown to be kinetically consistent. In common-sense terms, the peroxide intermediates which are formed on a mole for mole basis by the decomposition of dithionite can react either with sulfite molecules already formed to form sulfate or with

SO_2^- radical ions to form more sulfite and regenerate peroxide intermediates. Since the concentration of sulfite ions in solution greatly exceeds that of SO_2^- ions after the first second of the reaction, the preponderance of sulfite rather than sulfate in the products requires that $k_7 >> k_6$ in the above scheme. A steady state concentration of intermediates need not be postulated in this hypothetical analysis.

CONCLUSIONS

The chemistry of reactions of sulfur-oxygen species in aqueous solution is sufficiently complex to inject a certain amount of ambiguity into the interpretation of nearly all practicable experiments. Such is the case for the work described herein. A true and unambiguous understanding would require considerably more experimentation and methods that are far more subtle than the ones used in the present experiments.

As shown earlier, only a very specific investigation was conducted. The study of the effects of other variables such as the addition of certain ionic species, both anionic and cationic, was omitted entirely. Undoubtedly, a study in this direction would contribute to the understanding of this complex problem.

A brief summary of the major results obtained in the study of the air-oxidation of dithionite is given as follows:

1. The reaction was one-half order with respect to dithionite.
2. The reaction was first order with respect to molecular oxygen.
3. The activation energy based on the Arrhenius Equation for the specific rate-constant of reaction was 9.3 kcal/mole. The frequency factor A, was found to be 7×10^{-5} $(\text{moles/liter})^{-1/2}\text{sec}^{-1}$. The rate of reaction is given by the expression

$$r = k_c^{o}[S_2O_4]^{1/2}[O_2].$$

4. The rate of sulfite oxidation to sulfate was low compared to the oxidation rate of dithionite.
5. The small pH change from 13 to approximately 12.8 indicated the generation of hydrogen ion in the reaction. This result agrees with the observed overall stoichiometry that there is a net increase in acidic sulfur anions.
6. The ratio of sulfite to sulfate in the reacted mixture was 3 to 1 on a mole basis.

A mechanism which satisfied the established order with respect to dithionite and oxygen and in which the initial step was dissociation of dithionite is proposed as follows:

$$S_2O_4^{=} \rightleftharpoons 2SO_2^{-} \qquad (6)$$

$$SO_2^{-} + O_2 \longrightarrow \text{products} \qquad (7)$$

Since the first step is an instantaneous equilibrium process, the second step must be rate determining. Hence the measured rate must have a direct relationship to the second step. The kinetic expression becomes:

$$r = k_2[SO_2^{-}][O_2] \qquad (11)$$

From the first step, the equilibrium constant can be

written as:

$$K_c = \frac{[SO_2^-]^2}{[S_2O_4^=]} \tag{12}$$

A substitution of the concentration of SO_2^- from the equilibrium expression into the rate expression gives:

$$r = k_2 K_c^{1/2} [S_2O_4^=]^{1/2} [O_2] \tag{13}$$

Unfortunately, the value of K_c was indeterminate since the concentration of SO_2^- was experimentally inaccessible.

The rate constant k_c^o, which was calculated directly from the data, is related to k_2 by:

$$k_c^o = k_2 K_c^{1/2} \tag{14}$$

Thus the derived rate expression, which is equivalent to the experimental rate expression, is given as follows:

$$r = k_c^o [S_2O_4^=]^{1/2} [O_2] \tag{24}$$

The temperature variation of k_c^o is given by

$$k_c^o = 7 \times 10^5 \, e^{-\frac{9300}{RT}} \quad (\text{moles/liter})^{-1/2} \text{sec}^{-1} \tag{25}$$

Values of k_c^o are listed in Figures 8-11.

The observed order of reaction with respect to dithionite and molecular oxygen and the stoichiometry of the reaction products suggest that hydrogen-peroxide-type intermediates are involved in steps subsequent to the rate-determining step. A hypothetical mechanism can be described to account for the observed kinetic and stoichiometric facts.

PART 2. DITHIONITE STRUCTURE STUDIES

INTRODUCTION

Perhaps the earliest attempt to elucidate the structure of sodium dithionite by purely physical methods was made by Klemm (20) in 1937. He determined by gross magnetic susceptibility measurements that the anhydrous salt of sodium dithionite is diamagnetic.

It was of some interest, therefore, when Van der Heijde (21) in 1953 found that the exchange rate of S^{35} between dithionite and sulfur dioxide in neutral or acid solution was almost instantaneous, indicating the ready cleavage of the S-S dithionite bond. The exchange reactions were stopped by the addition of a large excess of formaldehyde, which complexed the dithionite and bisulfite ions according to the following equations:

$$Na_2S_2O_4 + 2CH_2O + H_2O \longrightarrow CH_2(OH)SO_2Na + CH_2(OH)SO_3Na \quad (1)$$

$$NaHSO_3 + CH_2O \longrightarrow CH_2(OH)SO_3Na \quad (2)$$

No exchange occurred, however, between SO_2 and trithionate ($S_3O_6^{=}$) which presumably has a normal S-S bond.

The first crystal structure studies of sodium dithionite were reported by Dunitz (22) in 1956. He found that the dithionite anion, in the crystal structure of sodium dithionite, consists of two SO_2^- units, joined by an unusually long S-S

bond which is 2.389 Å in length. By assuming the usual S-S single-bond distance of 2.08 Å, application of Pauling's (23) relationship $-\Delta R_{(n)} = 0.353 \log n$ between bond number, n, and the bond-type correction, $\Delta R_{(n)}$, relative to a single bond, predicts 0.36 for the bond strength. In the crystal, the dithionite anion has an eclipsed configuration with the planes of opposite SO_2^- groups inclined at 30° to one another. From these observations, Dunitz concluded that there should be ready cleavage of the S-S bond in dithionite.

An electron-paramagnetic-resonance (EPR) investigation by Hodgson, Neaves, and Parker (24) showed that anhydrous crystals of dithionite at the temperature of liquid oxygen gave weak electron-spin resonance. They reported a spectroscopic splitting factor of 2.01 ± 0.01 and a peak width of 12 ± 3 gauss. By treating the crystals with a small amount of degassed water or ethyl alcohol but not enough to dissolve them, the radical-ion content increased. When enough water was added to dissolve the crystals at room temperature and the mixture was frozen in liquid oxygen, no resonance could be detected. Upon evaporation of part of the water to re-form the crystals, a radical-ion signal was again observed. The radical-ions disappeared only very slowly when air was admitted. Hodgson, et al., estimated that approximately 0.01% of the dithionite ions was dissociated into SO_2^- radical-ions. They further stated that it was not clear whether the radical-ions were present only in the crystals or whether they were also present in the aqueous solution.

SUMMARY

A study of the electron-paramagnetic-resonance (EPR) properties of saturated dithionite solutions, which were stabilized at room temperature with sodium hydroxide, showed the presence of the SO_2^- radical-ion. On the EPR trace, the sharp resonance peak of this paramagnetic ion gave a peak width at half-height of 1.3 gauss and a spectroscopic splitting factor of 2.0051 at a klystron frequency of 9.453×10^9/sec and a magnetic-field strength of 3365 gauss. Observations on dithionite solutions of various dilutions showed that the SO_2^- concentration varied as the square root of the dithionite concentration so that the equilibrium relationship may be written as:

$$K_c = \frac{[SO_2^-]^2}{[S_2O_4^=]} \qquad (3)$$

Dry sodium dithionite powder was also observed to exhibit paramagnetism. This phenomenon is explicable in terms of minute amounts of $NaSO_2$ radicals occluded in dithionite powder.

Sodium formaldehyde sulfoxylate solutions were likewise shown to exhibit paramagnetism when adjusted to pH 6 or lower. The acidified solutions appeared to contain free radicals identical with those detected in dithionite solutions.

APPARATUS AND PROCEDURE

Chemically pure sodium dithionite (Baker Chemical Company, batch No. 3712, lot JTB 6113) was further purified by three fractional crystallizations from oxygen-free aqueous solutions at 0°C. The crystallization procedure was the same as that described in Air Oxidation Studies. The purified crystalline product was then used to make a saturated, oxygen-free alkaline solution at 0°C which was 0.5 molar in sodium hydroxide to inhibit thermal decomposition of the dithionite at room temperature.

Pyrex sample tubes with outside diameters of 1 mm and lengths of 76 mm were filled with the solution and sealed at both ends. Another set of sealed tubes of the same dimensions was prepared by filling with a tenfold and a hundredfold dilution of the saturated dithionite. A third set was prepared by filling with a completely oxidized sample of the saturated dithionite solution. Finally, a fourth set was prepared by filling with an acidified sample of a saturated thiosulfate solution, to provide a source of colloidal sulfur.

Each of the sealed tubes was analyzed in an EPR apparatus which had a cavity diameter slightly greater than 5 mm and a length of approximately 23 mm. During the EPR measurements, some difficulty was experienced in obtaining cavity resonance because of the dipole heating of the water molecules.

A calibration tube was made up from 0.1 molar manganous

chloride in order to compare the known values of the splitting factor and the gauss separation between resonance peaks for the free electron of the manganous ion with the resonance trace of the dithionite samples. In the calibration runs, the instrument settings for the sweep rate of the magnetic field were kept the same as those used for the dithionite.

In the experiments with dry $Na_2S_2O_4$ powder, the purified material was dried at 100°C in a vacuum over P_2O_5 for several days before sampling. The finely-divided, dry powder was loaded into a pyrex tube in a desiccator.

Eastman Kodak sodium formaldehyde sulfoxylate, m.p. 65°C, was recrystallized from water-methanol and dried at 50°C in a vacuum. The dry powder, saturated solutions in pure water, 1 molar NaOH, and 1 molar HCl were examined for paramagnetism.

RESULTS

The results of the EPR studies are shown in Figures 16 and 17. An arbitrary signal voltage which was a first-derivative function of the phase-sensitive detection system of the EPR apparatus is plotted against magnetic field strength in Figure 16a. Since the klystron frequency of the apparatus was held constant, the magnetic field strength was varied over the range in which resonance was expected to occur. The rate of magnetic scanning in relationship to chart speed on the graphic recorder fixed the time constant from which the magnetic field strength at resonance and the resonance peak width were calculated. The scale factor for conversion of instrument readings to corresponding field-strength values was obtained from a calibration using the resonance peaks of manganous ions which have a peak to peak distance of 98 gauss.

Only the three samples which contained oxygen-free stabilized dithionite of different dilutions showed paramagnetism. Sharp resonance occurred at 3.365 kilogauss with a fixed klystron frequency of 9.453×10^9 cycles/sec. The width of the single resonance peak for each sample was approximately 1.3 gauss at half-peak height, and the spectroscopic splitting factor g was found to be 2.0051 based upon a comparison with the free-electron g-value of 2.0023 for manganous ion in aqueous solution.

Figure 17 shows the absorption peaks of the three dithionite concentrations studied. An estimate of the area ratios of the absorption peaks for the saturated solution, the tenfold dilution and the hundredfold dilution was 10 to 3 to 1, respectively. This indicated that the SO_2^- concentration varied as the square root of the dithionite concentration, so that they are related by the expression:

$$K_c = \frac{[SO_2^-]^2}{[S_2O_4^=]} \qquad (3)$$

No absolute concentration of the SO_2^- was determined from these few tests, but the limiting concentration of the paramagnetic species which could be detected in the 5 mm cavity was estimated to be 2×10^{-6} molar or 10^{-9} moles.

In agreement with Hodgson et al. (24), dry $Na_2S_2O_4$ powder was also observed to exhibit paramagnetism. The width of the single resonance peak, measured at half-peak height, was 5 gauss. Ultraviolet irradiation of the dry powder for several hours did not increase the paramagnetism in an experiment carried out at room temperature.

Sodium formaldehyde sulfoxylate crystals did not exhibit paramagnetism. Saturated aqueous solutions in pure water or 1 molar NaOH gave the same result. The acidified solution, however, either at pH 5-6 or pH 1, gave a sharp resonance peak whose width and g-value are indistinguishable from that obtained from dithionite solutions. Figure 16b shows

the resonance absorption obtained from the acidified sodium formaldehyde sulfoxylate solution and from the solid $Na_2S_2O_4$ powder when both samples were placed in the cavity. Two peaks, superimposed upon one another, can be distinguished. The narrower, inner peak corresponds to the liquid sample and the outside peak shows the resonance absorption in the solid. Likewise, Figure 16c shows the superposition of the same solid sample on the aqueous dithionite resonance absorption. Within the limits of experimental detection, the peak widths and g-factors of these free radicals are identical.

DISCUSSION AND CONCLUSIONS

The observation that the SO_2^- free radical exhibits a single resonance absorption is consonant with the fact that no nuclear spins are present in the molecule, and therefore one would expect no hyperfine splitting.

The close proximity of the observed g-value to that of a free electron indicates that spin-orbit interactions are probably small. Since the EPR studies were conducted at only one frequency, however, it cannot be concluded that there is no orbital contribution to the paramagnetism.

The narrow peak observed for the aqueous SO_2^- indicates that the rate of combination-dissociation between the dimer dithionite and the monomer SO_2^- ions must be low compared with the free electron relaxation time of 10^{-9} seconds. Moreover, the fact that the absorption peak width changed only slightly upon dilution by 100-fold suggests that exchange narrowing is not a significant process in this instance.

The observed paramagnetism of dry dithionite powder is somewhat surprising since aqueous solution results require the interpretation that the undissociated dithionite dimer be diamagnetic. Crystal structure studies (22) indicate that dithionite is not dissociated in the crystal. Although a completely unambiguous explanation of this phenomenon cannot be given at this time, it seems likely that extremely small amounts of SO_2^- or $NaSO_2$ are occluded or trapped in the

crystals. Certainly the similarity of g-value and narrow line width suggests that again an SO_2^- radical ion is involved. Since extremely small concentrations of SO_2^- would be required to give the observed resonance, i.e., about one part in 100,000, crystal structure studies would not detect these occlusions.

The observed paramagnetism of acidic solutions of sodium formaldehyde sulfoxylate is also surprising since the unprotonated complex is diamagnetic in neutral and basic solutions. Evidently protonation of the ionized complex causes cleavage of the carbon-sulfur bond with liberation of the radical-ion SO_2^-. Thus:

$$CH_2(OH)SO_2^- + H^+ \longrightarrow SO_2^- + ? \qquad (4)$$

That the free radical obtained upon acidification is SO_2^- has not been definitely established. The only evidence offered in support of the thesis that it is SO_2^- is the fact that sodium formaldehyde sulfoxylate is formed from formaldehyde and dithionite in basic solution:

$$S_2O_4^= + CH_2O + H_2O \longrightarrow CH_2(OH)SO_2^- + SO_3^= + H^+ \qquad (5)$$

and similarities in the resonance absorptions shown in Figures 16b and c. Heretofore three investigators (6,21,25) believed that acidification of the complex liberated the anion

of sulfoxylic acid and regenerated formaldehyde.

$$CH_2(OH)SO_2^- + H^+ \longrightarrow CH_2O + SO_2^= + 2H^+ \qquad (6)$$

The fact that this is not the case explains the instability of pyridine nucleotide complexes (25,26,27,28), which are similar to formaldehyde complexes, with dithionite and sulfoxylate in acidic media. Also explicable is the rapid decomposition of neutral and acidic solutions of formaldehyde sulfoxylate complex with metal ions known to catalyze free radical decompositions (6).

The unambiguous demonstration that appreciable concentrations of SO_2^- ion exist in equilibrium with $S_2O_4^=$ in solutions of sodium dithionite supports the mechanism proposed for the air oxidation of dithionite solutions. SO_2^- radical-ions are confirmed to be real intermediates in the air oxidation mechanism. Moreover, the limit of sensitivity of the detection apparatus and the results of the dilution experiments enable one to make order-of-magnitude calculations of the equilibrium constant, K_c. The concentrations of dithionite corresponding to the absorption curves in Figure 17 are 7.4×10^{-1}, 7.4×10^{-2} and 7.4×10^{-3} molar in decreasing order. Estimating that one more tenfold dilution of dithionite to 7.4×10^{-4} molar would decrease the SO_2^- concentration to the limit of detection of the apparatus, i.e., 2×10^{-6} molar, permits a rough calculation of K_c to be made:

$$K_c \approx \frac{(2 \times 10^{-6})^2}{7.4 \times 10^{-4}} \approx 5 \times 10^{-9} \text{ moles/liter} \qquad (7)$$

This order-of-magnitude calculation is in reasonable agreement with the order-of-magnitude calculation of 8×10^{-11} moles/liter based upon air oxidation studies.

PART 3. ELECTROLYTIC STUDIES

INTRODUCTION

The electrolytic synthesis and electrochemical properties of sodium dithionite were first investigated nearly a hundred years ago by Schutzenberger (2), one of the pioneers in dithionite chemistry. Schutzenberger reduced a solution of sodium bisulfite electrolytically and obtained a crystalline solid which proved to have powerful reducing properties. He assigned the molecular formula $NaHSO_2$ to the substance.

Nearly half a century later, Jellinek (29) used electrochemical methods to investigate the equilibrium

$$H_2 + 2HSO_3^- \rightleftharpoons S_2O_4^= + 2H_2O \qquad (1)$$

Determination of the emf corresponding to the electrode reaction

$$S_2O_4^= + 2H_2O \rightleftharpoons 2HSO_3^- + 2H^+ + 2e^- \qquad (2)$$

enabled him to calculate the heat of reaction for the equilibrium process. He reported the following, for equilibrium at 21°C:

$$S_2O_4^= + 2H_2O \rightleftharpoons 2HSO_3^- + H_2 \quad \Delta H = -15{,}300 \text{ cal} \qquad (3)$$

In a later article (30) Jellinek stated that the electrolytic reduction of $NaHSO_3$ to $Na_2S_2O_4$ gave decreasing yields of dithionite during electrolysis. He concluded that this decrease in yield resulted from thermal decomposition of the dithionite formed according to the equation:

$$2Na_2S_2O_4 + H_2O \longrightarrow Na_2S_2O_3 + 2NaHSO_3 \qquad (4)$$

He discounted the possibility that the dithionite itself could be reduced to thiosulfate in the electrolytic reduction.

The first precise electrochemical work reported in the literature was by Gossman (31) in 1930. Studying the reduction of sulfur dioxide in aqueous solutions at the dropping mercury electrode, Gossman postulated that $H_2S_2O_4$ was formed by reduction of SO_2 in strongly acidic media. At a cathode potential of -0.2v vs S.C.E. in 1 molar HCl, 2 moles of electrons were believed to be transferred to 2 moles of aqueous SO_2 yielding $H_2S_2O_4$, which he incorrectly believed to be stable in strongly acidic media. Thus:

$$2SO_2 + 2H^+ + 2e^- \longrightarrow H_2S_2O_4 \qquad (5)$$

At pH 6, two smaller cathodic waves were observed. He postulated that the dithionite was unstable at pH 6 and decomposed thus:

$$H_2S_2O_4 \longrightarrow H_2SO_2 + SO_2 \qquad (6)$$

The second cathodic wave he ascribed to the reduction of the liberated SO_2. Above pH 7 no cathodic waves were observed at potentials less than that required to reduce sodium ion at the mercury electrode.

Kolthoff and Miller (32) in 1941 repeated Gossman's work and obtained the same experimental data. Their interpretation of the data, however, was quite different. They stated that the reduction of sulfur dioxide in 1 molar HCl is a two electron transfer process, instead of the one electron transfer process postulated by Gossman. Thus:

$$SO_2 + 2H^+ + 2e^- \longrightarrow H_2SO_2 \qquad (7)$$

Sulfoxylic acid, not dithionous acid, was stated to be the reduction product. They reasoned that the diffusion coefficient for SO_2 calculated from the data and the use of Ilkovic's equation for one and two electron transfer reactions agreed with the previously known diffusion coefficient of oxygen under similar conditions only in the case of the two electron transfer. In order to explain the two cathodic waves at pH 6, they reverted to a one-electron transfer reaction which is followed by a dimerization reaction and subsequent reduction of the dimer to thiosulfate. Thus:

$$HSO_3^- + 2H^+ + e^- \longrightarrow HSO_2 + H_2O \qquad (8)$$

$$2HSO_2 \longrightarrow H_2S_2O_4 \longrightarrow S_2O_4^{=} + 2H^+ \qquad (9)$$

$$2H^+ + S_2O_4^{=} + 2e^- \longrightarrow S_2O_3^{=} + H_2O \qquad (10)$$

No analyses of reduction products were reported.

In a series of articles published between 1949 and 1953 Patel and Rao (17) described investigations of the feasibility of producing sodium dithionite electrolytically on a commercial basis. The effects of a great number of reaction conditions were systematically studied in an attempt to maximize the yield of sodium dithionite. The cathodic potential used in all cases, however, was sufficiently negative to reduce sodium ion; hence the reducing agent was actually sodium-mercury amalgam. Using a reactor maintained at 5°C and pH 5 to 5.5 with a HSO_3^- concentration of 30% by weight (maintained by constant SO_2 gas feed), dithionite concentrations of 20% by weight could be obtained with 91% current efficiency. Under optimal conditions, a current density of 2.0 - 2.6 x 10^{-2} amps/sq cm was maintained between a rapidly stirred mercury cathode, which contained 0.13% Zn, and a carbon rod anode.

The present investigation of the electrochemical synthesis and properties of sodium dithionite was designed to seek answers

to several problems left unsolved by the investigations described above. Knowledge of the fact that SO_2^- radical ions exist in aqueous solution in equilibrium with undissociated dithionite suggested that the cathodic waves obtained by Gossman and Kolthoff and Miller corresponded to reduction of SO_2 to SO_2^- by a one electron transfer reaction:

$$SO_2 + 1e^- \longrightarrow SO_2^- \qquad (11)$$

Identification of the reduction product by its ability to reduce methylene blue and the paramagnetism of its solutions would confirm the suggestion that dithionite is formed. Furthermore, a study of the efficiency of the reduction process and the stability of the dithionite formed would be of interest.

Since the completion of the work described in the following sections, two important studies have been reported in the literature.

Munemori (33) reported the coulometric titration of dyestuffs with electrolytically generated dithionite. Electrolyses of solutions 0.01 molar in bisulfite ion between pH 3 and 5 with cathode potential -0.63v vs S.C.E. and constant currents between 3.1 and 5.0 milliamps produced dithionite at essentially 100% current efficiency.

Cermak (34,35) reported extensive studies of the polarographic properties of dithionite solutions. His experiments included the effects of pH, concentration and reaction tempera-

ture. His results are in agreement with the existence of SO_2^- radical-ions in aqueous solutions of dithionite. In order to explain the anodic and cathodic kinetically-controlled waves obtained, it was necessary to postulate the dissociation of the dimer $S_2O_4^=$ to monomer SO_2^- ions. Two anodic waves corresponding to the oxidation of SO_2^- to SO_2 and $S_2O_4^=$ to $S_2O_5^=$ were postulated. Two cathodic waves corresponding to the reduction of SO_2 to SO_2^- and SO_2^- to $SO_2^=$ were also postulated. The heights of the kinetically-controlled waves enabled him to calculate the ratio of the forward rate constant of the $S_2O_4^=$ dissociation to the square root of the equilibrium constant for the reaction

$$S_2O_4^= \underset{k_{-1}}{\overset{k_1}{\rightleftharpoons}} 2SO_2^- \qquad (12)$$

where $K_c = \frac{k_1}{k_{-1}}$

The value of $\frac{k_1}{\sqrt{K_c}}$ at 40°C was given as 6×10^{-3} $(\text{moles/liter})^{-\frac{1}{2}}$ sec^{-1}. Separate evaluation of the rate constants or equilibrium constant was not possible from this work.

SUMMARY

Dithionite ion has been established as the reduction product in the electrolysis of aqueous bisulfite solutions of pH 5-5.3 at cathode potentials of -0.60 to -0.98v vs S.C.E. That the reduction is a one-electron transfer process by which SO_2^- ions are formed from aqueous sulfur dioxide at the cathode seems likely, although the possibility of two electron transfer has not been excluded.

APPARATUS AND PROCEDURE

A simple electrolysis cell consisting of a 600 ml Berzelius beaker with a tight-fitting plexiglas lid was immersed in an ice bath. The cathode consisted of a pool of clean mercury 7 mm deep and 49 sq cm in area. The cathode was connected to a terminal on the plexiglas lid by a platinum wire shielded from the electrolyte by glass tubing. The cathodic pool was not stirred. The anode consisted of a platinum electrode, with surface area 1 sq cm, placed in an anode compartment. The anode compartment consisted of a fine-mesh gas-dispersion frit mounted on the end of a length of a 1 cm glass tubing fixed to the plexiglas lid. Fresh electrolyte solution was added to the compartment at intervals in order to maintain a positive pressure differential between the anode compartment and the bulk of the electrolyte solution. A Heathkit Model PS-3 power supply was used to drive the cathode potential negative and measure the current in milliamperes. A Leeds and Northrup Model 7664 pH meter measured the potential of the cathode with respect to a saturated calomel electrode immersed in the electrolyte solution and fixed to the plexiglas lid. The electrolyte solution was stirred rapidly and at constant speed with a glass paddle-stirrer.

The electrolyte solution was prepared by saturating 250 ml of distilled water with reagent grade sodium bisulfite and by adding reagent grade sodium acetate and water, as needed, to

produce a saturated solution at the desired pH of 5.0-5.3.

One- or two-cc samples were withdrawn from the electrolyte by a pipette at suitable time intervals and titrated with standardized methylene blue as described in Air Oxidation Studies.

A total of three experiments were conducted at constant currents of 100, 150, and 200 milliamperes. The cathode potential varied between -0.67 and -0.98 v. At the conclusion of the 200 milliampere experiment the electrolysis was allowed to proceed for several hours. The electrolysis was then stopped, the solution made alkaline by the addition of 1 molar NaOH solution, and pure crystalline NaCl added to salt out a white precipitate. This white precipitate was collected by centrifugation and quickly loaded, as a wet paste, into a pyrex tube for examination by EPR.

RESULTS AND CONCLUSIONS

Figure 18 and Table 12 present the data obtained from the three electrolysis experiments. Evidently dithionite can be generated at constant current efficiency of about 75% under the conditions studied. The rather low current efficiency obtained probably results, at least in part, from the fact that the cathode was not stirred.

Electron paramagnetic resonance absorption similar in all respects to the one shown in Figure 16a was obtained from the sample of precipitated reduction product. This confirms the identity of SO_2^-, and hence $S_2O_4^=$, as the reduction product.

The question of whether the reduction is a one or two electron transfer, however, has not been unambiguously solved. The two possibilities are

$$SO_2 + 1e^- \longrightarrow SO_2^- \qquad (11)$$

and

$$SO_2 + 2e^- \longrightarrow SO_2^= \qquad (13)$$

The identification of SO_2^- as the reduction product is not sufficient to distinguish between these two mechanisms. It is possible that $SO_2^=$, if generated, could react with aqueous SO_2 to yield $S_2O_4^=$ and hence SO_2^-. Thus:

$$SO_2^{=} + SO_2 \longrightarrow S_2O_4^{=} \rightleftharpoons 2SO_2^{-} \qquad (14)$$

Since it has been demonstrated by EPR that sodium formaldehyde sulfoxylate, heretofore believed (6,21,25) to be a source of $SO_2^{=}$ ions, liberates SO_2^{-} in solution of pH 6 or less, the reaction written above cannot be tested using sodium formaldehyde sulfoxylate as the source of $SO_2^{=}$ ions. An experiment using another source has not been attempted.

The polarographic studies of aqueous SO_2 solutions (31, 32,34,35) as interpreted by Cermak indicate that $SO_2^{=}$ is not formed by the reduction of SO_2^{-} ions until a cathode potential of -1.23v is reached. This seems to be an entirely reasonable interpretation of the polarographic waves observed, although it is not a unique one.

Use of the Cermak relation $k_1/\sqrt{K_c} = 6 \times 10^3$ $(\text{moles/liter})^{\frac{1}{2}}$ sec^{-1} together with order-of-magnitude calculations of the equilibrium constant, K_c, from air oxidation and EPR studies enables one to obtain order-of-magnitude values for k_1 and k_{-1}. The values of K_c estimated from air oxidation and EPR studies are 8×10^{-11} and 5×10^{-9} moles/liter respectively. If one uses a logarithmic average value, namely 6×10^{-10} moles/liter and solves for k_1 and k_{-1} in equation 12 using the Cermak relation, k_1, and k_{-1} are found to be 2×10^{-7} sec^{-1} and 3×10^2 $(\text{moles/liter})^{-1/2}\text{sec}^{-1}$, respectively. The bimolecular rate constant, k_{-1}, seems rather low, although the approximate nature of these calculations does not justify any further conclusions which might be drawn.

PART 4. THERMAL DECOMPOSITION STUDIES

INTRODUCTION

The first careful study of the thermal decomposition of sodium dithionite solutions was reported by Jellinek (36) in 1919. Examining the decomposition reaction in neutral and sodium-bisulfite-containing solutions, he found that dithionite decomposed almost quantitatively in accordance with the equation:

$$2Na_2S_2O_4 + H_2O \longrightarrow 2NaHSO_3 + Na_2S_2O_3 \qquad (1)$$

In reactions carried out at constant temperature, the rate constant was found to be proportional to the square of the initial bisulfite concentration. The variation in rate constant with temperature, at constant initial bisulfite concentration, was in a manner predicted by the Arrhenius equation.

Bassett and Durrant (6) in 1927 reviewed all of the literature pertaining to the interrelationships of the sulfur acids and attempted a correlation with the results of extensive experimental work of their own. In order to explain the complexity of products of dithionite reactions, they postulated that dithionite exists in three isomeric forms. Each isomer was believed to decompose in a way such that all of the observed reaction products could be explained by one or more of the mechanisms. Although Bassett and Durrant's work is of

considerable value as a compilation of experimental observations of dithionite reactions, subsequent work has invalidated their interpretation of these reactions.

Lynn (8) carried out the most extensive investigation of the thermal decomposition reaction reported to date. He found that an aqueous solution of purified sodium dithionite at 60°C decomposed slowly at first, and then, after a certain elapsed time, decomposed very rapidly. This behavior suggested to him a degenerate chain-branching mechanism. He assumed the stoichiometry of the reaction to be that described by Equation 1 above. He observed that the hydrogen ion concentration increased in a manner which was almost a mirror image of the decreasing dithionite concentration. At low pH, the dithionite decomposed in a few seconds. In addition, the presence of colloidal sulfur accelerated to a lesser extent the onset of the rapid decomposition reaction.

Lynn also studied the effects of added salts on the reaction rate. The addition of sodium hydroxide or sodium sulfite was observed to inhibit the onset of the rapid decomposition reaction. Addition of sodium chloride catalyzed this reaction, presumably by a Brönsted positive-salt effect. Sodium thiosulfate, likewise, accelerated the onset of the rapid decomposition reaction. Sodium bisulfite, however, had a different effect. At concentrations less than the initial dithionite concentration its effect was similar to that of sodium thiosulfate, but when greater, it changed the course

of the reaction entirely. The reaction became apparently first order in both bisulfite and dithionite concentrations. Moreover, when thiosulfate was added to this mixture, the reaction became apparently first order in thiosulfate as well as in bisulfite and dithionite. The third order rate constant, however, was found to be an undetermined function of hydrogen ion and initial dithionite concentrations.

Superimposed on this complex reaction system, Lynn found that the observed rate was periodic with time, i.e. periodically increased and decreased as the reaction proceeded. In order to explain this curious phenomenon, he postulated the presence of an unknown product species having properties similar to dithionite. In addition, there was a significant lack of reproducibility in many of the experiments reported. This was believed to result from the presence of differing amounts of suspended sulfur particles in the initial dithionite solutions.

SUMMARY

A study of the thermal decomposition of sodium dithionite was conducted in buffered and unbuffered media in the pH range 4.0 to 7.0. The concentration of the dithionite was measured as a function of time at 60, 70, and 80°C. Initial concentrations varied from 5.5 to 11.5 x 10^{-3} molar. The pH of the unbuffered systems was measured as a function of time with a Beckman Model G pH meter. The reaction was observed to consist of an induction period in which the decomposition was slow, followed by a decay period, in which the concentration of dithionite rapidly decreased to zero. Apparent periodic increases and decreases in dithionite concentration during the induction period were observed and could not be explained solely on the basis of experimental error. One possible explanation of this unusual phenomenon is the formation of unstable intermediate(s) possessing reducing potentials comparable to dithionite with respect to methylene blue. The amplitude of the apparent oscillations in dithionite concentration decreased with increasing temperature, suggesting that the concentration of the hypothetical reactive intermediate(s) likewise decreased with increasing temperature. Absence of oscillations in solutions of pH greater than 7 suggests that the hypothetical intermediate(s) either are not formed or are unstable in alkaline solution.

During the induction period, the reaction was observed

to be 1/2 order with respect to H^+ and 3/2 order with respect to dithionite, giving a rate expression of the following form:

$$r_{induction} = k_c[H^+]^{1/2}[S_2O_4^=]^{3/2}$$

The variation of k_c with temperature gives a straight line on an Arrhenius equation plot. The activation energy ΔE was found to be 12 kcal/mole and the frequency factor A was found to be 1.3×10^8 $(moles/liter)^{-1}sec^{-1}$.

The anions $SO_3^=$, HSO_3^-, $SO_4^=$, and $S_2O_3^=$ had no specific effects in buffered reactions. Colloidal sulfur catalyzed the reaction by decreasing the length of the induction period.

The rapid increase in the rate of dithionite decomposition during the decay period followed an exponential relationship with time. This fact together with the catalysis by colloidal sulfur suggests that an autocatalytic or a degenerate branching chain mechanism is occurring.

APPARATUS

In general, the apparatus for the thermal decomposition studies was the same as that described in Air Oxidation Studies. The only change was to eliminate the presence of oxygen from the reaction system. This was accomplished by partially diverting the oxygen-free nitrogen from the scrubbing system previously described into the reactor. It is important to note that the nitrogen was not allowed to pass through the reactor in a steady stream. The pressure of the nitrogen above the reaction mixture was maintained slightly above atmospheric and was controlled manually by occasionally adjusting a by-pass valve upstream from the reactor. A water-filled manometer which was connected directly to the exit line indicated the pressure.

EXPERIMENTAL PROCEDURE

The preparation of the recrystallized dithionite was accomplished in the same manner as described in the experimental procedure of the Air Oxidation Studies. Also, by the same procedure, the saturated solution of dithionite was subsequently prepared from the crystals and used to supply the initial concentration to the reactor.

The volume of the liquid mixture in the reactor was approximately 500 cc. The composition of the solution before addition of the saturated dithionite varied according to the desired hydrogen-ion concentration. The majority of tests were performed in water that had been triply distilled. Other tests were performed in buffered solutions wherein the pH was varied from 4.0 to 7.0. The buffering agents were mixtures of KH_2PO_4 and NaOH or $KHC_8H_4O_4$ and NaOH in proportions commensurate with the desired pH. In Appendix I, the compositions of the buffer solutions are described in detail.

Experiments at 60, 70 and 80°C were conducted with the unbuffered systems in order to determine the effect of temperature on the rate of decomposition. The buffered systems were studied only at 60°C since, in this case, the effect of a controlled pH was of primary importance. At each temperature and for both the buffered and unbuffered systems, the initial concentration of dithionite was varied from 5.5 to 11.5 x 10^{-3} molar.

In the unbuffered systems, no products of reaction such as HSO_3^-, $S_2O_3^=$, $SO_3^=$, S, and H^+ were added to the system in order to determine their specific catalytic effects. This work had been done previously by Lynn (8). To the buffered reactions, however, HSO_3^-, $S_2O_3^=$, $SO_4^=$, and $SO_3^=$ were added in concentrations ranging from one-half to three halves of the stoichiometric quantities according to the reaction:

$$2S_2O_4^= + H_2O \longrightarrow S_2O_3^= + 2HSO_3^- \qquad (2)$$

These anion additions were always made while the decomposition experiments were in progress. The purpose of their addition was to determine their catalytic effects in the presence of controlled H^+ ion.

By conducting successive tests in the reactor without removing the contents of the previous runs, the catalytic effects of the product species $S_2O_3^=$ and sulfur were determined. Usually, three dithionite solutions were decomposed in each experiment, and in all cases the systems were buffered at a pH of 5.00. After the first decomposition which was begun with fresh solution, and after each successive decomposition, enough buffer solution was added to restore the volume of the reactor contents to 500 cc. Also, the initial dithionite concentrations which varied from 5.5 to 6.0 x 10^{-3} molar, originated from the same saturated solution. A pH measurement was taken at the beginning and end of each decomposition

in order to insure that sufficient buffer was present.

Great care was taken to prevent oxygen contamination. When transferring samples from the reactor to the titration flasks, for example, the sampling syringe was flushed with nitrogen several times prior to removing a sample from the reactor. As a further precaution to prevent contamination, the syringe was rinsed several times with oxygen-free distilled water after taking each sample.

Reactant and Product Analysis

The concentration of $S_2O_4^=$ was estimated by titration with methylene blue as described in the experimental procedure of the Air Oxidation Studies. The sample flasks which received a measured volume of the reaction mixture were initially filled with 50 cc of 0.1 molar KOH and 30 cc of CH_3OH. Titration of the samples with methylene blue was done immediately in order to minimize the errors due to slight oxygen contamination or further thermal decomposition. Occasionally, titrations were performed at approximately 5°C to check for any significant effects of temperature upon the results. No effect was noted, so that titrations at room temperature were done with confidence.

In order to determine the relative concentrations of the end-products, an unbuffered reaction at 30°C was carried out in a sealed vessel with an initial dithionite concentration of 7.32×10^{-3} molar. The completion of reaction was determined

by titration of a 10 cc sample with methylene blue. The concentration of the product $S_2O_3^=$ was estimated by iodometric titrations of samples from the sealed vessel. The sampling flasks were initially filled with 10 cc of formaldehyde, 30 cc of distilled water, and 20 cc of acetate buffer with a pH of about 5. The purpose of the formaldehyde was to complex the HSO_3^- by the reaction,

$$CH_2O + NaHSO_3 \longrightarrow CH_2(OH)SO_3Na \qquad (3)$$

This reaction was allowed 20 minutes for completion. In the complexed form, the HSO_3^- was unaffected by I_3^- so that the concentration of $S_2O_3^=$ alone could be determined.

The HSO_3^- ion was analyzed by an iodometric oxidation in which the excess iodine was titrated with a standardized 0.01 normal $S_2O_3^=$ solution. The sampling flasks were initially filled with 50 cc of standardized 0.01 normal iodine solution and 25 cc of acetate buffer with a pH of about 5. The resulting sum of the concentrations of $S_2O_3^=$ and HSO_3^- allowed the concentration of HSO_3^- to be calculated by difference.

Hydrogen Ion Concentration

The pH of the reacting mixtures was measured with a standard Beckman Model G pH meter, which was connected to electrodes inserted into the reactor through standard-taper glass fittings. pH readings were taken approximately every 100 seconds. In this way, depending upon the duration of reaction, between

twenty and forty measurements of pH were obtained for each run.

With the buffered systems, the pH was measured only before and after reaction to insure that the hydrogen ion concentration had been held constant.

RESULTS

Unbuffered Reactions--General

The experimental data on the concentration of dithionite as a function of time for the unbuffered systems are presented in Tables 13-15 and Figures 19-21. The general trend of the curves as shown in the figures is in substantial agreement with Lynn's results. The decomposition began with an induction period in which the dithionite concentration decreased slowly. In most cases, this was followed by an abrupt and rapid decrease in the concentration.

In Table 13 and Figures 19a, b, c, which present experimental results of the decomposition at 60°C, it is noted that the total time of reaction was a function of initial dithionite concentration. Also, independently of the initial concentration, the curves show marked oscillations which have amplitude variations as high as ± 15%, with the average being closer to ± 5%.

The data at 70°C, which are plotted in Figure 20 and listed in Table 14, show a similar dependence of total time of reaction on initial concentration. The amplitude of the oscillations, however, is considerably less than at 60°C and varies as high as ± 6% with an average variation of ± 2%.

In Figure 21 and Table 15, the amplitude of the oscillations at 80°C is practically negligible. The maximum variation is only ± 1.5% with an average variation of less than ± 0.5%.

Variation of pH in Unbuffered Reactions

As stated under Apparatus and Procedure, the pH of unbuffered decompositions was measured continually during many of the tests. Typical plots of H^+ concentration vs time for 60 and 70°C are shown in Figures 22 and 23. The data for the plots are listed in Table 17. For comparison, the dithionite concentrations as a function of time are also plotted in the same figures. The curves show that the H^+ concentration varies almost as the mirror image of the dithionite concentration. Particularly interesting is the fact that the H^+ curves oscillate. There appears, however, to be no simple relationship in frequency or amplitude between the oscillations of the dithionite curves and the H^+ curves.

Buffered Reactions--General

The experimental data on the concentration of dithionite as a function of time for the buffered systems are presented in Table 16 and Figures 25a,b. With the exception of the results at a pH of 7.00, the curves for concentration vs time are practically the same as those obtained for the unbuffered systems. Again there is an induction period followed by a rapid decrease in dithionite concentration giving rise to curves which are convex. Also, the characteristic oscillations which were present in the unbuffered systems were found to exist for the buffered reactions. At a pH of 7.00, the concentration of dithionite decreased so slowly that the rapid decomposition period was not reached during the time in which

the reaction was studied. Significant oscillations were still present.

Effect of pH on Buffered Reactions

It was found experimentally that the induction time and likewise the total time of reaction decreased with increasing H^+ concentration. As presented in Table 19 and Figure 24 for the pH range of 4.80 to 6.00 and at an initial dithionite concentration of 11.0×10^{-3} molar, the time of the induction period was inversely proportional to the first power of the H^+ concentration, i.e.

$$\theta_I \propto \frac{1}{C_b} \qquad (4)$$

where θ_I is the time of the induction period and C_b is the concentration of H^+ in the buffered solution. At a pH lower than 4.5, the decomposition was very rapid and could not be studied with the analytical methods used.

Effect of Additives on the Buffered Reactions

The addition of HSO_3^-, $S_2O_3^=$, $SO_4^=$ and $SO_3^=$ had no measurable effect on the rate of dithionite decomposition. This is presented in Table 20 and Figures 27a,b in which the concentration of dithionite is plotted vs time at a pH of 7.00. On the plots are shown the concentrations of the additives and the time of their injection into the reactor.

The addition of air to the decomposition reaction at pH of 7.00 also had no measurable effect on the rate. This is

shown on Figure 27a.

In Table 21 and Figures 28a,b are presented the results of two identical experiments. As stated under Experimental Procedure, for each experiment three successive decomposition reactions were conducted wherein the reactor contents consisted of the products of the previous tests. The figures show the dithionite concentration as a function of time. The rate of reaction showed a marked increase in each successive test, and this indicated that a product, probably sulfur, catalyzed the decomposition. It is interesting to note that the curves for the two experiments are almost identical even with respect to the oscillations.

Product Analysis

The end-products of the thermal decomposition reaction were found to consist mainly of thiosulfate and bisulfite in an approximate molar ratio of 1 to 2, respectively. A typical analysis is listed in Table 22 for an experiment at 30°C. From a knowledge of the initial dithionite concentration, a sulfur material balance indicated that other products such as free sulfur were present but in low concentrations. The analysis listed in Table 22 does not represent the only product distribution to be expected in every dithionite decomposition experiment. The relative amount of sulfur in the products apparently depends on conditions of acidity, temperature and catalysis.

Appearance of Sulfur in Buffered and Unbuffered Reactions

The formation of sulfur as one of the products of dithionite decomposition was not measured quantitatively in this investigation. Its formation, however, was definitely established by visual inspection. As the reaction proceeded toward completion it was found that the reactor contents acquired a slight milky appearance which sometimes disappeared and reformed several times before the end of the induction period. At the onset of the rapid decrease in dithionite concentration, the milky appearance reached a maximum opacity. This phenomenon was considered to be the formation of solid particles of sulfur which either coalesced to form colorless macromolecules or reacted with other species in the solution. The appearance of sulfur was found in both unbuffered and buffered reactions at a pH less than or equal to 7.0. At a pH greater than 7.0, no sulfur was found by visual inspection.

Order of Reaction with Respect to the Concentration of Dithionite for the Induction Period

The dependence of the rate during the induction period upon the concentration of dithionite was obtained from the results of the unbuffered systems. For each temperature, the initial rates were plotted vs the initial concentrations on logarithmic paper and the slope of the best line through the points gave the order of the reaction with respect to dithionite. This calculation was based on the rate expression,

$$-\frac{d[S_2O_4^{=}]_o}{d\theta} = k[S_2O_4^{=}]_o^n \qquad (5)$$

and the results are presented in Table 23 and Figure 29. A value of $n = 1.5 \pm 0.2$ was obtained for the order of reaction with respect to dithionite. The use of Equation 5 assumes that the initial rate is a function only of the initial concentration of dithionite. This would be correct if all other independent variables such as temperature and the concentrations of other reactants were held constant. All of the experiments were performed under conditions of constant temperature. Most of the experiments were performed in unbuffered systems in which the H^+ was not controlled. Measurements of the H^+ concentration were taken, however, and since it was found that the initial H^+ concentration did not vary by more than a factor of 2, the error introduced by using Equation 5 was not significant. This conclusion was in agreement with the results of tests in buffered solutions, which were designed primarily to determine the order of reaction with respect to H^+. Thus at a pH of 5.00 and at a temperature of 60°C, decomposition experiments were conducted for several initial concentrations of dithionite. The order of reaction with respect to dithionite was obtained in the same way as noted above and was found to be 1.6. These results are presented in Table 24 and Figure 30.

Order of Reaction with Respect to the Concentration of H^+ for the Induction Period

The dependence of the rate during the induction period upon the concentration of H^+ was obtained from the buffered reactions. The initial rate was determined at each value of pH for the same initial concentration of dithionite (11.0×10^{-3} molar).

The rate of dithionite decomposition was found to increase in proportion to the square root of the H^+ concentration. These results are presented in Table 19 and Figure 31. The fact that the rate of reaction varied as the square root of the H^+ concentration explains why the initial rate of dithionite decomposition in unbuffered systems was reasonably insensitive to a twofold variation in H^+ concentration.

Rate Expression for the Induction Period

The 3/2 order dependence of rate upon the concentration of dithionite and the 1/2 order dependence upon the concentration of H^+ were combined to give a rate expression for the induction period. The relationship is given as follows:

$$r_{induction} = k_c[S_2O_4^{=}]^{3/2}[H^+]^{1/2} \qquad (6)$$

for which the values of k_c as a function of temperature are given in Table 25. The temperature dependence of k_c is given by the Arrhenius equation, $k = Ae^{-\Delta E/RT}$ in which the value of ΔE and A were obtained from a plot of log k_c vs 1/T given

in Figure 32. Therefore, the equation for k_c is:

$$k_c = 1.3 \times 10^8 \, e^{-\frac{12,000}{RT}} \quad (\text{moles/liter})^{-1}\text{sec}^{-1} \qquad (7)$$

It is important to note here that since the thermal decomposition of dithionite was complicated by the oscillatory nature of the reaction, there was considerable uncertainty both in the initial concentration of dithionite and in the initial reaction velocity. Since the order of reaction is contingent upon these parameters the established order of reaction with respect to both the H^+ and $S_2O_4^=$ is an approximation which is good to only ± 15%.

Rate Expression for the Decay Period

The convex nature of the concentration-time relationship for dithionite and the apparent catalytic effect of sulfur suggested that either an autocatalytic or degenerate branching chain process might be occurring. Both of these processes can be described by an exponential relationship between rate and time (37). A brief discussion of the application of these theories to the present data is given under DISCUSSION OF RESULTS AND CONCLUSIONS.

From the exponential law that

$$-\frac{dC}{d\theta} = Ae^{B\theta} \qquad (8)$$

the algebraic relationship between the concentration of di-

thionite C and time θ is found by integration to be

$$C_o - C = \frac{A}{B}(e^{B\theta} - 1) \qquad (9)$$

For degenerate, branching-chain reactions the term $(e^{B\theta} - 1)$ can be approximated by $e^{B\theta}$ since this term becomes very large after branching begins. Hence, with the above simplification, the logarithm of Equation 9 gives

$$\log(C_o - C) = \log \frac{A}{B} + \frac{B}{2.303}\theta \; . \qquad (9a)$$

By plotting $(C_o - C)$ vs θ on a semi-logarithmic scale, series of straight lines for the decay period were obtained for the data at 60, 70 and 80°C. The plots are presented in Table 26 and Figures 33-35; and as shown, the curves were non-linear for the induction period as would be expected. Also, the non-linearity near the end of reaction was not surprising since in this region the accuracy of analysis was a limiting factor. The fact that the lines at a given temperature are not parallel and do not have a common intercept, by extrapolation, indicates that both constants A and B are a function of initial dithionite concentration. The observed increase in slope with increase in temperature shows that B is also a function of temperature. Inspection of the curves indicates that these functional relationships are complex.

DISCUSSION OF RESULTS AND CONCLUSIONS

Oscillations in Dithionite Concentration vs Time Curves

Lynn (8) was unable to explain the oscillations which occurred during the decomposition of dithionite. The present experimental investigation of the thermal decomposition was undertaken primarily to determine the validity of these oscillations. No amount of care in removing sources of error or contamination succeeded in eliminating them. It may be pointed out that reproducibility of the oscillations was not in general obtained in the unbuffered systems (See Figures 19a,b). Oscillation reproducibility was, however, found to be more prevalent among the buffered systems than in the unbuffered systems. An example of this reproducibility is presented in Table 21 and Figures 28a,b for a pH of 5.00.

The amplitude of the oscillations was in many experiments too large to be explained solely on the basis of experimental error. The magnitude of these errors is discussed briefly as follows:

1. The calibrated syringe which was used to remove samples from the reactor had a capacity of 2 cc and was found to give reproducibility with a precision of $\pm$ 0.2%.
2. Further reaction of the sample after injection into a sample flask at 25°C was considered negligible since the flask contained 0.1 molar NaOH under a

nitrogen atmosphere. Furthermore, the sample experienced a 70 to 1 dilution. Titrations at 5°C did not affect the oscillations. Simultaneous samples which were titrated at different times, one immediately and one approximately 10 min later, did not show any measurable differences. Therefore, errors introduced by further reaction in the sample flasks were considered to be less than the titration error.

3. The concentrations of methylene blue solutions were selected to give differences in burette readings up to 40 cc for each dithionite sample titrated. The color of methylene blue is so intense that a drop of 0.0001 molar solution gives a clearly discernible blue color in 150 ml of water. For all the titrations in the present investigation, however, methylene blue with a concentration of about 0.001 molar was used. Rapid titrations could be carried out to $\pm$ 0.05 cc or an average error of $\pm$ 0.5%.

4. The ultimate products of the decomposition, $NaHSO_3$, $Na_2S_2O_3$, and varying amounts of sulfur did not reduce methylene blue under the conditions described in the experimental procedure. In fact, concentrations of $S_2O_3^=$, $SO_3^=$ and $S^=$ in quantities greater than one hundred times the concentration of $S_2O_4^=$ did not interfere. Lynn (8) stated that a very accurate but time-consuming chromate test for $S_2O_4^=$ gave results that compared closely with the methylene blue approach.

5. Perhaps the most unpredictable source of error was contamination by oxygen. In spite of the many precautions, this possibility cannot be ruled out, and it would be expected to cause errors in a completely random way. As described previously, however, there was some degree of reproducibility in the oscillations under certain conditions. Hence if the oscillations were caused entirely by oxygen contamination, it would be difficult to explain their semi-reproducibility. Also as stated previously, small amounts of air appeared to have no measurable effects on the systems buffered at a pH of 7.00. Yet these systems displayed oscillations in the curves of dithionite concentration vs time. Another argument opposed to oxygen contamination as the sole cause of the oscillations is the fact that the amplitude of the oscillations decreased with increase in temperature, as shown in Figures 19-21. This result is the converse of what would be expected on the basis of oxygen effects.

Therefore, excluding the small random error of oxygen contamination, the overall error in the analysis for $S_2O_4^=$ was $\pm$ 1%. This value is on the average much lower than the per cent changes in concentration of $S_2O_4^=$ as a result of the oscillations.

Several other factors related to the oscillation problem should be mentioned here. Significantly, there were no oscillations in the air-oxidation experiments. Yet the same method

of analysis for dithionite was used with both systems. Secondly, the H^+ concentrations of unbuffered systems not shown here, but similar in all respects to the H^+ concentration shown in Figure 22, were analyzed by use of pH electrodes without disturbing the system through removal of samples. Still, oscillations were present in the H^+ concentration as a function of time.

The above arguments would rule out experimental errors and oxygen contamination as the only cause of the oscillations. The fact that oscillations were semi-reproducible under certain conditions suggests that a series of reactions involving unstable intermediates of reducing potential comparable to dithionite was responsible for this unusual phenomenon.

Effect of Oxygen on the Thermal Decomposition of Dithionite

In the unbuffered decomposition of dithionite, the addition of small volumes of air (2 - 5 cc) during the reaction caused erratic changes in the concentration of dithionite. Several such additions of air usually shortened the induction period of the decomposition. This effect of the oxygen was apparently related to the effect of hydrogen ion concentration because in the buffered decomposition of dithionite at a pH of 7.00, erratic changes in concentration by addition of acid did not appear. It is likely that in both cases the oxygen reacted with species in solution such as SO_2^- or HSO_3^- by a chain mechanism to form anions of greater acidity. The increase of hydrogen ion had an imperceptible effect on the buffered

system, but in the unbuffered system increased the H^+ concentration. Indeed, the marked decrease in pH is illustrated by Figure 24, in which the concentration of H^+ vs time is shown for the decomposition of dithionite after several additions of air. That small amounts of oxygen caused relatively large changes in the H^+ ion concentrations suggests a chain or catalytic reaction which is inhibited in solutions of pH 7 or greater. Others (15,37,38) have found, for example, that HSO_3^- ion, which is present in the products of dithionite decomposition, reacts with O_2 by a chain mechanism in which oxygen is one of the chain initiators.

Catalytic Effects of Additives

The results of the present investigation show that the anions $SO_3^=$, $SO_4^=$, HSO_3^-, and $S_2O_3^=$ have no catalytic effect on the thermal decomposition of dithionite under conditions of controlled pH. These results are in disagreement with Lynn's work. He found that both HSO_3^- and $S_2O_3^=$ catalyzed the decomposition, but his investigations were conducted without careful control of the H^+ concentration.

In agreement with Lynn, it was found that sulfur does catalyze the decomposition by shortening the induction period in either buffered or unbuffered solutions. A discussion of the mechanism of the catalysis is presented below under The Decay Period.

Sensitivity of Reaction to H^+

The thermal decomposition of dithionite was found to be very sensitive to changes in H^+ concentration. At a pH greater than 7 the rate of decomposition was very low. In highly alkaline solutions from which air was rigorously excluded, reaction times were observed to be of the order of several hundred hours. At a pH lower than 4.8 the rate of decomposition was extremely rapid and could not be studied by the methods used in this work. In fact, at a pH of 4.0 the acidity was high enough for detectable concentrations of H_2S to be observed in the gas phase above the reacted mixture. H_2S formation would be expected from the acid decomposition of thiosulfate, which is a product of the dithionite decomposition reaction. The fact that H^+ also has a large effect on the decomposition of thiosulfate has been carefully studied by La Mer (40). A mechanism given by Davis (41) explains the experimental results of La Mer. His proposed mechanism consists of a series of nucleophilic substitution reactions between protonated anions. Briefly, this mechanism is as follows:

$$S_2O_3^{=} + H^+ \rightleftharpoons HS_2O_3^-$$

$$HS_2O_3^- + S_2O_3^{=} \rightleftharpoons HS_3O_3^- + SO_3^{=} \qquad (10)$$

(etc. until molecule contains 9 sulfur atoms)

$$HS_9O_3^- \rightleftharpoons S_8 + HSO_3^-$$

With increasing acidity, the products of the individual reactions in the above mechanism can produce sulfur having less than eight atoms per molecule, i.e.

$$HS_3O_3^- \overset{H^+}{\rightleftharpoons} S_2 + HSO_3^- \qquad (11)$$

This could possibly explain the various forms of sulfur that probably exist during the decomposition of dithionite.

Similarity of $S_2O_3^=$ and $S_2O_4^=$ Decomposition

It is interesting to note that the rate of S_8 formation during the initial decomposition of thiosulfate was found by LaMer (40) to follow the rate expression:

$$\frac{dS_8}{d\theta} = k[H^+]^{1/2}[S_2O_3^=]^{3/2} \qquad (12)$$

This expression is the same type found for the initial rate of dithionite disappearance with the exception that $S_2O_3^=$ is replaced by $S_2O_4^=$. The fact that addition of thiosulfate has been shown to have no effect on dithionite decomposition in buffered systems excludes the possibility, on mass action principles, that $S_2O_4^=$ is in equilibrium with $S_2O_3^=$, whose decomposition is the rate controlling factor as described by the equation above. Moreover, a dithionite decomposition mechanism parallel to the thiosulfate decomposition mechanism proposed by Davis seems unlikely since no sulfate is found in

the reaction products. One must conclude, therefore, on the basis of information gathered to date, that the similarity in rate expressions is fortuitous.

Mechanism of the Induction Period

In the past, dithionite has been postulated to dissociate into $SO_2^{=} + SO_2$ (6), $SO + SO_3^{=}$ (42), and $SO^{-} + SO_3^{-}$ (39) by various investigators attempting to explain the thermal decomposition and solution reactions of dithionite. There has been no experimental confirmation of any of these dissociation reactions, or of the presence of these intermediates in dithionite solutions, reported to date. Moreover, unsymmetrical dissociation reactions of the types suggested do not lead in a straightforward way to the observed 3/2 order of the reaction with respect to dithionite.

The reality of the symmetrical dissociation of dithionite into SO_2^{-} radical-ions has been confirmed by air oxidation kinetics, EPR spectra, and polarographic studies. The observed sensitivity of the thermal decomposition reaction to changes in hydrogen-ion concentration suggests that protonated forms of the ions SO_2^{-} or $S_2O_4^{=}$ are involved in the rate-determining step. Two alternative mechanisms are suggested for the rate-determining step:

$$HS_2O_4^{-} + SO_2^{-} \longrightarrow HSO_3 + S_2O_3^{=}$$

and (13)

$$S_2O_4^{=} + HSO_2 \longrightarrow HSO_3 + S_2O_3^{=}$$

Either mechanism would be followed by the faster reactions:

$$HSO_3 + HSO_2 \longrightarrow HSO_3^- + SO_2 + H^+ \qquad (14)$$

$$SO_2 + H_2O \longrightarrow HSO_3^- + H^+ \qquad (15)$$

If one makes the assumption that HSO_2 is a much weaker acid than $HS_2O_4^-$, for which Jellinek (4) established an ionization constant of 3.25×10^{-3} at 25°C by conductance measurements, then most of the experimental facts about the decomposition reaction can be explained in terms of either or both the above mechanisms. The observed rate of reaction would be 3/2 order with respect to dithionite concentration. In the pH interval 5 to 6.5 the reaction would appear 1/2 order with respect to hydrogen ion. Below pH 4.5 the rate of reaction would be extremely high, indicating greater than 1/2-order dependence. In neutral or alkaline solutions the rate of decomposition would be extremely low and would appear insensitive to changes in hydrogen ion concentration. The only products of the primary decomposition reaction would be sulfite and thiosulfate, and in the observed stoichiometric ratio. Finally, the acidity of the reaction medium would increase during the reaction because of the ionization of the sulfurous acid formed.

It is impossible, on the basis of established experimental facts, to distinguish between the alternative mechanisms sug-

gested. Unfortunately the positive salt effect reported by Lynn is not sufficiently well documented by facts, and this evidence cannot be used in favor of the first mechanism suggested. Both mechanisms are incomplete to the extent that periodic increases in dithionite concentration with time cannot be explained. Therefore, these mechanisms are offered merely as suggestions.

The Decay Period

The concentration vs time curves shown in Figures 19-21 for the unbuffered systems and in Figures 25a,b for the buffered systems suggest that chain reactions are involved and, in particular, the degenerate branching type. According to theory (37), during the induction period, only a primary chain exists. As the chain progresses, it generates a stable intermediate which later reacts to form new active centers. These centers cause branching of the primary chain; or if it has already disappeared as is often the case, the active centers form new primary chains with branching. It is often difficult to distinguish between degenerate branching chain reactions and autocatalyzed reactions in which the catalyst is formed during the progress of reaction. Although in the case of the degenerate chain reactions the induction period always exists, there may or may not be an induction period in autocatalysis. In both cases, following the induction period, there is usually a rapid decrease in the concentration of the primary reactant resulting in a convex curvature of the

concentration vs time function. Attempts to resolve the problem as to which type of reaction, if either, occurred during the dithionite decomposition were not too successful. Some discussion of the experimental results from the point of view of these theories is presented here.

Sulfur, either as a polymer S_8 or as a colloid $(S_8)_x$ was the only species under conditions of controlled pH, temperature, and initial dithionite concentration, that caused a decrease in the time of the induction period and hence the time of the overall reaction. This effect might be explained by several possible mechanisms:

1. Polymeric sulfur which is formed as a product may combine with one of its predecessor ions to form a reactive complex. After a series of decomposition steps, the sulfur is regenerated. An example of this type of chain-branching intermediate is $S_x \cdot SO_3^{=}$ or $S_x \cdot S_2O_3^{=}$.
2. Colloidal or polymeric sulfur may act autocatalytically as an adsorption catalyst which accelerates the rate-determining step of the thermal decomposition reaction.
3. The several forms of sulfur that might exist in the solution could each have a specific effect on the reaction rate. Thus in the form of a monomer, the sulfur could suppress the equilibrium step in which it is formed, i.e. $HS_2O_3^- \overset{H^+}{\rightleftharpoons} S + HSO_3^-$. Eventually,

the monomer may polymerize to S_8 and then to colloidal sulfur. These higher aggregates can adsorb the monomer sulfur and thus accelerate the overall decomposition autocatalytically.

Conclusions

The thermal decomposition of sodium dithionite solutions in buffered and unbuffered media in the pH range of 4.0 to 7.0 was observed to consist of an induction period in which the decomposition was slow, followed by a decay period, in which the concentration of dithionite rapidly decreased to zero. Apparent periodic increases and decreases in dithionite concentration during the induction period were observed and could not be explained solely on the basis of experimental error. One possible explanation of this unusual phenomenon is the formation of unstable intermediate(s) possessing reducing potentials comparable to dithionite with respect to methylene blue. The amplitude of the apparent oscillations in dithionite concentration decreased with increasing temperature, suggesting that the concentration of the hypothetical reactive intermediate(s) likewise decreased with increasing temperature. Absence of oscillations in solutions of pH greater than 7 suggests that the hypothetical intermediate(s) either are not formed or are unstable in alkaline solution.

During the induction period, the reaction was observed to be 1/2 order with respect to H^+ and 3/2 order with respect to dithionite, giving a rate expression of the following form:

$$r_{induction} = k_c[H^+]^{1/2}[S_2O_4^{=}]^{3/2} \qquad (6)$$

The variation of k_c with temperature gives a straight line on an Arrhenius equation plot. The activation energy ΔE was found to be 12 kcal/mole and the frequency factor A was found to be 1.3×10^8 $(moles/liter)^{-1}sec^{-1}$.

The anions $SO_3^{=}$, HSO_3^{-}, $SO_4^{=}$, and $S_2O_3^{=}$ had no specific effects in the buffered systems. Colloidal sulfur catalyzed the reaction by decreasing the length of the induction period.

The rapid increase in the rate of dithionite decomposition during the decay period followed an exponential relationship with time. This fact together with the catalysis by colloidal sulfur suggests that an autocatalytic or a degenerate branching chain mechanism is occurring.

REFERENCES

1. Schonbein, J. prakt. Chem., 61, 193 (1852).
2. Schutzenberger, P., Compt. Rend., 69, 196 (1869).
3. Jellinek, K., Zeit. Anorg. Chem., 70, 93 (1911).
4. Jellinek, K., Zeit. physik. Chem., 76, 257 (1911).
5. Meyer, J., Zeit. Anorg. Chem., 34, 43 (1903).
6. Bassett, H., and Durrant, R. G., J. Chem. Soc., 2, 1401 (1927).
7. Nicloux, M., Compt. Rend., 196, 616 (1933).
8. Lynn, S., Ph.D. Thesis, Calif. Inst. (1954).
9. Welcher, F. J., "Organic Analytical Reagents," D. Van Nostrand Co., New York (1948).
10. Kolthoff, I. M., and Cohn, G., J. Biol. Chem., 148, 711 (1943).
11. Rosin, J., "Reagent Chemicals," D. Van Nostrand, New York (1937).
12. Fritz, J. S., and Freland, M. Q., Anal. Chem., 26, 1593 (1954).
13. Swift, E., "Systematic Quantitative Analysis," Prentice-Hall, New York (1939).
14. Lange, N. A., "Handbook of Chemistry," 7th ed., Handbook Publishers, Inc., Sandusky, Ohio (1949).
15. Alyea, H. N., and Backstrom, H. L. J., J. Am. Chem. Soc., 51, 90 (1929).
16. Yost, D. M., and Russell, H., "Systematic Inorganic Chemistry," Prentice-Hall, Inc., New York (1944).
17. Rao, M. R. A., and Patel, C. C., Proc. Nat. Inst. Sc. India, 19, 211 (1953).
18. Uri, N., Chem. Revs., 50, 375 (1952).
19. Frost, A. A., and Pearson, R. G., "Kinetics and Mechanism," Wiley, New York (1953).

20. Klemm, L., Zeit. Anorg. Chem., 231, 136 (1937).

21. Van der Heijde, H. B., Rec. Trav. Chim. Pays-Bas, 72, 95 (1953).

22. Dunitz, J. D., Acta Chryst., 9, 579 (1956).

23. Pauling, L., J. Am. Chem. Soc., 69, 542 (1947).

24. Hodgson, W. G., Neaves, A., and Parker, C. A., Nature, 178, 489 (1956).

25. Yarmolinsky, M. B., and Colowick, S. P., Biochim. Biophys. Acta, 20, 177 (1956).

26. Karrer, P., and Benz, F., Helv. Chem. Acta, 19, 1028 (1936).

27. Schlenk, F., Hellström, H., and von Euler, H., Ber. 71, 1471 (1938).

28. Kosower, E. M., personal communication.

29. Jellinek, K., Zeit. Elektrochem., 17, 157 (1911).

30. Jellinek, K., Zeit. Elektrochem., 17, 245 (1911).

31. Gossman, B., Coll. Czech. Chem. Commun., 2, 185 (1930).

32. Kolthoff, I. M., and Miller, C. S., J. Am. Chem. Soc., 63, 2818 (1941).

33. Munemori, M., Talenta, 1, 110 (1958).

34. Cermak, V., Chemicke Zvesti, 8, 714 (1954).

35. Cermak, V., Coll. Czech. Chem. Commun, 23, 1471 (1958).

36. Jellinek, K., and Jellinek, E., Zeit. physik Chem., 93, 325 (1919).

37. Semenoff, N., "Chemical Kinetics and Chain Reactions," Oxford Clarendon Press (1935).

38. Haber, and Franck, Naturw., 19, 450 (1931).

39. Fujinawa, K., J. of Ind. Chem., Japan, 54, 160 (1951).

40. Dinegar, R. H., Smellie, R. H., and La Mer, V. K., J. Am. Chem. Soc., 73, 2050 (1951).

41. Davis, R. E., J. Am. Chem. Soc., 80, 3565 (1958).

42. Von Deines, O., and Elstner, G., Zeit. Anorg. Allgem. Chem., 191, 340 (1930).

LIST OF FIGURES

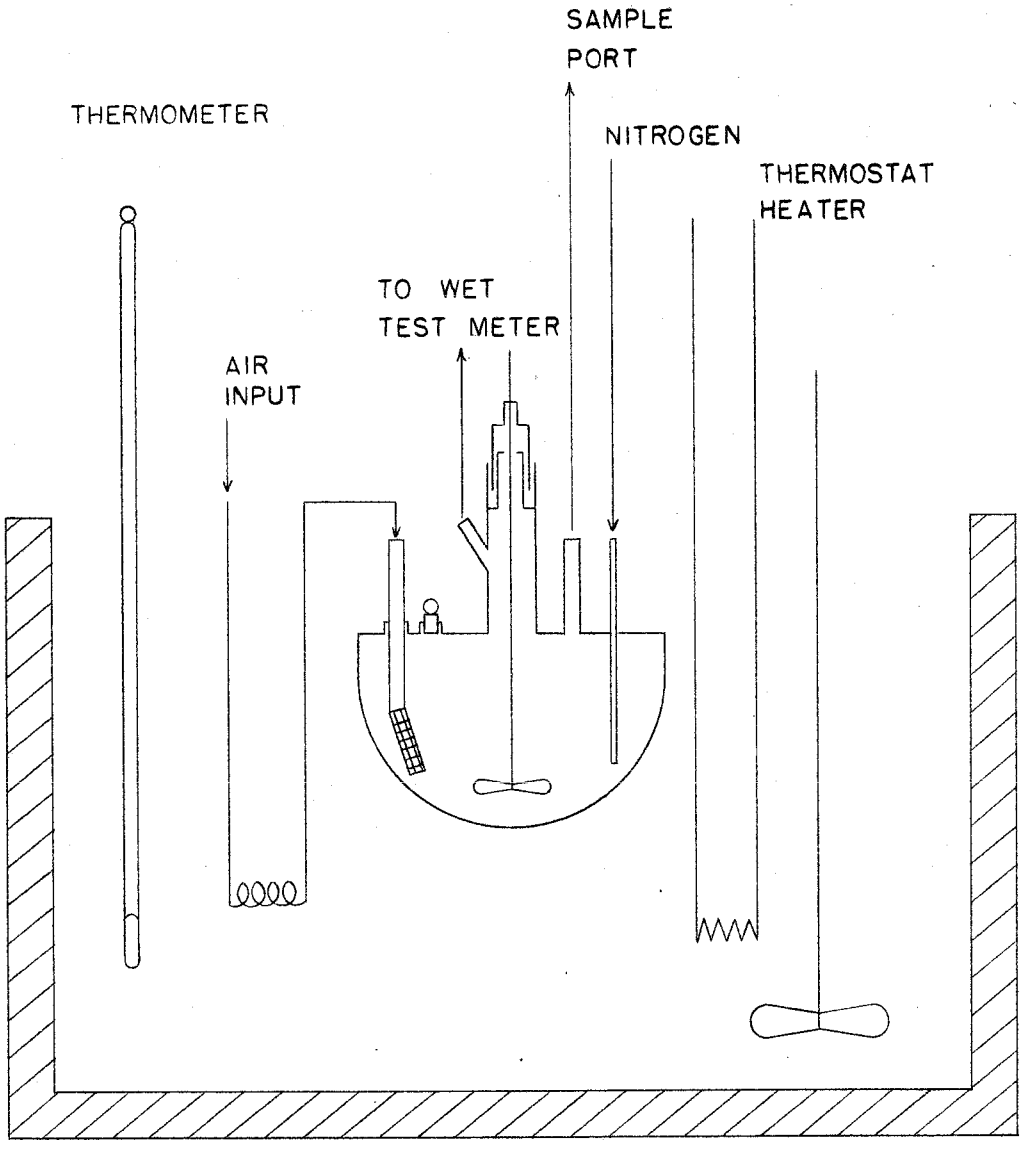

Figure 1--Diagram of Apparatus

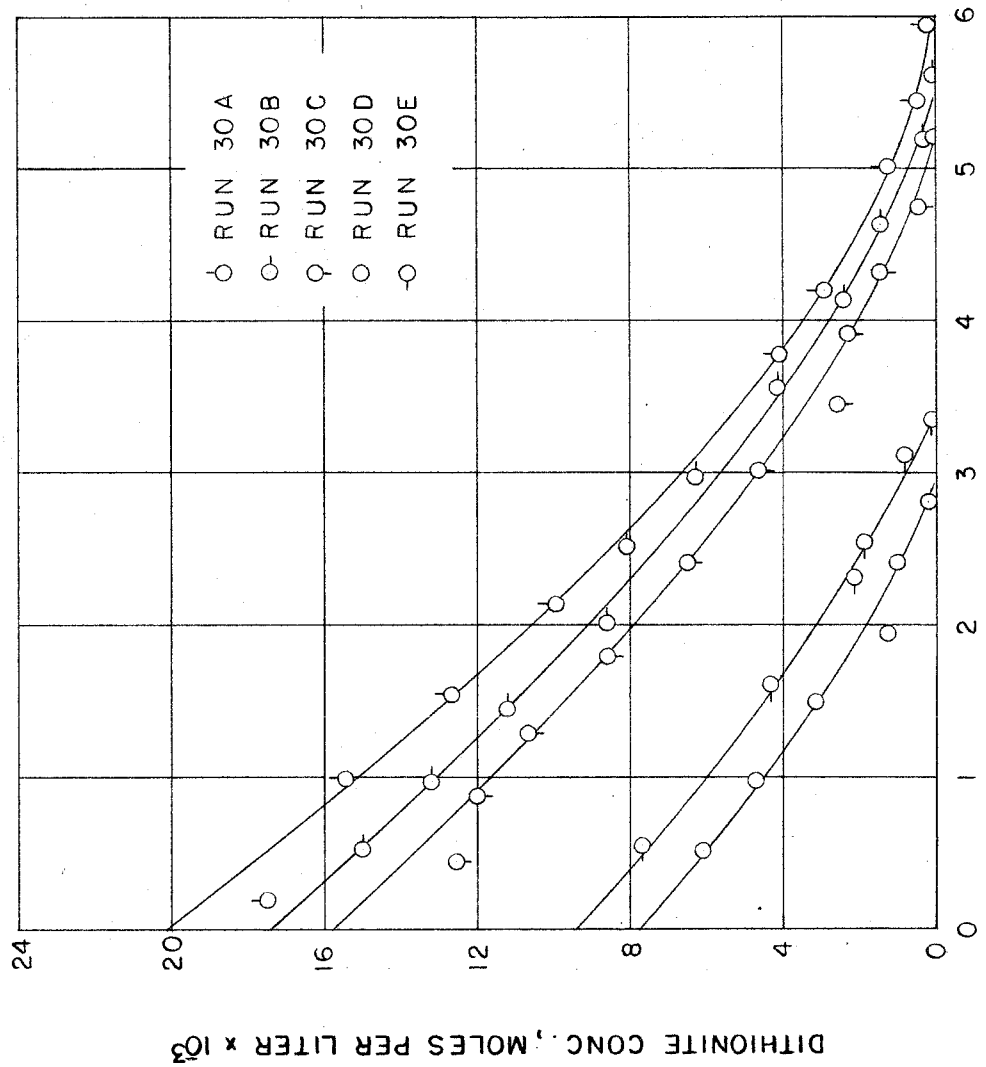

Figure 2--Air Oxidation Studies. Dithionite Concentration vs Time at 30°C

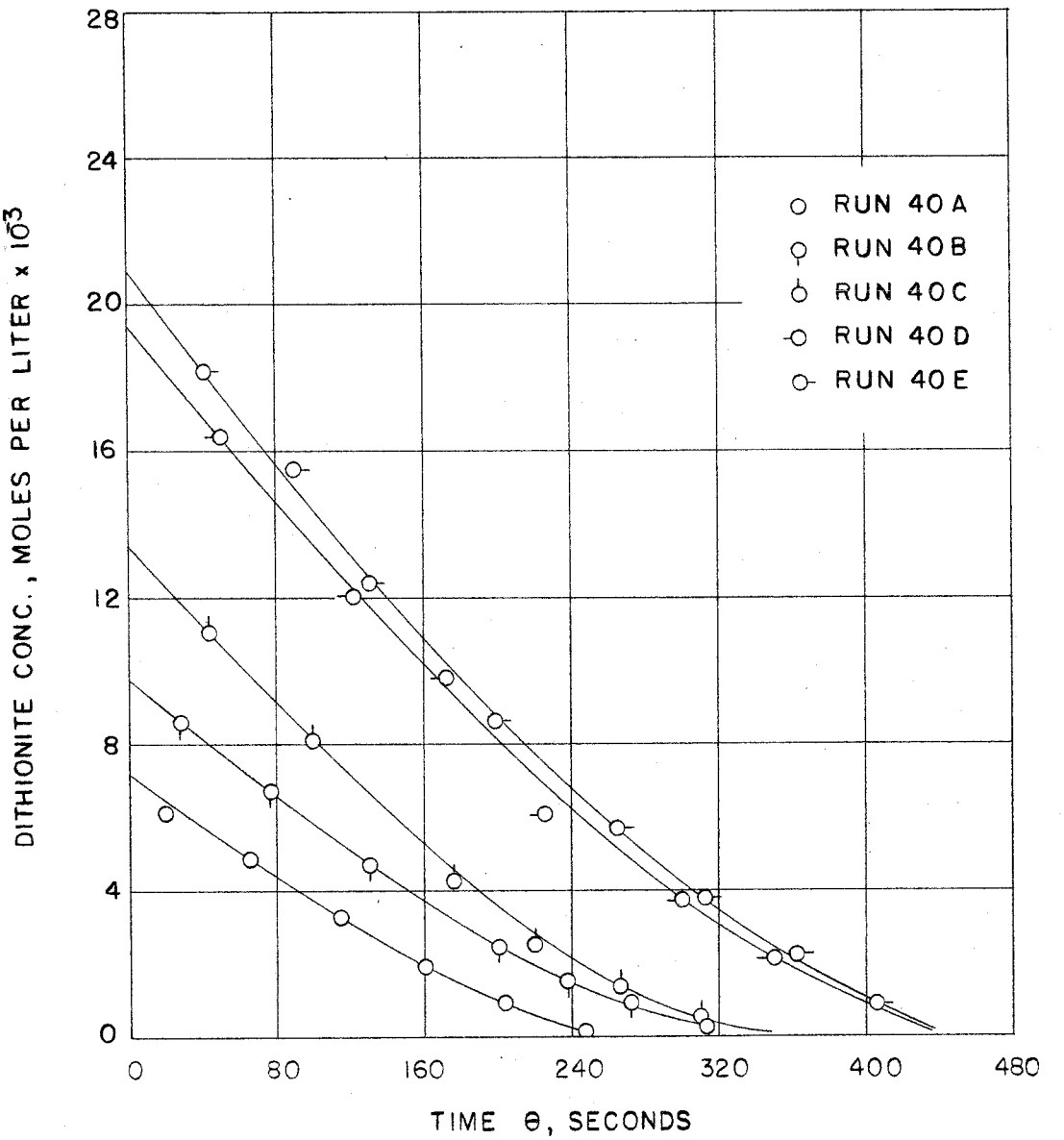

Figure 3--Air Oxidation Studies. Dithionite Concentration vs Time at 40°C

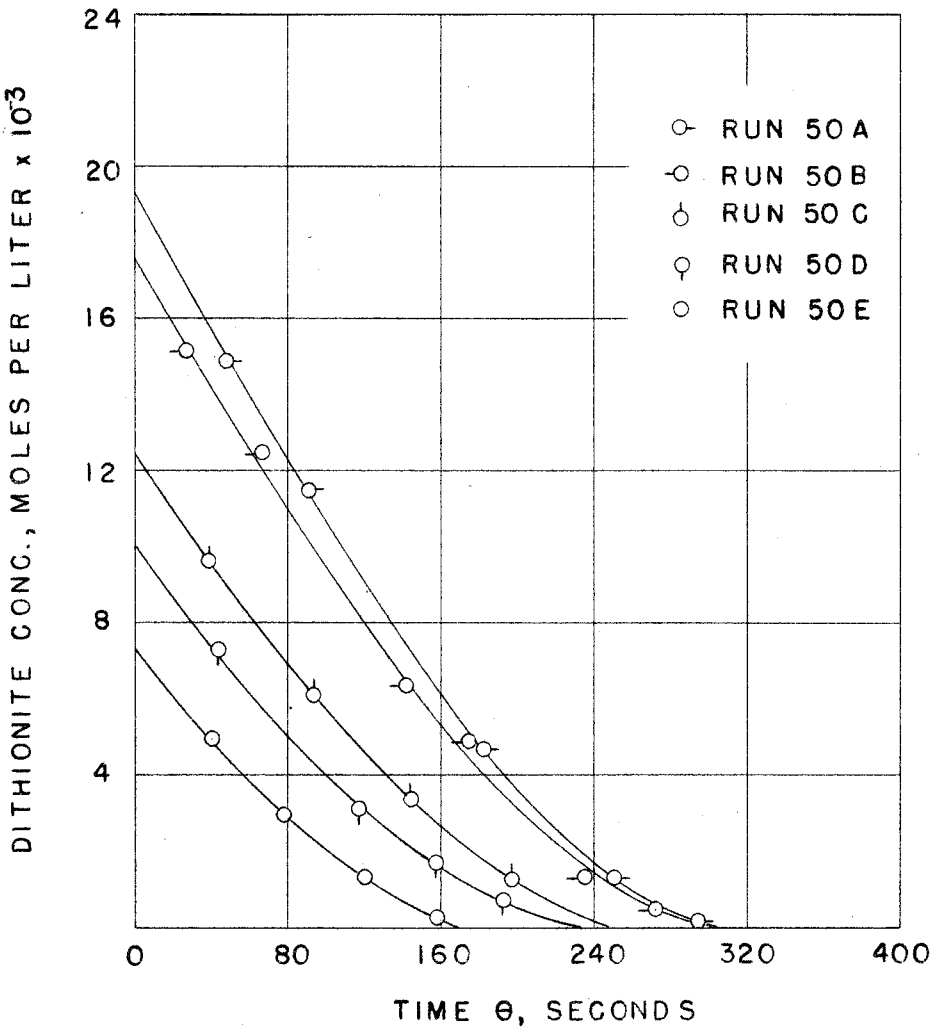

Figure 4--Air Oxidation Studies. Dithionite Concentration vs Time at 50°C

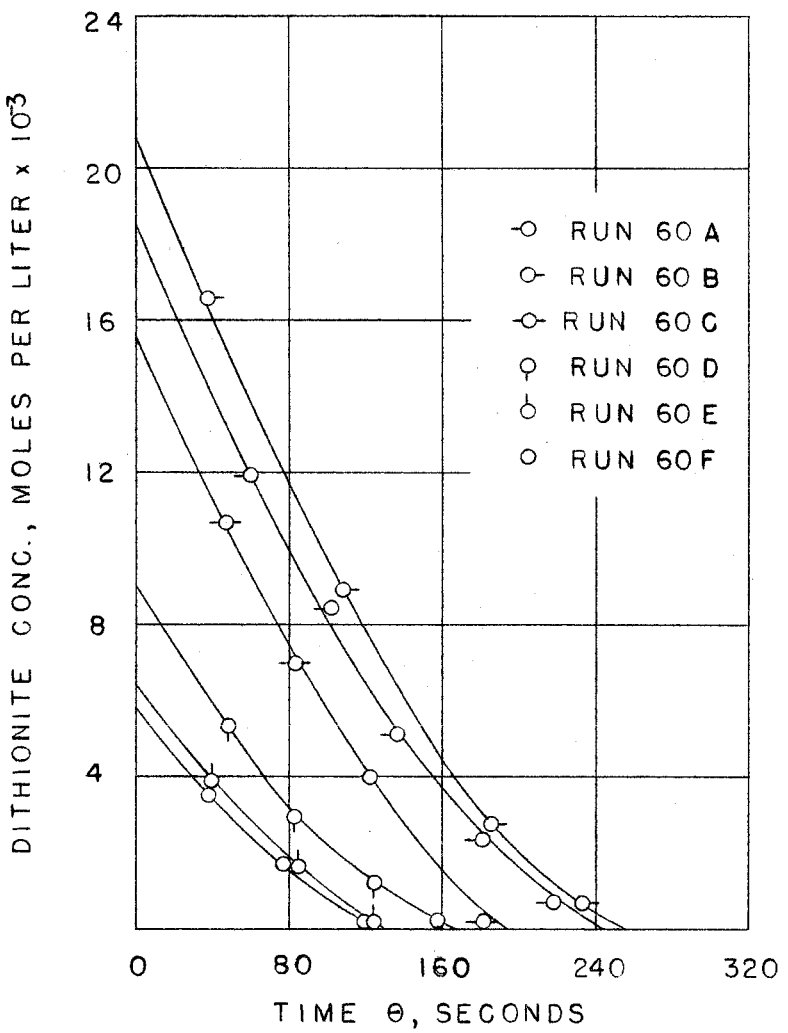

Figure 5--Air Oxidation Studies. Dithionite Concentration vs Time at 60°C

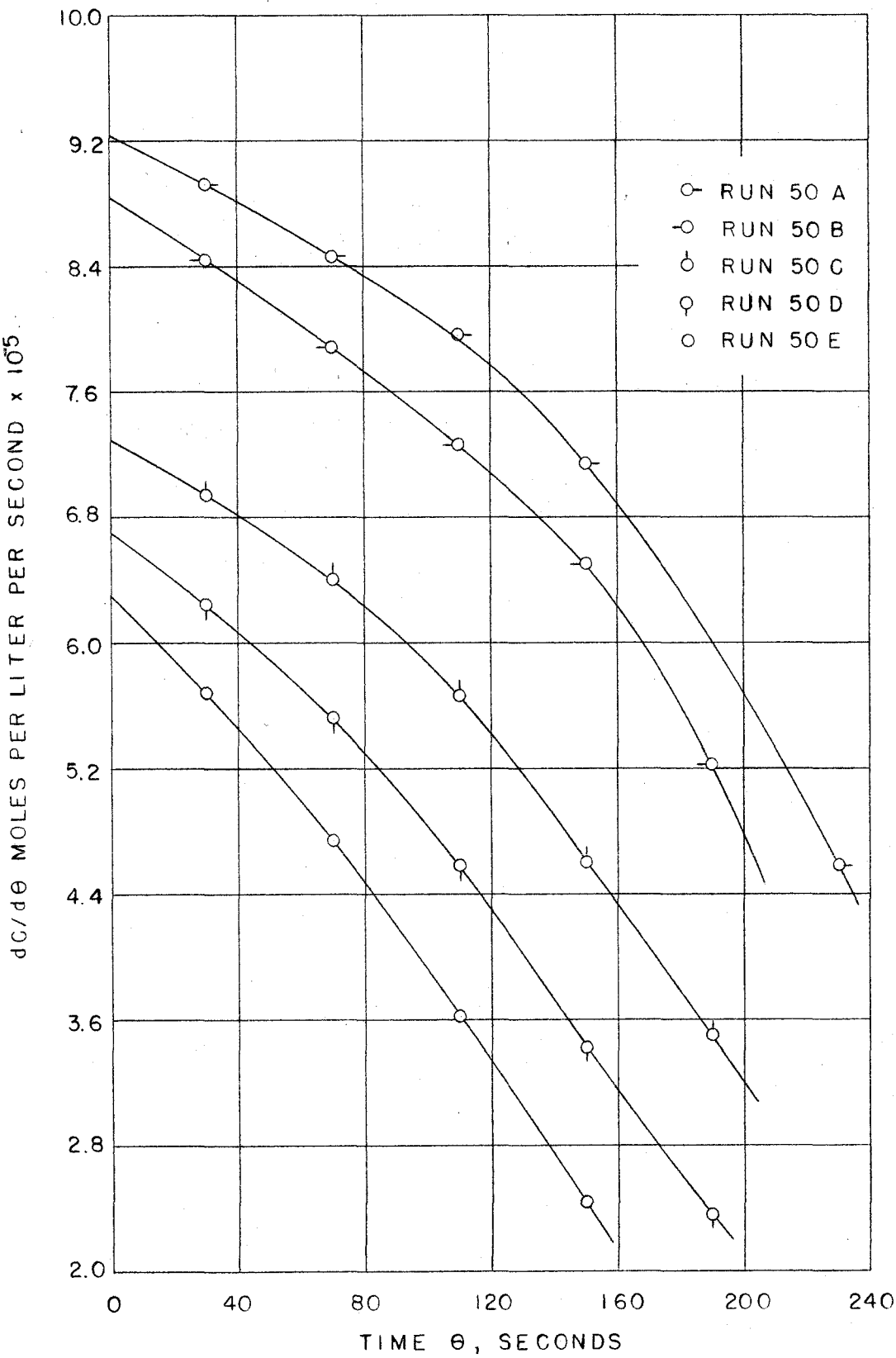

Figure 6--Air Oxidation Studies. Determination of Initial Rates. (dC/dθ) vs Time at 50°C

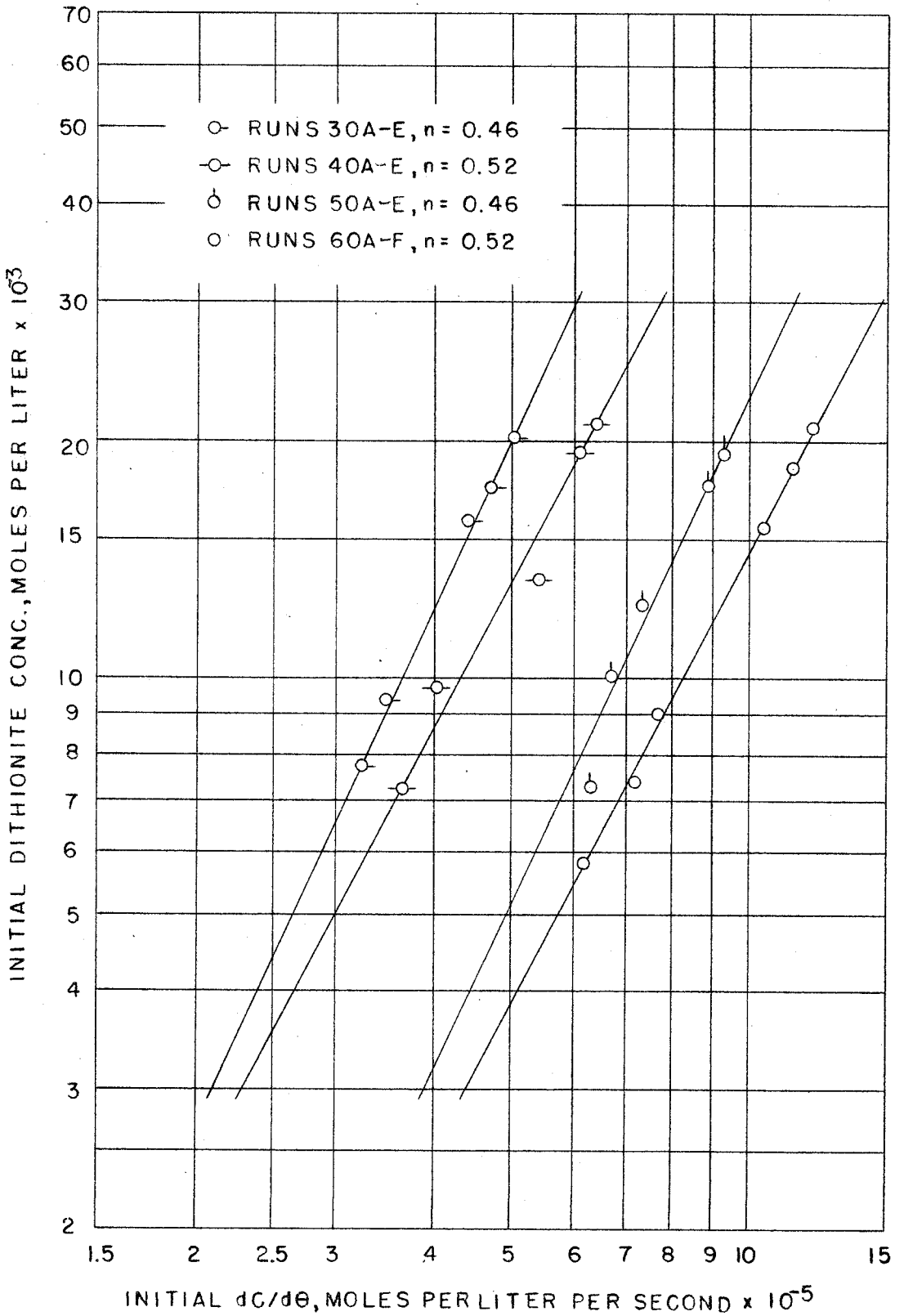

Figure 7--Air Oxidation Studies. Determination of n. Log $(dC/d\theta)_o$ vs Log C_o at 30, 40, 50, and 60°C

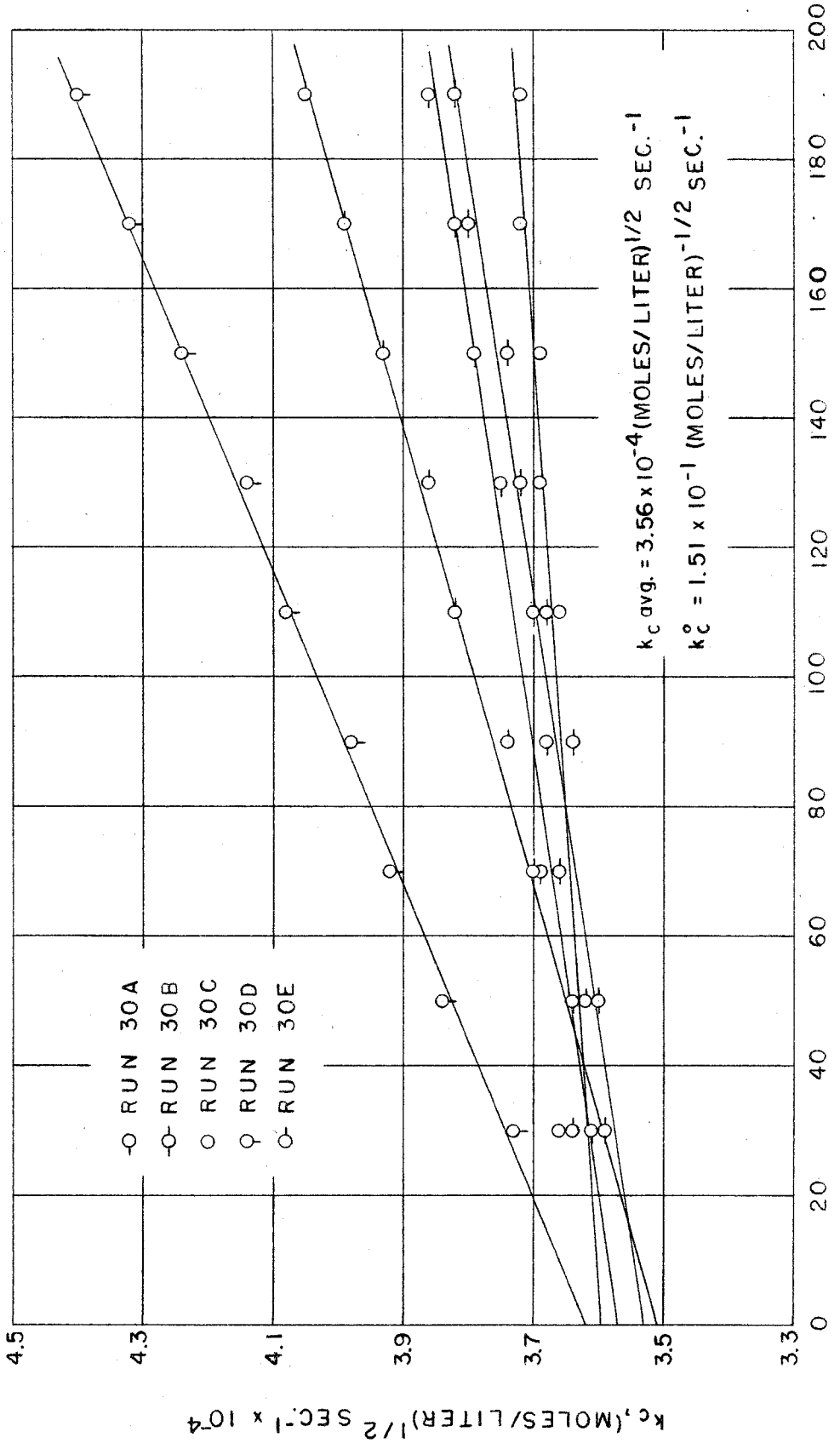

Figure 8--Air Oxidation Studies. Determination of k_c^o. k_c vs Time at 30°C

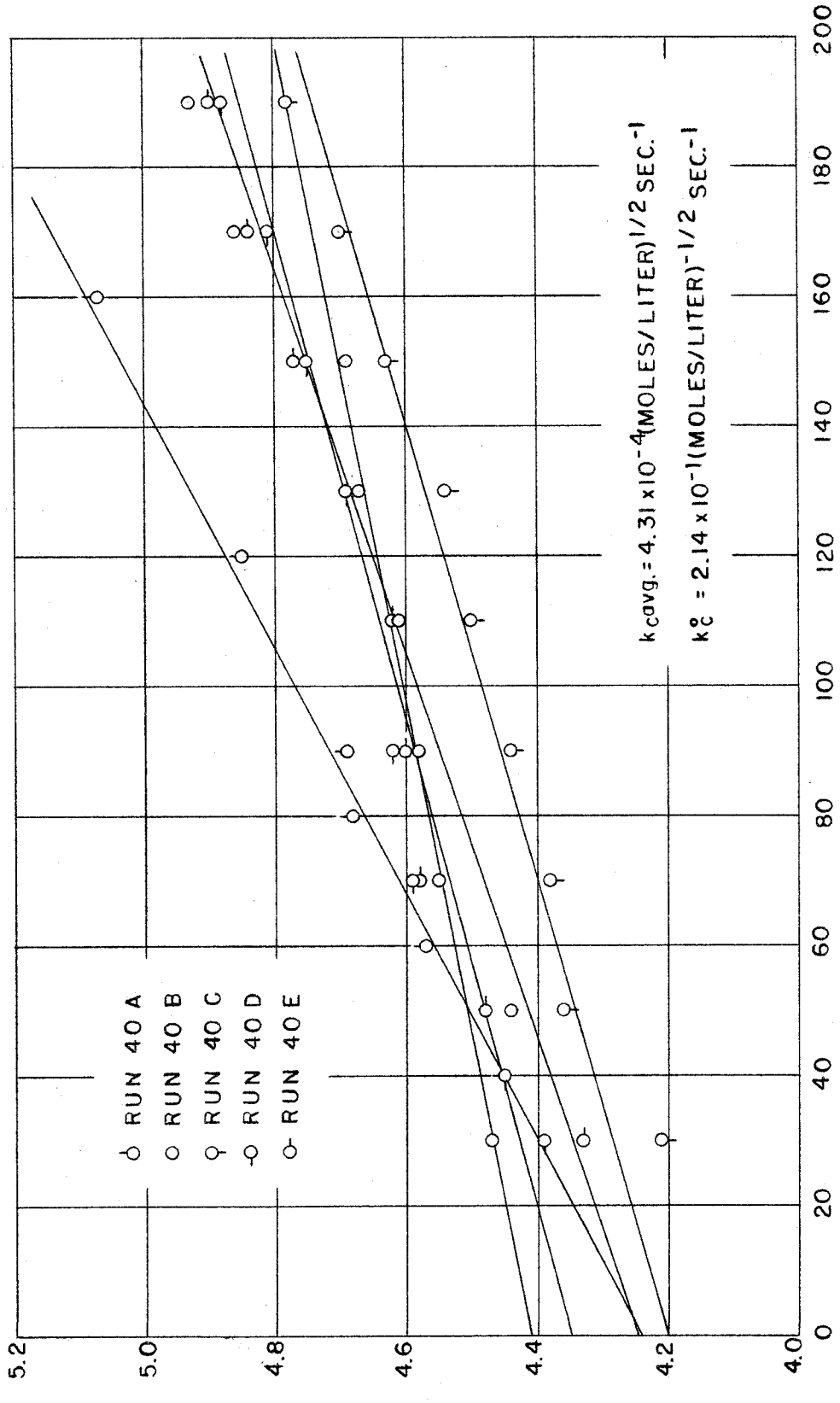

Figure 9--Air Oxidation Studies. Determination of k_c^o. k_c vs Time at 40°C

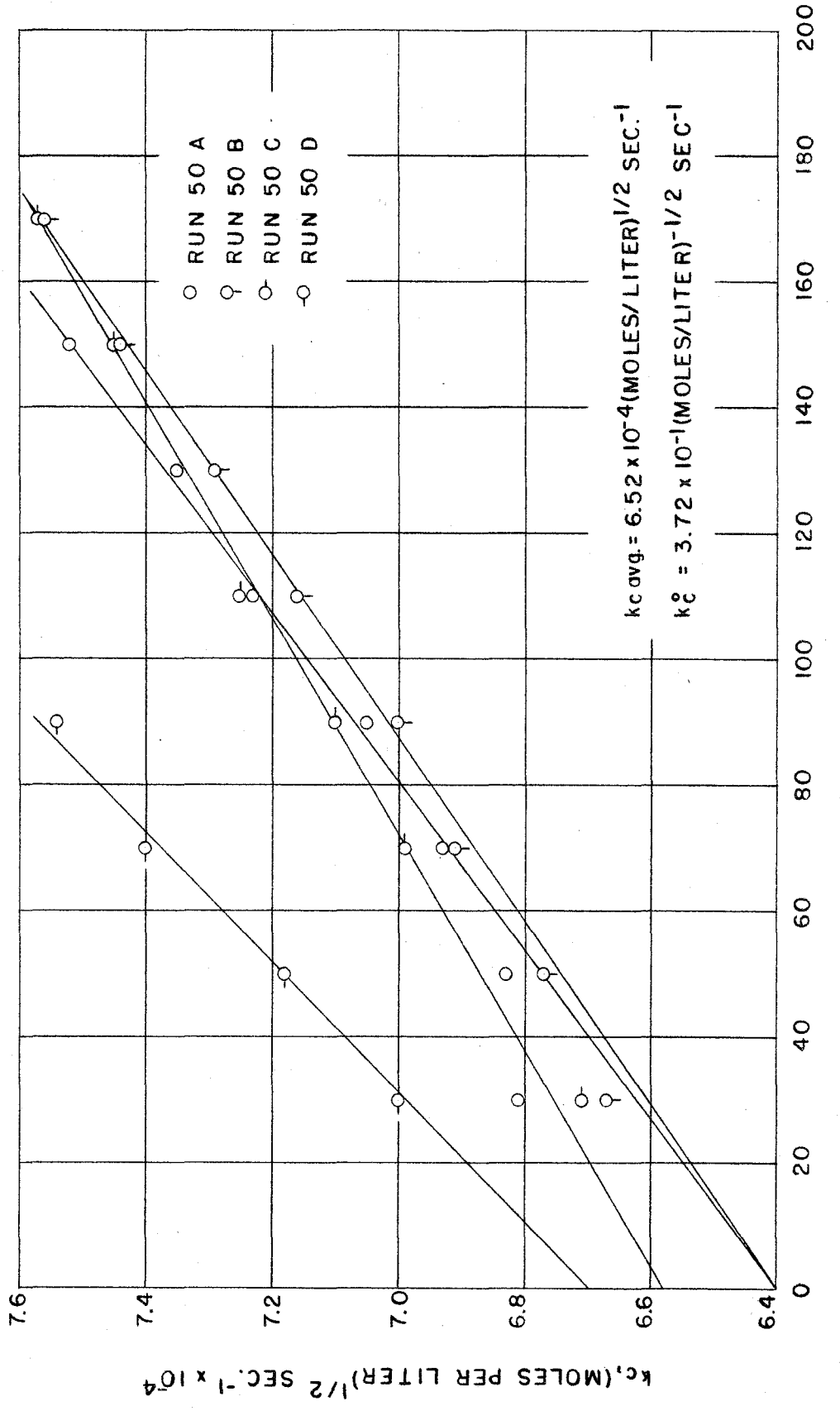

Figure 10--Air Oxidation Studies. Determination of k_c^o. k_c vs Time at 50°C

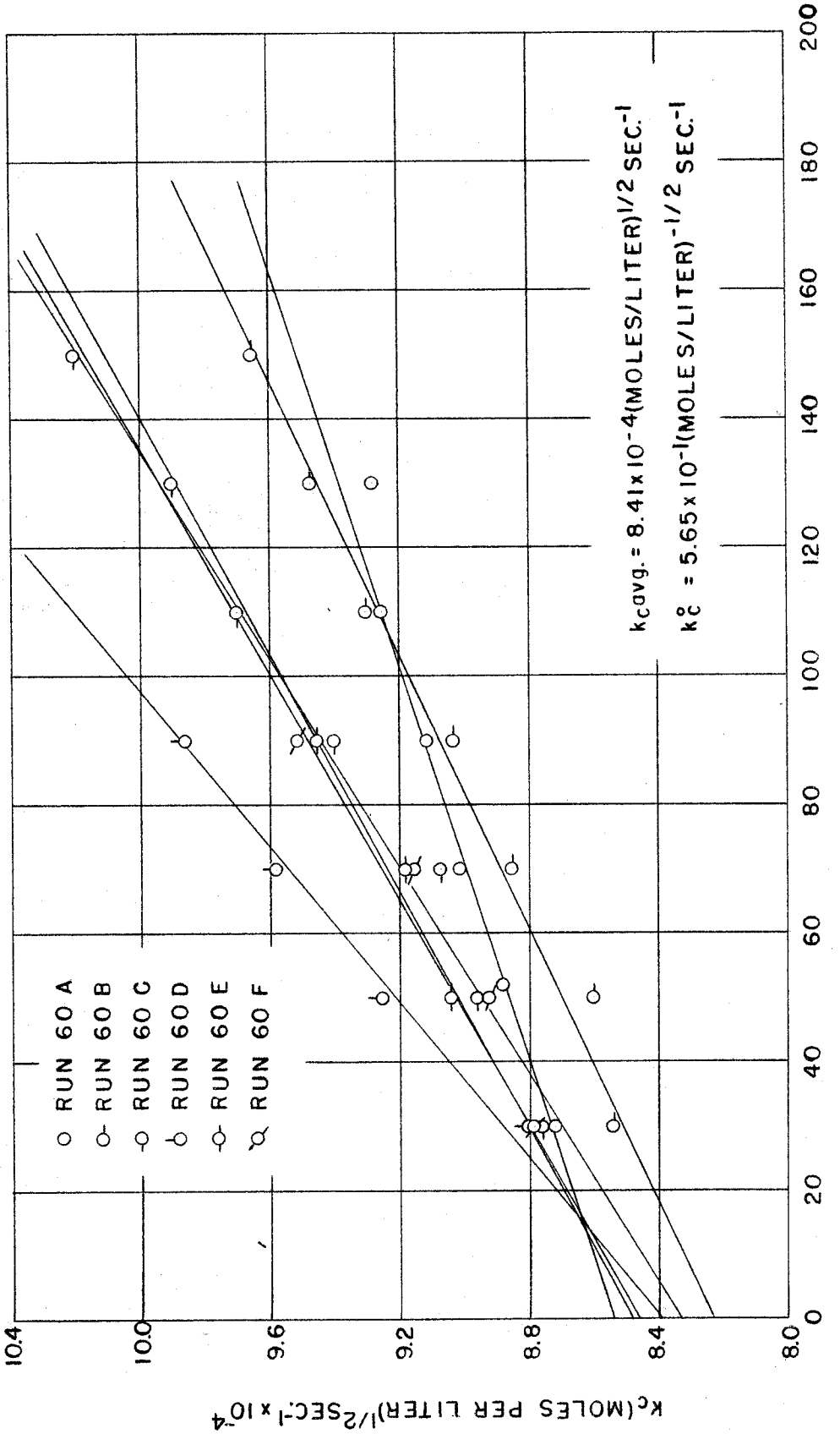

Figure 11--Air Oxidation Studies. Determination of k_c^o. k_c vs Time at 60°C

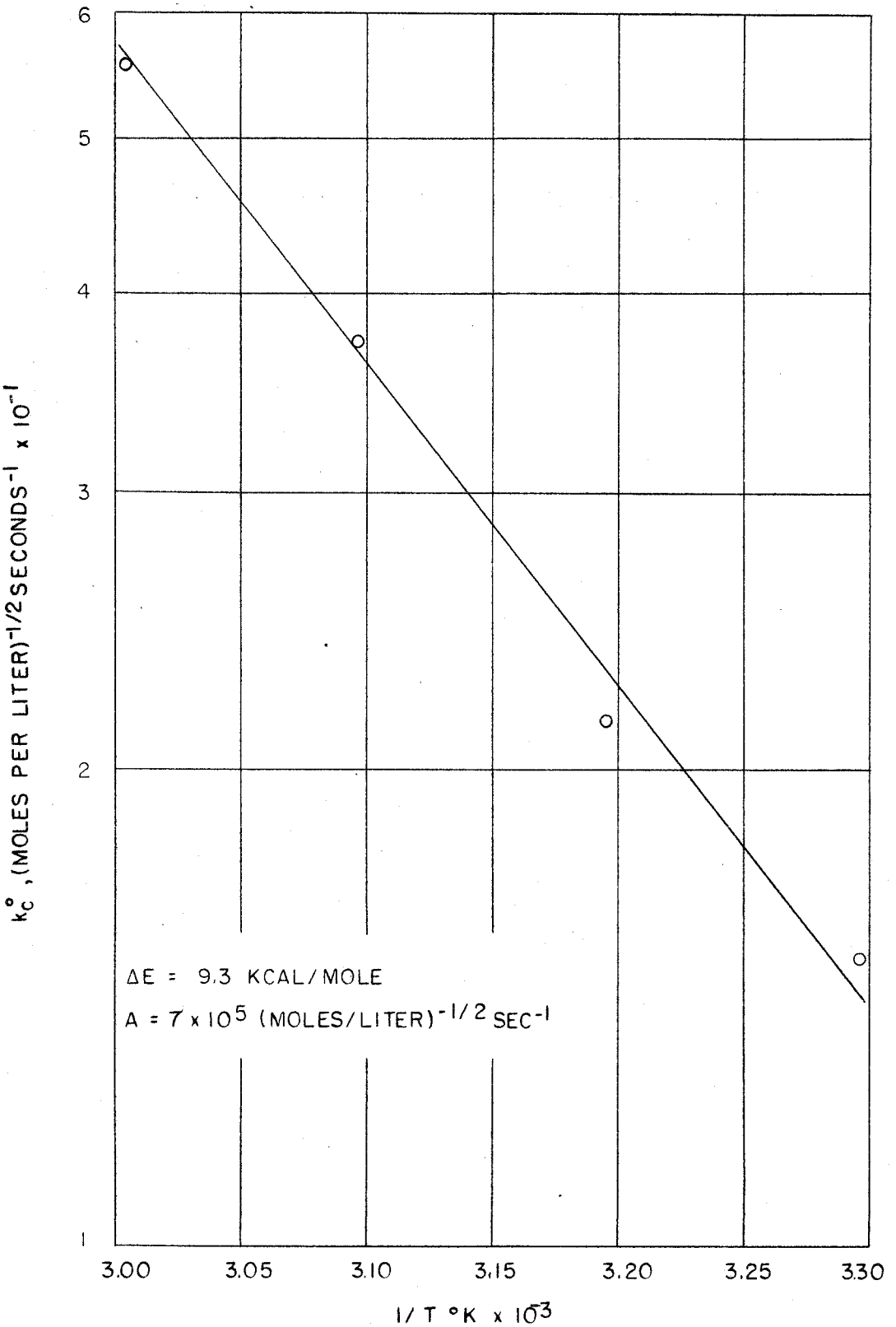

Figure 12--Air Oxidation Studies. Arrhenius plot.
Log k_c° vs 1/T°K

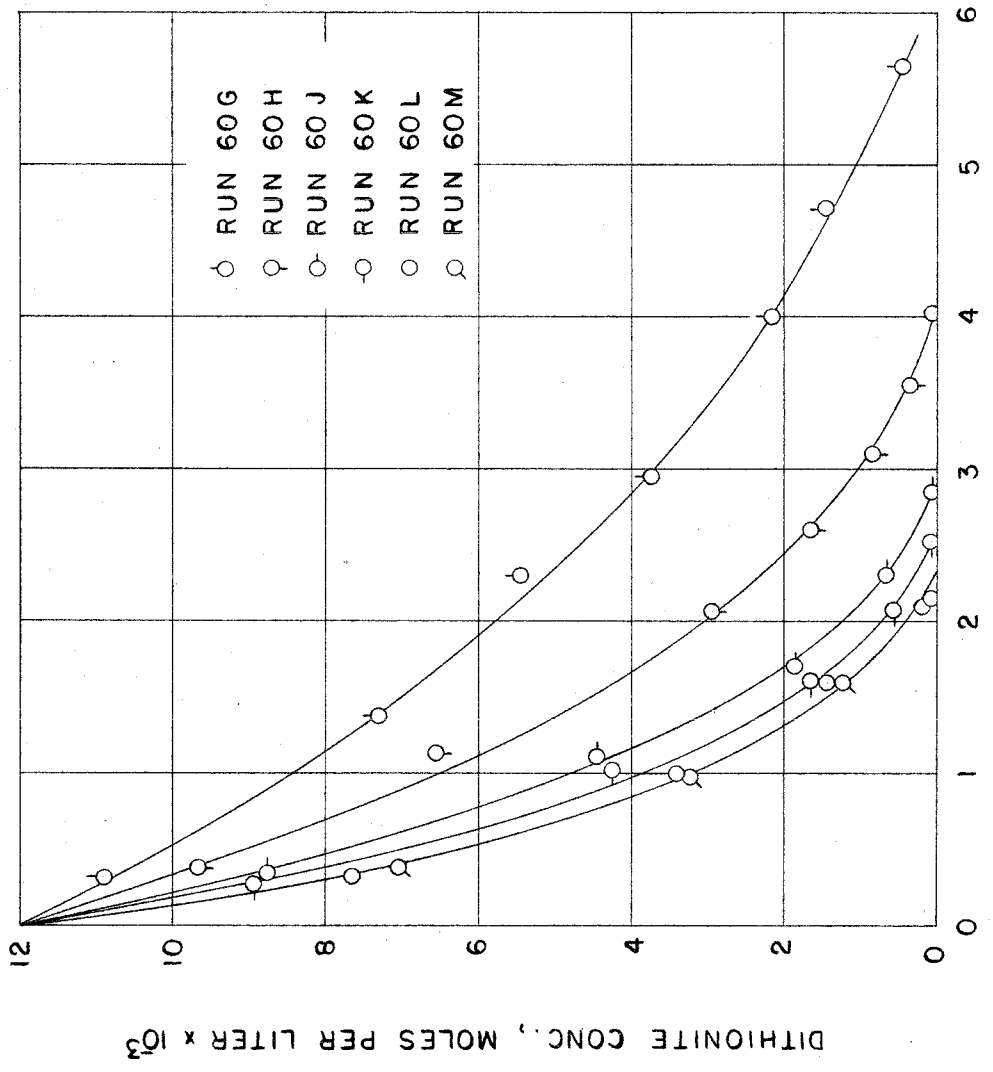

Figure 13--Air Oxidation Studies. Effects of Stirring Rate and Air Flow. Dithionite Concentration vs Time

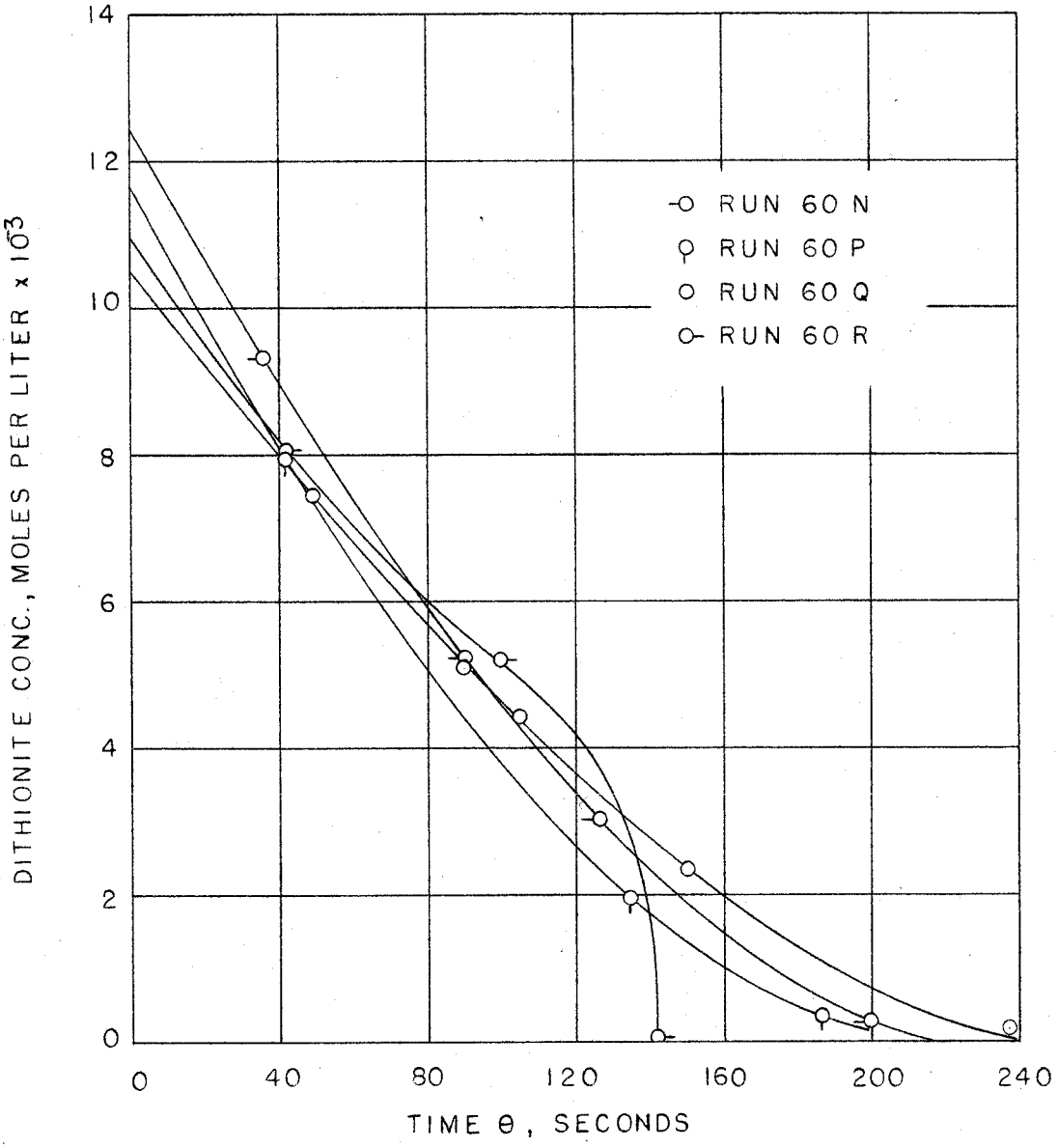

Figure 14--Air Oxidation Studies. Effects of Ionic Strength. Dithionite Concentration vs Time

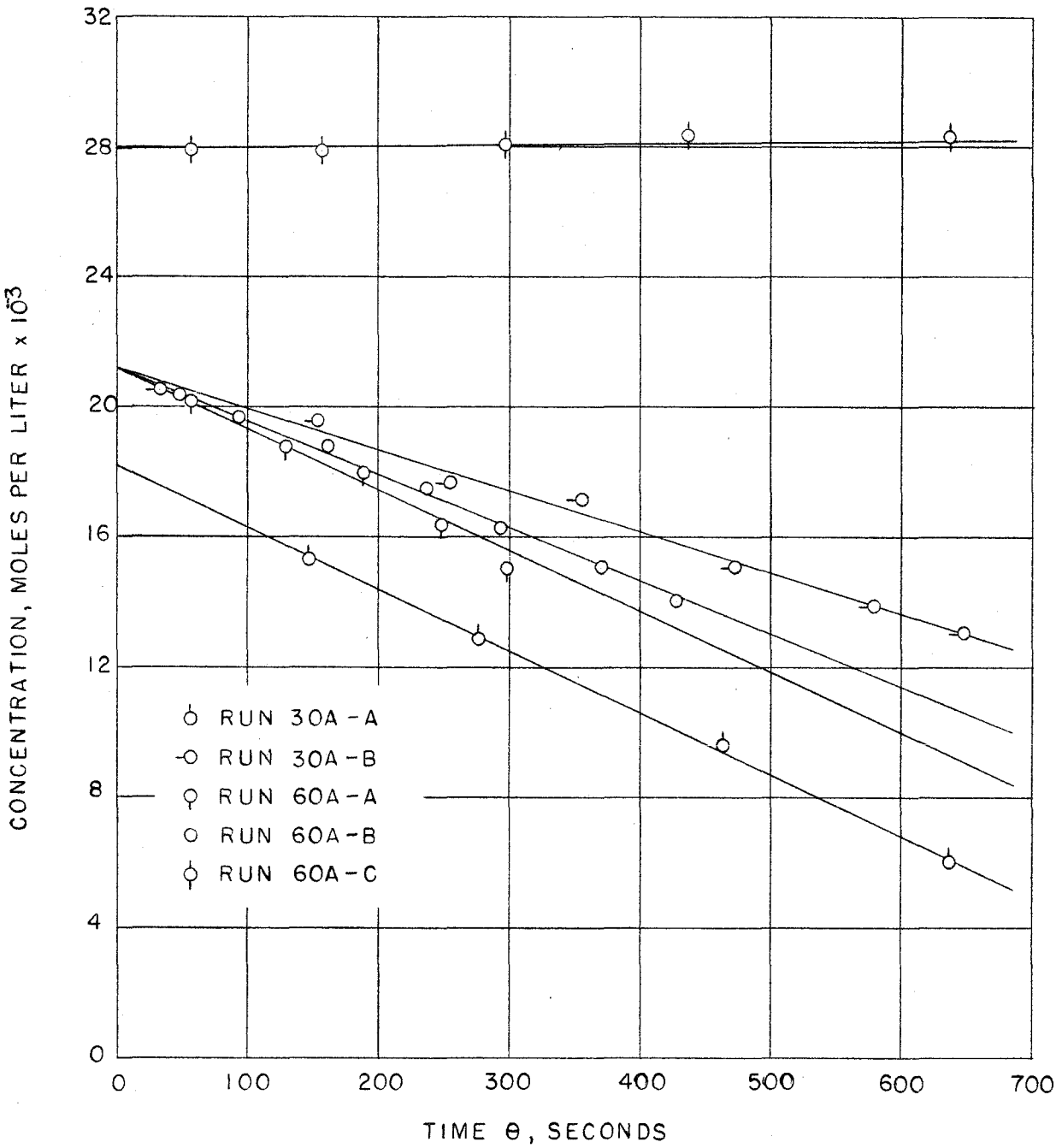

Figure 15--Air Oxidation Studies. Sulfite and Thiosulfate Concentration vs Time

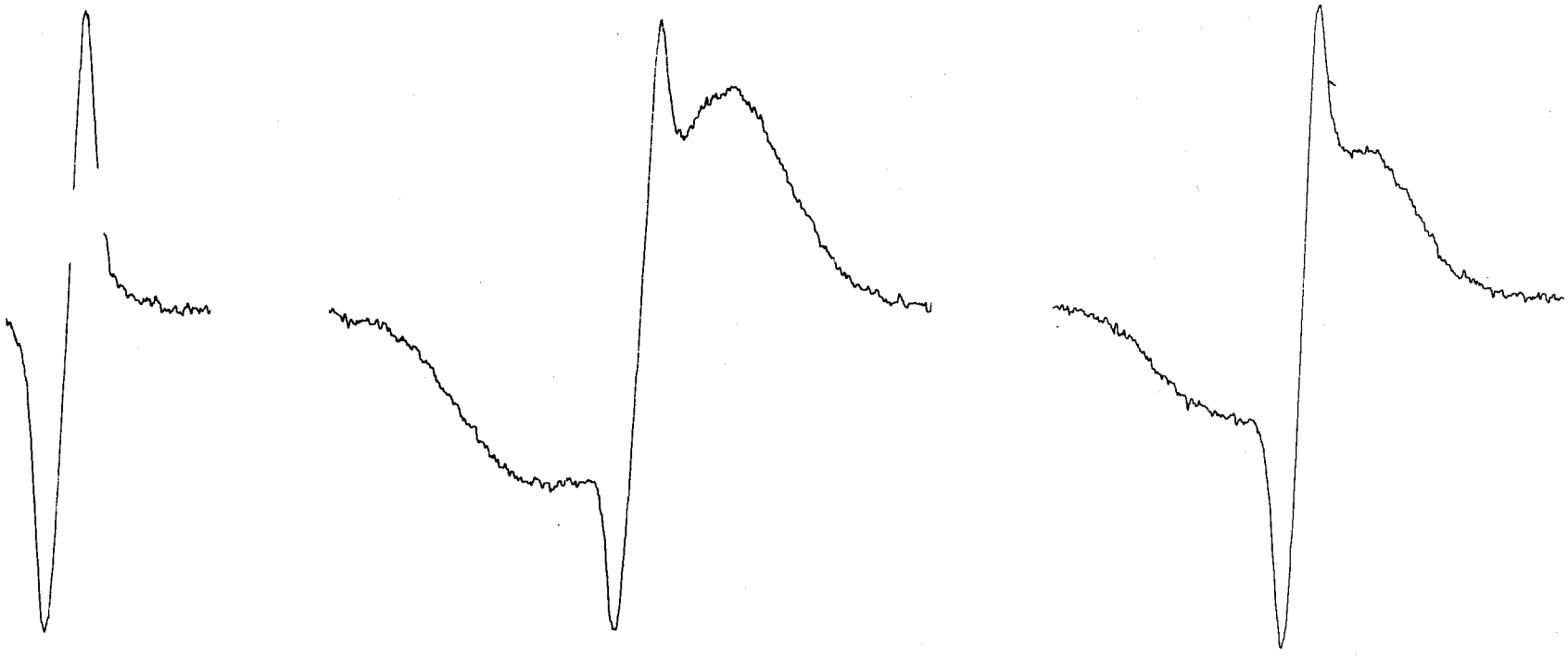

A - EPR of Aqueous Dithionite

B - EPR of Acidified Sulfoxylate and Solid Dithionite

C - EPR of Aqueous Dithionite and Solid Dithionite

Figure 16--Dithionite Structure Studies.

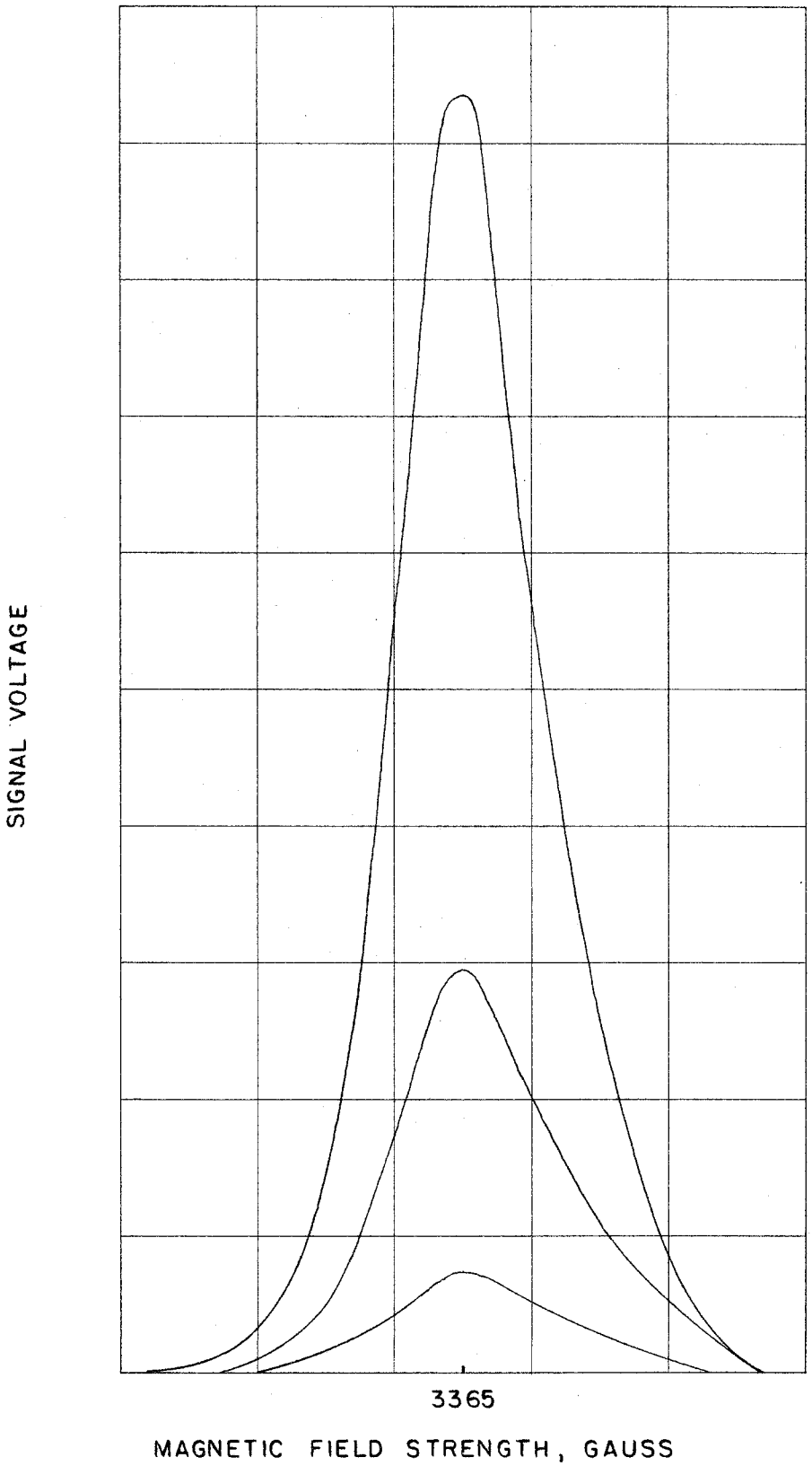

Figure 17--Dithionite Structure Studies. EPR Absorption Peaks for Diluted Dithionite Solutions

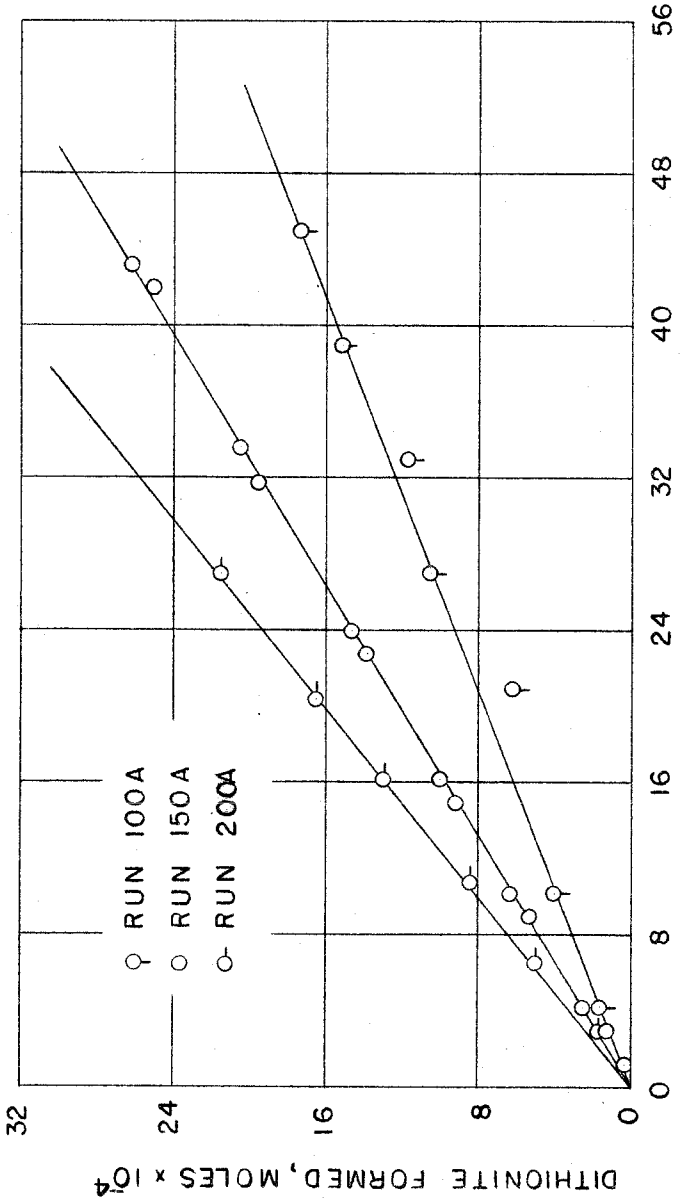

Figure 18--Electrolytic Studies. Electrolytic Generation of Dithionite. Dithionite Formed vs Time at 100, 150, and 200 ma

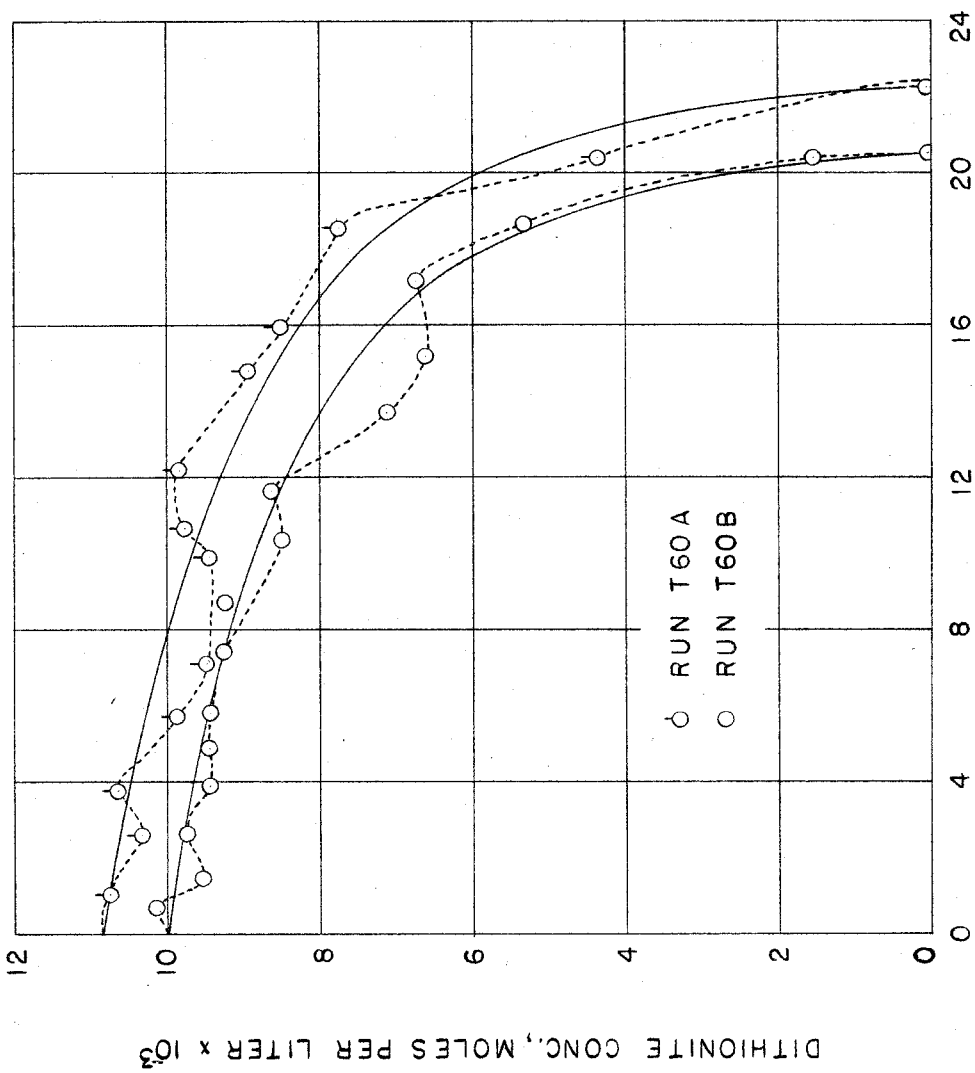

Figure 19a--Thermal Decomposition Studies. Dithionite Concentration vs Time at 60°C

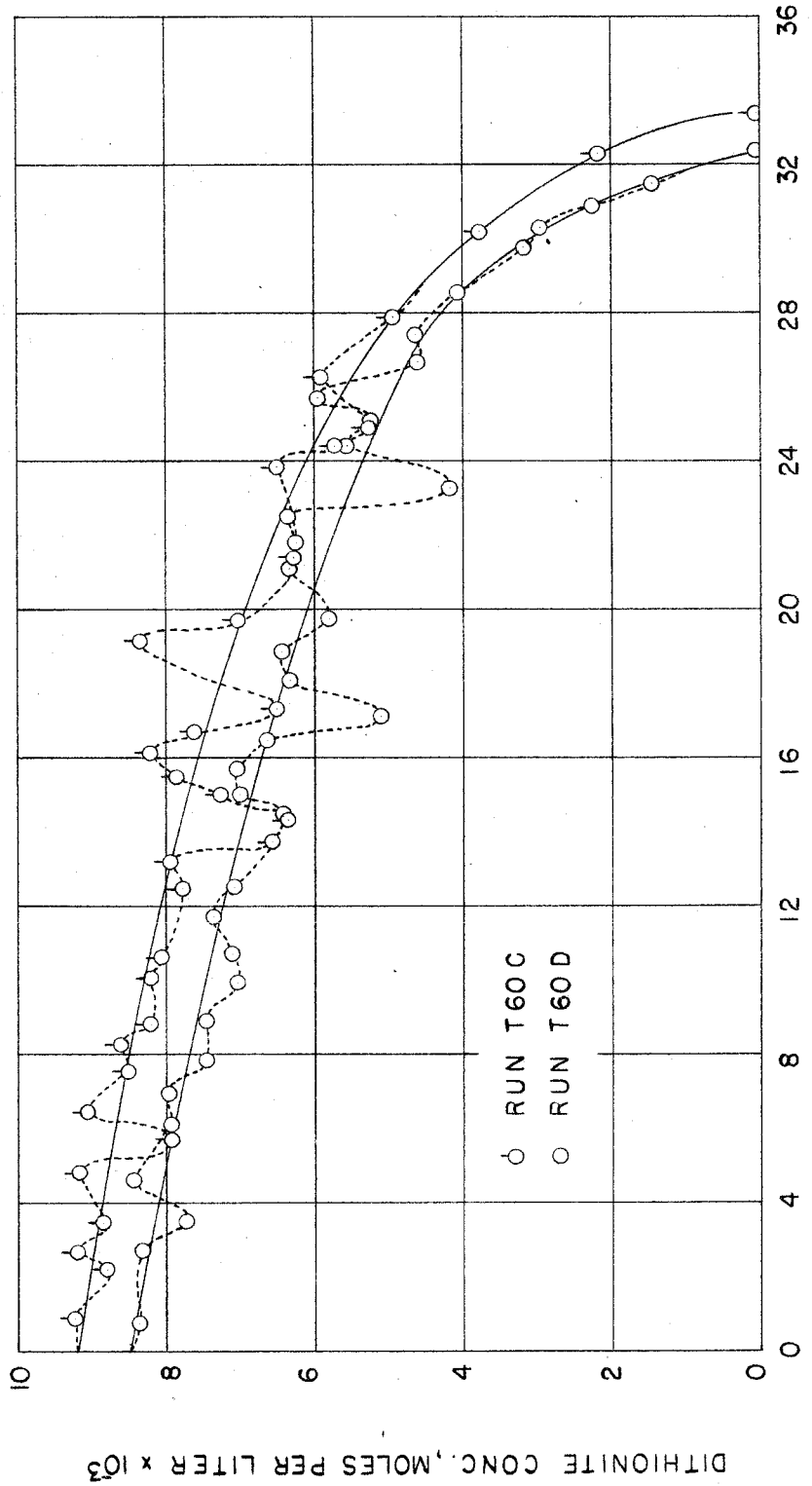

Figure 19b--Thermal Decomposition Studies. Dithionite Concentration vs Time at 60°C

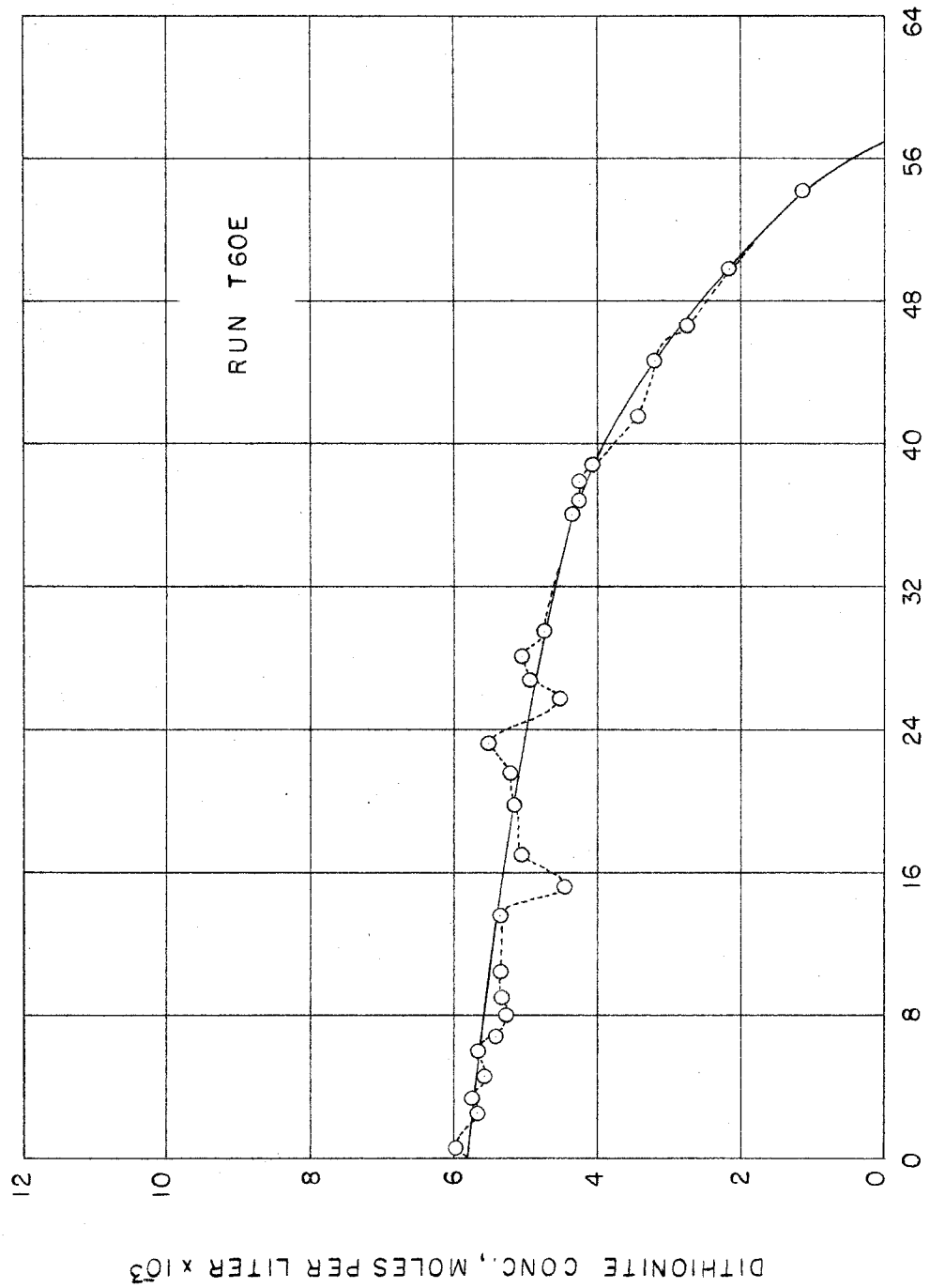

Figure 19c--Thermal Decomposition Studies. Dithionite Concentration vs Time at 60°C

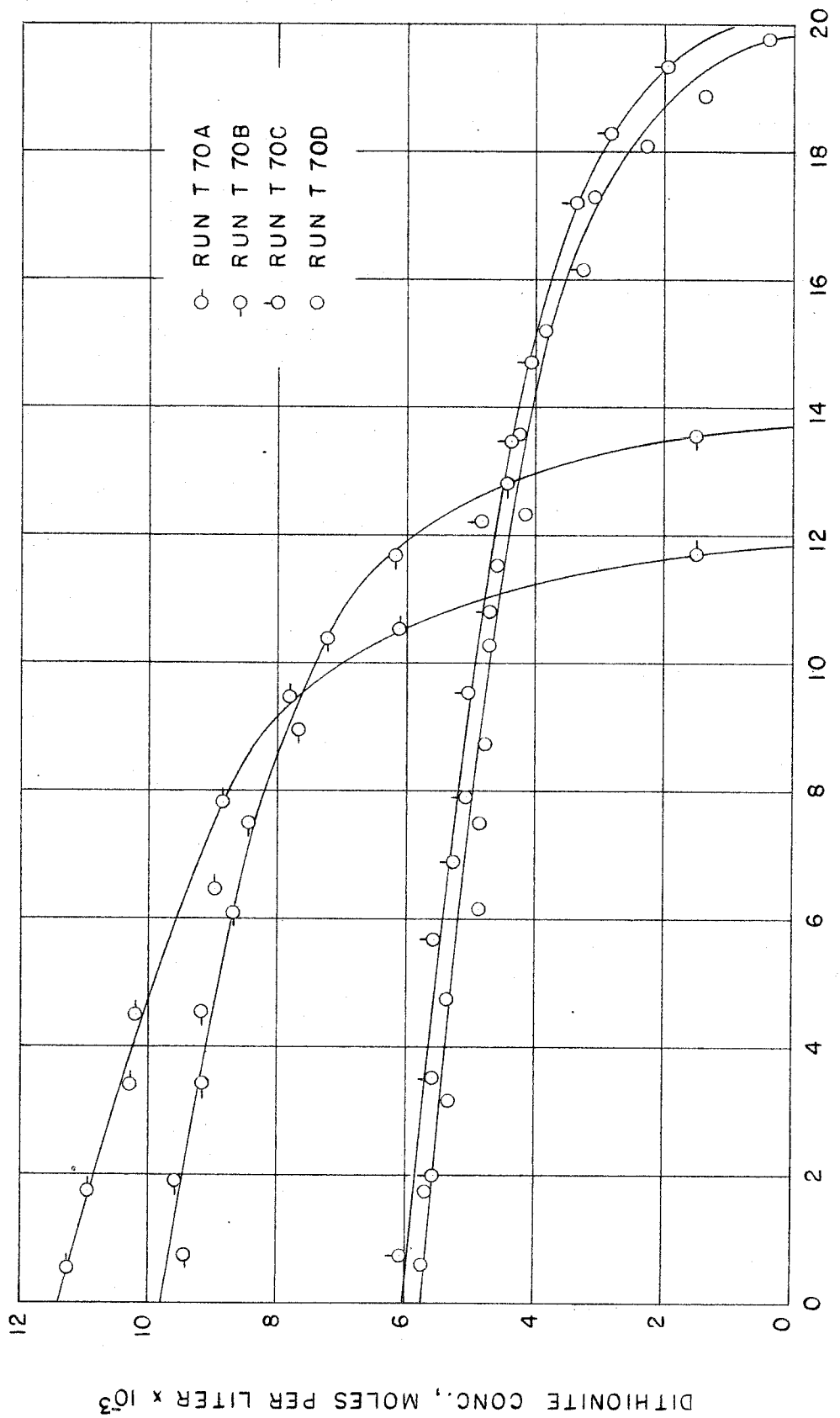

Figure 20--Thermal Decomposition Studies. Dithionite Concentration vs Time at 70°C

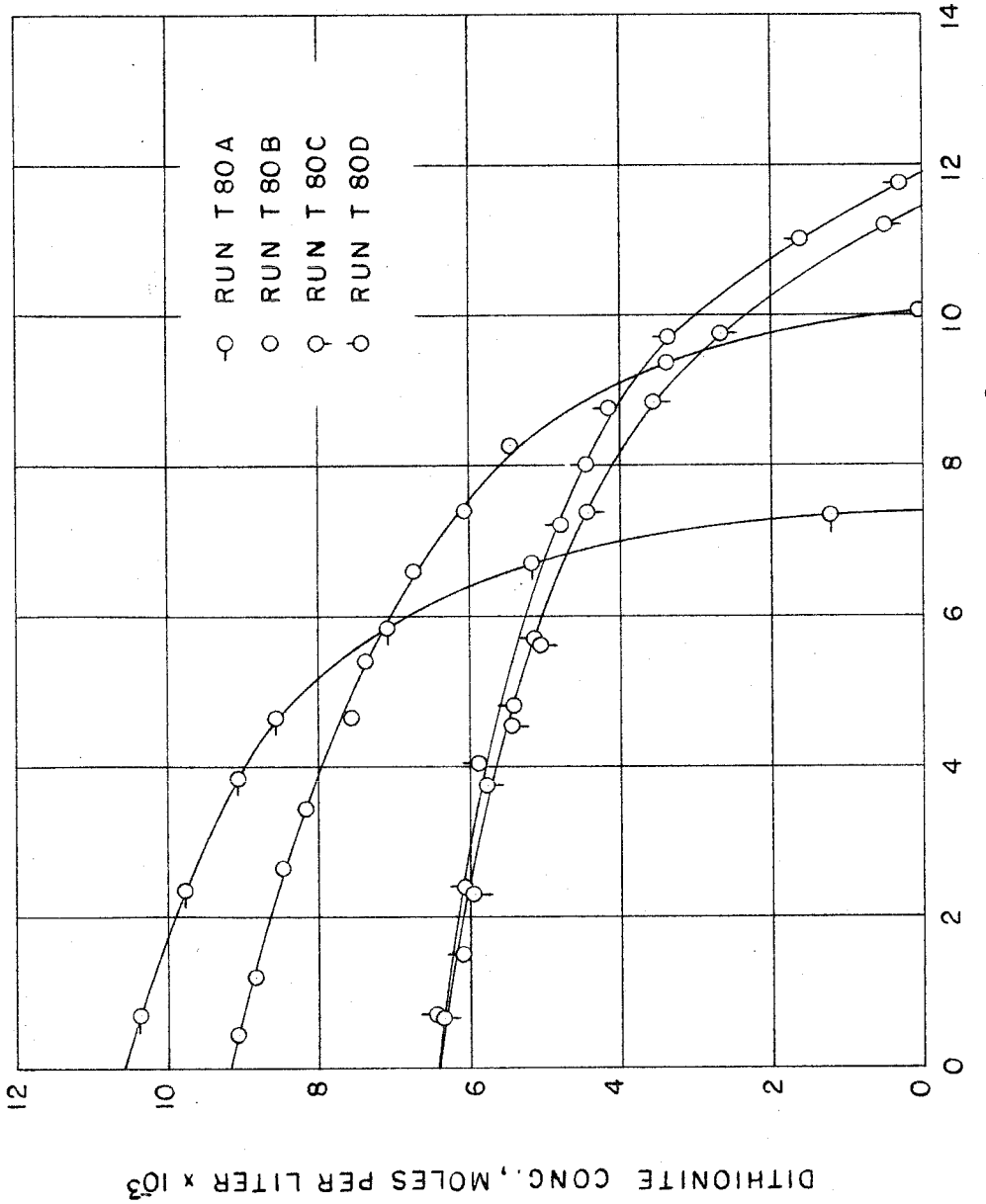

Figure 21--Thermal Decomposition Studies. Dithionite Concentration vs Time at 80°C

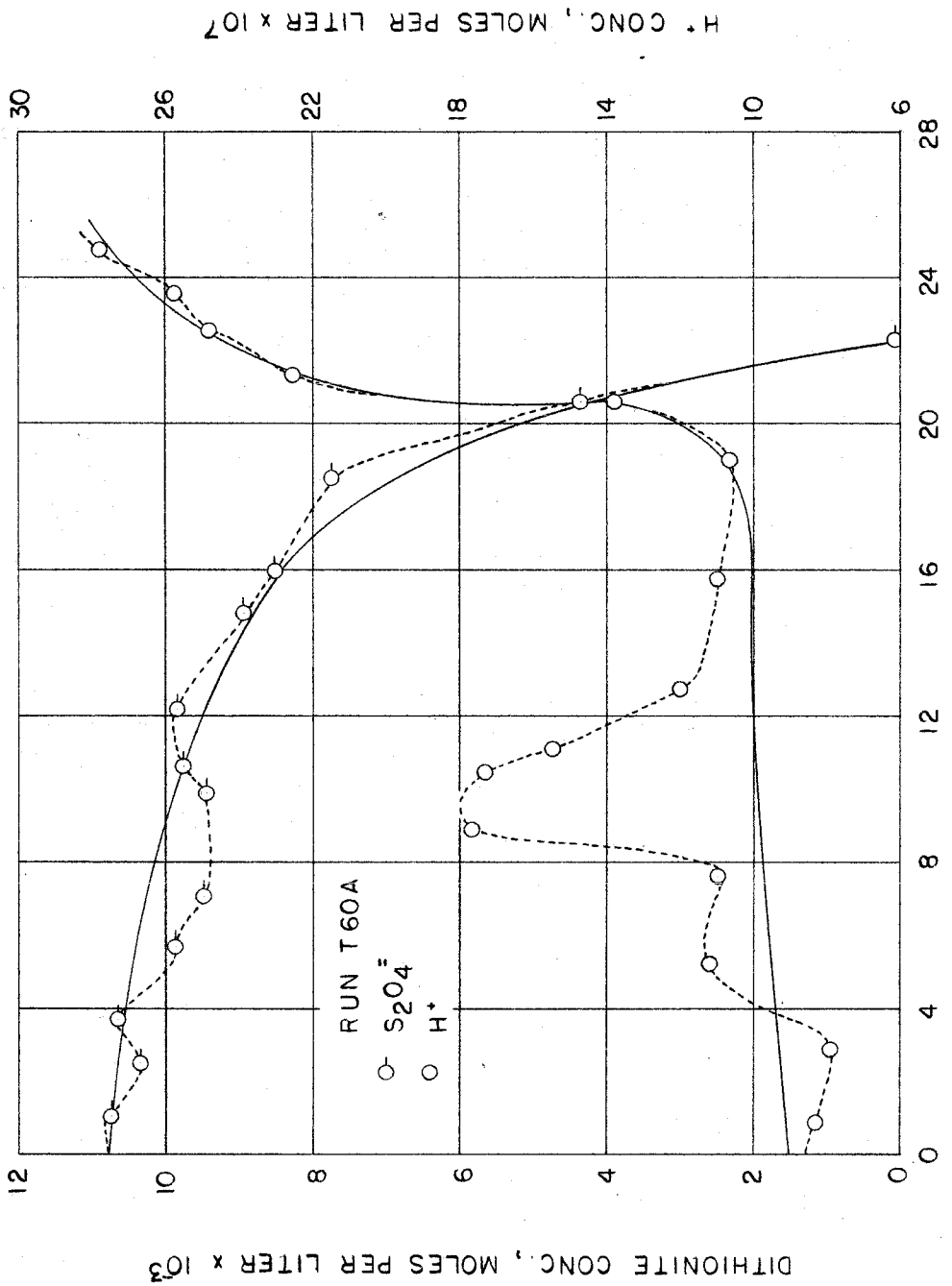

Figure 22--Thermal Decomposition Studies. H^+ and Dithionite Concentration vs Time at 60°C

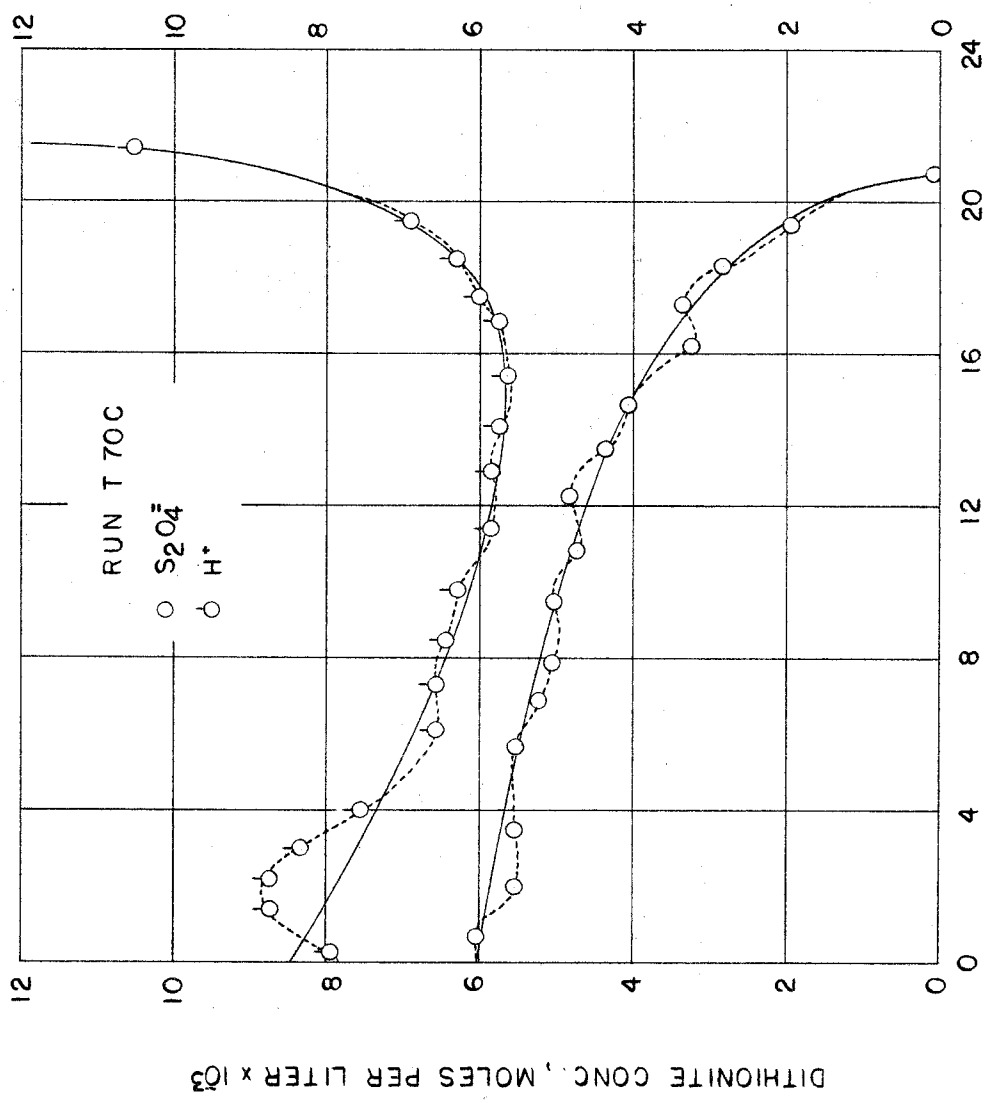

Figure 23--Thermal Decomposition Studies. H^+ and Dithionite Concentration vs Time at 70°C

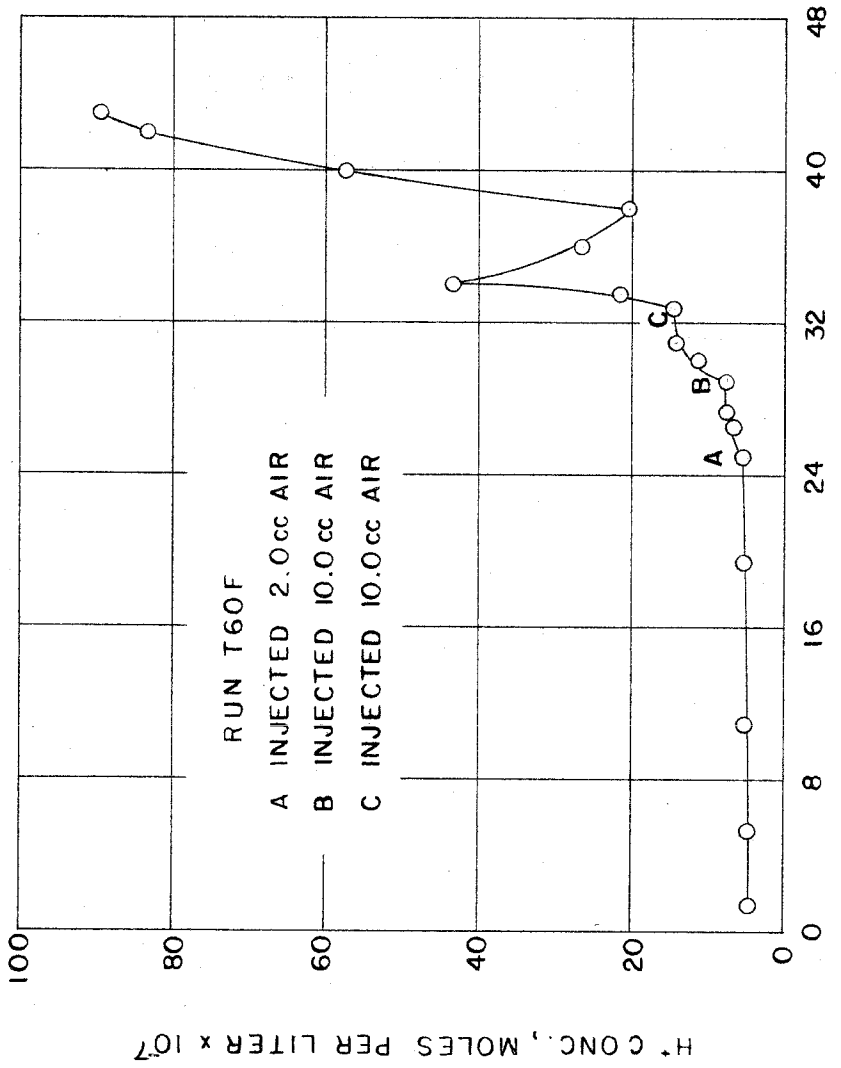

Figure 24--Thermal Decomposition Studies. O_2 Effects on H^+. H^+ Concentration vs Time at 60°C

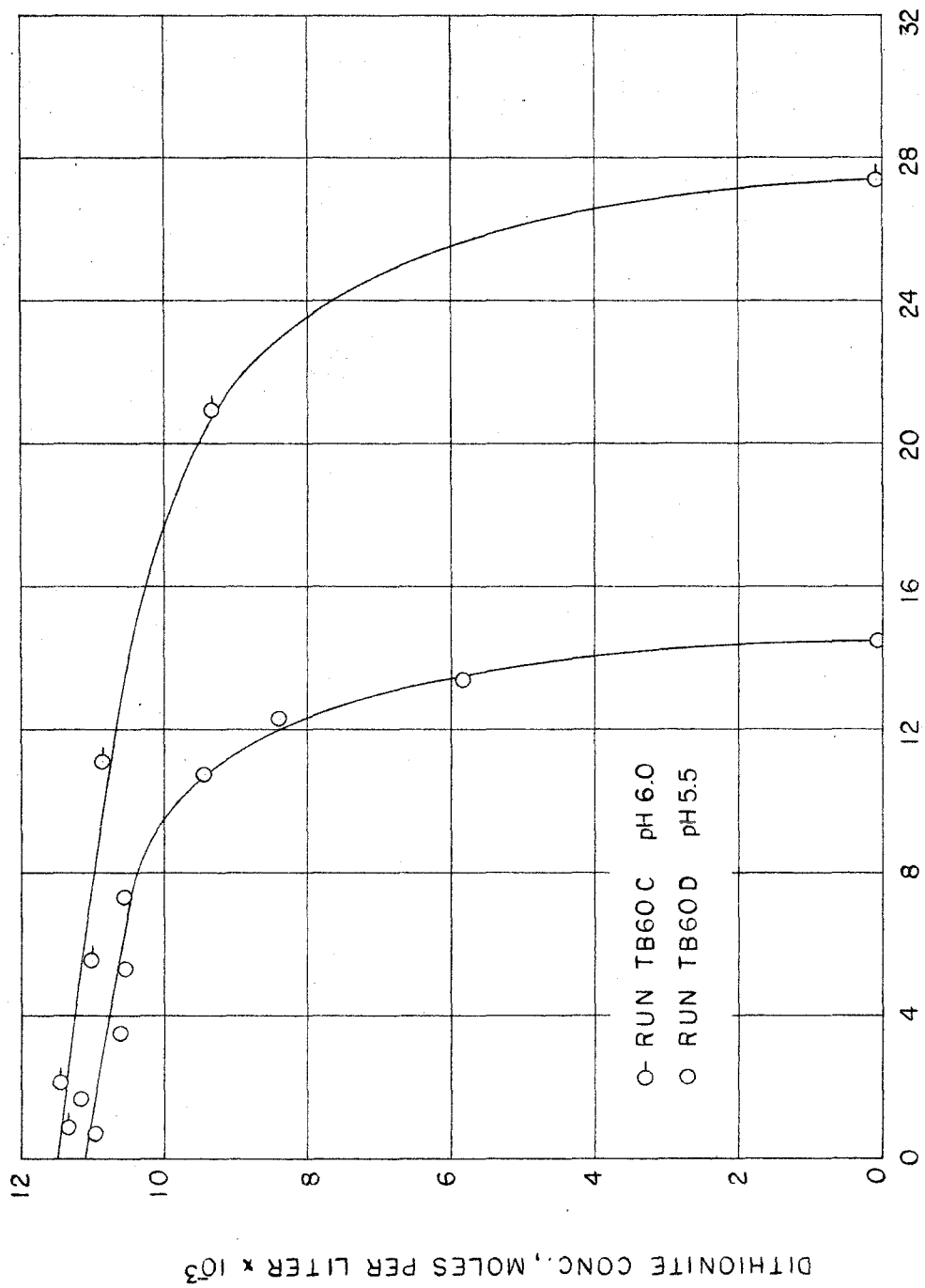

Figure 25a--Thermal Decomposition Studies. Dithionite Concentration vs Time at 60°C in Buffered Systems

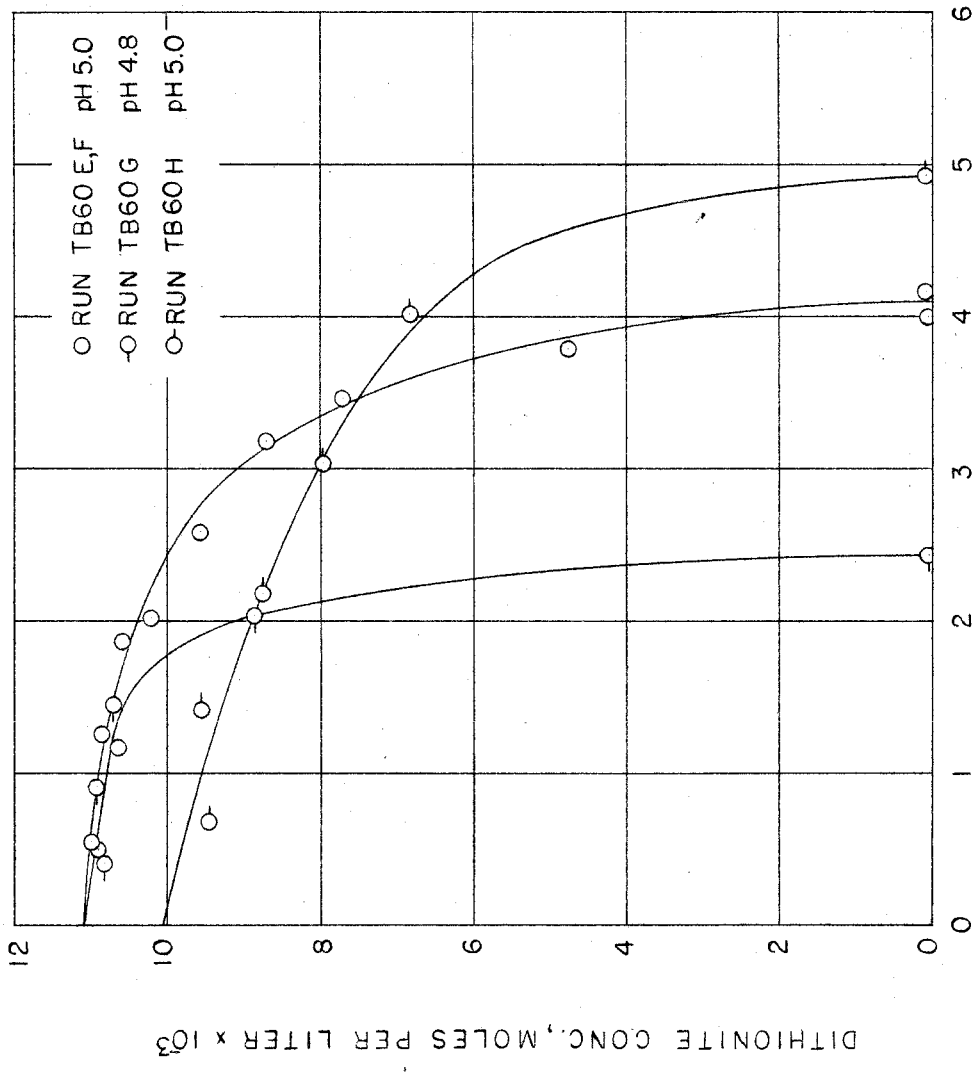

Figure 25b--Thermal Decomposition Studies. Dithionite Concentration vs Time at 60°C in Buffered Systems

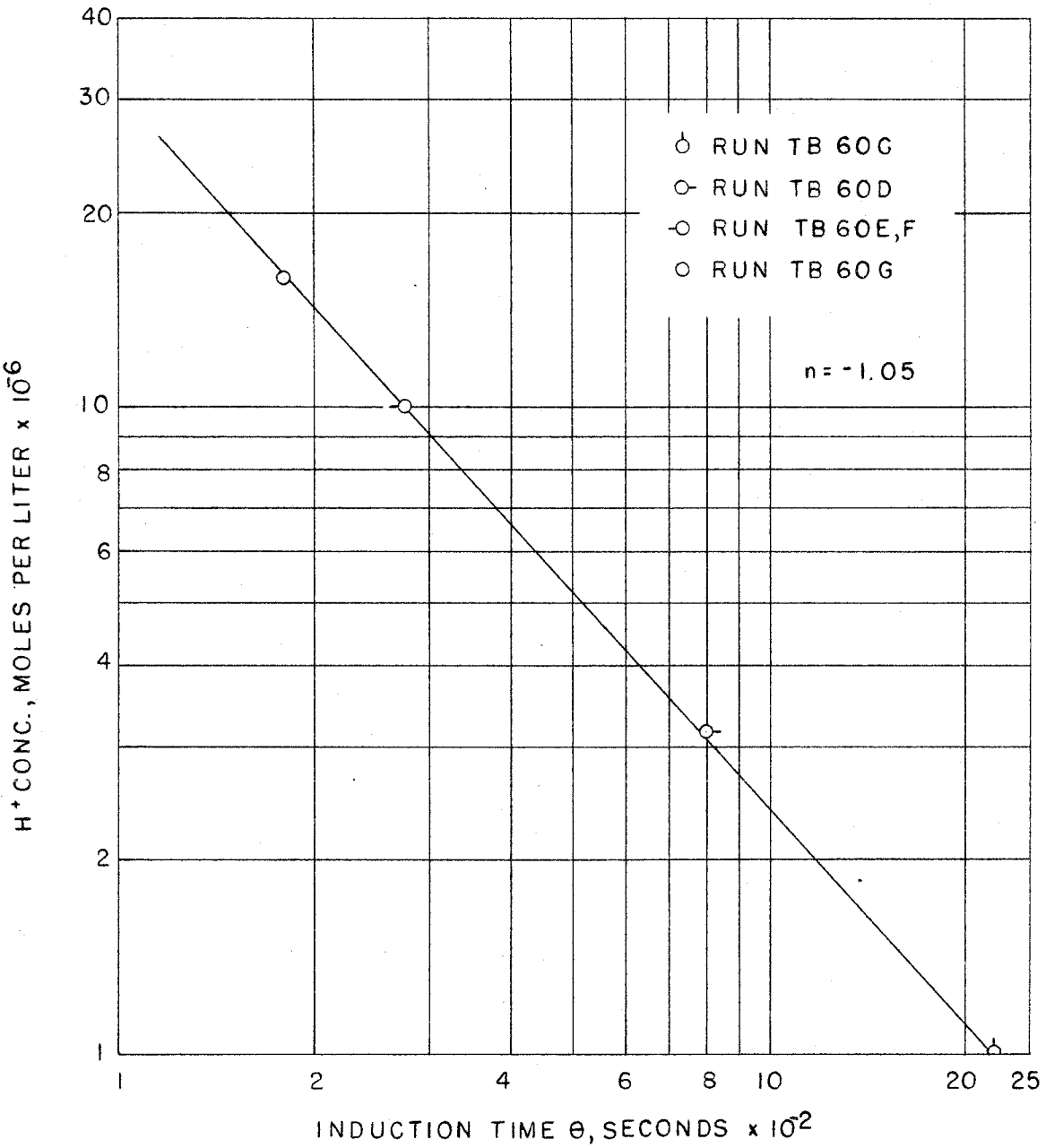

Figure 26--Thermal Decomposition Studies. Log of Induction Time vs Log of H^+ Concentration

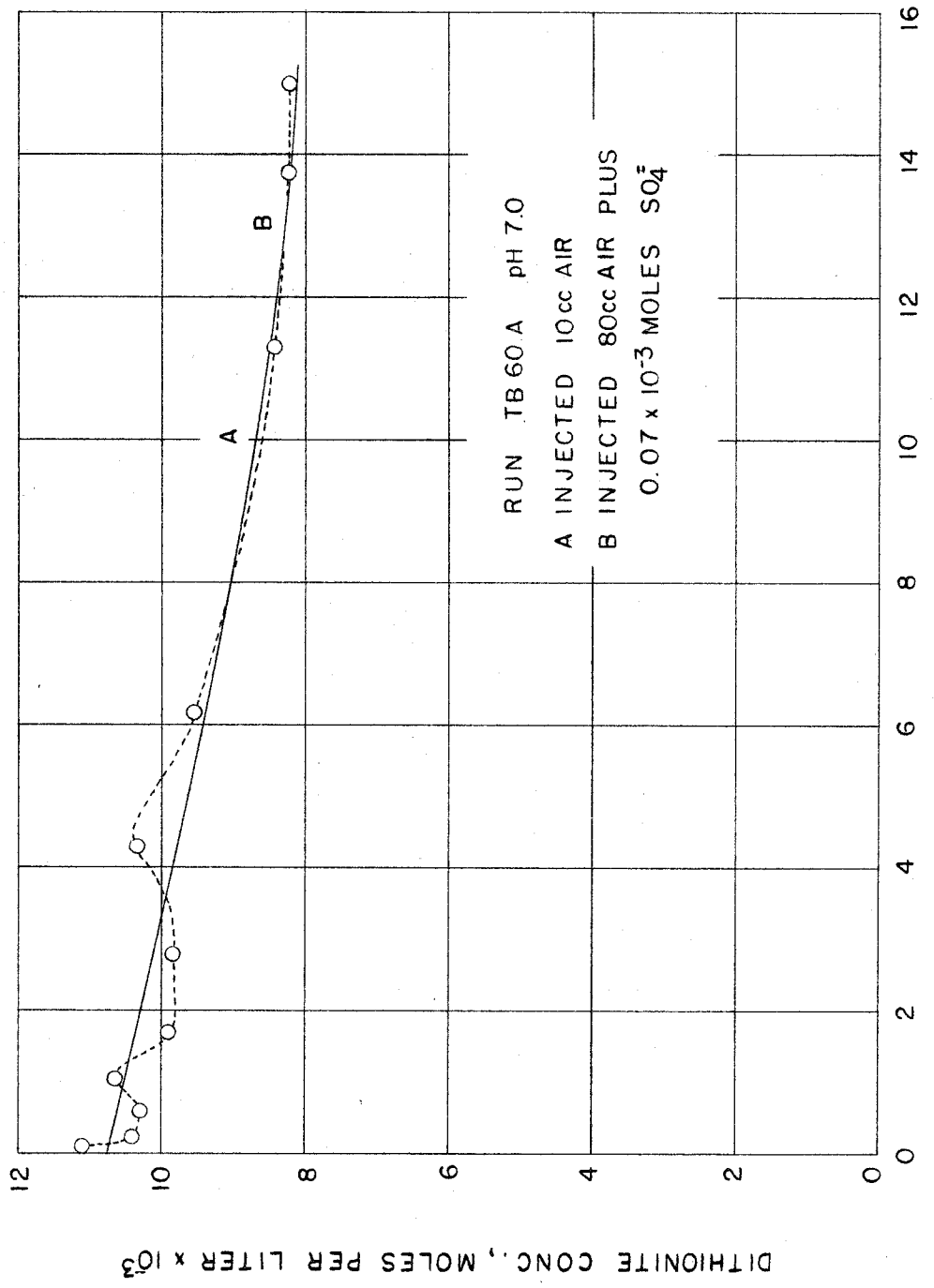

Figure 27a--Thermal Decomposition Studies. Effects of Air and $SO_4^=$. Dithionite Concentration vs Time at 60°C in System Buffered at pH 7

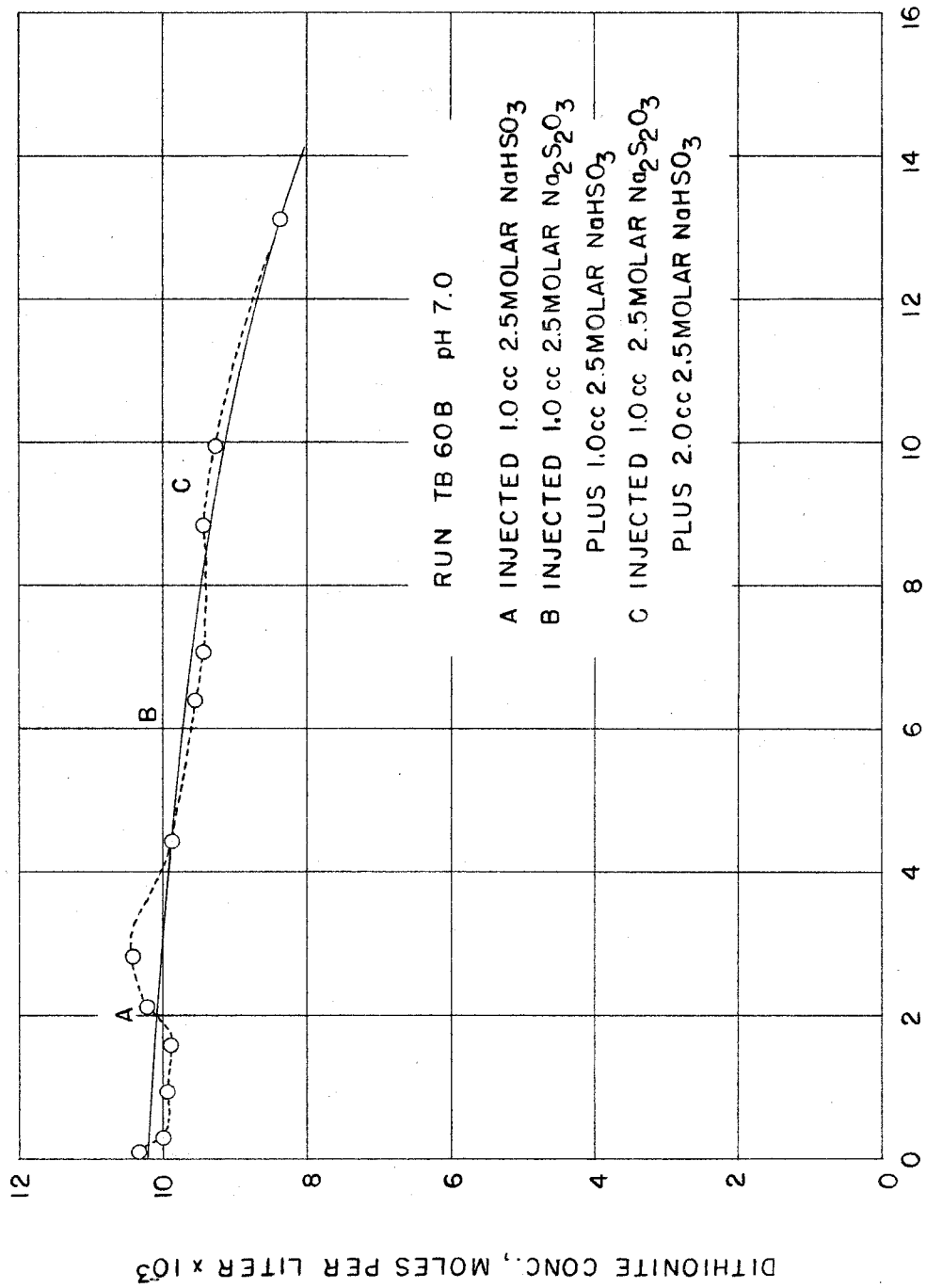

Figure 27b--Thermal Decomposition Studies. Effects of $S_2O_3^=$ and HSO_3^-. Dithionite Concentration vs Time at 60°C in System Buffered at pH 7

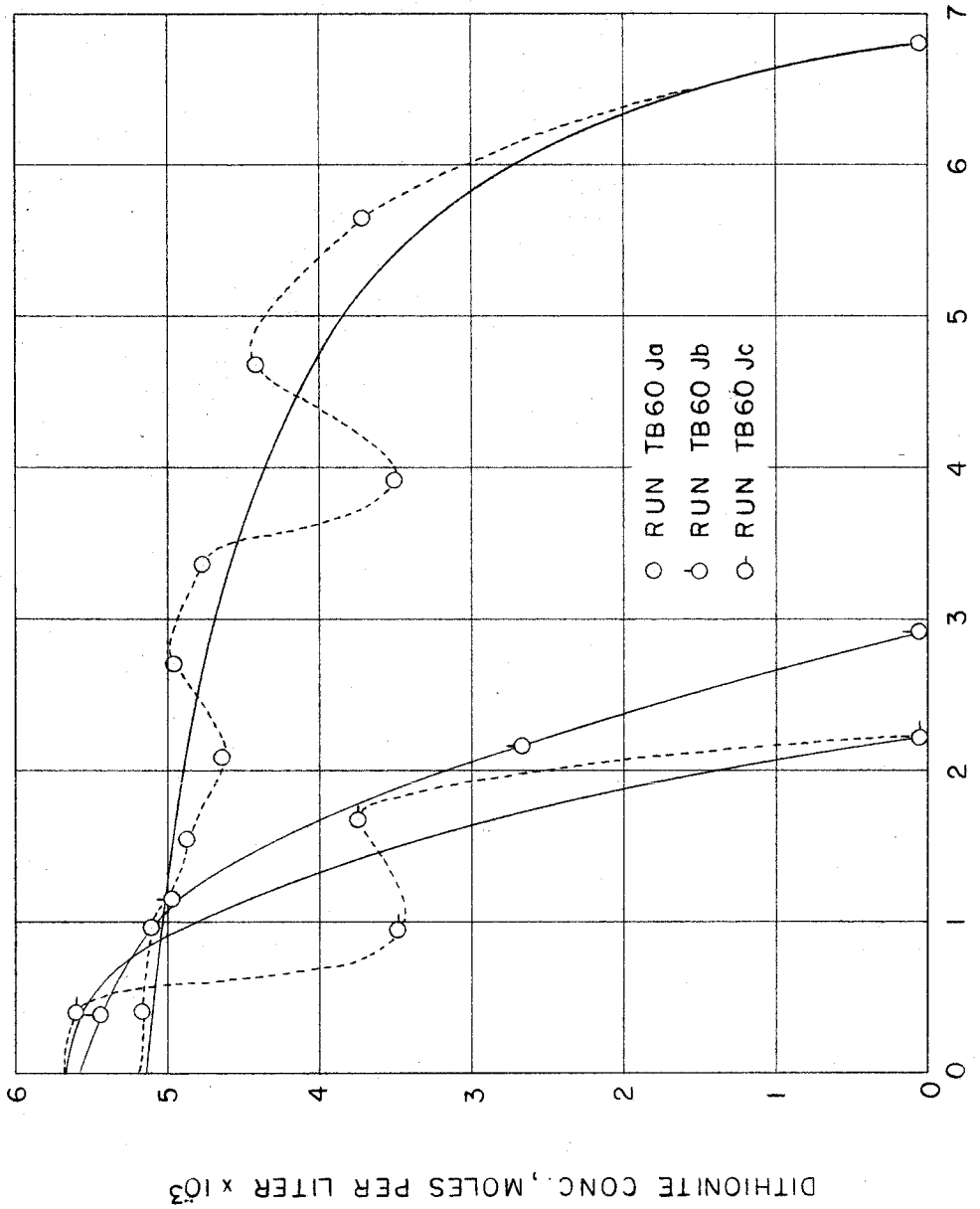

Figure 28a--Thermal Decomposition Studies. Effects of End Products. Dithionite Concentration vs Time at 60°C in System Buffered at pH 5

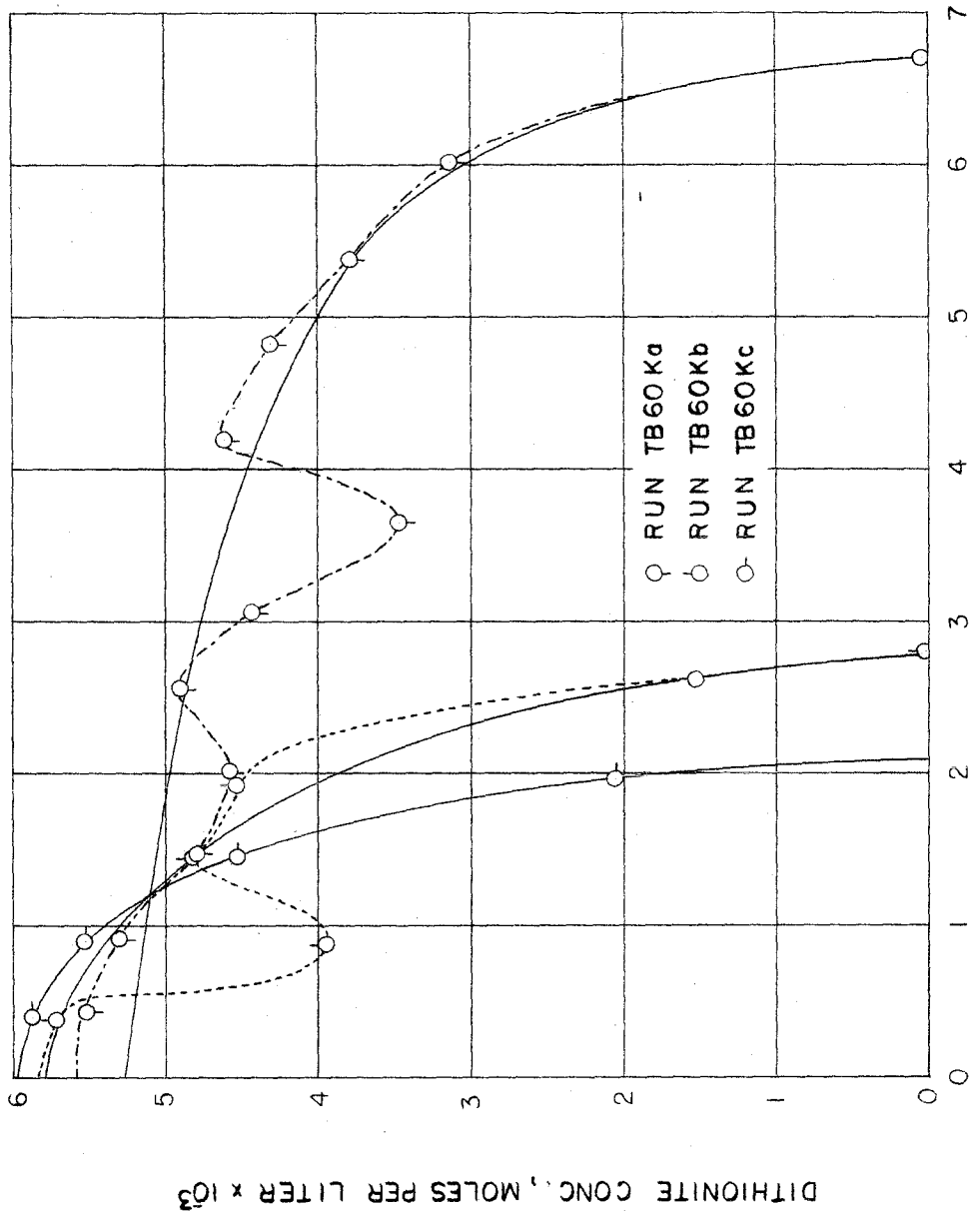

Figure 28b--Thermal Decomposition Studies. Effects of End Products. Dithionite Concentration vs Time at 60°C in System Buffered at pH 5

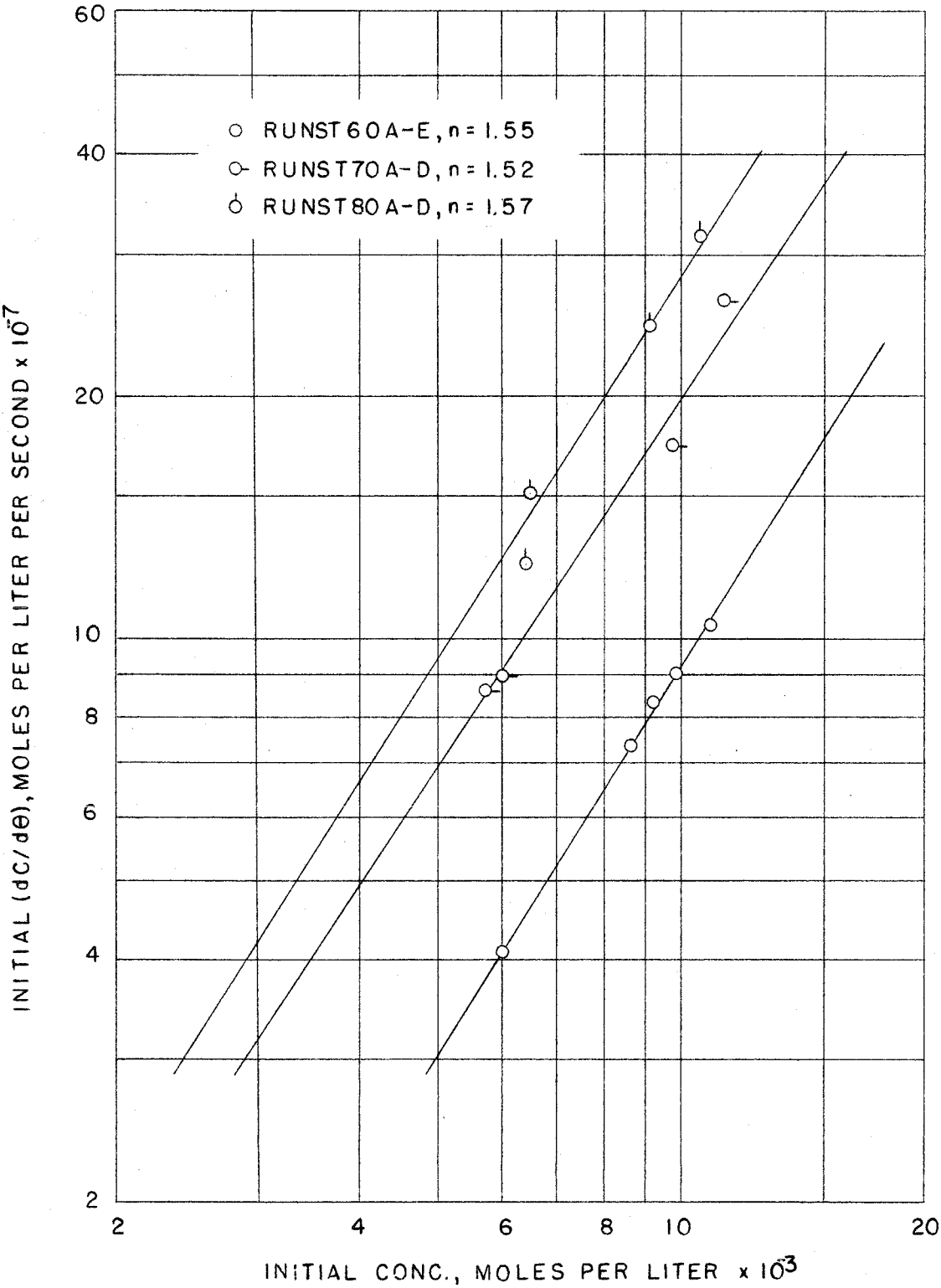

Figure 29--Thermal Decomposition Studies. Determination of n. Log $(dC/d\theta)_o$ vs log C_o at 60, 70, and 80°C

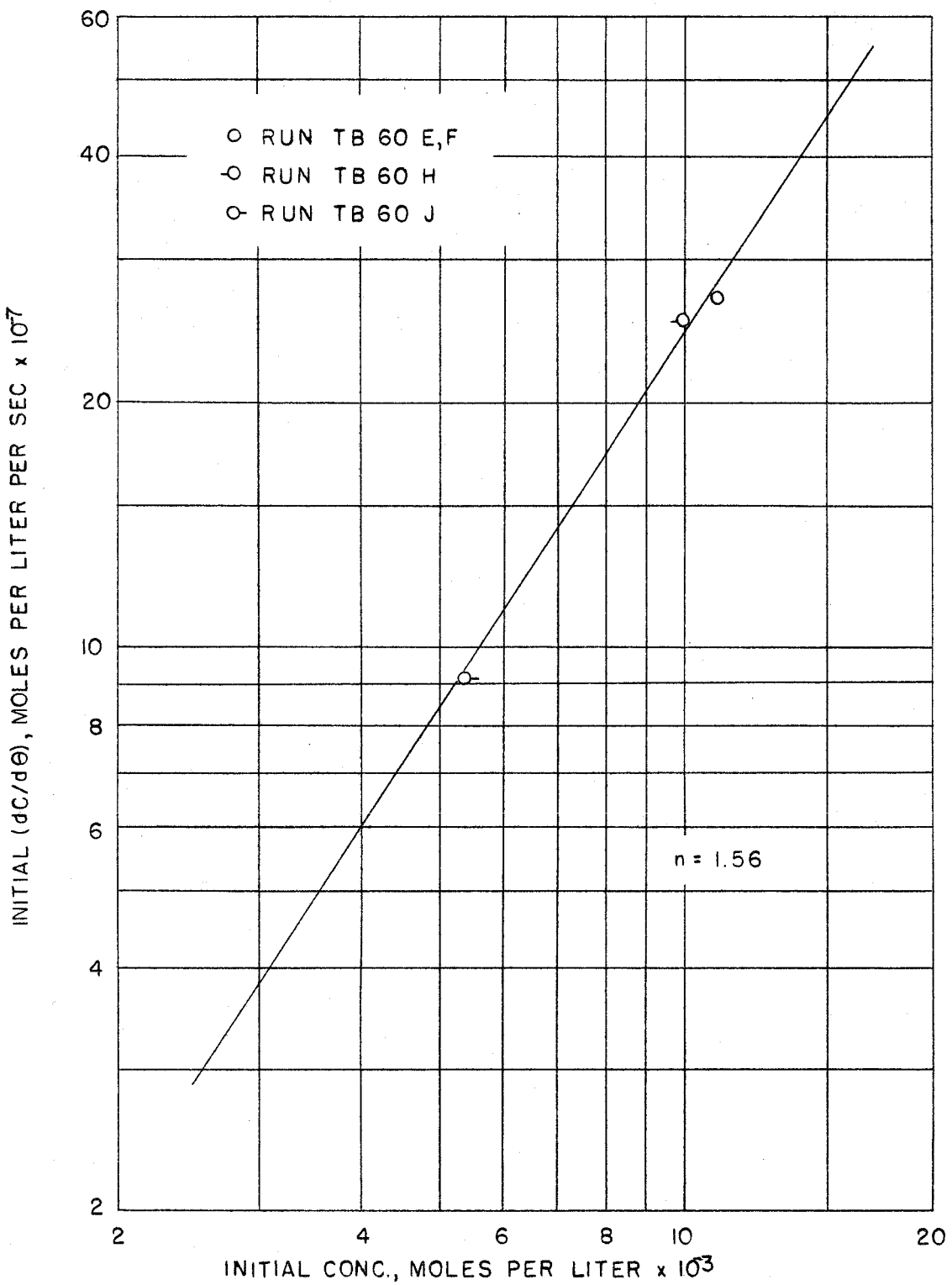

Figure 30--Thermal Decomposition Studies. Determination of n. Log $(dC/d\theta)_o$ vs log C_o at 60°C and pH 5.

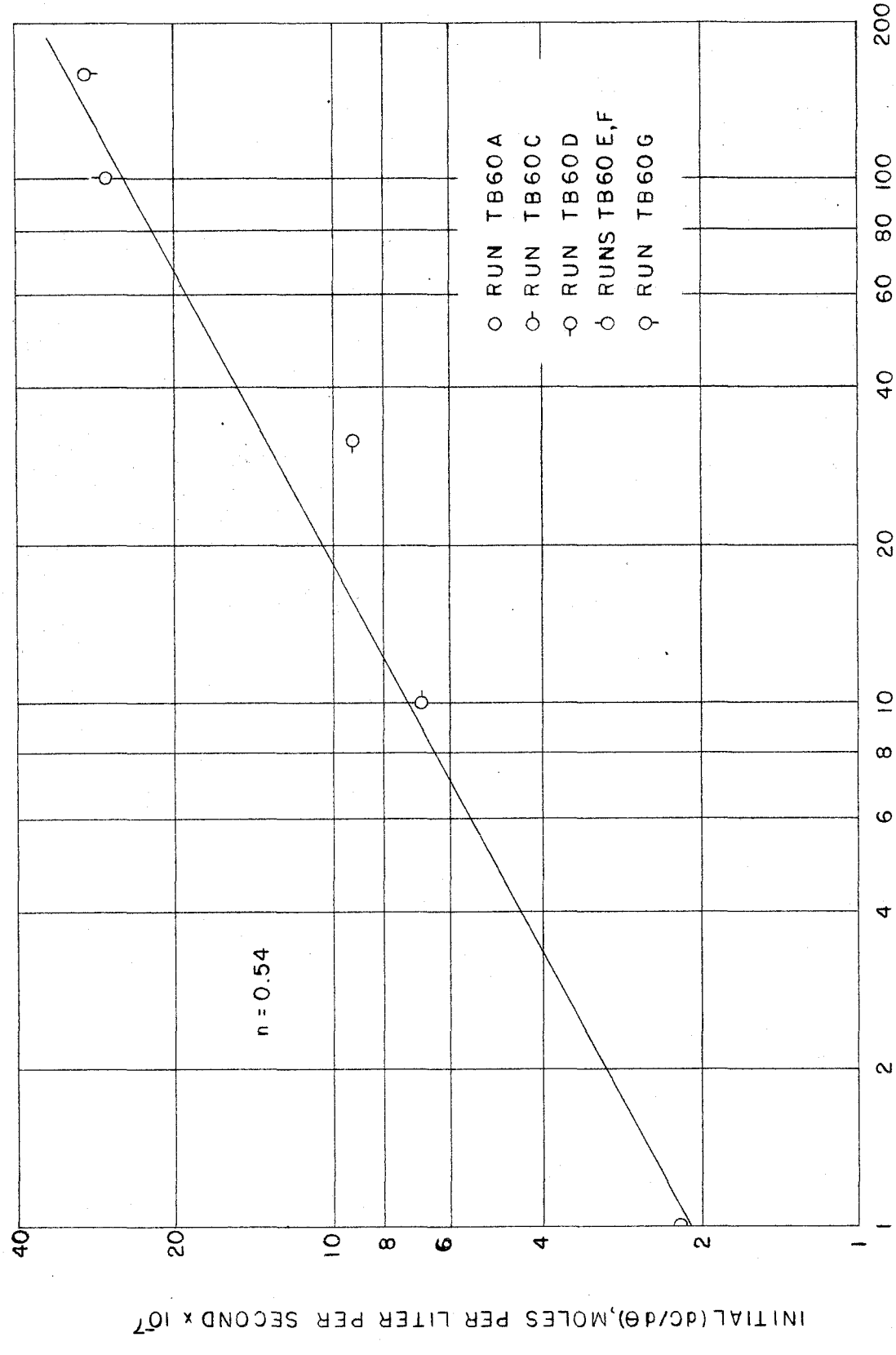

Figure 31--Thermal Decomposition Studies. Effect of H^+. Log $(dC/d\theta)_o$ vs log H^+ Concentration at 60°C for C_o = 11.00 x 10^{-3} Molar

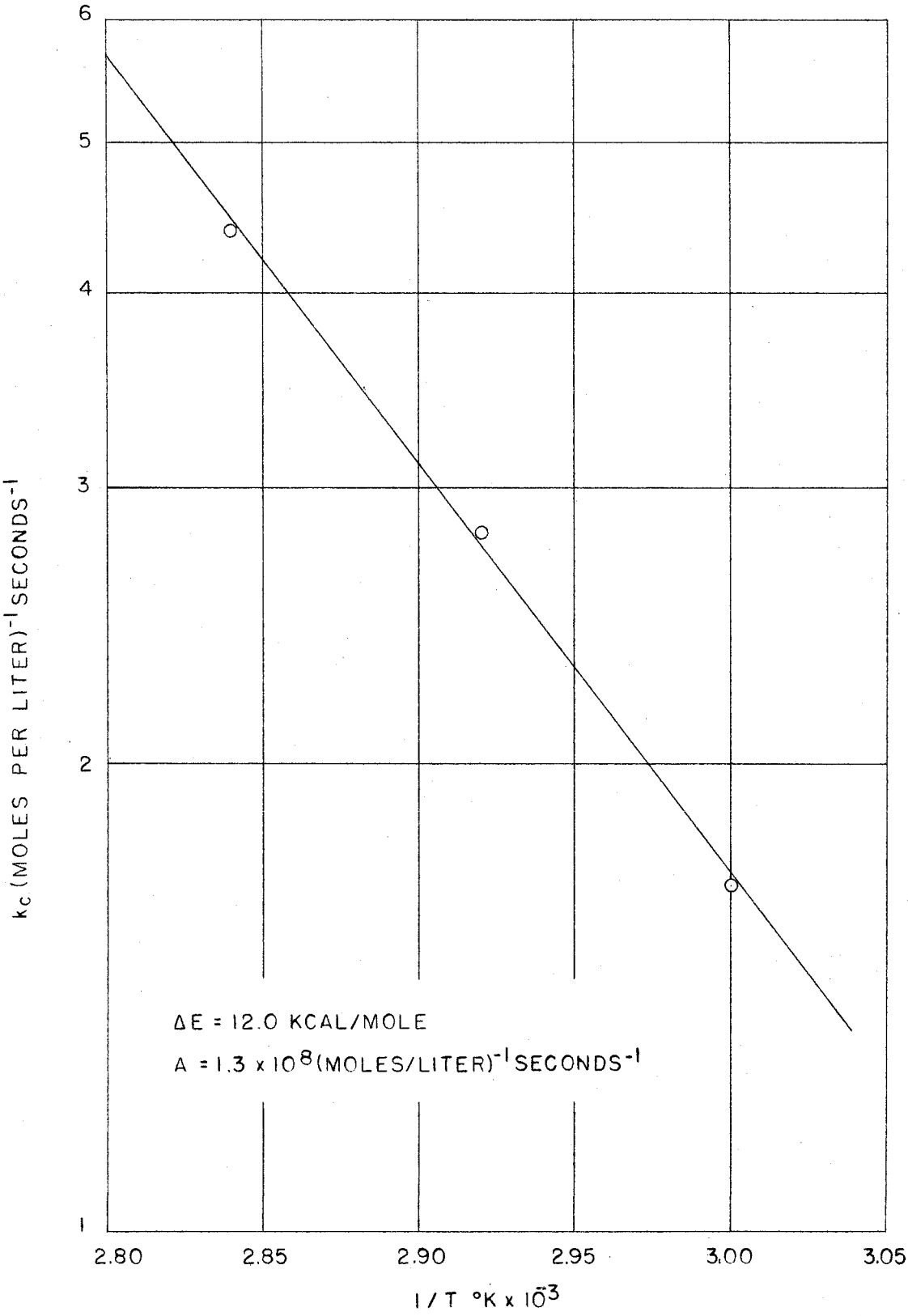

Figure 32--Thermal Decomposition Studies. Arrhenius Plot. Log k_c vs 1/T °K

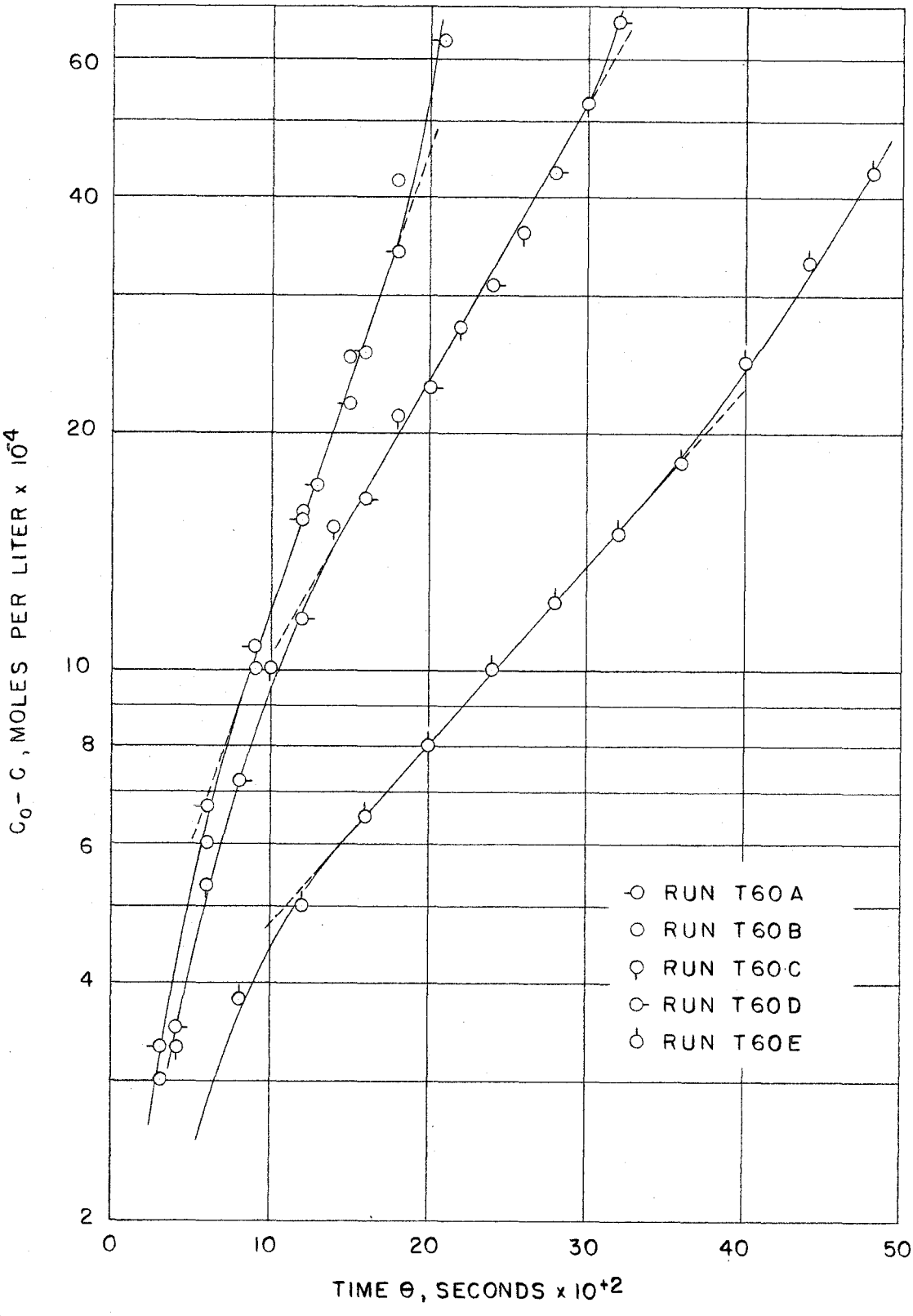

Figure 33--Thermal Decomposition Studies. Log (C_o - C) vs Time at 60°C

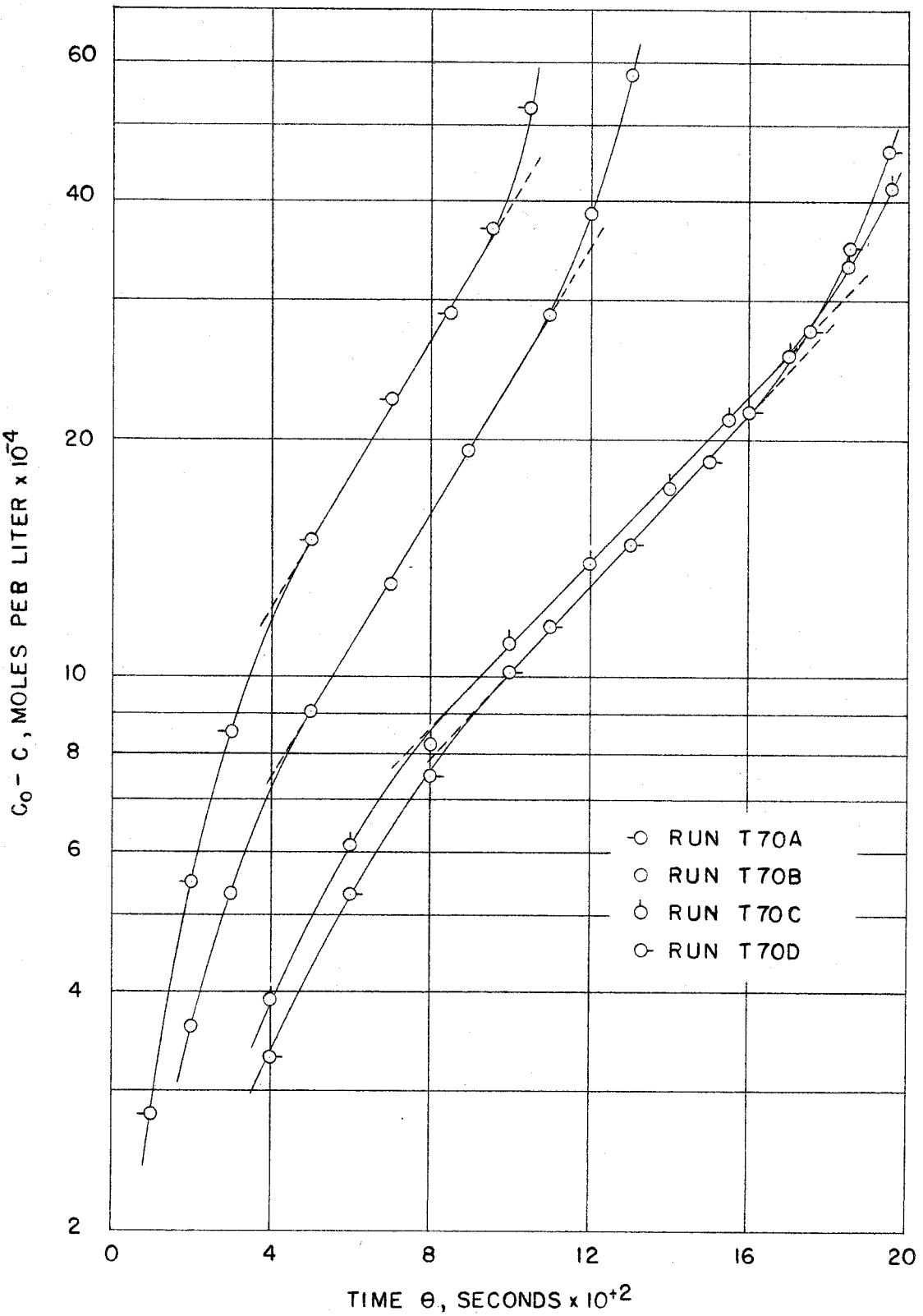

Figure 34--Thermal Decomposition Studies. Log (C_o - C) vs Time at 70°C

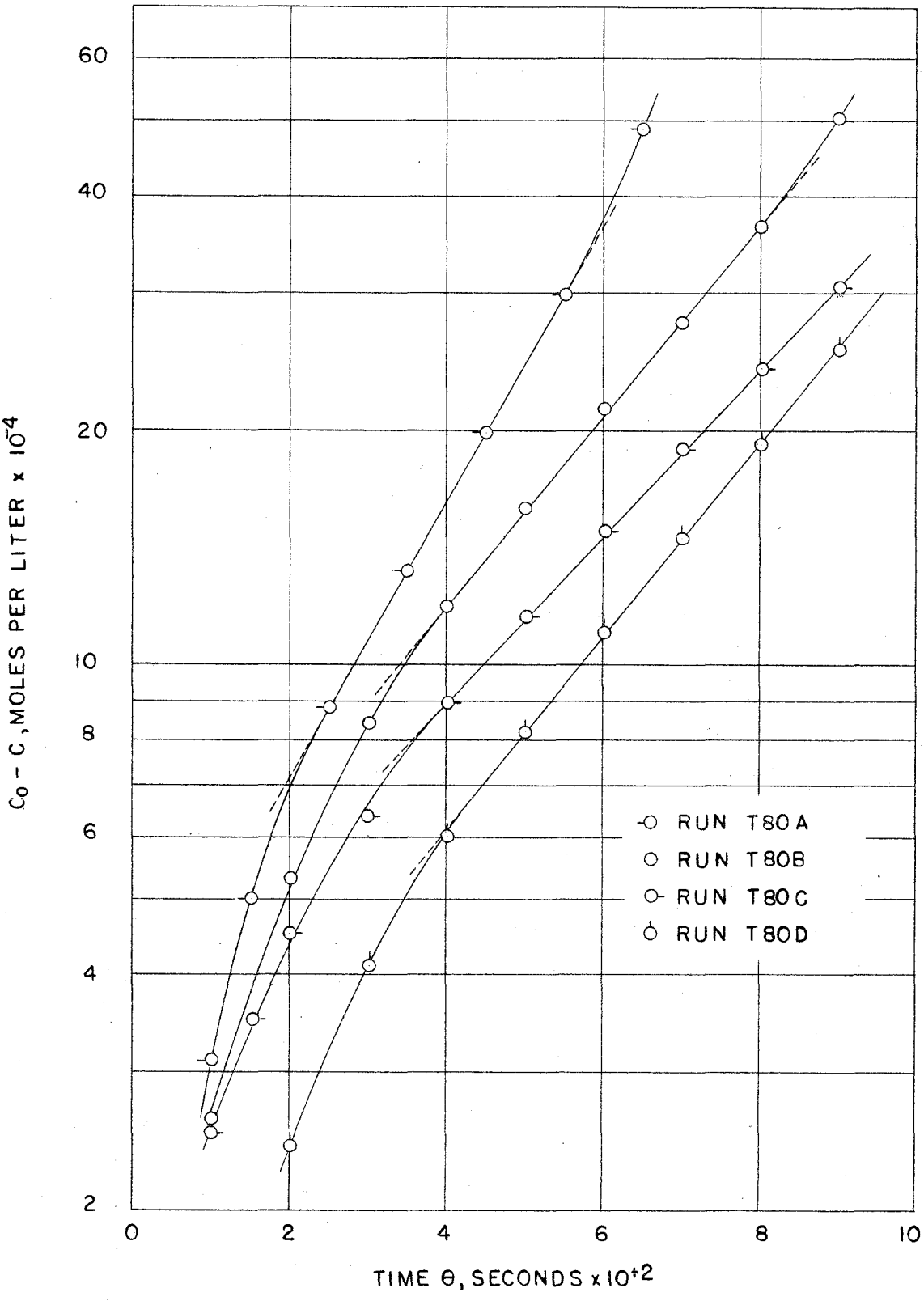

Figure 35--Thermal Decomposition Studies. Log (C_o - C) vs Time at 80°C

LIST OF TABLES

TABLE I

AIR OXIDATION STUDIES
DITHIONITE CONCENTRATION VS TIME AT 30°C

Run 30A

θ, Sec	$S_2O_4^=$ x 10^3 Moles/Liter
45	17.67
100	15.42
155	12.75
215	9.98
378	4.07
420	2.94
502	1.26
545	0.46
600	0.04

Run 30B

θ, Sec	$S_2O_4^=$ x 10^3 Moles/Liter
53	15.00
98	13.20
145	11.24
202	8.64
251	8.03
298	6.38
357	4.19
414	2.40
464	1.46
520	0.38
562	0.04

Run 30C

θ, Sec	$S_2O_4^=$ x 10^3 Moles/Liter
47	12.58
88	12.00
130	10.67
179	8.60
243	6.53
301	4.62
345	2.58
392	2.28
432	1.46
475	0.44
522	0.05

Run 30D

θ, Sec	$S_2O_4^=$ x 10^3 Moles/Liter
52	6.03
98	4.76
150	3.14
195	1.23
242	1.00
282	0.19
326	0.04

Run 30E

θ, Sec	$S_2O_4^=$ x 10^3 Moles/Liter
56	7.60
78	5.15
165	4.18
132	3.65
235	2.04
255	1.93
312	0.85
335	0.10

TABLE 2

AIR OXIDATION STUDIES

DITHIONITE CONCENTRATION VS TIME AT 40°C

Run 40A

θ, Sec	$S_2O_4^=$ x 10^3 Moles/Liter
20	6.02
66	4.86
115	3.27
159	1.94
203	0.91
247	0.15
280	0.03

Run 40B

θ, Sec	$S_2O_4^=$ x 10^3 Moles/Liter
28	8.58
77	6.72
130	4.73
199	2.42
238	1.53
273	0.95
314	0.29
352	0.04

Run 40C

θ, Sec	$S_2O_4^=$ x 10^3 Moles/Liter
44	11.03
100	8.06
175	4.20
220	2.44
265	1.28
310	0.43
350	0.03

Run 40D

θ, Sec	$S_2O_4^=$ x 10^3 Moles/Liter
52	16.42
122	12.00
172	9.81
225	6.02
300	3.63
350	2.12
395	1.16
437	0.07

Run 40E

θ, Sec	$S_2O_4^=$ x 10^3 Moles/Liter
41	18.18
91	15.50
130	12.33
198	8.60
264	5.64
313	3.77
362	2.25
406	0.81
448	0.05

TABLE 3

AIR OXIDATION STUDIES

DITHIONITE CONCENTRATION VS TIME AT 50°C

Run 50A

θ, Sec	$S_2O_4^=$ x 10^3 Moles/Liter
48	14.82
91	11.48
182	4.65
250	1.27
294	0.17
330	0.04

Run 50B

θ, Sec	$S_2O_4^=$ x 10^3 Moles/Liter
27	15.15
67	12.47
142	6.36
175	4.86
235	1.29
272	0.42
320	0.04

Run 50C

θ, Sec	$S_2O_4^=$ x 10^3 Moles/Liter
39	9.61
93	6.10
144	3.34
197	1.23
247	0.04

Run 50D

θ, Sec	$S_2O_4^=$ x 10^3 Moles/Liter
43	7.30
117	3.11
158	1.68
193	0.68
230	0.04

Run 50E

θ, Sec	$S_2O_4^=$ x 10^3 Moles/Liter
39	4.98
78	2.92
120	1.31
158	0.22
198	0.04

TABLE 4

AIR OXIDATION STUDIES
DITHIONITE CONCENTRATION VS TIME AT 60°C

Run 60A

θ, Sec	$S_2O_4^=$ x 10^3 Moles/Liter
60	11.94
102	8.54
137	5.10
181	2.37
218	0.67
289	0.02

Run 60B

θ, Sec	$S_2O_4^=$ x 10^3 Moles/Liter
38	16.59
108	8.90
185	2.76
233	0.68
272	0.04

Run 60C

θ, Sec	$S_2O_4^=$ x 10^3 Moles/Liter
47	10.69
84	6.98
122	3.97
181	0.19
196	0.04

Run 60D

θ, Sec	$S_2O_4^=$ x 10^3 Moles/Liter
48	5.35
83	2.94
124	1.20
158	0.23
192	0.05

Run 60E

θ, Sec	$S_2O_4^=$ x 10^3 Moles/Liter
39	3.92
85	1.64
124	0.18
160	0.04

Run 60F

θ, Sec	$S_2O_4^=$ x 10^3 Moles/Liter
38	3.52
77	1.70
120	0.21
156	0.02

TABLE 5

AIR OXIDATION STUDIES
DETERMINATION OF ORDER OF REACTION, n,
$(dC/d\theta)_o$ VS C_o AT 30, 40, 50, and 60°C

Run	Temperature °C	$(dC/d\theta)_o \times 10^5$ Moles/Liter, Sec	$C_o \times 10^3$ Moles/Liter, Sec
30A	30	5.06	20.20
30B	30	4.72	17.50
30C	30	4.43	15.85
30D	30	3.49	9.40
30E	30	3.25	7.72
40A	40	3.63	7.22
40B	40	4.01	9.73
40C	40	5.42	13.37
40D	40	6.11	19.37
40E	40	6.40	20.97
50A	50	9.24	19.25
50B	50	8.84	17.55
50C	50	7.29	12.40
50D	50	6.70	10.10
50E	50	6.30	7.30
60A	60	11.40	18.50
60B	60	12.07	20.77
60C	60	10.50	15.50
60D	60	7.70	9.00
60E	60	7.21	7.41
60F	60	6.20	5.80

TABLE 6

AIR OXIDATION STUDIES

k_c VS θ AT 30°C

Run 30A

θ, Sec	$k_c \times 10^4$ (Moles/Liter)$^{\frac{1}{2}}$Sec^{-1}
30	3.61
50	3.64
70	3.69
90	3.68
110	3.70
130	3.75
150	3.79
170	3.82
190	3.86

Run 30B

θ, Sec	$k_c \times 10^4$ (Moles/Liter)$^{\frac{1}{2}}$Sec^{-1}
30	3.59
50	3.66
70	3.66
90	3.64
110	3.68
130	3.72
150	3.74
170	3.80
190	3.82

Run 30C

θ, Sec	$k_c \times 10^4$ (Moles/Liter)$^{\frac{1}{2}}$Sec^{-1}
30	3.66
50	3.60
70	3.66
90	3.64
110	3.66
130	3.69
150	3.69
170	3.72
190	3.72

Run 30D

θ, Sec	$k_c \times 10^4$ (Moles/Liter)$^{\frac{1}{2}}$Sec^{-1}
30	3.73
50	3.84
70	3.92
90	3.96
110	4.08
130	4.14
150	4.24
170	4.32
190	4.40

Run 30E

θ, Sec	$k_c \times 10^4$ (Moles/Liter)$^{\frac{1}{2}}$Sec^{-1}
30	3.64
50	3.62
70	3.70
90	3.74
110	3.82
130	3.86
150	3.93
170	3.99
190	4.05

TABLE 6 (CONTINUED)

k_c VS θ AT 40°C

Run 40A

θ, Sec	$k_c \times 10^4$ $(\text{Moles/Liter})^{\frac{1}{2}}\text{Sec}^{-1}$
30	4.33
40	4.45
60	4.57
80	4.68
90	4.69
120	4.85
160	5.07

Run 40B

θ, Sec	$k_c \times 10^4$ $(\text{Moles/Liter})^{\frac{1}{2}}\text{Sec}^{-1}$
30	4.47
50	4.44
70	4.55
90	4.58
110	4.61
130	4.67
150	4.69
170	4.86
190	4.93

Run 40C

θ, Sec	$k_c \times 10^4$ $(\text{Moles/Liter})^{\frac{1}{2}}\text{Sec}^{-1}$
30	4.21
50	4.36
70	4.38
90	4.44
110	4.50
130	4.54
150	4.63
170	4.70
190	4.78

Run 40D

θ, Sec	$k_c \times 10^4$ $(\text{Moles/Liter})^{\frac{1}{2}}\text{Sec}^{-1}$
30	4.39
50	4.56
70	4.59
90	4.62
110	4.77
130	4.69
150	4.75
170	4.81
190	4.88

Run 40E

θ, Sec	$k_c \times 10^4$ $(\text{Moles/Liter})^{\frac{1}{2}}\text{Sec}^{-1}$
30	4.33
50	4.48
70	4.58
90	4.60
110	4.62
130	4.69
150	4.77
170	4.84
190	4.90

TABLE 6 (CONTINUED)

k_c VS θ AT 50°C

Run 50A

θ, Sec	$k_c \times 10^4$ $(\text{Moles/Liter})^{\frac{1}{2}}\text{Sec}^{-1}$
30	6.81
50	6.83
70	6.93
90	7.05
110	7.23
130	7.35
150	7.52
170	7.67
190	7.81
210	7.94

Run 50B

θ, Sec	$k_c \times 10^4$ $(\text{Moles/Liter})^{\frac{1}{2}}\text{Sec}^{-1}$
30	6.67
50	6.77
70	6.91
90	7.00
110	7.16
130	7.29
150	7.44
170	7.56
190	7.70
210	7.79

Run 50C

θ, Sec	$k_c \times 10^4$ $(\text{Moles/Liter})^{\frac{1}{2}}\text{Sec}^{-1}$
30	6.71
50	6.83
70	6.99
90	7.10
110	7.25
130	7.35
150	7.45
170	7.57
190	7.69
210	7.87

Run 50D

θ, Sec	$k_c \times 10^4$ $(\text{Moles/Liter})^{\frac{1}{2}}\text{Sec}^{-1}$
30	7.00
50	7.18
70	7.40
90	7.54
110	7.60
130	7.58
150	7.59
170	7.64
190	7.70

TABLE 6 (CONTINUED)

k_c VS θ AT 60°C

Run 60A

θ, Sec	$k_c \times 10^4$ $(\text{Moles/Liter})^{\frac{1}{2}}\text{Sec}^{-1}$
30	8.72
50	8.88
70	9.01
90	9.11
110	9.25
130	9.28

Run 60B

θ, Sec	$k_c \times 10^4$ $(\text{Moles/Liter})^{\frac{1}{2}}\text{Sec}^{-1}$
30	8.54
50	8.60
70	8.85
90	9.03
110	9.30
130	9.47
150	9.65

Run 60C

θ, Sec	$k_c \times 10^4$ $(\text{Moles/Liter})^{\frac{1}{2}}\text{Sec}^{-1}$
30	8.76
50	8.96
70	9.07
90	9.40
110	9.70
130	9.90
150	10.20

Run 60D

θ, Sec	$k_c \times 10^4$ $(\text{Moles/Liter})^{\frac{1}{2}}\text{Sec}^{-1}$
30	8.80
50	9.25
70	9.58
90	9.86
110	9.94

Run 60E

θ, Sec	$k_c \times 10^4$ $(\text{Moles/Liter})^{\frac{1}{2}}\text{Sec}^{-1}$
30	8.80
50	9.04
70	9.18
90	9.45

Run 60F

θ, Sec	$k_c \times 10^4$ $(\text{Moles/Liter})^{\frac{1}{2}}\text{Sec}^{-1}$
30	8.79
50	8.92
70	9.15
90	9.51

TABLE 7

AIR OXIDATION STUDIES
EFFECT OF STIRRING RATE AND AIR FLOW RATE.
DITHIONITE CONCENTRATION VS TIME AT 60°C

Run 60G

*Air Flow Rate = 295cc/min
Stirring Rate = 800 rpm

θ, Sec	$S_2O_4^=$ x 10^3 Moles/Liter
31	10.90
138	7.30
230	5.47
295	3.71
400	2.18
472	1.45
565	0.47
622	0.33
685	0.02

Run 60H

Air Flow Rate = 495cc/min
Stirring Rate = 800 rpm

θ, Sec	$S_2O_4^=$ x 10^3 Moles/Liter
38	9.67
113	6.55
206	2.98
260	1.81
310	0.85
355	0.34
401	0.02

Run 60J

Air Flow Rate = 720cc/min
Stirring Rate = 800 rpm

θ, Sec	$S_2O_4^=$ x 10^3 Moles/Liter
35	8.78
112	4.42
170	1.83
230	0.68
286	0.04

Run 60K

Air Flow Rate = 960cc/min
Stirring Rate = 800 rpm

θ, Sec	$S_2O_4^=$ x 10^3 Moles/Liter
27	8.92
102	4.27
162	1.63
208	0.57
252	0.02

Run 60L

Air Flow Rate = 1200cc/min
Stirring Rate = 800 rpm

θ, Sec	$S_2O_4^=$ x 10^3 Moles/Liter
33	7.65
100	3.40
160	1.41
210	0.20
250	0.03

Run 60M

Air Flow Rate = 2500cc/min
Stirring Rate = 1100 rpm

θ, Sec	$S_2O_4^=$ x 10^3 Moles/Liter
39	7.01
99	3.25
160	1.22
214	0.09
255	0.02

TABLE 8

AIR OXIDATION STUDIES
IONIC STRENGTH EFFECTS. DITHIONITE
CONCENTRATION VS TIME

Run 60N
μ = 0.50

θ, Sec	$S_2O_4^=$ x 10^3 Moles/Liter
36	9.42
127	3.00
200	0.27
265	0.04

Run 60P
μ = 0.30

θ, Sec	$S_2O_4^=$ x 10^3 Moles/Liter
42	7.95
135	1.94
187	0.35
222	0.04

Run 60Q
μ = 0.10

θ, Sec	$S_2O_4^=$ x 10^3 Moles/Liter
55	7.46
107	4.55
150	2.36
203	0.97
242	0.06

Run 60R
μ = 0.01 N

θ, Sec	$S_2O_4^=$ x 10^3 Moles/Liter
42	8.06
90	5.20
142	0.05

TABLE 9

AIR OXIDATION STUDIES
SULFITE AND THIOSULFATE CONCENTRATION VS TIME
AT 30° AND 60°C AND CONSTANT AIR RATE

Run 30A-A at 30°C

θ, Sec	$SO_3^=$ x 10^3 Moles/Liter
147	15.27
276	12.85
463	9.58
637	6.02

Run 30A-B at 30°C

θ, Sec	$SO_3^=$ x 10^3 Moles/Liter
33	20.50
153	19.54
255	17.64
355	17.13
472	15.03
578	13.84
648	13.03

Run 60A-A at 60°C

θ, Sec	$SO_3^=$ x 10^3 Moles/Liter
56	20.15
138	18.75
188	17.94
248	16.36
298	15.02

Run 60A-B at 60°C

θ, Sec	$SO_3^=$ x 10^3 Moles/Liter
48	20.37
93	19.66
161	18.77
237	17.44
293	16.22
370	15.03
427	14.02

Run 60A-C at 60°C

θ, Sec	$S_2O_3^=$ x 10^3 Moles/Liter
56	27.88
156	27.85
297	28.07
436	28.37
637	28.29

TABLE 10

AIR OXIDATION STUDIES

END PRODUCT ANALYSES

Run EP - A Diffusion controlled oxidation

Initial $[S_2O_4^{=}]$ = 10.30×10^{-3} moles/liter
Reaction time = 29 hrs
Average analyses:

$[SO_3^{=}]$ = 13.14×10^{-3} moles/liter

$[SO_4^{=}]$ = 5.72×10^{-3} moles/liter

$[S_2O_3^{=}]$ = 1.60×10^{-3} moles/liter

$$\frac{[SO_3^{=}]}{[SO_4^{=}]} = 2.3$$

Run EP - B Air oxidation

Initial $[S_2O_4^{=}]$ = 9.50×10^{-3} moles/liter
Analysis (corrected for 8.8% thermal decomposition):

$[SO_3^{=}]$ = 13.16×10^{-3} moles/liter

$[SO_4^{=}]$ = 4.16×10^{-3} moles/liter

$[S_2O_3^{=}]$ = 0.42×10^{-3} moles/liter

$$\frac{[SO_3^{=}]}{[SO_4^{=}]} = 3.16$$

Run EP - C Air oxidation

Initial $[S_2O_4^{=}]$ = 10.10×10^{-3} moles/liter
Analysis (corrected for 21% thermal decomposition):

$[SO_3^{=}]$ = 11.90×10^{-3} moles/liter

$[SO_4^{=}]$ = 4.26×10^{-3} moles/liter

$[S_2O_3^{=}]$ = 1.00×10^{-3} moles/liter

$$\frac{[SO_3^{=}]}{[SO_4^{=}]} = 2.78$$

Average: $\frac{[SO_3^{=}]}{[SO_4^{=}]} = 2.97$

TABLE 11

AIR OXIDATION STUDIES
SOLUBILITY OF SODIUM DITHIONITE AT 0°C

Run No.	Solubility in gms/100 ml H_2O at 0°C
S-A	14.39
S-B	14.38
S-C	14.35
S-D	13.85
S-E	13.69
S-F	12.51
S-G	11.63
S-H	11.68
S-I	13.15
S-J	13.52
S-K	12.00

Average = 13.20 σ = 1.08 or 8% of 13.20

TABLE 12

DITHIONITE STRUCTURE STUDIES. ELECTROLYTIC GENERATION OF DITHIONITE

Run 100A pH = 5.3 Temperature = 2.2°C Current = 100 ma

Time sec	Cathode Potential	Total Moles of $S_2O_4^=$ formed x 10^4	Moles of Electrons passed x 10^4
120	-0.67	0.35	1.244
420	-0.68	1.58	4.351
1020	-0.68	4.03	10.57
2100	-0.71	6.20	21.77
2700	-0.71	10.51	28.00
3300	-0.72	11.74	34.20
3900	-0.73	15.12	40.41
4500	-0.73	17.36	46.64

Average Current Efficiency = 75.0%

Run 150A pH = 5.0 Temperature = 2.8°C Current = 150 ma

300	-0.73	1.25	4.66
420	-0.74	2.49	6.53
900	-0.74	5.33	13.98
1020	-0.75	6.32	15.85
1500	-0.75	9.16	23.32
1620	-0.75	10.00	25.18
2280	-0.75	13.92	35.43
2400	-0.75	14.64	37.30
3180	-0.75	19.51	49.40
3360	-0.75	20.47	52.20
4200	-0.75	24.97	65.30
4320	-0.75	26.16	67.18

Average Current Efficiency = 78.5%

Run 200A pH = 5.1 Temperature = 2.8°C Current = 200 ma

300	-0.98	1.69	6.22
660	-0.97	5.00	13.68
1080	-0.96	8.40	22.38
1620	-0.97	12.87	33.58
2040	-0.96	16.44	42.30
2700	-0.96	21.46	55.92

Average Current Efficiency = 77.2%

TABLE 13

THERMAL DECOMPOSITION STUDIES. DITHIONITE CONCENTRATION VS TIME AT 60°C

T 60A		T 60B		T 60C	
θ, Sec	$S_2O_4^=$ x 10^3 Moles/Liter	θ, Sec	$S_2O_4^=$ x 10^3 Moles/Liter	θ, Sec	$S_2O_4^=$ x 10^3 Moles/Liter
105	10.75	68	10.14	89	9.23
258	10.33	145	9.52	220	8.80
375	10.63	265	9.74	267	9.20
573	9.89	390	9.44	343	8.85
708	9.49	488	9.45	480	9.18
993	9.45	582	9.45	567	7.92
1065	9.77	742	9.27	644	9.05
1218	9.83	870	9.23	757	8.50
1479	8.94	1036	8.50	823	8.60
1595	8.51	1164	8.62	882	8.20
1856	7.74	1368	7.11	1005	8.20
2040	4.37	1515	6.61	1058	8.03
2225	0.05	1716	6.73	1244	7.78
		1863	5.32	1317	7.93
		2036	1.53	1375	6.57
		2050	0.03	1433	6.36
				1496	7.27
				1551	7.86
				1610	8.20
				1669	7.61
				1727	6.50
				1915	8.32
				1971	7.02
				2139	6.29
				2383	6.50
				2438	5.71
				2487	5.27
				2624	5.90
				2788	4.93
				3019	3.78
				3233	2.18
				3340	0.03

TABLE 13 (CONTINUED)

T 60D		T 60E	
θ, Sec	$S_2O_4^{=}$ x 10^3 Moles/Liter	θ, Sec	$S_2O_4^{=}$ x 10^3 Moles/Liter
74	8.38	58	5.98
272	8.32	250	5.68
350	7.72	336	5.76
460	8.43	461	5.58
606	7.93	594	5.67
694	7.97	681	5.41
786	7.46	807	5.28
893	7.47	900	5.32
994	7.02	1150	5.35
1071	7.10	1365	5.35
1171	7.37	1512	4.46
1251	7.08	1700	5.05
1437	6.42	1983	5.17
1500	7.00	2155	5.21
1571	7.02	2324	5.51
1644	6.62	2572	4.52
1712	5.10	2665	4.92
1803	6.31	2810	5.04
1886	6.42	2947	4.74
1976	5.80	3400	4.36
2111	6.32	3480	4.27
2178	6.23	3585	4.24
2250	6.36	3685	4.07
2324	4.18	3950	3.43
2441	5.55	4059	3.20
2508	5.22	4255	2.74
2570	5.94	4587	2.17
2665	4.60	5025	1.13
2739	4.62		
2854	4.06		
2977	3.19		
3030	2.95		
3089	2.26		
3148	1.45		

TABLE 14

THERMAL DECOMPOSITION STUDIES. DITHIONITE CONCENTRATION VS TIME AT 70°C

T 70A

θ, Sec	$S_2O_4^=$ x 10^3 Moles/Liter
55	11.23
176	10.92
340	10.26
450	10.18
648	8.96
785	8.84
950	7.80
1057	6.10
1175	1.40
1240	-

T 70B

θ, Sec	$S_2O_4^=$ x 10^3 Moles/Liter
75	9.40
190	9.54
342	9.12
455	9.14
610	8.63
750	8.41
900	7.64
1040	7.21
1170	6.16
1285	4.42
1360	1.45
1445	-

T 70C

θ, Sec	$S_2O_4^=$ x 10^3 Moles/Liter
75	6.06
200	5.52
352	5.56
570	5.52
690	5.22
795	5.04
955	5.03
1085	4.71
1225	4.81
1350	4.36
1475	4.07
1620	3.22
1728	3.36
1835	2.85
1940	1.96
2125	-

T 70D

θ, Sec	$S_2O_4^=$ x 10^3 Moles/Liter
60	5.71
175	5.66
316	5.31
475	5.36
618	4.85
750	4.84
875	4.78
1030	4.70
1155	4.58
1235	4.41
1360	4.25
1525	3.83
1627	3.25
1732	3.08
1812	2.26
1892	1.33
1993	0.35
2025	-

TABLE 15

THERMAL DECOMPOSITION STUDIES. DITHIONITE CONCENTRATION VS TIME AT 80°C

Run T 80A

θ, Sec	$S_2O_4^=$ x 10^3 Moles/Liter
70	10.37
237	9.76
385	9.05
465	8.56
585	7.09
670	5.17
735	1.20
840	-

Run T 80B

θ, Sec	$S_2O_4^=$ x 10^3 Moles/Liter
45	9.05
120	8.82
265	8.48
345	8.17
465	7.55
540	7.37
660	6.71
740	6.05
828	5.45
935	3.39
1005	-

Run T 80C

θ, Sec	$S_2O_4^=$ x 10^3 Moles/Liter
65	6.35
230	5.95
375	5.78
452	5.44
560	5.07
738	4.42
882	3.55
975	2.67
1120	0.49
1195	-

Run T 80D

θ, Sec	$S_2O_4^=$ x 10^3 Moles/Liter
70	6.42
150	6.09
240	6.06
402	5.89
480	5.40
570	5.11
720	4.78
800	4.43
875	4.14
970	3.35
1100	1.60
1175	0.29
1240	-

TABLE 16

THERMAL DECOMPOSITION STUDIES. DITHIONITE CONCENTRATION VS TIME IN BUFFERED SYSTEMS AT 60°C

Run TB 60C pH = 6.00

θ, Sec	$S_2O_4^=$ x 10^3 Moles/Liter
88	11.35
215	11.45
554	11.00
1108	10.86
2095	9.32
2740	0.09

Run TB 60D pH = 5.50

θ, Sec	$S_2O_4^=$ x 10^3 Moles/Liter
70	10.96
164	11.18
350	10.60
532	10.52
728	10.53
1074	9.43
1230	8.39
1338	5.82
1456	0.03

Run TB 60E pH = 5.00

θ, Sec	$S_2O_4^=$ x 10^3 Moles/Liter
55	10.99
126	10.84
202	10.20
258	9.57
346	7.70
417	0.08

Run TB 60F pH = 5.00

θ, Sec	$S_2O_4^=$ x 10^3 Moles/Liter
50	10.90
117	10.62
187	10.59
318	8.70
378	4.76
400	0.04

Run TB 60G pH = 4.80

θ, Sec	$S_2O_4^=$ x 10^3 Moles/Liter
41	10.81
91	10.91
145	10.70
203	8.86
244	0.04

Run TB 60H pH = 5.00

θ, Sec	$S_2O_4^=$ x 10^3 Moles/Liter
68	9.47
142	9.55
218	8.75
304	7.97
401	6.81
493	0.09

TABLE 17

THERMAL DECOMPOSITION STUDIES. H^+ CONCENTRATION VS TIME AT 60° AND 70°C

Run T 60A		Run T 70C	
θ, Sec	$H^+ \times 10^7$ Moles/Liter	θ, Sec	$H^+ \times 10^7$ Moles/Liter
170	7.95	30	7.95
290	7.75	140	8.73
340	7.75	220	8.73
410	7.75	300	8.32
525	11.20	400	7.57
540	11.50	610	6.58
610	12.60	730	6.58
670	11.75	850	6.44
760	11.00	980	6.30
810	11.00	1140	5.87
890	17.75	1295	5.87
910	18.60	1410	5.74
930	19.10	1540	5.62
990	17.75	1685	5.74
1050	17.35	1755	6.00
1120	15.50	1855	6.30
1185	14.10	1950	6.90
1210	13.80	2140	10.50
1275	12.00	2210	12.90
1330	11.75	2325	12.90
1410	11.50		
1435	11.20		
1570	11.00		
1540	10.70		
1660	10.00		
1750	10.00		
1820	10.00		
1900	10.70		
1930	11.20		
1980	11.50		
2060	13.80		
2130	22.50		
2210	23.80		
2251	24.80		
2320	27.80		
2357	25.80		
2475	27.80		

TABLE 18

THERMAL DECOMPOSITION STUDIES. EFFECT OF O_2 ON H^+ IN UNBUFFERED SYSTEM AT 60°C

Run T 60F $C_o = 9.28 \times 10^{-3}$ Moles/Liter

(Continued)

θ, Sec	$H^+ \times 10^7$ Moles/Liter	θ, Sec	$H^+ \times 10^7$ Moles/Liter
150	4.80	3200	14.75
300	4.90	3290	14.75
550	4.90	3300	air injected (10cc)
750	5.15	3320	21.45
950	5.15	3350	31.60
1100	5.15	3360	37.22
1300	5.25	3400	43.50
1450	5.37	3450	42.55
1650	5.37	3500	37.22
1950	5.25	3550	31.60
2050	5.25	3600	26.80
2150	5.37	3650	24.65
2550	5.37	3700	21.95
2560	air injected (2cc)	3750	20.90
2600	5.87	3800	20.50
2650	6.90	3850	21.95
2700	7.10	3900	37.22
2750	7.40	3950	48.90
2800	7.60	4000	57.25
2900	7.60	4050	66.20
2970	air injected (10cc)	4100	72.25
2990	7.95	4150	77.50
3000	11.20	4200	83.25
3050	13.45	4250	87.30
3100	14.10	4300	89.35
3150	14.45	4350	93.70

TABLE 19

THERMAL DECOMPOSITION STUDIES. EFFECTS OF H^+ ON INDUCTION PERIOD TIME, AND $\left[\frac{dc}{d\theta}\right]_o$ VS H^+ AT 60^oC AND $C_o = 11.0 \times 10^{-3}$ MOLES/LITER

Run	$H^+ \times 10^7$ Moles/Liter	Time of Induction Period, Sec	$\left[\frac{dc}{d\theta}\right]_o \times 10^7 \frac{\text{Moles}}{\text{Liter}}\ \text{sec}^{-1}$
TB 60A	1	Not measured	2.2
TB 60C	10	2200	6.8
TB 60D	31.6	800	9.1
TB 60E & F	100	275	26.9
TB 60G	158.2	180	29.1

TABLE 20

THERMAL DECOMPOSITION STUDIES. EFFECTS OF ADDITIVES.
DITHIONITE CONCENTRATION VS TIME AT
60°C IN SYSTEM BUFFERED AT pH 7

Run TB 60A		Run TB 60B	
θ, Sec	$S_2O_4^{=}$ x 10^3 Moles/Liter	θ, Sec	$S_2O_4^{=}$ x 10^3 Moles/Liter
112	11.10	94	10.35
241	10.40	299	10.00
599	10.29	946	9.94
1044	10.64	1621	9.90
1694	9.90	2129	10.21
2781	9.85	2845	10.41
4281	10.32	4476	9.89
6178	9.52	6434	9.56
11297	8.41	7073	9.45
13754	8.24	8863	9.46
14965	8.21	9878	9.29
		13162	8.38

TABLE 21

THERMAL DECOMPOSITION STUDIES. EFFECTS OF END PRODUCTS.
DITHIONITE CONCENTRATION VS TIME AT
60°C IN SYSTEM BUFFERED AT pH 5

Run TB 60Ja

θ, Sec	$S_2O_4^=$ x 10^3 Moles/Liter
42	5.16
97	5.10
155	4.86
209	4.64
271	4.95
337	4.76
392	3.50
469	4.41
565	3.72
682	-

Run TB 60Jb

θ, Sec	$S_2O_4^=$ x 10^3 Moles/Liter
39	5.45
115	4.97
216	2.66
293	-

Run TB 60Jc

θ, Sec	$S_2O_4^=$ x 10^3 Moles/Liter
40	5.60
95	3.49
167	3.75
224	-

Run TB 60Ka

θ, Sec	$S_2O_4^=$ x 10^3 Moles/Liter
44	5.51
91	5.30
148	4.80
202	4.58
256	4.90
306	4.43
365	3.46
419	4.61
481	4.32
538	3.79
601	3.14
671	-

Run TB 60Kb

θ, Sec	$S_2O_4^=$ x 10^3 Moles/Liter
38	5.71
89	3.94
147	4.81
193	4.54
262	1.53
334	-

Run TB 60Kc

θ, Sec	$S_2O_4^=$ x 10^3 Moles/Liter
40	5.86
89	5.51
145	4.51
197	2.06
256	-

TABLE 22

THERMAL DECOMPOSITION STUDIES. END PRODUCT ANALYSIS OF 30°C RUN

Initial Dithionite Concentration = 7.32×10^{-3} Moles/Liter

Final HSO_3^- Concentration = 7.32×10^{-3} Moles/Liter

Final $S_2O_3^=$ Concentration = 3.32×10^{-3} Moles/Liter

Ratio of $HSO_3^-/S_2O_3^=$ = 2.2

Sulfur Balance:

Sulfur in = 14.64×10^{-3} Moles/Liter

Sulfur out = 7.32×10^{-3}
$+6.64 \times 10^{-3}$
13.96×10^{-3} Moles/Liter

Sulfur unaccounted for = 0.68 Moles/Liter

Therefore, % of dithionite forming other products

$$= \frac{0.34 \times 10^{-3}}{7.38 \times 10^{-3}} \times 100 = 4.6\%$$

TABLE 23

THERMAL DECOMPOSITION STUDIES. DETERMINATION OF ORDER OF REACTION, n, IN UNBUFFERED SYSTEMS. $(dc/d\theta)_o$ VS C_o AT 60, 70, AND 80°C

Run	Temperature °C	$C_o \times 10^3$ Moles/liter	$(dc/d\theta)_o \times 10^7$ Moles/liter, Sec^{-1}
T 60A	60	10.85	10.32
T 60B	60	9.90	8.98
T 60C	60	9.25	8.28
T 60D	60	8.67	7.35
T 60E	60	6.00	4.05
T 70A	70	11.38	26.2
T 70B	70	9.78	17.3
T 70C	70	6.02	8.96
T 70D	70	5.72	8.58
T 80A	80	10.58	31.5
T 80B	80	9.17	24.4
T 80C	80	6.50	15.1
T 80D	80	6.42	12.3

TABLE 24

THERMAL DECOMPOSITION STUDIES. DETERMINATION OF ORDER OF REACTION, n , IN SYSTEM BUFFERED AT pH 5. $(dc/d\theta)_o$ VS C_o AT 60°C

Run	$C_o \times 10^3$ Moles/Liter	$(dc/d\theta)_o \times 10^7$ (Moles/Liter)(Sec^{-1})
TB 60 E & F	11.05	26.9
TB 60H	9.95	25.2
TB 60J	5.40	9.1

TABLE 25

THERMAL DECOMPOSITION STUDIES

k_c VS C_o AT 60, 70, AND 80°C

Run	Temperature °C	$C_o \times 10^3$ Moles/Liter	k_c $\frac{\text{Moles}}{\text{Liter}}^{-1}$ Sec^{-1}
T 60A	60	10.85	1.70
T 60B	60	9.90	1.70
T 60C	60	9.25	1.60
T 60D	60	8.67	1.70
T 60E	60	6.00	1.62
	$[H^+]_{o(avg)}^{\frac{1}{2}}$	$= 5.38 \times 10^{-4}$ Moles/Liter	$k_{c(avg)} = 1.67$ $\frac{\text{Moles}}{\text{Liter}}^{-1}$ Sec^{-1}
T 70A	70	11.38	3.09
T 70B	70	9.78	2.56
T 70C	70	6.02	2.75
T 70D	70	5.72	2.84
	$[H^+]_{o(avg)}^{\frac{1}{2}}$	$= 6.98 \times 10^{-4}$ Moles/Liter	$k_{c(avg)} = 2.81$ $\frac{\text{Moles}}{\text{Liter}}^{-1}$ Sec^{-1}
T 80A	80	10.58	4.67
T 80B	80	9.17	4.49
T 80C	80	6.50	4.65
T 80D	80	6.42	3.86
	$[H^+]_{o(avg)}^{\frac{1}{2}}$	$= 6.20 \times 10^{-4}$ Moles/Liter	$k_{c(avg)} = 4.38$ $\frac{\text{Moles}}{\text{Liter}}^{-1}$ Sec^{-1}

TABLE 26

THERMAL DECOMPOSITION STUDIES. $(C_o - C)$ VS TIME AT 60, 70, AND 80°C

Run T 60A $C_o = 10.85 \times 10^{-3}$ moles/liter Run T 60B $C_o = 10.00 \times 10^{-3}$ moles/liter

Sec	$C_o - C$ $\times 10^3$	C $\times 10^3$	Sec	$C_o - C$ $\times 10^3$	C $\times 10^3$
0	0	10.85	0	0	10.00
100	0.10	10.75	100	0.11	9.89
200	0.22	10.63	200	0.21	9.79
300	0.33	10.52	300	0.30	9.70
400	0.44	10.41	400	0.40	9.60
500	0.55	10.30	500	0.50	9.50
600	0.67	10.18	600	0.60	9.40
700	0.80	10.05	700	0.70	9.30
800	0.93	9.92	800	0.84	9.16
900	1.07	9.78	900	1.00	9.00
1000	1.22	9.63	1000	1.16	8.84
1100	1.37	9.48	1100	1.35	8.65
1200	1.55	9.30	1200	1.58	8.42
1300	1.72	9.13	1300	1.84	8.16
1400	1.93	8.92	1400	2.14	7.86
1500	2.19	8.66	1500	2.50	7.50
1600	2.52	8.33	1600	2.94	7.06
1700	2.91	7.94	1700	3.48	6.52
1800	3.40	7.45	1800	4.20	5.80
1900	4.05	6.80	1900	5.25	4.75
2000	4.90	5.95	2000	7.15	2.85
2100	6.30	4.55	2100	10.00	0.00
2200	10.85	0.00			

TABLE 26 (CONTINUED)

$(C_o - C)$ VS TIME AT 60, 70, AND 80°C

Run T 60C

Sec	$C_o - C$ x 10^3	C x 10^3
0	0	9.20
200	0.19	9.01
400	0.35	8.85
600	0.54	8.66
800	0.72	8.48
1000	0.92	8.28
1200	1.16	8.04
1400	1.40	7.80
1600	1.65	7.55
1800	1.95	7.25
2000	2.28	6.92
2200	2.65	6.55
2400	3.09	6.11
2600	3.60	5.60
2800	4.30	4.90
3000	5.25	3.95
3200	6.68	2.52
3400	9.20	0.00

Run T 60D

Sec	$C_o - C$ x 10^3	C x 10^3
0	0	8.50
200	0.15	8.35
400	0.33	8.17
600	0.53	7.97
800	0.75	7.75
1000	1.00	7.50
1200	1.27	7.23
1400	1.52	6.98
1600	1.80	6.70
1800	2.10	6.40
2000	2.40	6.10
2200	2.72	5.78
2400	3.12	5.38
2600	3.60	4.90
2800	4.25	4.25
3000	5.25	3.25
3200	7.50	1.00
3400	8.50	0.00

Run T 60E

Sec	$C_o - C$ x 10^3	C x 10^3
0	0	6.00
200	0.10	5.90
400	0.20	5.80
600	0.29	5.71
800	0.38	5.62
1000	0.42	5.58
1200	0.50	5.50
1400	0.58	5.42
1600	0.65	5.35
1800	0.72	5.28
2000	0.80	5.20
2200	0.90	5.10
2400	1.00	5.00
2600	1.10	4.90
2800	1.22	4.78
3000	1.35	4.65
3200	1.49	4.51
3400	1.63	4.37
3600	1.83	4.17
3800	2.11	3.89
4000	2.48	3.52
4200	2.86	3.14
4400	3.30	2.70
4600	3.80	2.20
4800	4.30	1.70
5000	4.87	1.13

TABLE 26 (CONTINUED)

$(C_o - C)$ VS TIME AT 60, 70, AND 80°C

Run T 70A $C_o = 11.38 \times 10^{-3}$ moles/liter

Sec	$C_o - C$ $\times 10^3$	C $\times 10^3$
0	0	11.38
100	0.28	11.10
200	0.55	10.83
300	0.85	10.53
400	1.17	10.21
500	1.49	9.89
600	1.86	9.52
700	2.24	9.14
800	2.62	8.76
850	2.88	8.50
900	3.23	8.15
950	3.80	7.68
1000	4.35	7.03
1050	5.23	6.15
1100	6.38	5.00
1150	8.28	3.10

Run T 70B $C_o = 9.78 \times 10^{-3}$ moles/liter

Sec	$C_o - C$ $\times 10^3$	C $\times 10^3$
0	0	9.78
100	0.18	9.60
200	0.36	9.42
300	0.53	9.25
400	0.72	9.06
500	0.90	8.88
600	1.09	8.69
700	1.31	8.47
800	1.58	8.20
900	1.94	7.84
1000	2.36	7.42
1100	2.88	6.90
1150	3.29	6.49
1200	3.86	5.92
1250	4.66	5.12
1300	5.78	4.00
1350	7.78	5.00

Run T 70C $C_o = 6.02 \times 10^{-3}$ moles/liter

Sec	$C_o - C$ $\times 10^3$	C $\times 10^3$
0	0	6.02
200	0.20	5.82
400	0.39	5.63
600	0.61	5.41
800	0.82	5.20
1000	1.10	4.92
1100	1.23	4.79
1200	1.39	4.63
1300	1.55	4.47
1400	1.74	4.28
1500	1.99	4.03
1550	2.11	3.91
1600	2.24	3.78
1650	2.41	3.61
1700	2.57	3.45
1750	2.77	3.25
1800	3.02	3.00
1850	3.32	2.70

Run T 70D $C_o = 5.72 \times 10^{-3}$ moles/liter

Sec	$C_o - C$ $\times 10^3$	C $\times 10^3$
0	0	5.72
200	0.15	5.57
400	0.33	4.29
600	0.53	5.19
800	0.75	4.97
1000	1.02	4.70
1100	1.16	4.56
1200	1.32	4.40
1300	1.48	4.24
1400	1.65	4.07
1500	1.88	3.84
1550	2.02	3.70
1600	3.18	3.54
1650	2.37	3.35
1700	2.56	3.16
1750	2.82	2.90
1800	3.12	2.60
1850	3.50	2.22
1900	3.95	1.77
1950	4.64	1.98

TABLE 26 (CONTINUED)

$(C_o - C)$ VS TIME AT 60, 70, 80°C

Run T 80A $C_o = 10.58 \times 10^{-3}$ moles/liter Run T 80B $C_o = 9.17 \times 10^{-3}$ moles/liter

θ Sec	$C_o - C$ $\times 10^3$ moles/liter	C $\times 10^3$ moles/liter	θ Sec	$C_o - C$ $\times 10^3$ moles/liter	C $\times 10^3$ moles/liter
0	0	10.58	0	0	9.17
50	0.16	10.52	50	0.14	9.03
100	0.31	10.27	100	0.26	8.91
150	0.50	10.08	150	0.38	8.79
200	0.68	9.90	200	0.53	8.64
250	0.88	9.70	250	0.68	8.49
300	1.08	9.50	300	0.84	8.33
350	1.32	9.26	350	0.99	8.18
400	1.61	8.97	400	1.18	7.99
450	1.98	8.60	450	1.37	7.80
500	2.43	8.15	500	1.59	7.58
550	2.99	7.59	550	1.85	7.32
600	3.78	6.80	600	2.13	7.04
650	4.88	5.70	650	2.44	6.73
700	6.60	3.98	700	2.77	6.40
725	8.21	2.37	750	3.17	6.00
740	10.58	0	800	3.67	5.50
			850	4.26	4.91
			900	5.05	4.12
			950	6.18	2.99
			975	7.01	2.16
			1000	8.42	0.75

TABLE 26 (CONTINUED)

$(C_o - C)$ VS TIME AT 60, 70, 80°C

Run T 80C $C_o = 6.50 \times 10^{-3}$ moles/liter Run T 80D $C_o = 6.42 \times 10^{-3}$ moles/liter

Sec	$C_o - C$ $\times 10^3$	C $\times 10^3$	Sec	$C_o - C$ $\times 10^3$	C $\times 10^3$
0	0	6.50	0	0	6.42
50	0.15	6.35	50	0.04	6.38
100	0.25	6.25	100	0.12	6.30
150	0.35	6.15	150	0.18	6.24
200	0.45	6.05	200	0.24	6.18
250	0.53	5.97	250	0.32	6.10
300	0.64	5.86	300	0.41	6.01
350	0.76	5.74	350	0.50	5.92
400	0.89	5.61	400	0.60	5.82
450	1.01	5.49	450	0.70	5.72
500	1.15	5.35	500	0.82	5.60
550	1.30	5.20	550	0.94	5.48
600	1.48	5.02	600	1.10	5.32
650	1.67	4.83	650	1.26	5.16
700	1.89	4.61	700	1.45	4.97
750	2.11	4.39	750	1.67	4.75
800	2.40	4.10	800	1.92	4.50
850	2.71	3.79	850	2.22	4.20
900	3.07	3.43	900	2.54	3.88
950	3.50	3.00	950	2.94	3.48
1000	4.00	2.50	1000	3.42	3.00
1050	4.63	1.98	1050	4.04	2.38
1100	5.52	0.98	1100	4.82	1.60
			1150	5.67	0.75
			1190	6.42	0

SECTION I

APPENDIX I

TABLE 1A

COMPOSITION OF THE BUFFER SOLUTIONS

TOTAL VOLUME OF WATER SOLUTION = 1000 cc

Acid Salt	Weight of Acid-Salt grams	Weight of NaOH grams	pH
KH_2PO_4	6.800	1.190	7.0
KH_2PO_4	6.800	0.228	6.0
$KHC_8H_4O_4$	10.220	1.506	5.5
$KHC_8H_4O_4$	10.220	0.954	5.0
$KHC_8H_4O_4$	10.220	0.708	4.8
$KHC_8H_4O_4$	10.220	0.160	4.0

TABLE IIA

AIR OXIDATION STUDIES
EFFECT OF PURE OXYGEN ON RATE.
DITHIONITE CONCENTRATION VS TIME AT 30°C

Run 30F

θ, Sec	$S_2O_4^=$ x 10^3 Moles/Liter
0	12.6
14	10.80
46	6.46
85	1.63
126	0.0

Run 30G

θ, Sec	$S_2O_4^=$ x 10^3 Moles/Liter
0	12.6
23	8.27
52	5.37
82	0.88
118	0.0

Run 30H

θ, Sec	$S_2O_4^=$ x 10^3 Moles/Liter
0	19.3
19	15.01
36	11.62
56	6.79
75	3.52
98	1.09
135	0.0

Run 30J

θ, Sec	$S_2O_4^=$ x 10^3 Moles/Liter
0	19.3
11	16.11
29	11.80
49	8.71
70	4.94
94	1.56
115	0.43
138	0.0

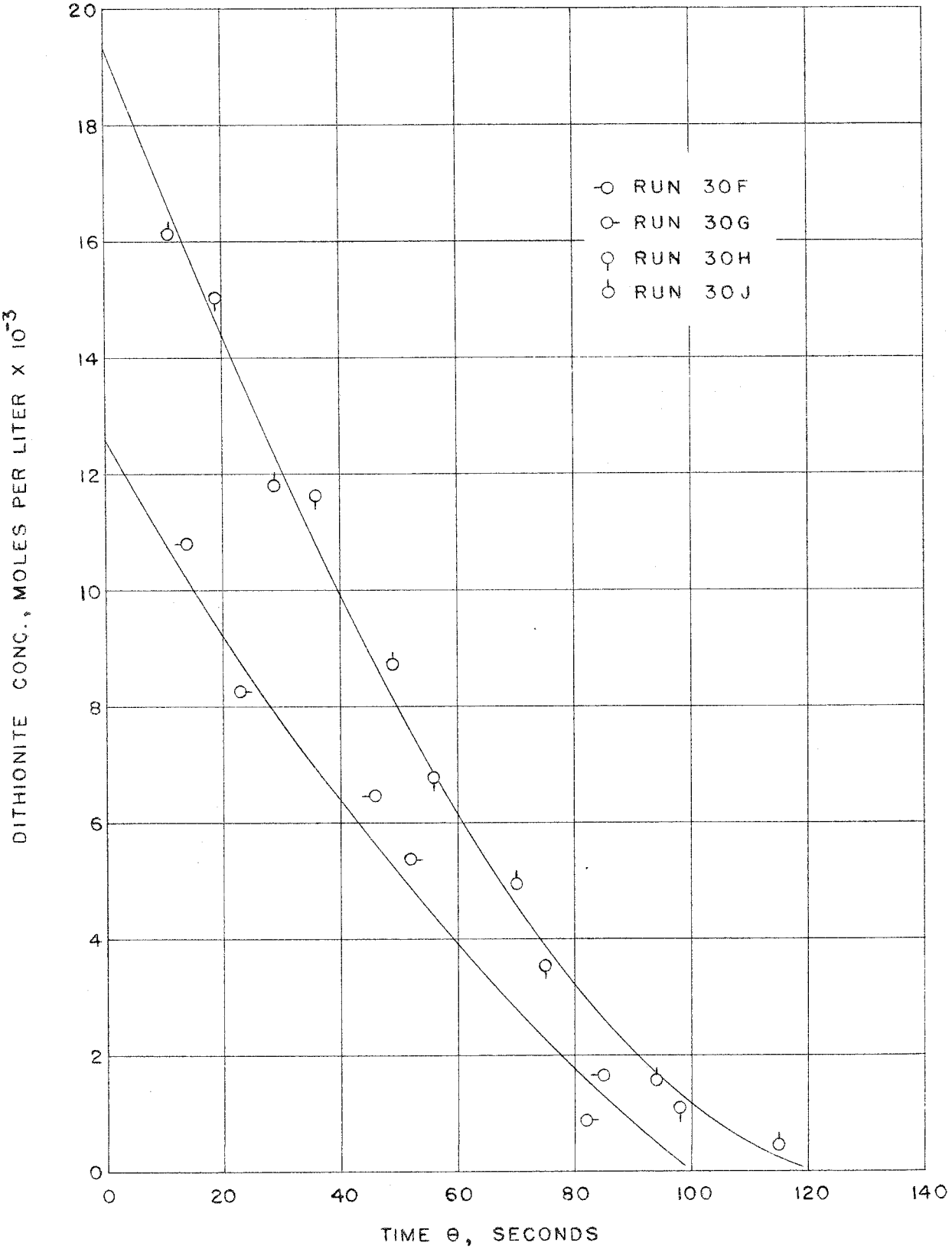

Figure IA--Air Oxidation Studies. Effect of Pure Oxygen on Rate. Dithionite Concentration vs Time at 30°C

SECTION II

A PRELIMINARY STUDY OF THE CATALYZED ADDITION OF HYDROGEN CHLORIDE TO VINYL CHLORIDE IN A STIRRED REACTOR

INTRODUCTION

Review of the Chemical and Kinetic Studies in Reactions between Hydrogen Halides and Vinyl Halides

Probably the first systematic study of the general behavior and conditions for the addition of hydrogen halides to vinyl halides was conducted in 1930 by Wibaut, et al (1,2,3). Since his work was rather extensive, only that portion pertaining to the addition reaction between hydrogen chloride (HCl) and vinyl chloride (CH_2CHCl) or acetylene (C_2H_2) is discussed here. His experiments consisted of passing a gaseous mixture of hydrogen chloride and either vinyl chloride or acetylene through a tube reactor filled with solid catalyst. The depth of the catalyst layer was maintained nearly constant at 55 cm in the reactor which consisted of a glass tube 80 cm long and 25 mm inside diameter, giving a reactor volume of 0.39 liter.

In all cases, at temperatures ranging from 25 to 200°C, the addition reaction was found to be very slow when the tube packing consisted of catalyst carriers such as silica gel, charcoal, glass wool and asbestos fiber. To improve the rate of addition of the HCl to acetylene, the silica gel carrier was impregnated with $HgCl_2$. (For all the experiments, the same amount of catalyst was used, namely 220 gm, containing 0.1 gm mole of an anhydrous metallic chloride per 100 gm of carrier.) The formation of vinyl chloride, which was the main

product of reaction, occurred rapidly at 25°C and higher. Only a small amount of 1,1 dichloroethane (CH_3CHCl_2) was formed as a by-product even when the HCl was added to the feed stream in large excess. A brief tabulation of the results of this experiment is presented below:

Rate of Flow of Acetylene = 1.5 liters/hr.

Rate of Flow of HCl = 2.2 liters/hr.

Temperature °C	Volume C_2H_2 Liters	% Yield of * Vinyl Chloride	% Yield of ** 1,1 Dichloroethane
25	5.1	93	3
80	7.2	93	3
110	4.7	90	2
195	6.5	98	1

* Based on the molar conversion of acetylene.

** Based on the molar conversion of vinyl chloride.

In order to determine the relative yields of the two separate reactions, namely,

(1) $C_2H_2 + HCl \longrightarrow CH_2 : CHCl$ and

(2) $CH_2 : CHCl + HCl \longrightarrow CH_3CHCl_2$,

Wibaut performed experiments under identical conditions of temperature, rate of gas flow, and type of catalyst. These results are briefly listed as follows:

Temperature = 100°C

Rate of Flow of Acetylene or Vinyl Chloride = 1.5 liters/hr.

Rate of Flow of HCl = 2.2 liters/hr.

Catalyst on Silica Gel	% Yield of Vinyl Chloride from Acetylene and HCl	% Yield of 1,1 Dichloroethane from Vinyl Chloride and HCl
$HgCl_2$	95	11
$BiCl_3$	18	18
$FeCl_3$	3.7	13
$ZnCl_2$	15	66

From this experiment, Wibaut concluded that $HgCl_2$ was a good catalyst for the addition of HCl to acetylene but had only a slight influence on the rate of addition to HCl to vinyl chloride. On the other hand, $ZnCl_2$ was a good catalyst for the second reaction whereas the first reaction proceeded at a low rate in its presence. Ferric chloride catalyzed both reactions but favored the addition of HCl to vinyl chloride. According to Wibaut's conclusions, the $FeCl_3$ had a much lower activity in comparison to the $HgCl_2$ and $ZnCl_2$. This conclusion, however, is questionable in light of the present work because Wibaut did not correct for loss of activity due to fouling. Finally, in the presence of $BiCl_3$, the yields of both reactions were practically the same.

Wibaut's final experiment was to determine the effect of temperature on the relative yields of the two reactions in the presence of different catalysts. The following is a convenient

summary of the experimental results he obtained.

Rate of Flow of Acetylene or Vinyl Chloride = 1.5 liters/hr.

Rate of Flow of HCl = 2.2 liters/hr.

Catalyst	Temperature °C	% Yield of Vinyl Chloride from Acetylene and HCl	% Yield of 1,1 Dichloroethane from Vinyl Chloride and HCl
$HgCl_2$ - Charcoal	155	84	16.5
$HgCl_2$ - Silica Gel	165	100	9
$BiCl_3$ - Silica Gel	165	42	-
$BiCl_3$ - Silica Gel	148	-	9
$FeCl_3$ - Silica Gel	200	4.5	9

This experiment showed that $HgCl_2$ and $BiCl_3$ gave excellent yields at various temperatures in the reaction between HCl and acetylene. For the reaction between HCl and vinyl chloride, the catalysts $FeCl_3$ and $BiCl_3$ gave low yields, which could probably be attributed to their loss of activity within a short period of time.

The fact that addition of HCl to vinyl chloride occurred with some difficulty even in the presence of catalysts, while HBr and vinyl bromide (not discussed above) reacted rapidly on the surface of asbestos or glass wool, was convincing evidence to Wibaut that in general HCl reacts more slowly with alkenes than HBr. Perhaps more significant was the fact that independent of the temperature and of the nature of the catalyst,

the only product of the reaction between HCl and vinyl chloride was 1,1 dichloroethane. This suggested to him that the course of the addition reaction was governed by directed adsorption at the catalyst surface.

Between 1928 and 1940, Kharasch, et al (4,5,6,7,8,9,10,11) conducted a long series of comparative experiments pertaining to the mechanism of the addition reactions of HCl, HBr and HI to vinyl chloride. The important results of this work are briefly discussed here.

1. The Peroxide Effect

The peroxide content of a vinyl chloride-hydrogen bromide mixture was the most important single factor governing the direction and velocity of the resultant addition reaction. In the absence of a solvent or a good antioxidant, the addition of HBr to vinyl chloride resulted in a rapid, nearly quantitative, formation of the abnormal product, 1-bromo-2-chloroethane (CH_2BrCH_2Cl). On the other hand, the addition of HCl or HI to vinyl chloride under similar conditions was not affected in direction or velocity by the peroxide content. The normal products, 1,1 dichloroethane and 1-iodo-1-chloroethane (CH_3CHICl) were formed; but the hydrogen chloride added very slowly at room temperature whereas the addition of hydrogen iodide occurred rapidly.

2. The Antioxidant Effect.

When an antioxidant was added to the reacting mixture of HBr and vinyl chloride, the normal product 1-bromo-1-chloro-

ethane was predominantly formed. Some of the most effective antioxidants were p-thiocresol, diphenylamine, a mixture of t-butylcarbylamine and diphenylamine, and a mixture of t-butylcarbylamine and p-thiocresol. It was interesting to note that the velocity of the reaction in the presence of t-butylcarbylamine was increased by four- or five-fold. Antioxidants had practically no effect on the addition reactions of HCl or HI with vinyl chloride.

3. The Catalyst Effect.

In the presence of a catalyst, such as $FeCl_3$, the peroxide effect was destroyed, and nearly quantitative yields of 1-bromo-1-chloroethane resulted from the mixture of HBr and vinyl chloride. Ferric chloride increased tremendously the rate of HCl addition, but the 1,1 product was still formed. Hence, the results of the catalyzed reactions were in substantial agreement with the results that Wibaut obtained.

A tabulated summary of Kharasch's experiments is presented in Table 1A of Appendix I.

Kharasch arrived at several generalizations from his experiments. First of all, the additions of HCl and HI to double bonds, although different in rate, occur by similar mechanisms which do not involve chain reactions. On the other hand, the addition of HBr involves chains in which Br is the chain carrier. Secondly, the effect of the peroxides and metallic halides on the direction and/or rate of addition could be explained. Particularly, the addition of HCl with or without

$ZnCl_2$ or $FeCl_3$, and the addition of HBr with $FeCl_3$ to vinyl chloride were mechanistically equivalent to the normal uncatalyzed addition of HBr to vinyl chloride, i.e., 1-bromo-1-chloroethane. Hence, the addition of HCl to any ethylene derivative with or without catalysis would give only the normal addition product. It appeared evident to Kharasch that in these addition reactions, especially with HBr, antioxidants and metallic halides are negative and positive catalysts, respectively. Their concordant influence upon the direction of addition could be adequately explained by the thesis that the antioxidant retarded or suppressed the abnormal addition reaction, whereas the metallic halides accelerated the normal reaction.

Lonza (12) in 1944, reported a patented process for manufacturing 1,2 dichloroethane from the addition reaction between HCl and vinyl chloride. This was accomplished by charging a tube-reactor containing Raschig rings with $AlCl_3$ and aluminum-bronze suspended in liquid 1,2 dichloroethane on the surface of the rings. Gaseous vinyl chloride and HCl were passed through the column in a continuous stream. After separation of the product, the reactants were recycled. Apparently, the only impurity in the product was tri-chlorobutane with no detectable traces of 1,1 dichloroethane. It is interesting to note, here, that Lonza's results were in direct opposition to the results predicted from the generalizations of Kharasch and Wibaut.

Extensive experiments on the rate of thermal decomposition of 1,1 and 1,2 dichloroethane in a tube flow-reactor were conducted by Barton (13) in 1949. In a series of reactions involving the addition of small amounts of O_2 or Cl_2 to the feed, he observed that the rate of pyrolysis of the 1,2 dichloroethane was greatly increased whereas that of the 1,1 dichloroethane was unaffected. He concluded that in the case of the former compound, the mechanism of the pyrolysis was of the radical-chain type. Both reactions gave the same products, namely, vinyl chloride and HCl. Barton found that the 1,1 dichloroethane decomposed in the temperature range of 356-453°C by a homogeneous, first-order reaction. In the pressure range of 20-200 mm Hg, the rate constant varied with temperature according to the equation $k = 1.2 \times 10^{12} e^{-\frac{49,500}{RT}} \text{ sec}^{-1}$. Significantly, the frequency factor was close to the value 10^{13} usually expected for unimolecular decompositions. The complete absence of any inhibiting effect by propylene in the pyrolysis of 1,1 dichloroethane, together with the absence of an induction period and the excellent adherence to first-order kinetics well beyond the 50% decomposition point, proved conclusively to him that the mechanism of the 1,1 dichloroethane decomposition was quite different from that of 1,2 dichloroethane, namely, that it is not a radical-chain reaction.

In 1952, Howlett (14,15) studied the homogeneous decomposition of 1,1 dichloroethane and like Barton concluded that the reaction was unimolecular. He performed the pyrolysis experi-

ments in a batch reactor at 412, 433 and 449°C. At pressures above 4 mm of Hg, the first-order rate constant varied with temperature according to the equation, $k = 10^{11.65} e^{-\frac{48,300}{RT}}$ sec^{-1}. Below a pressure of 4 mm of Hg, the order with respect to 1,1 dichloroethane increased and became 1.5 at a pressure of 1 mm of Hg. The reaction was found to be insensitive toward O_2, Cl_2 and propene. These observations along with the fact that there was no induction period were strong evidence in favor of a unimolecular reaction.

Previous Reactor Systems

All the experiments described above were conducted in either batch reactors or continuous-flow tube reactors. Prior to the experiments described in the present work, no studies of the addition reactions between vinyl halides and hydrogen halides had been made in a continuous-flow stirred reactor. The use of the stirred reactor in general kinetic studies, however, is not a new concept. Denbigh's pioneering work (16,17, 18,19) beginning in 1944, showed that the instantaneous rate of a chemical reaction could be measured by balancing the reaction rate against a rate of flow of fluid in a steady-state, stirred reactor. By simple algebra, he equated the rate of reaction r, whether it be the formation of any reactant, any intermediate, or any product, to the quantity $\frac{u}{V}(C_o - C)$ where u is the constant flow rate of entering reactants into the stirred reactor of constant volume V. C is the concentration of the substance in the steady state system, and C_o

its concentration in the entering fluid. Denbigh extended the generality of this simple analysis by showing that its validity for any substance was not impaired by the presence of competing or consecutive reactions.

Previous Methods of Product Analysis for the Vinyl Halide-Hydrogen Halide Reactions

Wibaut (3) determined quantitatively the proportions of the reaction products by fractional distillation followed by purity checks on the separated fractions by means of boiling points or refractive indices.

Kharasch (9) eliminated the fractional distillation step. His first step was to remove the unsaturated products by chemical means followed by a determination of the boiling point or refractive index of the alkyl-halide mixture. The results of these latter measurements were compared with calibrated samples.

The uses of spectroscopic methods for the analysis of mixtures of vinyl halides, hydrogen halides and their addition products have not been reported in the literature. The infrared spectra of the individual components, however, are well documented (20,21).

The present experimental work was greatly facilitated by the use of gas-phase chromatography which provides a relatively accurate and rapid method of quantitative analysis. A number of publications have described types of columns and conditions of operation for the chromatographic analysis of systems which

contain individually or collectively the vinyl halides, hydrogen halides and/or the alkyl halides. A published report by Beckman Instruments, Inc. (22) is of particular value in this respect.

Present Work

The purpose of the present work was to extend the knowledge of reactions between vinyl halides and hydrogen halides by studying the addition of HCl to vinyl chloride from a kinetics standpoint. With this objective, the catalyzed reaction was studied in a stirred reactor, and the products were analyzed chromatographically.

SUMMARY

The catalyzed addition reaction between gaseous HCl and vinyl chloride was studied in a continuous-flow stirred reactor at 164, 215 and 299°F. Preliminary investigation showed that in the temperature range of 150 to 400°F the homogeneous rate, even in the presence of $FeCl_3$ vapor, was immeasurably low for retention times up to 12 hours. The catalyst used was $ZnCl_2$ supported on 1/8 in. Celite pellets in the ratio of 0.2 gm $ZnCl_2$/1.0 gm Celite. This choice was based upon tests performed in batch systems in which a variety of carriers and metallic halides were examined. Among the metallic halides tested, $FeCl_3$ showed a greater activity than $ZnCl_2$ but was deactivated, by fouling, much more rapidly than the latter.

The total flow rates through the stirred-reactor were varied from 2.0×10^{-3} to 27.4×10^{-3} lb/hr, corresponding to retention times of 11.2 to 0.76 hr, respectively. The ratio of vinyl chloride to HCl on a weight basis was varied from 2.16 to 2.46.

Starting with 120 gm of freshly prepared catalyst, the sequence of temperatures investigated was 215, 164 and 299°F, in that order. As predicted from the batch experiments, fouling of the catalyst by decomposition of the vinyl chloride was observed. The decreasing conversion at 215°F reached an asymptotic value greater than zero, which ruled out the possibility of irreversible single-site fouling. Further changes in the catalyst activity were not observed at 164°F but additional

fouling was observed at 299°F. The fact that one of the fouling products was elementary carbon or a carbonaceous residue suggested that an irreversible dual-site mechanism was in operation.

An empirical fit of the observed rate data was obtained by the equation,

$$r_{1,1} = C\left(p_{HCl}\, p_{v.c.} - \frac{p_{1,1}}{K_p}\right) \qquad (10a)$$

wherein $r_{1,1}$ was obtained from the equation,

$$r_{1,1} = \frac{F}{W}\ (n_{1,1}) \qquad (8)$$

Published values (30) of the thermodynamic equilibrium constant K, assuming unit activity coefficients, could not be used in Equation 10a to solve for C, because the experimentally observed conversions exceeded the predicted equilibrium values by a factor of nearly 20 in the initial runs. From data for the non-fouling period at 215°F, K_p was determined empirically by a least-squares analysis. The resulting value of 17.2 atm^{-1} was used in the Van't Hoff equation to determine K_p's at 164 and 299°F. The values obtained were 86.2 and 2.0 atm^{-1}, respectively.

Values of C were computed for both the fouling and non-fouling periods at each temperature. In terms of concentration units, the C's were plotted against catalyst-exposure time to obtain a fouling factor. Sufficient data were not available to compute the temperature dependence of the fouling factor.

Hence, its determination was limited to the results at 215°F. An equation which includes the effects of fouling and which can be used to predict the approximate conversion of 1,1 dichloroethane at 215°F was obtained as follows:

$$n_{1,1} = \frac{W}{F}\left[\frac{(0.589 + 10.341\, e^{f(t_e)})}{(RT)^2/M_{1,1}}\left(p_{HCl}\, p_{v.c.} - \frac{p_{1,1}}{17.2}\right) \times 10^2\right] \tag{13}$$

where

$$f(t_e) = (2.303)(0.001378\, t_e - 2.87278 \times 10^{-5}\, t_e^{\,2} + 4.2623 \times 10^{-8}\, t_e^{\,3} - 1.814 \times 10^{-11}\, t_e^{\,4}) \tag{12}$$

The average values of C_c for the non-fouling periods at 215 and 164°F and for the initial fouling period at 299°F were correlated with temperature by a straight-line fit on an Arrhenius plot. This linearity indicates that the second-order rate law given by Equation 10a describes, at least empirically, the behavior of the reacting system.

Based upon the hypothesis that C_c for the non-fouling periods obey an Arrhenius-type equation, a straight line was then drawn through the values of C_c at 215 and 299°F on an Arrhenius plot and extrapolated to 164°F. At that temperature, the extrapolation value of C_c is 16.5 (lb moles 1,1 dichloroethane)$(ft^3)^2$/(hr)(lb catalyst)(lb moles)^2.

From these results, the temperature dependence of C_c is given by the equation,

$$C_c = 4.07 \times 10^8 \, e^{-\frac{21,100}{RT}} \qquad (14)$$

Equation 14 can be combined with Equations 10a and 8 to give an expression for predicting the conversion during the non-fouling period.

$$n_{1,1} = \frac{W}{F}\left[\frac{(4.07 \times 10^8 \, e^{-\frac{21,100}{RT}})}{(RT)^2/M_{1,1}}\left(p_{HCl}\, p_{v.c.} - \frac{p_{1,1}}{K_p}\right)\right] \qquad (15)$$

Equation 15 is applicable under varying conditions of residence time for the temperature range of 164 to 299°F, for mass ratios of vinyl chloride to HCl in the range of 2.16 to 2.46, and for catalyst-exposure times up to 1800 hr. Small changes in total pressure would not be expected to noticeably affect the final, steady-state fouling.

An empirical test of the assumed second-order mechanism for the forward reaction indicated that exponents of 1 for p_{HCl} and $p_{v.c.}$ gave a minimum drift in C_c. This result, in addition to the fact that C_c was practically linear on an Arrhenius plot, suggested that the reaction was second order. It is probable that because of the relatively low rate of reaction, even in the presence of a catalyst, the addition occurred by a four-center-type mechanism. In this case, the catalyst $ZnCl_2$ increased the probability of reaction by orienting the reacting molecules.

APPARATUS

General

A simplified flow diagram of the experimental equipment is shown in Figure 1. This should be helpful to the reader in following the detailed discussion of the individual parts of the system.

The front view of the steel framework which contained the reactor and auxiliary equipment is shown in Figure 2A. As noted in the figure, this framework consisted of 3 compartments each of which served a specific purpose. One of the compartments contained the stirred reactor, a drive motor for the stirrer, an oil bath surrounding the reactor, and a sampling system on the exit line of the reactor. For safety reasons, the reactor compartment was equipped with steel doors. During operation, the doors were bolted shut and thus provided an explosion-proof enclosure.

The second compartment contained the purification and conditioning system for the feed streams and included also a vacuum manifold which could be connected to any portion of the entire apparatus.

Finally, the third compartment contained the thermostated oil-bath from which silicone oil was pumped to the reactor oil-bath through insulated pipe. The functions of the equipment in each compartment are discussed in greater detail in the paragraphs to follow.

An instrument bench shown in Figure 2B contained equipment for controlling and measuring temperatures.

Reactor and Accessories

The complete assembly of the glass reactor is shown in Figure 3. This six-liter vessel consisted of two parts, namely, a lower shell and a lid containing four entrance ports, one centrally located and the remaining three spaced 120° apart in a peripheral pattern. All four ports were 29/42 standard-taper fittings. A ground-glass flange on both the lid and shell provided a means of joining them to form a sealed vessel. To give a better seal and to allow for stress relief when the two parts were clamped together, a teflon gasket was inserted between the matched faces of the flanges.

As shown in the figure, the entire assembly was suspended from the heavy steel lid of the oil bath by means of an adjustable ring-clamp which was held in position by set screws. This arrangement provided a rigid support for the reactor and made it possible to transport the glassware to and from the oil bath without any mishaps.

Through the central port of the reactor lid passed the shaft of the glass stirrer. The stirrer consisted of a 3/16 in. glass rod with four impeller blades at each of three positions along its length. The blades were 2 in. in length and were mounted on a 30° pitch. Outside of the reactor and above the central port of the reactor lid, the stirrer shaft was clamped in a steel-jacketed, teflon bearing. To prevent over-

heating, the bearing housing was jacketed with copper tubing through which cooling water was circulated. Although the teflon required no lubrication and at the same time provided a good seal, its expansion due to a 50 degree rise in temperature was sufficient to cause undue frictional drag on the rotating shaft of the stirrer. Hence, the cooling coils were a necessity.

One of the problems in assembling the reactor was to connect the stirrer bearing to the glass lid with a gas-tight seal which was also free of stresses. This was accomplished by using the combination of a standard-taper fitting and flange fabricated from teflon as a single unit. The taper was inserted in the central port of the reactor lid and the flange was clamped against a matched teflon surface in the bearing.

At the upper end of the bearing shown in Figure 3, the stirrer shaft was joined to a stainless-steel drive pulley by means of neoprene gaskets which gripped the shaft on their inner surfaces and gripped the internal wall of the pulley-housing with their outer surfaces. A screwdown follower which compressed the gaskets was adjusted until no slippage between the pulley and stirrer shaft occurred. The pulley was belt driven because this appeared to be the simplest method of transmitting power from the drive motor. Also, there was no danger of breaking the stirrer shaft in case it froze in position.

The two feed lines consisting of 7-mm pyrex tubing entered by means of ring seals through two of the standard taper ports on the lid and extended to the bottom of the reactor. It was found that sealing the tapers with stopcock grease of which several varieties were tested proved to be unsatisfactory. A satisfactory seal was obtained by using a teflon sleeve 1/1000 in. thick between the matching faces of each taper. The maximum temperature of operation, namely 400°F, appeared to have no damaging effect on the teflon seals. Also, the seals were chemically inert toward the reactants and products.

Through the one remaining port passed the product line and thermocouple probe for which the method of sealing was identical to that of the feed lines. The thermocouple probe consisted of a 7-mm pyrex tube with five side-arms, 1/2 in. in length, extending 45° from the tube axis and spaced evenly along its length. Each of the side arms contained a copper-constantan thermocouple junction (No. 40 wire) and was sealed on the end by a thin glass wall. The leads from the five junctions passed collectively through the main tube to the outside and terminated in a Cannon plug which is shown in Figure 3. All external connections to the feed lines and product line were made by means of standard ball-and-socket joints.

In order to disperse a fixed catalyst bed inside the reactor, a glass-tray system was used. As shown in Figure 3

the trays were arranged in the form of a spiral to provide for good circulation of the gas stream throughout the entire volume of the reactor. Another feature of this arrangement was the fact that a group of stirrer blades was positioned between each set of four trays. Hence, there was very little chance for stagnation to develop within the rather complex configuration.

For the purpose of maintaining the temperature of the reactor constant, an oil bath was used. Figure 4A shows the upper portion of the reactor oil-bath which was nothing more than an adiabatic container having a capacity of about 10 gal. Dow Corning No. 550 silicone oil was pumped into the bottom of the bath from a controlled thermostat which is discussed in the next subsection. The oil returned to the thermostat by gravity from an overflow pipe at the top of the bath. The depth of oil was adjusted to the maximum overflow capacity by means of a valve installed in the feed line or by means of a by-pass valve on the pump. At this capacity, the reactor was completely submerged with at least 2 in. of oil above the lid.

Three thermocouples enclosed in pyrex tubes were inserted in the oil bath at various depths, namely, near the top and bottom and in the middle. As a safety precaution, in case the pumping rate exceeded the overflow rate, a float was used to indicate the level of oil during operation. It was provided with electrical contacts which were connected to signal lights on the control panel. Whenever the oil level was either above

or below the desired value, a signal was given. Figure 3 shows the float attached to the oil-bath lid.

Thermostat for Supplying Constant-Temperature Oil

As stated previously, the silicone oil which was pumped into the reactor oil-bath was first brought to a controlled temperature in a thermostat. A good view of the thermostat is shown in the foreground of Figure 2A. It consisted of two concentric, cylindrical containers which were made of steel. The inner container was provided with a cylindrical baffle and a high-speed, belt-driven impeller; and it contained the silicone. The outer container was insulated and was separated from the inner container by an air gap of at least 2 in. Four, 500-watt heaters were wound evenly on the outer surface of the inner container to provide the energy necessary to heat the oil within a few degrees of operating conditions. An additional four heaters, two of which were controlled by variacs, were wound on the insulated outer container and supplied energy to compensate for convection and conduction losses from the inner container.

Two control elements for the thermostat were located near the top of the inner container. One element was a coiled heater which received energy by electrical means from a thyratron unit having a two-derivative control circuit. The thyratron unit was installed in the instrument bench shown in Figure 2B. The second element was a coiled-iron resistance-thermometer which was balanced against a resistance bridge

installed in the instrument bench. Any out-of-balance in the resistance bridge was detected by a ballistic galvanometer which caused a reflected beam of light to shine on a photocell connected to the thyratron. During an experiment, the resistance bridge was adjusted to a predetermined value, equivalent to the resistance of the iron-coil thermometer at the operating temperature. Deviations from balance because of changes in the thermometer resistance were detected by the ballistic galvanometer which, in turn, reflected a carefully focused beam of light to the window of the photoelectric cell. Variations in the amount of light received by the cell created similar variations in the electrical signal from the cell to the thyratron unit. Thus, the thyratron unit, having been signaled that the bridge and thermometer were not in balance, supplied a first- and second-derivative surge of energy to the heater coil in the thermostat. As a result, the temperature was automatically controlled to $\pm$ 0.02°F.

The absolute value of the thermostat temperature was measured by means of a platinum resistance thermometer immersed in the silicone and connected to a Mueller bridge on the instrument bench. Care was taken to insure that the thermometer was well immersed in the circulating oil and that the connections between the platinum leads and the standard cable leading to the instrument bench were cooled with circulating water. Although the temperature measured by the platinum thermometer in the thermostat was not the same as

that measured in the reactor oil-bath, because of slight heat losses, the thermometer was useful in getting the system up to a control point. In calibrating the thermocouples, however, the platinum thermometer was extremely useful as a standard since the calibrations were conducted in the thermostat. More discussion of the calibrations will be given under EXPERIMENTAL PROCEDURE.

The thermostated silicone was circulated through heavily insulated pipe to the reactor oil-bath by means of a centrifugal pump. Including the connecting pipe, the volume of the circulating system was approximately 21 gal. All the electrical energy to the pumps, drive motors, and heaters for the entire apparatus was controlled from a power panel mounted on the thermostat compartment.

Conditioning System for the Feed Streams

The chemicals to be fed to the reactor, namely, hydrogen chloride and vinyl chloride were supplied by the manufacturer as compressed gases in steel cylinders. A means of removing impurities, drying the gases, and measuring their flow rates in a continuous process was essential.

The gases were transported through 1/8 in. pipe from the cylinders to the conditioning compartment shown in Figure 5. On the front panel of this compartment, the metal feed lines were terminated at needle valves made of stainless steel. These, in addition to the pressure-regulating valves on the steel cylinders, provided a means of controlling the flow of the feed streams.

Proceeding from a needle valve through glass tubing, the hydrogen chloride was first passed upward through a 5-liter glass tower containing approximately 3 liters of crystal oil. In order to obtain good dispersion of the gas and to minimize pulsing in the system, the hydrogen chloride entered the bubble tower through a medium glass-frit. The vinyl chloride was handled similarly except that the bubble tower was constructed of steel and contained approximately 3 liters of an aqueous solution containing 20% by weight of sodium hydroxide. Dispersion of the gas was accomplished by means of a porous steel thimble located on the inlet line.

Impurities removed from the hydrogen chloride by absorption in the crystal oil were primarily organic in nature. The only impurities of consequence in the vinyl chloride were phenol, which was added as an inhibitor, plus small amounts of hydrogen chloride. The two bubble towers are shown in Figure 5.

From the bubble towers, the gases flowed into pre-dryers filled with anhydrous calcium chloride. To insure complete drying, the gas streams were then directed into large drying tubes which, as shown in Figure 5, were located to the right of the pre-dryers. These, too, were filled with calcium chloride.

The dried gases next flowed to a set of separate glass coils immersed in an isothermal water bath which was controlled at 25°C. Each coil, although compact in a spiral arrangement,

contained an equivalent of 12 feet of 7-mm glass tubing. This provided sufficient surface area for the gas streams to reach a steady temperature close to that of the bath. Immediately downstream from the conditioning coils, each feed line was interrupted first by a side arm leading to a manometer, secondly by a thermocouple junction inserted directly in the path of flow and finally by a Tri-flat rotameter which could easily be installed or removed from the feed line by means of standard taper fittings. The water bath and rotameters were housed in an aluminum-covered cabinet located to the left of the bubble columns as shown in Figure 5. This eliminated large temperature fluctuations which resulted from convection currents in the room.

A knowledge of the pressure, temperature, and scale reading on the rotameter was sufficient to determine the mass rate of flow for each component. More discussion of this calculation is given under EXPERIMENTAL PROCEDURE. Since the pressure of each gas beyond the conditioning coils was only slightly above atmospheric, it was necessary to fill the manometers with a low-density fluid such as dibutyl phthalate. The difference between liquid levels in the manometer legs was measured with a cathetometer.

The emf's of the feed-line thermocouples in addition to all other thermocouples were measured by means of a K-type potentiometer installed in the instrument bench. Connections between the thermocouple leads and the potentiometer were

accomplished with jumpers on a plug board.

Product-Stream and Feed-Stream Sampling

Beyond the rotameters, the feed-lines led directly to the reactor. The product stream leaving the reactor was directed through a manifold as shown in Figure 4B, from which samples could be removed. The remaining waste mixture was then passed through a wash-bottle containing strong alkali.

Just before the manifold, the product line was interrupted by a manometer which was used to measure sample pressures and to indicate pressure fluctuations in the upstream system. The sample ports on the manifold were conveniently fitted with ball-and-socket joints, thus making it possible to install or remove samplers with great facility. Also, the sampling manifold was connected by a separate line to a vacuum manifold shown in Figure 6. This provided means of evacuating samplers and filling them without removal from the sampling manifold.

The purity of the feed streams was determined by sampling the gases prior to their flow into the conditioning coils. Here, also, a sampling manifold was used and in like manner was connected to the vacuum system.

Gas Chromatography Equipment

The determination of the feed-stream purity and the composition of the reactor products was accomplished by means of gas-phase chromatography. The chromatograph unit which is shown in Figure 7 was designed and constructed as a general-purpose analytical tool, with sufficient capacity to contain

at least twelve columns. The cabinet was constructed from 1/16 in. sheet steel, and its overall volumetric dimensions were 8 x 3 x 3 ft.

On each of two sides, the unit was provided with two sets of doors. One set measured 6-1/2 ft in height, and the other set, above the first, measured only 1 ft in height. The larger doors were used only when a column was to be installed or removed from the cabinet, whereas the smaller doors were used during operation when a sample was to be injected into a column from a portable sampler. By using the small doors, the temperature control within the cabinet was not disrupted to any large degree.

All instrumentation for the unit was placed on the outside unless a controlled temperature for a particular instrument was necessary in its operation. Hence, the detector cells and flowmeters for the exit streams were placed on the inside since these instruments required isothermal surroundings.

The inner space of the cabinet was divided in half by a vertical steel panel. With an opening at the top and bottom of the panel, it was possible to circulate the air between the two sections of the cabinet in a continuous path. This was accomplished with a 3-bladed fan operating at 1700 rpm. It was located in the bottom opening of the partition panel. A 500-watt heater and a refrigeration coil were placed directly in front of the fan. Details of the construction are shown

in Figures 8 and 9. In order to reduce the heat transfer between the cabinet and surroundings, the inner walls of the cabinet were covered with Fiberglas insulation, 1 in. thick.

A mercury-filled sensing element, located in the top opening of the partition panel was used as a thermostatic control-switch by detecting variations in the cabinet temperature. To improve its sensitivity, the element was constructed, in the form shown in Figure 10, from a 10 ft length of 3/16 in. stainless steel tubing, which provided a relatively large surface area and a large heat transfer coefficient. The sensing element could detect a temperature fluctuation of $\pm$ 0.01°C. In principle, the expansion or contraction of the mercury due to temperature variations opened or closed an electronic-relay circuit located on top of the chromatograph unit. This, in turn, electrically opened or closed a power relay which energized the cabinet heater. A variac in the heater circuit was used to control the amount of power up to 500 watts. Figure 10 shows the detailed circuit diagram for the control relay and Figure 11 shows the details of the heater circuit.

Also, as shown in Figure 11, a safety feature in the heater circuit was the installation of a Fenwal, bimetallic thermo-switch. Its purpose was to take over control of the cabinet in the event the mercury-filled sensing element became electrically shorted. The Fenwal, however, was only capable of detecting variations of $\pm$ 0.5°C, but this was sufficient

to prevent gross changes in the cabinet temperature.

The temperature of the chromatograph cabinet was measured by means of copper-constantan thermocouples (No. 30 wire) which were located on each side of the partition panel. Under ideal conditions, the temperature difference between the two sections of the cabinet amounted to only 0.05°C corresponding to an emf difference of approximately 2 microvolts.

The details of the column which was used in the gas analysis are shown in Figure 12. It consisted of three concentric pyrex tubes. The central column contained the packing and consisted of a 4-ft length of 7-mm tubing, with 10/30 standard taper fittings on each end. The middle concentric tube, 1 in. in diameter, was wrapped in a spiral pattern over its entire length with a 200-watt heater. Finally, the outside tube, 1-1/2 in. in diameter, served as a shield to buffer any sudden changes in the air temperature surrounding the column. The entire assembly was mounted vertically in the chromatograph cabinet.

The column heater was controlled by a variac mounted externally on the cabinet. Since the electrical power to the entire unit was supplied through a voltage regulator, the voltage output of the column-heater variac was relatively constant. This, coupled with good control of the cabinet temperature, provided a satisfactory means of controlling the column temperature. Thermocouples, mounted at the top and bottom of the column, were used to measure its temperature.

The packing in the center column consisted of 60-80 mesh Dicalite which had been acid washed and coated with a partition liquid. Its chemical composition, according to the Johns-Manville Co., is as follows:

SiO_2	-	83.13% (weight basis)
H_2O	-	5.30%
Al_2O_3	-	4.60%
CaO	-	2.50%
Fe_2O_3	-	2.00%
Na_2O	-	1.60%
MgO	-	0.64%
TiO_2	-	0.18%
P_2O_5	-	0.05%

The purpose of the acid washing was to reduce the Fe content to a minimum. It was not at all improbable that its presence in large enough concentrations could catalyze undesirable decomposition reactions in at least two of the sample components, namely, vinyl chloride and 1,1 dichloroethane.

The two major criteria which determined the optimal mesh size of the packing were a large surface area per unit weight and a low pressure drop through the column. Since these criteria were in direct opposition with respect to mesh size, a compromise was reached by choosing 60-80 mesh.

Of the many types of packing available, it was desirable to use one which had relatively large pore diameters. Although, with increasing pore size, there was a decrease of surface area per unit weight, the undesirable hold-up inherent in small

pores was reduced. Dicalite has relatively large pore diameters averaging approximately 22,000 Å as compared to the relatively small pore diameters of 15-200 Å in ordinary silica gel. The average specific surface area of Dicalite is approximately 6×10^6 cm^2/gm, wherein the unit diatom of a particle is cylindrical in shape and approximately 3 microns in length.

A number of criteria determined, within a range of compounds, the type of partition liquid to use. The most important of these was its ability to separate the components of a sample with little or no overlapping, but with a minimum time of retention.

Another criterion, namely, chemical properties, was important in two respects. First the compound must be thermally stable, and second its chemical reactions with the sample components must be easily reversible at the temperature of operation. In the present work, however, the use of weak chemical bonding as a means of separation was not used. Thus, it was desirable to choose a liquid which was chemically inert toward the sample components.

Of no less importance were the physical properties of the partition liquid such as viscosity, specific gravity, and vapor pressure. Since the transport at the interfacial surfaces between the mobile and stationary phase was primarily molecular, a liquid of low viscosity was required. Furthermore, since the column was to be used for a large number of samples and with minimum contamination of the separated components,

the partition liquid was required to have a low vapor pressure at the temperature of operation. A rule of thumb in this regard is that its boiling point should be at least 150°C higher than either the column temperature or the boiling point of the least volatile component in the sample, whichever is higher.

The partition liquid chosen for the desired separation was didecylphthalate, which has the following characteristics (23):

Molecular Weight	446.65
Specific Gravity at 20°C/20°C	0.966
Boiling Point at 5 mm of Hg	261°C
Viscosity at 20°C	11.9 cps
Vapor Pressure, mm of Hg at 200°C	0.3
Solubility of Water in it at 20°C, % by weight	0.3

In preliminary experiments, didecylphthalate was found to give a good separation of carbon dioxide, vinyl chloride and 1,1 dichloroethane when used as a partition liquid. An illustrative example of the peak separations is shown in Figure 13. Here, it is noteworthy to give an explanation for the presence of carbon dioxide in the samples. Since the samples from the reactor contained hydrogen chloride, there was reason to believe that if allowed to pass through the column packing, it either would react irreversibly with the partition

liquid or, in the presence of minute quantities of Fe in the Dicalite, would react further with one of the other components in the sample, namely vinyl chloride. Its corrosive effect on the detection system was also an undesirable feature. Therefore, a 6 in. column of 100 mesh $NaHCO_3$ was placed on the upstream side of the partition column. The HCl reacted quantitatively with the bicarbonate to form an equimolar amount of CO_2, along with H_2O and NaCl. A discussion of the effects of water upon the component separations is given under Results.

The maximum column temperature was never greater than 90°C, and the boiling point of the least volatile component, namely 1,1 dichloroethane, is 57°C. In comparison to the boiling point of didecylphthalate both of these temperatures were well below the allowable maximum of approximately (260-150)°C or 110°C. The viscosity of didecylphthalate was somewhat high and for this reason was probably responsible for part of the tailing in the peaks. This disadvantage, however, was not intolerable.

The amount of didecylphthalate which was used in coating the Dicalite with a thin film was 35% by weight. Here, the ratio between the packing and stationary phase was not a rigid specification except when it was desirable to have identical characteristics in two different columns. Experience had shown that a weight per cent in the range 30-40% was optimal. Too large a quantity of partition liquid greatly increased the resistance to the flow of the mobile phase, which in all cases

was helium. For the weight per cent of liquid used in the 4 ft column, a pressure drop of 25 psi was required for a helium flow rate of 28 cc/min, corrected to 70°F and 1 atm pressure.

The flow rate of helium was measured on the down-stream end of the column by means of a Tri-flat rotameter which was located inside the cabinet. The helium rate was also measured on the upstream or high-pressure side, but this measurement was used only as a means of checking for leaks. The high-pressure rotameter was mounted on the outside of the cabinet as shown in Figure 7. Prior to entering the partition column, the helium passed through a 6 ft length of 1/4 in. copper tubing, the purpose of which was to condition the gas to the temperature of the cabinet.

The method chosen for detecting and measuring the quantity of eluted components was the measurement of the differences in thermal conductivity between the components and the carrier gas. For this purpose, a thermal-conductivity cell was constructed as shown in Figure 14. It consisted of a coiled tungsten filament mounted near the central axis of a 1/4 in., stainless-steel tube. The tube was approximately 6 in. in length and was fitted on one end with a 10/30 standard taper joint by means of a glass-to-metal seal. With the tapered joint, the cell could be easily attached to the column exit.

Since the thermal-conductivity cell was inside the chromatograph, its wall temperature became that of the cabinet. A

concentric metal jacket, as shown in Figure 14, was placed on the 1/4-in. steel tubing in order to serve as a buffer against sudden changes in the cabinet temperature. In this manner, the temperature of the cell was held constant to at least within the limits of the cabinet temperature, namely $\pm$ 0.05°C.

Electrical power to the tungsten sensing element was supplied by four Willard 20-2 storage cells each having a 2-volt output. The batteries were connected to give a steady 4-volt signal to the element, and their capacity was high enough such that recharging was necessary only once a month.

During an analysis, the changes in resistance of the sensing element as a result of changes in composition of the effluent gas were measured on the bridge circuit shown in Figure 15. Detection of the out-of-balance of the bridge was accomplished by means of a Variac G-10 graphic recorder. The full-scale sensitivity of the recorder was 10 millivolts, but this could be attenuated to a less sensitive scale by means of a Helipot resistor connected as shown in Figure 15. In order to reduce the noise level resulting from pulsating magnetic fields, the detector bridge was housed in a metal box, and all electrical leads to and from the circuit were made from shielded cable. In Figure 7 it is shown mounted on the outside of the chromatograph cabinet.

Samples were introduced into the column by means of a portable apparatus which is shown in Figure 16. The sampler

was provided with a ball-and-socket fitting on each end so that it could be installed or removed rapidly and without appreciable disturbance to the cabinet temperature. In this regard, only the small cabinet doors were opened momentarily. As shown in the figure, there were two collecting arms on the sampler. Either could be used to collect a known volume (approximately 2 cc) of sample; but for each analysis, only one arm was filled with sample whereas the empty arm was used as a by-pass for purging the air out of the end-sections. By proper manipulation of the three-way stopcocks, a sample could be collected and analyzed with negligible contamination by air.

In order to prevent a pressure surge on the column during analysis, the sample was always pressurized to the column pressure immediately following the air-purging operation but prior to its entrance into the column. This procedure provided a satisfactory means of analyzing the products with reasonable accuracy and within a short period of time.

EXPERIMENTAL PROCEDURE

Calibration of Equipment

All thermocouples used in the stirred-reactor equipment were calibrated in the thermostat which was described under APPARATUS. For each point of calibration, the thermostat was first allowed to reach a steady temperature with a variation not exceeding ± 0.05°F. At steady conditions, the emf's of the thermocouples and the resistance of the platinum thermometer were measured repeatedly over a period of several hours. The same procedure was used at 10 different temperatures over the range 150 to 300°F. An air-saturated ice bath was used to maintain the reference junctions of the thermocouples at 0.02 ± 0.01°C. Using the platinum resistance thermometer (Ser. No. 1170781) as a standard, the temperatures corresponding to the thermocouple emf's were calculated. A tabulation of these results is presented in Table 2A of Appendix I.

The Tri-flat rotameters which were used to meter the feed streams to the reactor were calibrated in place by a volumetric procedure. Figure 17 shows a schematic diagram of the equipment used. The collecting vessel was a 44-liter carboy which was immersed in water in a 50-gal drum. A capillary, pyrex tube connected the interior of the bottle to a mercury-filled manometer. Another pyrex tube, used as a feed line, connected the carboy to the product manifold of the reactor. At the mouth of the carboy, the feed line was

terminated in a three-way stopcock which could be used to by-pass the gas stream before and after a calibration run. A third tube was connected directly to the vacuum manifold. Both the manometer line and the vacuum line could be closed off from the system by stopcocks located at the mouth of the carboy. Prior to a calibration run, the carboy was evacuated to an arbitrary low pressure. Also, the gas stream was allowed to flow in series through the rotameter, the reactor, the product-line manifold, and finally through the by-pass line of the carboy until steady conditions with respect to temperature, pressure and the metering rate were obtained at the rotameter. It is noteworthy to mention here that the rotameters were calibrated under conditions identical to those used in all other experiments. At steady conditions, the by-pass line was closed and the gas stream was directed into the carboy. A careful control of the flow into the carboy was maintained by a continuous adjustment of the stopcock on the feed line. The amount of adjustment was determined by the difference in liquid levels appearing in the manometer connected to the reactor product line. This procedure was necessary because of the large capacity of the carboy with respect to the rest of the system. Some buffering, however, was afforded by the reactor.

The time of a run was recorded to the nearest 0.1 sec. Other measurements included the initial and final pressure in the carboy to the nearest 0.05 mm of Hg, the temperature in

the carboy to the nearest 0.1°C, the temperature of the gas at the rotameter to the nearest 0.1°C, the pressure of the gas at the rotameter to the nearest 0.001 mm Hg and finally the flow rate of gas through the system to the nearest 0.1 division on the rotameter scale. Ordinarily, a calibration run was conducted over a period of 1 to 2 hours. Such a long period provided a truer average of the flow rate than if the runs had been conducted in much shorter periods of time. The calibration results for both the hydrogen chloride and vinyl chloride are presented in Figures 1A and 2A and Table 3A in Appendix I.

The volume of the reactor, with and without the catalyst support and tray system, was measured to the nearest 3 cc by filling it with a known volume of water. The amount of catalyst support was the same as that used in the kinetic experiments, namely 100 gm. Without the catalyst support and tray system, the volume was 6020 ± 3 cc at 25°C; and with them, it was 5870 ± 3 cc. These quantities were required in the determination of retention times for the various feed rates.

The volume of the sampler was determined at 25°C to the nearest 0.05 cc by weighing it empty and filled with mercury. Its volume was 1.84 ± 0.05 cc. The weighings were accurate to the nearest 0.5 milligram.

Calibration Samples for the Chromatograph Column

Within experimental error, the conditions of operation in the chromatograph were identical for all samples. The only exception was the size of sample to be analyzed. The following

list of conditions was compiled from the recorded data for nearly 200 samples.

Helium pressure at 25°C	25.0 ± 0.5 psig
Helium flow rate (upstream) at 25°C and 25 psig	10.6 ± 0.5 cc/min
Helium flow rate (downstream) at 70°F and 1 atm	28.0 ± 0.1 cc/min
Current in sensing element	260 ± 1 ma
Full scale sensitivity for CO_2 and vinyl chloride peaks	66.7 ± 0.1 mv
Full scale sensitivity for 1,1 dichloroethane peaks	10.0 ± 0.1 mv
Column jacket-heater	42.0 ± 0.5 V
Column temperature, top	184 ± 2°F
Column temperature, bottom	194 ± 2°F
Cabinet temperature	88.71 ± 0.05°F
Thermal conductivity cell temperature	88.71 ± 0.05°F
Chart speed on recorder	4 in./min
Penwal setting for safety control	5.1
Cabinet control-heater setting	40-60V

Calibration mixtures of the reaction products, namely HCl, vinyl chloride and 1,1 dichloroethane, were prepared by first obtaining a known mixture of HCl and vinyl chloride. This was accomplished by collecting the two gases, either individually from the feed lines or as a mixture from the reactor, in a 500 cc sample-bulb. The 1,1 dichloroethane was added as either a gas or liquid. When added as a liquid, it was injected into

the bulb through a serum-bottle cap. When added as a gas, the liquid was first heated to increase its vapor pressure, and then a small portion of the vapor was admitted to the bulb. In both cases, the 1,1 dichloroethane had previously been solidified, followed by evacuation to remove dissolved air.

All mixtures were prepared on the feed-line sampling system which was connected to the vacuum manifold. A mercury-filled manometer indicated the pressure in the bulb as each component was added. By assuming that the mixtures were ideal solutions and using compressibility factors (24) at 25°C of 1.00, 0.92 and 0.87 for HCl, vinyl chloride and 1,1 dichloroethane, respectively, the molal concentration of each component was computed.

For each calibration sample, a distinct chromatographic separation was obtained, and the areas under the elution peaks representing each component were measured with a planimeter to a precision of $\pm$ 0.5%. In this regard, the relatively high chart speed of 4 in./min was advantageous in that spreading out the elution peaks greatly improved the accuracy and precision of area measurement.

By considering the areas to be a function of the mole fraction or weight fraction of the components, a comparison of the composition calculated from the peak-areas with the known composition provided a series of correction factors. It was found that the composition represented by the uncorrected areas more closely represented the weight fractions than the

mole fractions of the components. Hence, the correction factors were based upon weight fractions.

The assumption of ideal solutions in the calibration mixtures was checked by eluting the pure components in quantities equivalent to the amounts present in the mixtures. Satisfactory agreement was obtained. The sample calibration results are listed in Table 4A of Appendix I. Included also are the average values of the correction factors. All subsequent chromatograms, including those obtained for the products of the kinetic experiments, were corrected by these factors.

In sampling the reactor products, the gases were allowed to flow through the sampler, which was attached to the product manifold by means of a ball-and-socket joint. Over a period of time, usually 30 min, the air in the sampler was sufficiently purged, and there remained a representative sample of the reactor product. This method was preferred to the one in which the sampler would have been evacuated, because there was less manipulation required and there was less disturbance to the system.

Studies of the Homogeneous Reaction

In the absence of a catalyst, the reaction was studied over a temperature range of 150 to 400°F and at a pressure of 1 atm. The stirring rate was fixed at 300 rpm, and the flow rates of the feed streams were varied from 3×10^{-3} to 29×10^{-3} lbs/hr, corresponding to retention times from

7 to 1/2 hr, respectively.

Homogeneous catalysis was studied under similar conditions. In this case, however, $FeCl_3$ was added as a vapor to the HCl feed stream. The amount added was determined by the relationship (25):

$$\text{Log}_{10} P_{mm} = \frac{-6449.345}{T°K} + 13.742$$

where P is the vapor pressure. Hence, at a temperature of 396.6°F (475.7°K) this corresponded to a mole fraction of approximately 0.002 in the HCl stream. Figure 4A shows the apparatus which contained the anhydrous salt; and as noted, the vaporizer was heated to the desired temperature with a 200-watt heating-tape. Good contact between the HCl and $FeCl_3$ was obtained by passing the HCl directly through the heated solid in the vaporizer. A rough approximation as to the amount of $FeCl_3$ added was determined by withdrawing a 20 cc sample of the HCl with a syringe and injecting it into a few milliliters of standard potassium ferrocyanide. Accurate control of the $FeCl_3$ concentration was impossible by the above method, but this was of no consequence since the experiment was devised only to be qualitative.

Preliminary Studies of Heterogeneous Catalysis in Batch Systems

A series of experiments were performed to determine the relative effectiveness of various metallic halides and carriers in catalyzing the addition reaction between HCl and

vinyl chloride. These reactions were conducted in glass ampules each having a volume of 155 cc. The ampules were assembled in two parts by means of a standard-taper joint and were equipped with a sampling line which could be opened or closed by means of a stopcock.

In all the experiments, the ampules and their contents were placed in an oven which was maintained at a temperature of 100.0 ± 0.5°C. The time of reaction was varied from 2 to 12 hr.

In the filling procedure, a weighed portion of catalyst was placed in the lower half of an ampule. Next, the two parts of the ampule were joined and clamped, and then it was attached to the product manifold which is shown in Figure 48. Here, it was evacuated and filled to a pressure slightly above atmospheric with a known mixture from the stirred reactor. In all cases, the ratio of HCl to vinyl chloride was 1.2 on a mole basis.

The sampler shown in Figure 16 was used to transfer samples from the ampules to the chromatographic column. By placing the sampler and the ampule in series on the vacuum manifold an air-free sample was obtained. Since the samples were only 2 cc, several could be removed from a given ampule when checking for reproducibility.

Whenever it was desirable to re-use the catalyst of a previous experiment, the ampule was heated to 100°C and evacuated for several hours. This removed essentially all the

adsorbed, volatile materials which could interfere with subsequent analyses.

A variety of catalysts and catalyst supports were studied. In fact, the purpose of the experiments was to determine the optimal combination of catalyst and carrier which could be used in subsequent kinetic studies. It was of interest also to repeat in part the experiments of Wibaut (3) and Kharasch (6,9).

The catalysts which were studied included Hg_2Cl_2, $CoCl_2$, $FeCl_3$, $ZnCl_2$, $NiCl_2$, $MnCl_2$, $CdCl_2$ and $BiCl_3$, whereas the carriers included asbestos short and long fiber, 10-20 mesh silica gel, 60-80 mesh Dicalite, 6-12 mesh or 1/8 in. pellets of Celite, and 1/4 in. spheres or 1/8 in. pellets of alumina.

The types of combinations placed in the ampules included:

1. 1.00 gm. or 1.2 millimoles of the pure metallic halide.

2. 1.00 gm of the unimpregnated carrier.

3. 1.00 or 0.05 gm of catalyst plus carrier, wherein the amount of catalyst was 1.5 millimoles/gm of carrier.

Since there was a possibility that side reactions could occur in the presence of a catalyst, a qualitative analysis of the reaction products, in addition to the quantitative analysis, was desirable. Hence, samples from an ampule containing $ZnCl_2$ supported on Celite were analyzed by infrared spectroscopy. The analyses were conducted in a gas cell having a 10 cm light path. For a comparison and for the purpose

of calibration, samples of natural gas containing methane, ethane and propane were analyzed. It appeared that these components as well as acetylene, ethylene and hydrogen would be the most likely products of a side reaction. A Perkin-Elmer automatic infrared spectrometer was used in the analysis, and the instrument settings are listed in the legend of Figure 18.

Studies of Heterogeneous Catalysis in the Stirred Reactor

The catalyst chosen for the kinetic studies was based upon the results obtained in the ampule experiments. It was found conclusively, as discussed under RESULTS, that Celite pellets impregnated with $ZnCl_2$ performed the most satisfactorily as a catalyst. Hence, a catalyst was prepared by impregnating 1/8 in. Celite pellets with $ZnCl_2$ in the ratio of 0.200 gm $ZnCl_2$ per 1.000 gm of carrier. The extruded cylindrical pellets were designated by the Johns-Manville Co., Inc. as Celite #408 having the following properties:

Chemical composition - Diatomaceous silica

SiO_2	-	90.2% (weight basis)
TiO_2	-	0.2%
Fe_2O_3	-	1.6%
Al_2O_3	-	4.9%
P_2O_5	-	0.4%
CaO	-	0.8%
MgO	-	0.6%
Na_2O	-	0.6%
K_2O	-	0.7%

Average dimensions of pellet - 0.175 in. dia x 0.156 in. long

Average pore size - 22,000 Å

Packed density - 36 lbs/ft^3

Reaction in water - slightly acid to neutral

Surface area (measured by Union Oil Co. of California) based on nitrogen adsorption - 10.6 m^2/g

In preparing the catalyst, a weighed portion of anhydrous $ZnCl_2$ was dissolved in reagent-grade acetone. This solution was then mixed with a weighed amount of Celite pellets which had previously been dried under vacuum at 115°C for at least 12 hrs. The mixing was done in a weighed, air-tight container which was slowly evacuated to remove the acetone. By careful control of the evaporation rate, there was no difficulty in coating the Celite with reasonable uniformity.

When nearly all the acetone was removed, with only a small amount adsorbed on the pellets, the container was heated to 115°C and maintained at that temperature under a vacuum for several hours. By this treatment, essentially all the acetone was removed. The exact amount of $ZnCl_2$ adsorbed was determined by difference after weighing the empty container along with any unadsorbed residue on its walls. Samples of the dry, impregnated Celite were viewed under a 20-power binocular microscope and were found to contain no uneven aggregates of $ZnCl_2$ crystals.

Preliminary experiments in the ampules and in the reactor had shown that a relatively large amount of catalyst per unit volume of reactor, namely 3 gm/liter, was required to give measurable rates of 100°C and for retention times less than 12 hr. Upon this basis, 120.000 ± 0.001 gm of the impregnated Celite were placed in the reactor and distributed evenly among the eight trays. Figure 3 shows the catalyst loaded in the reactor, and Table 5A of Appendix I lists the weight in each tray.

After the loaded reactor had been checked for vacuum tightness, it was placed in the oil bath and brought to a temperature of 215°F. Following a period of evacuation at this temperature, it was filled with HCl through the feed lines to a pressure of 1 atm. Finally, the vinyl chloride was admitted to the reactor, and this was considered as the initial time of reaction. Sampling from the reactor was begun immediately in order to follow the transient build-up to steady state with respect to feed composition.

The range of conditions studied were as follows:

Stirring rate (fixed)	-	300 rpm
Temperature	-	165 to 300°F
Pressure	-	near atmospheric
Flow rates of HCl	-	0.60 to 8.58 x 10^{-3} lb /hr
Flow rates of Vinyl Chloride	-	1.38 to 18.82 x 10^{-3} lb /hr
Weight ratio of Vinyl Chloride to HCl	-	2.16 to 2.46

THEORY

General

The most important single factor determining the mathematical treatment of stirred reactor systems is the degree of mixing. In the ideal case, complete mixing occurs, and this results in a uniform composition, temperature and pressure throughout the reactor. Under these conditions, the material and energy balance equations are considerably simplified and in the case of steady state, can be reduced to simple algebraic equations. For the case of incomplete mixing, the equations describing the system become extremely complex, and usually cannot be solved by rigorous, analytical methods. In the equations that follow, it is assumed that complete mixing occurs and that diffusion at the entrance section can be neglected.

Material Balance

The general statement of material balance in a reacting system for product A is given as follows:

$$\left[\begin{array}{c}\text{Rate of product}\\ \text{addition in the}\\ \text{feed stream}\end{array}\right] - \left[\begin{array}{c}\text{Rate of product}\\ \text{removal in the}\\ \text{exit stream}\end{array}\right] + \left[\begin{array}{c}\text{Rate of product}\\ \text{formation in the}\\ \text{reactor}\end{array}\right] = \left[\begin{array}{c}\text{Rate of product}\\ \text{accumulation in}\\ \text{the reactor}\end{array}\right] \qquad (1)$$

The application of Equation 1 to a stirred reactor containing a solid catalyst which undergoes fouling can be written in mathematical form as,

$$F_i n_{Ai} - F_o n_{Ao} + r_{w_A} W = V_r \frac{dC_A}{d\Theta} \qquad (2)$$

where:

F_i and F_o = mass rate of feed stream and exit stream respectively, lb/hr.

n_{Ai} and n_{Ao} = the concentration of product A in the feed and exit stream respectively, lb A/lb of total material flow.

r_{w_A} = net instantaneous rate of product formation, lb A/(hr) (lb of catalyst)

W = weight of the catalyst, lb.

V_r = volume of the reacting system, ft^3.

C_A = mass concentration of A in the reacting system, lb A/ft^3 of reacting volume.

Θ = time, hr.

For a gaseous system which obeys the ideal gas law, the term C_A can be related to n_A by the following relationship, in which the concentration of product A in the exit stream is identical to that in the reacting system because of complete mixing.

$$C_A = \frac{n_{A_o}{}^m}{V_r} = \frac{PV_r}{RT} M_{av} \qquad (3)$$

where:

m = total mass of reacting system excluding the catalyst, lb.

M_{av} = average molecular weight of the reacting system, lb/lb mole

A combination of Equations 2 and 3 for conditions of constant temperature, pressure, and reactor volume results in,

$$F_i n_{A_i} - F_o n_{A_o} + r_{w_A} W = \frac{PV_r}{RT} \frac{d(M_{av}\, n_{A_o})}{d\theta} \qquad (4)$$

An overall material balance relates F_i and F_o by,

$$F_i = F_o + F_f \qquad (5)$$

where:

F_f = the mass rate of accumulation in the reacting system, lb/hr.

In the present work, F_f represents only the accumulation of material deposited on the surface of the catalyst due to a fouling reaction, since no consideration is given to transient conditions resulting from start-up.

The substitution of Equation 5 into Equation 4 gives the final form as follows:

$$F_i n_{A_i} - (F_i - F_f) n_{A_o} + r_{w_A} W = \frac{PV_r}{RT} \frac{d(M_{av}\, n_{A_o})}{d\theta} \qquad (6)$$

In the case of no fouling and steady state, the right-hand member of Equation 6 is zero, and also F_i equals F_o. The resulting equation becomes:

$$F_i(n_{a_i} - n_{A_o}) + r_{w_A} W = 0 \qquad (7)$$

For the case in which the feed contains no product, Equation 7 further simplifies to,

$$F_i n_{A_o} = r_{w_A} W \qquad (8)$$

A knowledge of the total feed rate, the weight fraction of component A in the product stream, and the weight of catalyst is necessary and sufficient to compute the instantaneous rate of reaction with respect to A by Equation 8. In comparing a series of tests and in determining the mechanism or specific rate of reaction, a knowledge of the feed composition and the total product composition is also necessary.

RESULTS

Chromatographic Analysis of Products

A partition column containing didecylphthalate coated on Dicalite was used in the chromatography unit for the purpose of analysis. The operating conditions are described under EXPERIMENTAL PROCEDURE. At these conditions, the retention times of CO_2, vinyl chloride, 1,1 dichloroethane, 1,2 dichloroethane, water and air were complied from data for nearly 200 samples and are listed in Table 1. Although the reactor product contained only HCl, vinyl chloride and 1,1 dichloroethane, the other materials listed above were indirectly a part of the analysis. As stated under APPARATUS, the HCl was not allowed to pass through the elution column but instead was passed through $NaHCO_3$ to form CO_2 and H_2O, which were subsequently eluted. A knowledge of the 1,2 dichloroethane retention time was desirable in case an unexpected peak were to appear in its vicinity.

The separation of components was primarily a function of their relative absorptivities in the partition liquid. The fact that the peaks shown in Figure 13 were not symmetrical, however, suggested that the absorption isotherms were non-linear.

Each elution peak also showed tailing. This was partially attributed to three effects, namely, longitudinal diffusion, diffusional resistance in the partition liquid and adsorption

on the column packing. Throughout the experimental work, an effort was made to minimize each of these effects without destroying the separation of peaks.

By an increase of the column temperature, the viscosity of the partition liquid was decreased, thereby reducing its resistance to diffusion. The increase in temperature also reduced the adsorptivity of the packing, and thus improved the reproducibility of the analysis. On the other hand, the increase in temperature reduced the absorptivity of the partition liquid and increased its vapor pressure. The latter effects placed an upper limit on the optimum column temperature.

Since the separation of the sample was a continuous process throughout the column length, a positive temperature gradient in the direction of flow improved the separation between the components. As stated under EXPERIMENTAL PROCEDURE, the gradient used was approximately 2.5°F/ft.

The undesirable effects of longitudinal diffusion were more noticeable at higher temperatures but were reduced to some extent by increasing the flow of the carrier gas, helium. Here again, a limitation was involved since an increase in flow rate usually decreased the time for equilibration between the sample and partition liquid. A reasonable compromise between these opposing phenomena was reached by using a helium flow rate of 28.0 cc/min corrected to 70°F and 1 atm.

Although good separation was obtained among the primary reactor products, overlapping occurred between air and CO_2 and

between 1,1 dichloroethane and H_2O. Since air and water were contaminants, it was desirable to keep the samples free of them. By carefully following a rigid sampling technique, contamination from air was eliminated. The water, however, was a more difficult problem, since it was a product of the reaction between HCl and $NaHCO_3$ in the column. Use of a drying agent in series with the bicarbonate column was not practicable, because the irreversible adsorption of the sample components on the dryer was a possibility.

It was apparent from the chromatograms that the water peaks were not reproducible and that considerable tailing occurred. This was attributed to irreversible adsorption of water on the column packing because its solubility in the partition liquid was negligible.

In order to correct for the overlap between the water and 1,1 dichloroethane, several techniques were tested. One method was to extrapolate the 1,1 dichloroethane peaks to the zero-baseline. Another was to extend a vertical line from the minimum portion of the overlap-curve to the zero-baseline. Here, an overlap curve is defined as two peaks partially superimposed on each other. A third method was to draw a new baseline which was tangent to the 1,1 dichloroethane peak at its origin on the zero baseline and to the minimum portion of the overlap curve. Finally, a fourth method was to compare the 1,1 dichloroethane peaks having water contamination with peaks of pure 1,1 dichloroethane. The validity of the latter

method was dependent upon the fact that the maximum point in the dichloroethane peak appeared before the origin of the overlap curve.

As shown in Table 1, the beginning of the water peak and hence the overlap curve was 905 sec, whereas the maximum in the 1,1 dichloroethane peak appeared at 825 sec. From this, it was reasonable to expect that the initial portion of the 1,1 dichloroethane peak, up to the peak maximum, was identical to the initial portion of a comparable peak for a pure sample. Here, the area included in the initial portion of the peak, for the purpose of further discussion, is called the symmetry area.

The ratio between the total area of the pure sample and twice its symmetry area provided an asymmetry factor which was used to correct the peaks of the contaminated samples. A plot of the asymmetry factor vs the symmetry areas of pure samples is shown in Figure 19 and the data are listed in Table 2. A sample calculation for correcting the contaminated peak is also shown in Table 2.

A comparison of the four correction methods outlined above showed that extrapolation of the elution curve and correction by an asymmetry factor agreed to within $\pm$ 3%. A comparison of these two with the vertical-line method showed agreement to within $\pm$ 6%, whereas the tangential-baseline method agreed only to within $\pm$ 10%. Because of its more logical basis, the correction by an asymmetry factor was used whenever necessary.

Following the correction for overlap, the calibration factors, which were discussed under EXPERIMENTAL PROCEDURE and are listed in Table 4A of Appendix I, were then used to convert the areas of each peak to a weight basis. Finally, the composition was determined by dividing each area by the sum of the areas.

The sensitivity of the thermal conductivity cell in detecting each component was estimated experimentally. In these experiments, measured quantities of a particular component were injected into the column from which a series of elution peaks was obtained. A plot of the quantity injected vs its peak area was extrapolated to zero area, and the intercept represented roughly the minimum detectable quantity. Without amplification, the sensitivity for each of the components corresponded to a 1.84 cc sample at a pressure of approximately 1 mm of Hg. For a sample containing only 0.3 mole% 1,1 dichloroethane, the error in detection was approximately $\pm$ 5% when the peak was amplified by a factor of 6.67. By comparing the areas for several known samples, the precision of detection was better than $\pm$ 2%.

It is well to mention here that another source of error in detection was the cell response time. The magnitude of this quantity was not measured, but since the elutions were performed at relatively low flow rates, its effect was considered to be negligible.

The areas of the peaks were measured to an accuracy of

± 3% with a polar planimeter, but in this case accuracy was not important since only the relative areas were required. The precision of these measurements was better than ± 0.5% for the CO_2 and vinyl chloride peaks and never exceeded ± 1% even for the smaller 1,1 dichloroethane peaks.

From a knowledge of the retention times, the retention volumes were computed from the following definition:

$$V_r = (F_v)(t_c) \qquad (7)$$

where:

V_r = corrected retention volume, cc at 70°C and 1 atm

t_c = corrected retention time, obtained by taking the difference between the measured retention time and the retention time of air, min.

F_v = flow rate of carrier gas, cc/min corrected to 70°F and 1 atm.

The calculated values of V_r for each component are listed in Table 1.

Studies of the Homogeneous Reaction

In the absence of a solid catalyst, no measurable reaction to form 1,1 dichloroethane occurred within the temperature limits of 200 to 400°F for retention times up to 12 hr. At 400°F, however, some cracking of the vinyl chloride was observed as indicated by a slight carbon deposit on the glass surfaces. Whether or not this was catalyzed by the glass was

investigated further.

Likewise, in the presence of $FeCl_3$ vapor no reaction was observed. It is possible, in this case, that insufficient $FeCl_3$ was present or that the vapor molecules were unable to decrease the activation energy of the reaction. Further work will be necessary to confirm these results.

Preliminary Studies of Heterogeneous Catalysis in Batch Systems

The results of the ampule tests were important in selecting the most favorable combination of catalyst and carrier to be used in subsequent studies.

Effect of Carriers.--With the exception of silica gel, all the carriers listed under EXPERIMENTAL PROCEDURE were found to be completely inert toward HCl and vinyl chloride.

The surface of the silica gel became discolored, which suggested that it was catalyzing the decomposition of monomeric or polymeric vinyl chloride. After prolonged contact, the discoloration increased until the surface was totally black.

Normal silica gel has a very large surface area, 800 m^2/gm, and also possesses an affinity for many organic and inorganic molecules. It is not unlikely, therefore, that physical adsorption or even chemisorption was occurring, both of which are normally exothermic processes. The resultant energy release may have been sufficient to induce the endothermic, cracking reaction.

An alternative explanation is the possibility that silica gel contains reactive sites capable of catalyzing the chemical

decomposition of vinyl chloride. Regardless of its mechanism, however, the decomposition was an undesirable reaction in the presence of a catalyst or a catalyst support.

Like the other catalyst supports, silica gel did not catalyze the addition of HCl to vinyl chloride. Its advantage over the other supports was a large surface area, but this was offset by its effect in decomposing reactants and by its small pore diameters. Celite possessed neither of these disadvantages and for this reason was used as the support in subsequent rate experiments.

Effect of Metallic Halides Without Carriers.--Among the pure metallic halides tested, only $ZnCl_2$ and $FeCl_3$ catalyzed the reaction between HCl and vinyl chloride to form 1,1 dichloroethane. A comparison between the catalytic activities of these two salts was obtained by varying the time of contact. The results of these tests are listed in Table 3 under Tests A and B.

For short periods of time, usually 2 hr, the ratio of conversion in the presence of $FeCl_3$ to that of $ZnCl_2$ was approximately 2, under identical conditions of initial composition and temperature. With increasing contact time, however, the difference in conversion for the two catalysts became smaller, and after 6 hr, the ratio was less than 1. For periods up to 12 hr, the ratio of conversion reached a value of 0.6 in favor of $ZnCl_2$.

These facts were explained on the basis that initially $FeCl_3$ was the more active catalyst of the two. The gradual

decrease in the ratio of conversions suggested that either equilibrium had been established in the presence of $FeCl_3$ or its activity was decreasing. The former alternative was ruled out since the ratio of conversions after 6 hr became less than 1. A repeated experiment with the same catalysts proved conclusively that $FeCl_3$ had lost its activity since no conversion was obtained. $ZnCl_2$ also showed some decrease in activity but not to the extent experienced by $FeCl_3$.

The loss of activity was explained when experiments showed that both $ZnCl_2$ and $FeCl_3$ as well as $BiCl_3$ catalyzed the decomposition of vinyl chloride. The net result was the gradual formation of a thin carbon film on the surfaces of these salts. Also, the rate of decomposition of vinyl chloride, and hence the rate of carbon formation, was much greater in the presence of $BiCl_3$ and $FeCl_3$ than in the presence of $ZnCl_2$. A subsequent analysis of the carbon-coated $FeCl_3$ showed that it had been reduced to $FeCl_2$, which was known to be inactive as a catalyst. Thus the rapid loss of activity in $FeCl_3$ was attributable to the occupation of active sites by decomposition products and to the reduction of the Fe^{+++} to a lower valence state during the decomposition reaction. In the case of $ZnCl_2$, the slower loss of activity was due only to the occupation of active sites.

Effect of Metallic Halides Supported on Carriers.--Results similar to the above were obtained for the catalyst supports impregnated with metallic halides. The most significant dif-

ference was the increased conversion per unit weight of salt. This was expected since, in comparison to the pure salts, greater exposure of $ZnCl_2$ and $FeCl_3$ was obtained on the large surfaces of the supports.

A series of tests at 100°C with $ZnCl_2$ supported on Celite were conducted as a function of contact time which was varied from 2 to 12 hr. The resultant conversions listed in Table 3 under Test C were conveniently based on 100 gm moles of initial mixture, and in each case the initial compositions in the ampules were practically the same at 1.2 moles of HCl per mole of vinyl chloride. Several significant conclusions can be drawn from these tests. Up to 12 hr, it was apparent that chemical equilibrium had not been attained because each succeeding test gave higher conversions. For 12 hr and beyond, a plot of percent vinyl chloride conversion vs contact time, which is presented in Figure 20 and Table 4, shows only a slight tendency to reach a plateau. It is probably safe to say, therefore, that equilibrium had not been attained even for 12 hr of contact time.

The functional relationship between the moles of unconverted vinyl chloride and contact time is presented in Figure 21 and Table 5. The curve shows that the rate of vinyl chloride disappearance decreased with time, which would be expected on the basis of a decrease in concentration and a decrease of catalyst activity. As shown under Tests E and F in Table 3, a comparison between the conversion obtained in the presence of

$ZnCl_2$ on 60-80 mesh Dicalite with that obtained in the presence of $ZnCl_2$ on 10-20 mesh silica gel indicated that a higher conversion was obtained in the presence of silica gel.

In an effort to determine the nature of the catalytic decomposition of vinyl chloride, samples of the product gas over a $ZnCl_2$ catalyst were analyzed as stated under EXPERIMENTAL PROCEDURE in an infrared spectrometer. The results of a typical spectrum are shown in Figure 18A. It was not unreasonable to suspect, based on the structure and chemical compositions of vinyl chloride, that HCl, methane, acetylene, hydrogen, ethylene or even ethane were among the gaseous products of decomposition. By comparing the spectrum of natural gas shown in Figure 18B with the spectrum shown in Figure 18A, the presence of methane or ethane in the product gas was eliminated. A similar comparison of the characteristic absorption bands for acetylene and ethylene, which are listed in the legend of Figure 18, eliminated these substances. The negative results were also an indication that the feed streams were free of the hydrocarbons mentioned above.

There still remained HCl, hydrogen and solid carbon as the possible products of decomposition. If these were the products of decomposition, the fouling may have begun by the splitting off of HCl from monomeric vinyl chloride. Then acetylene, an intermediate product, by a series of catalyzed decomposition steps finally yielded hydrogen and carbon.

The alternative possibility is that induced polymerization of the vinyl chloride occurred in the presence of the metallic

chlorides, and the resultant polymer decomposed to acetylenic residues on the surface of the catalyst.

A definite mechanism for the fouling reaction cannot be obtained on the basis of evidence collected to date. It can only be said that the absence of certain species and the positive identification of carbon limit to some extent the number of possibilities.

Rate Studies of Heterogeneous Catalysis in the Stirred Reactor

The results of the stirred-reactor experiments in which the amount of catalyst was 20 gm of $ZnCl_2$ supported on 100 gm of Celite pellets are listed in Tables 6a, 6b, 6c, and 6d.

Temperature Control.--For runs 1 through 25 inclusive, the average temperature was 215.0 ± 0.4°F, and the average difference in temperature between the top and bottom of the reactor was 0.22 ± 0.06°F. For runs 26 through 28, the corresponding values were 163.9 ± 0.1°F and 0.15 ± 0.01°F, and for runs 29 through 39, 299.0 ± 0.1°F and 0.25 ± 0.03°F. Tests showed that, for feed rates corresponding to a retention time of 45 min, a significant temperature gradient, on the order of 1°F/ft, developed within 3 or 4 min when the stirrer was stopped. The small temperature gradients, therefore, were an indication that the stirring rate was sufficiently high to obtain good mixing in the reactor. The temperature of the oil-bath in which the reactor was immersed differed from the average values in the reactor by only ± 0.2°F, which indicated that no large gradients existed in the radial direction.

Pressure Control.--An approximate indication of the pressure drop across the reactor was obtained from the rotameter manometer which measured the upstream pressure of both the reactor and the rotameters. As shown in Table 6a, the pressure drop varied slightly according to the flow rate through the system. For the maximum total feed rate of 27.4×10^{-3} lb/hr, the pressure drop was 0.0076 psi; and for the minimum rate of 1.98×10^{-3} lb/hr, it was 0.0040 psi. Hence, for all practical purposes the pressure in the reactor was uniform and equal to the absolute pressure of the surroundings.

Product Sampling.--In runs 1 and 2, corresponding to the first 30 hrs of operation, a small quantity of viscous liquid appeared on the cool surface of the product line. This was attributed to slight polymerization of the vinyl chloride. Its appearance as a polymer in the product line indicated that it was a low-molecular-weight material with a relatively high vapor pressure in comparison to the usual organic polymers. After approximately 6 hr, the rate of polymerization seemed to decrease sharply and by the end of 30 hr had essentially reached zero.

Since the conversion during the first 55 hr operation, which included runs 1 through 3, was relatively high, the method of sampling was modified during the experiments because of the possibility of 1,1 dichloroethane condensation in the product line. According to Radulescu (28), the vapor pressure of 1,1 dichloroethane is related to temperature by the following equation:

$$\log_{10} p_{cm} = 6.1560 - \frac{1258.1}{(T-36)} \qquad (8)$$

where

p = vapor pressure in cm Hg

T = temperature in °K

At 25°C, the equation predicts a vapor pressure of 22.6 cm which, by assuming ideal gases, represents a mole fraction of 0.30 in the gas phase. Thus, to prevent condensation, the product stream in passing through the sampler, was maintained at the reactor temperature. In Table 6a, the tabulated mole fractions of 1,1 dichloroethane for runs 1 through 3 are greater than the saturation value at 25°C, indicating the necessity of maintaining a high sampling temperature. After 55 hr, the conversion had decreased because of fouling so that heating the sampler was no longer necessary.

Feed Rates.--The feed rates of HCl and vinyl chloride were recorded at half-hour intervals during each run, which usually lasted from 15 to 18 hr. Between runs, the flow rates were reduced to very low values, but nevertheless the weight ratio of vinyl chloride to HCl was kept within the range of 2.16 to 2.46 at a constant temperature. In most cases, the rotameter readings varied over a range of ± 3% even with the temperature controlled at 25°C. For this reason, the net flow rates for each run were determined by graphical integration. The calibration charts in Figures 1A and 2A of Appendix I were

used to convert from rotameter-scale readings to mass rates. The mass rates of each reactant, the total mass rate, the weight ratio of vinyl chloride to HCl, and the weight ratio of total mass rate to catalyst weight are listed in Tables 6a and 6b.

Product Composition.--From the corrected areas of the chromatograms, the composition of the product stream was computed on a weight basis and converted to mole fractions. By assuming that the product stream could be adequately described by Dalton's law (29), the partial pressure of each component was computed from the product of its mole fraction and the total pressure. The composition in weight and mole fractions and the partial pressures in atmospheres are listed in Tables 6b and 6c.

Retention Times.--The capacity of the reactor, expressed in moles of ideal gas, is listed in Table 6c and was based upon the temperature and pressure of operation. From this value and the molar flow rates, the retention times were calculated. It is interesting to note that even for the highest molar flow, namely 53.6×10^{-5} lb moles/hr, the retention time of 45 min was probably sufficient for diffusion to occur between the gas phase and the catalyst surface, without limiting the rate of reaction.

Material Balance.--A useful method of determining the validity of the product analysis was to carry out a material balance. This was accomplished by assuming that each mole of

1,1 dichloroethane was formed from a mole each of HCl and vinyl chloride. Thus, a computation of the initial feed ratio required to give the products was compared with the experimental feed ratio. The calculated ratio and the percentage difference of the compared ratios are listed in Table 6d. During the first 350 hr of operation at 215°F the deviation averaged -15.6%, and similarly during the initial 200 hr at 299°F it averaged -9.0%. In both cases, the fact that the computed values of the vinyl chloride-HCl ratio were lower than the experimental values was evidence that a side reaction was consuming vinyl chloride. From the results of the batch experiments it was reasonable to assume that the side reaction was fouling of the catalyst.

After 350 hr at 215°F, the percentage deviation in the material balance decreased sharply and attained an average of ± 3.6%. Likewise, after 200 hr at 299°F, it became ± 3.8%, whereas at 164°F it averaged ± 2.6% for the entire period of 65 hr.

Catalyst Fouling.--The effect of fouling produced on a catalyst is best shown by plotting the conversion against the catalyst exposure-time for fixed conditions of temperature, pressure, feed ratio and space velocity. Significantly, the rate of catalyst fouling at any time is given by the slope of the curve. The catalyst exposure time is defined as the total time in which the catalyst has been exposed to the reacting mixture.

In Figure 22, the conversion at 215°F is plotted against catalyst exposure-time for parameters of feed ratio and F/W. The general trend of the curve shows that, because of fouling, the conversion continually decreased for approximately 450 hr. At the end of that time, it leveled off and remained reasonably constant for the remaining 650 hr. These results suggested that steady conditions with respect to fouling had been attained, but even more significant was the fact that the conversion had not decreased to zero. This was important evidence indicating that the fouling mechanism involved reversible fouling or irreversible, multi-site fouling but not irreversible single-site fouling. If the latter mechanism were the case, the conversion would have decreased to zero.

In runs 26 through 28 at 164°F, which followed the runs at 215°F, no fouling was observed. This was not too surprising since in going from a higher to a lower temperature the fouling rate, which reached nearly zero at 215°F, would be expected to decrease.

In runs 29 through 39 at 299°F, which followed the runs at 164°F, a fouling period followed by a non-fouling period was again observed. A plot similar to Figure 23 is presented in Figure 24. It shows that in comparison to the fouling at 215°F, the additional fouling at 299°F was much less. Under DISCUSSION OF RESULTS, a critical evaluation of the type of fouling at the three experimental temperatures is presented in detail.

Rate of Reaction.--For the rigorous determination of the rate of the primary reaction during the fouling period, Equation 6 under THEORY is applicable.

$$F_i n_{A_i} - (F_i - F_f) n_{A_o} + r_{w_A} W = \frac{pV_r}{RT} \frac{d(M_{av}\, n_{A_o})}{d\Theta} \qquad (6)$$

In the present work, n_{A_i} equals zero. The relative order of magnitude of F_f was determined approximately by the ratio of the total mass of fouling material, i.e. the carbonaceous deposit on the catalyst, to the total exposure time of the catalyst. The quantity was found to be 0.5% of the feed rate at early exposure times and thus can be neglected. The time derivative in Equation 6 was determined by measuring the slope of the curve in Figure 22 at zero exposure time. This method was valid in the present work, since the feed ratio of vinyl chloride to HCl was maintained relatively constant throughout the experimental program. The value of the slope at zero time, multiplied by its coefficient in Equation 6, was compared to the term $F_i n_{A_o}$ and found to be only 2% of that quantity. Based upon the above arguments, Equation 6 can be approximated by,

$$F_i n_{A_o} = r_{w_A} W \,, \qquad (6a)$$

which is equivalent to Equation 8 for the case of no fouling and steady state.

The rate was not computed for the first 6 hr of operation because of the transient conditions resulting from start-up.

A plot of conversion vs W/F at 215°F for an average feed ratio of 2.30 ± 0.04 is shown in Figure 24. The values in the plot were obtained from data for the non-fouling period which included runs 14 through 25. If the conversion in these experiments were near equilibrium, the curve would show an asymptotic slope, but its nearly linear trend indicates that the conversions were relatively low compared to equilibrium. The slope at any point on the curve is the instantaneous rate of reaction which is nearly constant for values of W/F up to 23 (lb catalyst/lb feed)(hr).

Order of the Primary Addition Reaction.--A procedure for determining empirically the order of reaction was based upon the following equation,

$$r_{1,1} = C\left(p_{HCl}^{\ a}\, p_{v.c.}^{\ b} - \frac{p_{1,1}}{K_p}\right) \qquad (9)$$

The exponents, a and b, were assigned values of 0.5, 1.0, 1.5, and 2.0 in all possible combinations and were applied to non-fouling data at large space velocities. Under these conditions, the term $p_{1,1}/K_p$ could be neglected. It was found that the drift in the calculated values of C was a minimum when the exponents of p_{HCl} and $p_{v.c.}$ were equal to 1. In further analyses of the data, therefore, the primary addition reaction

was assumed to be second order. This assumption was verified by the subsequent correlation of the data.

Interpretation of the Reaction Rate, $r_{1,1}$.--An attempt to determine the most plausible mechanism for the bimolecular reaction between HCl and vinyl chloride was based upon the assumption that one chemical step was rate-controlling. Upon this assumption, 10 different mechanisms seemed possible. Diffusion in the gas phase was not considered controlling under the conditions of complete mixing. The possible mechanisms, together with their corresponding rate equations, expressed in convenient form for comparison, are listed in Table 8A of Appendix I, wherein the nomenclature of Smith (37) and Emmett (43) is used. The mechanisms, which were chosen, in no way exhausted the possibilities but appeared to be the most logical ones for describing the catalyzed reaction between HCl and vinyl chloride.

The general form of the rate equations in Table 8A of Appendix I, can be written as,

$$r_{1,1} = C'\left(a_{HCl}\, a_{v.c.} - \frac{a_{1,1}}{K}\right) \qquad (10)$$

where: K = thermodynamic equilibrium constant.

a_i = activity of component i.

C' = a function of K, K_i, and a_i, depending on the rate-determining step.

K_i = adsorption equilibrium constant for component i.

The lack of activity data requires the use of concen-

trations or partial pressures or the assumption of unit values for activity coefficients. In terms of partial pressure, Equation 10 becomes,

$$r_{1,1} = C\left(p_{HCl}\, p_{v.c.} - \frac{p_{1,1}}{K_p}\right) \qquad (10a)$$

In testing each of the models separately, data for the non-fouling period at 215°F were used in a least-squares analysis, according to a method outlined by Hougen and Watson (26). A criterion used in establishing the rate-controlling mechanism requires that constants obtained from the least-squares analysis have positive or zero values.

None of the mechanisms tested gave all positive or zero values for the coefficients. This was an indication that either the correct mechanism had not been tested or that the calculations were too sensitive to small variations in the data. It is probable that the latter explanation was largely responsible for the apparent lack of correlation. If, for example, the adsorption constants had large differences in magnitude, a higher degree of precision would be required in the least-squares analysis.

A close examination of the negative coefficients obtained in the least-squares computation indicated that Equation 1-8A, i.e.

$$r_{1,1} = \frac{k_1 K_a K_b \left(p_a p_b - \frac{p_c}{K_p}\right)}{(1 + K_a p_a + K_b p_b + K_c p_c)^2} \qquad (1\text{-}8A)$$

gave values closer to zero compared to the other mechanisms. As stated in Table 8A, the above equation applies to the mechanism in which the surface reaction between two adsorbed molecules is controlling. On a comparative basis, therefore, Equation 1-8A appears to fit the experimental observations most favorably.

Another method of analyzing the data at 215°F in terms of the possible mechanisms, was by a simultaneous solution of each equation listed in Table 8A of Appendix I. In this case, the value for K_p was taken as 17.2 atm^{-1}. Since data from 12 runs (14 to 25, inclusive) were available, the simultaneous solutions to determine the four unknowns in each equation were obtained for all possible combinations of 12 runs. Only Equation 1-8A, for certain combinations of the 12 runs, gave all positive values of the computed coefficients. The results of these calculations, including the combinations of runs, are listed in Table 8A of Appendix I. The average values obtained are only relative orders of magnitude and could not be used with confidence in a general rate equation.

Empirical Calculations for the Equilibrium and Rate Constants.--Since the attempt to determine the mechanism of the reaction by calculating the equilibrium coefficients and rate

constant was unsuccessful, an empirical correlation of the rate data was obtained by assuming that the factor C in Equation 10a varies only with temperature and catalyst activity.

Published values (30) of the thermodynamic equilibrium constant, K, which had been obtained indirectly from heats of combustion could not be used in Equation 10a for the calculation of C. In fact, the conversions obtained experimentally exceeded those predicted from the published K by a factor of nearly 20. This unusually large difference could not be explained on the basis of experimental error. The internal consistency of the data plus the relatively good material balance in the non-fouling periods suggested that further experimentation is required to confirm the discrepancy.

An alternative analysis was chosen in which K_p was computed empirically from the rate data. For this calculation, Equation 10a was solved for K_p and C simultaneously by a least-squares procedure. Data from runs 14 through 25 at 215°F were used, because the fouling rate during these runs had decreased to nearly zero. A complete tabulation of the numerical values substituted into the least-squares equations is presented in Table 6A of Appendix I. The value obtained for K_p was 17.2 atm^{-1} whereas the published, thermodynamic K is 0.172 atm^{-1} at 215°F. Also, a solution of Equation 10a for C and K_p was obtained from runs 24 and 25, which were the final runs in the non-fouling period at 215°F. The value of 18.7 atm^{-1}, computed for K_p, agreed reasonably well with the least-squares value.

At 25°C, the standard free energy change corresponding to the above values of K is 4.67 kcal/gm mole for the computed K_p (17.2 atm^{-1}) and 1.94 kcal/gm mole for the published K.

K_p at 164 and 299°F was calculated from the Van't Hoff equation using published heats of formation and heat capacities (31,32,33,34,35,36). The values obtained are 86.2 and 2.0 atm^{-1}, respectively. The calculations are shown in detail in Table 7A of Appendix I.

With the computed values of K_p, Equation 10a was used to determine C for both the fouling and non-fouling periods at each temperature. Multiplication of C by $(RT)^2/M_{1,1}$ converted it to C_c which has conventional concentration units. Both C's are listed in Table 6d.

Effect of Catalyst Exposure Time on C_c.—A plot of C_c vs catalyst-exposure time at 215°F is shown in Figure 26. The values for runs 4, 5, and 9 are omitted from the plot because of experimental inaccuracies in the data. The curve shows a steady decline for the first 450 hr to an asymptotic value greater than zero. A similar plot for C_c at 299°F is shown in Figure 27. Since no fouling occurred at 164°F, C_c at that temperature did not drift as a function of catalyst exposure time.

Fouling Factor in the Rate Expression.—It is evident that the complete rate equation for a catalyst which undergoes fouling must include a fouling factor to account for the effect of catalyst exposure-time. According to other investi-

gators (26,37), there are not sufficient data available on any one system to establish with certainty the best procedure for introducing such a factor into a fundamental rate equation. Several alternatives are presently in use. Among the possibilities, a term may be introduced as a multiplying factor in the numerator of the rate equation, with the idea that fouling reduces the total number of active centers on the catalyst surface. The method used in the present work was based on this hypothesis. For this purpose, an equation relating C_c to catalyst exposure-time at 215°F was obtained for the curve shown in Figure 26. The resultant equation which is only an approximation is given as follows:

$$C_c = \left(0.589 + 10.341\, e^{f(t_e)}\right) \times 10^2 \qquad (11)$$

where $f(t_e)$, determined by least-squares, has the form

$$f(t_e) = (2.303)(0.001378\, t_e - 2.87278 \times 10^{-5}\, t_e^{\,2} + 4.2623 \times 10^{-8}\, t_e^{\,3} - 1.814 \times 10^{-11}\, t_e^{\,4}) \qquad (12)$$

The experimental data were insufficient to obtain a functional relationship between temperature and the fouling factor. In general, fouling experiments at each temperature, beginning with fresh catalyst, are required before a temperature function can be derived with confidence.

The final empirical equation which can be used to predict the amount of 1,1 dichloroethane formation, with a mass feed ratio of vinyl chloride to HCl in the range of 2.16 to 2.46, is given for 215°F as,

$$n_{1,1} = \frac{W}{F}\left[\frac{0.589 + 10.341\, e^{f(t_e)}}{(RT)^2/M_{1,1}}\left(p_{HCl}\, p_{v.c.} - \frac{p_{1,1}}{17.2}\right)x\ 10^2\right] \qquad (13)$$

With additional knowledge of the temperature dependence of fouling, Equation 13 could be modified to apply over the temperature range investigated.

Temperature Dependence of C_c based upon the Non-Fouling Activity Level at 215°F.—The average value of C_c at 164 and 215°F for the non-fouling periods, which corresponded to identical catalyst activity levels, were computed to be 8.75 and 60.19 (lb moles 1,1 dichloroethane)$(ft^3)^2$/(hr)(lb catalyst)(lb moles)^2, respectively. Since additional fouling at 299°F had decreased the catalyst activity, the value of C_c at that temperature corresponding to the same activity level was approximated by using its value obtained in the initial stage of the fouling period. This quantity was found to be 722.3 (lb moles 1,1 dichloroethane)$(ft^3)^2$/(hr)(lb catalyst) (lb moles)^2.

The fact that Equation 10a is similar in form to a

homogeneous rate equation suggested an Arrhenius-type temperature dependence of C_c. A plot of log C_c vs 1/T is shown in Figure 25 which gives a straight line. This linearity indicates that the second-order rate law given by Equation 10a describes, at least empirically, the behavior of the reacting system.

Temperature Dependence of C_c for Non-Fouling Activity Levels.--At 215 and 299°F, the average values of C_c for the non-fouling period were 60.19 and 339.8 (lb moles 1,1 dichloroethane)$(ft^3)^2$/(hr)(lb catalyst)(lb moles)^2, respectively. Since the fouling is assumed to be irreversible, the average C_c for runs 26 to 28 at 164°F does not represent the actual activity level of the catalyst for the non-fouling period at that temperature. This is true because the previous runs 1 to 25 were made at 215°F, at which the degree of fouling was greater than that obtainable at 164°F.

Based upon the hypothesis that C_c for the non-fouling periods obeys an Arrhenius-type equation, a straight line is then drawn through the values of C_c at 215 and 299°F on an Arrhenius plot in Figure 25a and extrapolated to 164°F. At that temperature, the extrapolation value of C_c is 16.5 (lb moles 1,1 dichloroethane)$(ft^3)^2$/(hr)(lb catalyst)(lb moles)^2.

From these results, the temperature dependence of C_c is given by the equation,

$$C_c = 4.07 \times 10^8 \, e^{-\frac{21,100}{RT}} \qquad (14)$$

Equation 14 can be combined with Equations 10a and 8 to give an expression for predicting the conversion during the non-fouling period.

$$n_{1,1} = \frac{W}{F}\left[\frac{4.07 \times 10^8 \, e^{-\frac{21,100}{RT}}}{(RT)^2/M_{1,1}}\left(P_{HCl}\, P_{v.c.} - \frac{P_{1,1}}{K_P}\right)\right] \qquad (15)$$

Equation 15 is applicable under varying conditions of residence time for the temperature range of 164 to 299°F, for mass ratios of vinyl chloride to HCl in the range of 2.16 to 2.46, and for catalyst-exposure times up to 1800 hr. Small changes in total pressure would not be expected to noticeably affect the final, steady-state fouling.

The equilibrium constant K_p is related to temperature by,

$$\ln K_p = 7.889 + \frac{1}{1.987}\left[\frac{13,559}{T} - 4.9 \ln T + 0.0054\, T - 19.15\right] \qquad (7\text{-}7A)$$

Equation 7-7A is derived in detail in Table 7A of Appendix I.

Because of the assumptions involved, Equation 15 is, at best, an empirical fit to the experimental data. Its general form, however, has some theoretical basis which is discussed in detail under DISCUSSION OF RESULTS.

DISCUSSION OF RESULTS

Reaction Mechanism for the Addition of HCl to Vinyl Chloride

In the arguments of Kharasch (6,9,10,11) and Wibaut (3), which are presented under INTRODUCTION, it was stated that mechanistically the addition of HCl to mono-olefins in the presence or absence of a catalyst is the same as the addition of HBr to vinyl chloride in the presence of $FeCl_3$. The 1,1 product, in all cases, is formed. Kharasch referred to these reactions as "normal" addition reactions which proceed according to Markownikoff's rule (38).

Kharasch further stated that the "abnormal" addition of HBr to olefins, especially in the presence of peroxides, was a chain reaction involving Br. The product, in this case, is always the 1,2 alkyl halide. His arguments were correct except that the free radical Br· is the chain carrier rather than Br.

In the present work, the fact that only the 1,1 product of the HCl addition to vinyl chloride was formed eliminated the possibility that the reaction was propagated by free radicals. A free radical reaction would occur as follows (39,40):

Mechanism A: $R\cdot + HCl \longrightarrow RH + Cl\cdot$ (A)

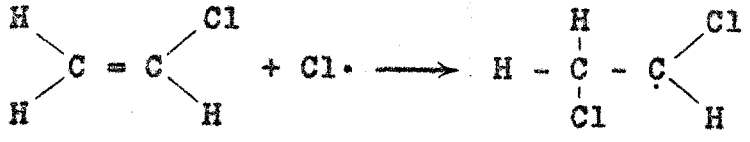

(B)

The resultant free radical would react further to form the product 1,2 dichloroethane by the reaction,

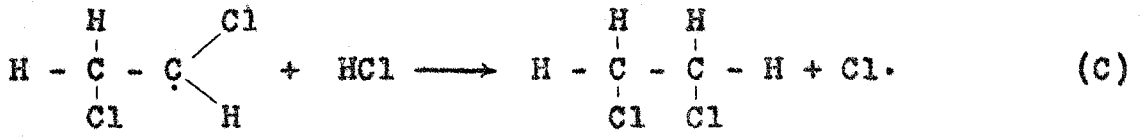

(C)

The major barrier preventing the occurrence of the above reaction is the difficulty in forming Cl· from HCl in which the hydrogen-chlorine bond is quite strong, i.e., 102.7 kcal/gm mole (41). Raley, et al (42), report, however, that the reaction can be accomplished in this manner.

From the above arguments, it is clear that the catalyzed or non-catalyzed addition of HCl to vinyl chloride must occur, under ordinary conditions, by a mechanism other than free-radical. One such mechanism would involve a bridged-carbonium ion (39) as a transition product and can be represented by the following steps:

Mechanism B:

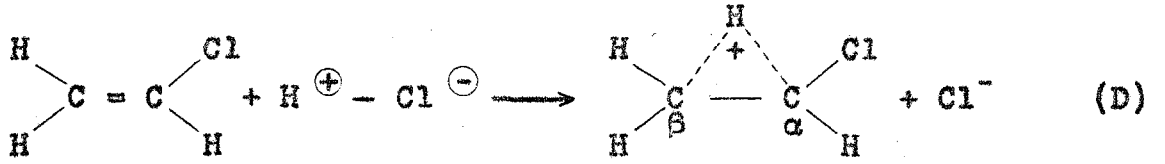

(D)

Reaction D requires that the molecule attacking the olefin be polar in nature. HCl has a dipole moment of 1.03×10^{-18} esu. The resultant bridged-carbonium ion acquires a net

positive charge on the α carbon relative to the β carbon, when it is attacked on the back-side by a Cl^- ion. This is because of the stabilizing effect of the Cl group on the α carbon. Thus:

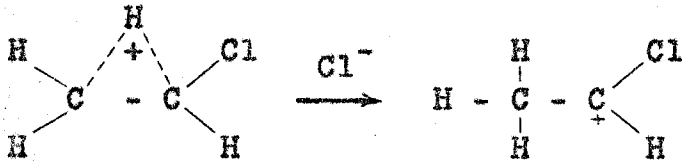

(E)

The classical carbonium ion of Equation E reacts with Cl^- to give 1,1 dichloroethane by the following reaction,

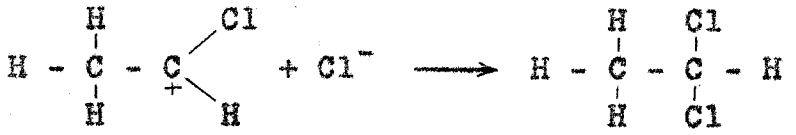

(F)

In the presence of an ion-solvating medium, Mechanism B can occur with relative ease because of the presence of H^+ and Cl^-. In the gas phase or on a non-solvating catalyst, Mechanism B becomes less probable. The solvating effect of anhydrous $ZnCl_2$ on adsorbed HCl is not known so that the contribution of Mechanism B in the catalyzed addition reaction is uncertain.

The second type of non-chain mechanism for addition reactions is frequently called a "four-center" reaction (39,40). In this case, the atoms in the reactants change their configuration to that of the product without the formation or destruction of ions. In the transition state resulting from the collision of an HCl molecule with a vinyl chloride molecule,

four atoms are each simultaneously forming a new bond and breaking an old one. It is especially important to note here that this type of reaction requires a high degree of molecular orientation before reaction occurs. A catalyst such as $ZnCl_2$ probably orients the molecules on the active sites and thus increases the probability of reaction. This reaction can be represented in the following manner:

Mechanism C:

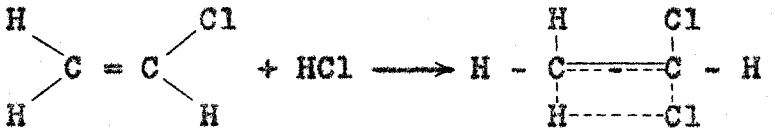

(G)

(H)

Mechanism C, in comparison to Mechanisms A and B, would be expected to give the lowest rate of reaction because of its small steric factor.

The very low rates encountered in the stirred reactor even with catalysis strongly suggest that Mechanism C is primarily responsible in forming the product. Moreover, the empirical fit of the rate data to a second-order, bimolecular reaction is a good indication that the activated complex whether formed by Mechanism B or C consists of a combination of a single HCl and vinyl chloride molecule.

Type of Fouling

It has been pointed out under RESULTS that the formation of a carbonaceous deposit on the catalyst surface was believed to be from the decomposition of vinyl chloride. The degree of reversibility of this reaction and the probable site characteristics of the catalyst surface are important phenomena which can be used to explain the decreasing conversion, in the primary reaction, to an asymptotic value. In the following discussion, several models of fouling are established and are used in a subsequent explanation of the experimental observations.

Model for Reversible Fouling.--For reversible fouling, an equilibrium expression can be written in terms of the activities of the components in the fouling reaction. This reaction may be presumed to occur as follows:

$$nA_1 \rightleftharpoons nA_a \rightleftharpoons B_a + \begin{matrix} m\ C_a \\ \Vert\downarrow \\ m\ C_1 \end{matrix} \qquad (17)$$

where:

A_1 and A_a = the primary fouling reactant in the gas phase and adsorbed phase, respectively.

B_a = a fouling product which is irreversibly adsorbed.

C_1 and C_a = a fouling product in the gas phase and adsorbed phase, respectively.

Representing the activities by the above definitions and the equilibrium constants by K, the following expressions can be written:

$$K_a = \frac{(C_1)^m B_a}{(A_1)^n} \qquad (18)$$

$$K_1 = \frac{A_a}{A_1}, \quad K_2 = \frac{B_a (C_a)^m}{(A_a)^n}, \quad \text{and} \quad K_3 = \frac{C_1}{C_a} \qquad (19a,b,\& c)$$

Combining Equations 18 and 19a,b & c, the expression for K_a becomes,

$$K_a = K_1^{\,n} K_2 K_3^{\,m} \qquad (20)$$

According to the evidence obtained in the batch experiments, the fouling reaction was probably endothermic so that K_2 would have a positive temperature coefficient. If, in this hypothetical mechanism, the net contributions of the positive temperature coefficients of K_2 and K_3 were greater than the negative coefficient of K_1, the coefficient of K_a would be positive.

Attainment of equilibrium in the fouling reaction would occur only if all the products and reactants were present in the system at near equilibrium concentrations. In the stirred reactor, however, a reversibly adsorbed fouling product, differing in composition from the primary reactants, would continually be purged from the reactor, so that equilibrium would

never be attained. If, on the other hand, the reversibly adsorbed product were identical to one of the reactants such as HCl, equilibrium could be attained for small changes in reactant concentrations.

An alternative assumption for reversible fouling would consider only the formation of an irreversibly adsorbed fouling product. The overall equilibrium constant would be given by,

$$K_a = K_1^{\,n} K_2 \qquad (21)$$

where:

$$K_1 = \frac{A_a}{A_1} \quad \text{and} \quad K_2 = \frac{B_a}{(A_a)^n} \qquad (22a \ \& \ b)$$

As in the previous case, K_a would have a positive temperature coefficient if the coefficient of K_2 for the endothermic decomposition were greater than the negative coefficient of K_1.

Model for Irreversible Fouling.--For irreversible, dual-site fouling the catalytic surface is assumed to contain two classes of active sites, namely, those which catalyze the primary reaction and those which catalyze either the primary reaction or a fouling reaction or both. This case is the simplest to treat theoretically because once fouling has occurred, changes in temperature and composition of the gas phase have no effect in changing the activity of the catalyst. The fouling curve for the irreversible dual-site model would

look similar to the curve for the reversible case wherein the conversion decreases to an asymptotic value different from zero. In Figure 22, which was discussed under RESULTS, such a curve resulted for the fouling data at 215°F.

Discussion of Experimental Observations with Respect to the Fouling Models.--With regard to the above discussion, the effects on the fouled catalyst of changing the temperature above and below 215°F are discussed briefly here.

If the fouling at 164°F were reversible, its equilibrium condition for K_a having a positive temperature coefficient would result in a lower conversion than that predicted by considering only the increase in reaction temperature relative to 215°F. The shift in equilibrium would show a steady decrease in conversion as a function of catalyst-exposure time. As shown in Figure 23, such a condition was observed. Thus, the hypothesis of reversible fouling, for which the equilibrium constant, K_a, has a positive temperature coefficient and in which the products and reactants are not removed from the reactor, would fit the observed facts at 299°F. The primary weakness in this hypothesis, however, is that re-forming the reactants from the carbonaceous deposit would be rather unlikely in the temperature range investigated.

The decreasing conversion at 299°F can also be explained on the basis of irreversible, dual-site fouling. As shown in Figure 22, the rate at 215°F had decreased to a very low value because of the diminishing concentration of foulable sites. It is possible that, with an increase in temperature,

the resulting increase in specific rate would be sufficient to give a measurable rate of additional fouling. The fact that the fouling curve again reached an asymptotic value was in agreement with the dual-site hypothesis. In this case, also, the formation of a carbonaceous deposit on the catalyst is more likely the product of an irreversible reaction than a reversible one. Until further investigation is conducted over a wider temperature range, the irreversible dual-site mechanism appears to fit the observed facts most favorably.

Relationship between Primary Reaction and Dual-Site Fouling Model.--Referring to the previous discussion that the primary reaction is probably a four-center-type mechanism, the dual sites on the catalyst may have different abilities in orienting the molecules. It is apparent, from experimental observation that both sites probably catalyze the primary reaction, but not necessarily at the same rate, and that only one site catalyzes the fouling reaction. Otherwise, either total deactivation or none at all would be observed with respect to the primary reaction.

Polymerization of Vinyl Chloride in the Initial Stages of the Reaction

As noted under RESULTS, slight polymerization of vinyl chloride was observed in the initial 30 hr of the stirred-reactor experiment. Its polymerization can be catalyzed by either acids, bases or free radicals (40). In the presence of Friedel-Craft catalysts such as $AlBr_3$ or $SnCl_4$, the presence

of small amounts of certain promoters, especially water, is usually required to polymerize vinyl chloride. The function of the water may be to solvate ions or furnish protons to the monomer. It is possible, therefore, that the vinyl chloride polymerization was initiated in the presence of both $ZnCl_2$ and minute quantities of moisture. After several hours, the water was probably purged by the dry gases flowing through the reactor. This may explain the rapid decline in polymerization after 6 hr of operation.

CONCLUSIONS

The catalyzed addition of HCl to vinyl chloride was found to occur by a non-free-radical mechanism to give exclusively 1,1 dichloroethane. It is probable that because of the relatively low rate of reaction, even in the presence of a catalyst, the addition occurred by a four-center-type mechanism. In this case, the catalyst $ZnCl_2$ increased the probability of reaction by orienting the reacting molecules.

A fouling reaction was also observed when $ZnCl_2$, supported on Celite, was used as a catalyst. Starting with fresh catalyst, the sequence of temperatures investigated was 215, 164 and 299°F, in that order. The decreasing conversion at 215°F reached an asymptotic value greater than zero, which ruled out the possibility of irreversible single-site fouling. Further changes in the catalyst activity were not observed at 164°F but additional fouling was observed at 299°F. The fact that one of the fouling products was elementary carbon or a carbonaceous residue, suggested that an irreversible dual-site mechanism was in operation.

Attempts to determine the reaction mechanism by computing the absorption equilibrium constants as well as the rate constant for a series of assumed models were unsuccessful. An empirical fit of the observed rate data, however, was obtained by the equation,

$$r_{1,1} = C \left(p_{HCl}\, p_{v.c.} - \frac{p_{1,1}}{K_p} \right) \qquad (10a)$$

wherein $r_{1,1}$ was obtained from the equation,

$$r_{1,1} = \frac{F}{W} \left(n_{1,1} \right) \qquad (8)$$

Published values (30) of the thermodynamic equilibrium constant K, assuming unit activity coefficients, could not be used in Equation 10a to solve for C, because the experimentally observed conversions exceeded the predicted equilibrium values by a factor of nearly 20 in the initial runs. From data for the non-fouling period at 215°F, K_p was determined empirically by a least-squares analysis. The resulting value of 17.2 atm^{-1} was used in the Van't Hoff equation to determine K_p's at 164 and 299°F. The values obtained were 86.2 and 2.0 atm^{-1}, respectively.

Values of C were computed for both the fouling and non-fouling periods at each temperature. In terms of concentration units, the C's were plotted against catalyst-exposure time to obtain a fouling factor. Sufficient data were not available to compute the temperature dependence of the fouling factor. Hence, its determination was limited to the results at 215°F. An equation which includes the effects of fouling and which can be used to predict the approximate conversion of 1,1 dichloroethane at 215°F was obtained as follows:

$$n_{1,1} = \frac{W}{F}\left[\frac{(0.589 + 10.341\, e^{f(t_e)})}{(RT)^2/M_{1,1}}(p_{HCl}\, p_{v.c.} - \frac{p_{1,1}}{17.2}) \times 10^2\right] \qquad (13)$$

where

$$f(t_e) = (2.303)(0.001378\, t_e - 2.87273 \times 10^{-5}\, t_e^{\,2} + 4.2623 \times 10^{-8}\, t_e^{\,3} - 1.814 \times 10^{-11}\, t_e^{\,4}) \qquad (12)$$

The average values of C_c for the non-fouling periods at 215 and 164°F and for the initial fouling period at 299°F were correlated with temperature by a straight-line fit on an Arrhenius plot. This linearity indicates that the second-order rate law given by Equation 10a describes, at least empirically, the behavior of the reacting system.

Based upon the hypothesis that C_c for the non-fouling periods obey an Arrhenius-type equation, a straight line was then drawn through the values of C_c at 215 and 299°F on an Arrhenius plot and extrapolated to 164°F. At that temperature, the extrapolation value of C_c is 16.5 (lb moles 1,1 dichloroethane)$(ft^3)^2$/(hr)(lb catalyst)(lb moles)^2.

From these results, the temperature dependence of C_c is given by the equation,

$$C_c = 4.07 \times 10^8 \, e^{-\frac{21,100}{RT}} \qquad (14)$$

Equation 14 can be combined with Equations 10a and 8 to give an expression for predicting the conversion during the non-fouling period.

$$n_{1,1} = \frac{W}{F}\left[\frac{(4.07 \times 10^8 \, e^{-\frac{21,100}{RT}})}{(RT)^2/M_{1,1}}\left(p_{HCl}\, p_{v.c} - \frac{p_{1,1}}{K_p}\right)\right] \qquad (15)$$

Equation 15 is applicable under varying conditions of residence time for the temperature range of 164 to 299°F, for mass ratios of vinyl chloride to HCl in the range of 2.16 to 2.46, and for catalyst-exposure times up to 1800 hr. Small changes in total pressure would not be expected to noticeably affect the final, steady-state fouling.

RECOMMENDATIONS

The preliminary rate studies discussed in the present work can be used as a starting point in future experiments. In the following list, several experiments are suggested.

1. An experiment should be conducted to determine the composition at chemical equilibrium for the system 1,1 dichloroethane, vinyl chloride and HCl. These tests can be performed over $ZnCl_2$ in a batch reactor which is thermostated at the temperatures used in the present work. A test for equilibrium can be obtained by using initially in one system, a mixture of HCl and vinyl chloride and, in another system, a sample of 1,1 dichloroethane.

2. An extensive series of experiments should be conducted to determine the effects of catalyst fouling as a function of both temperature and pressure, starting with fresh catalyst at each temperature investigated.

3. Data should be obtained in the stirred reactor over a wide range of conditions, at several different temperatures, in order to determine the rate-controlling mechanism by the method of least-squares (26).

4. An analysis of the carbonaceous deposit on the catalyst surface should be obtained by means of mass spectroscopy or by the usual methods of microorganic analysis.

5. Experiments should be conducted to determine the rate of HCl addition to vinyl bromide. A comparison of the results of these tests with the results of the HCl-vinyl chloride system would be useful in studying the contributions of steric effects.

REFERENCES

1. Wibaut, J. P., Dieckmann, J. J., and Rutgers, A. J., Rec. Trav. Chim., 47, 477 (1928).

2. Wibaut, J. P., Rec. Trav. Chim., 50, 313 (1931).

3. Wibaut, J. P., and Van Dalfsen, J., Rec. Trav. Chim., 51, 636 (1932).

4. Kharasch, M. S. and Darkis, F. R., Chem. Rev., 5, 571 (1928).

5. Kharasch, M. S. and Reinmuth, O., J. Chem. Ed., 8, 1703 (1931).

6. Kharasch, M. S., McNab, T. M., and Mayo, F. R., J. Am. Chem. Soc., 55, 2469, 2521, and 2531 (1933).

7. Kharasch, M. S. and Hannum, C. W., J. Am. Chem. Soc., 56, 712 (1934).

8. Kharasch, M. S., Engelmann, H., and Mayo, F. R., J. Org. Chem., 2, 288 (1937).

9. Kharasch, M. S., Kleiger, S. C., and Mayo, F. R., J. Org. Chem., 4, 428 (1939).

10. Kharasch, M. S., Norton, J. A., and Mayo, F. R., J. Am. Chem. Soc., 62, 81 (1940).

11. Kharasch, M. S., Haefele, W. R., and Mayo, F. R., J. Am. Chem. Soc., 62, 2047 (1940).

12. Lonza, Elektrizitatswerke und chemische Fabriken, Swiss 229422, (C.A. 43, 5410e).

13. Barton, D. H. R., J. Chem. Soc., 1949, 148, 155, and 165.

14. Howlett, K. E., Chemistry & Industry, 1952, 1175.

15. Howlett, K. E., J. Chem. Soc., 1952, 3695 and 4487.

16. Denbigh, K. G., Trans. Faraday Soc., 40, 352 (1944).

17. Denbigh, K. G., Trans. Faraday Soc., 43, 648 (1947).

18. Denbigh, K. G., Page, F. M., and Stead, B., Discussions of Faraday Soc., No. 2, 263 (1947).

19. Denbigh, K. G., Hicks, M., and Page, F. M., Trans. Faraday Soc., 44, 479 (1948).

20. Herzberg, G., "Infrared and Raman Spectra of Polyatomic Molecules," D. Van Nostrand Company, Inc., New York, 1945.

21. Randall, H. M., et al, "Infrared Determination of Organic Structures," D. Van Nostrand Company, Inc., New York, 1949.

22. Johns, Theron, "Beckman/Gas Chromatography Manual," Beckman Instruments, Inc., Fullerton, California.

23. Carbide and Carbon Chemicals Company, "Physical Properties," Company Publication, 1957.

24. Dow Chemical Company, personal communication.

25. Sano, K., J. Chem. Soc. of Japan, 59, 1073 (1938).

26. Hougen, Olaf A., and Watson, Kenneth M., "Chemical Process Principles," John Wiley and Sons, Inc., London, 1947.

27. Lucas, Howard J., "Organic Chemistry," American Book Company, New York, 1935.

28. Radulescu, D., and Alexa, M., Bul. Soc. Chim. Romania, 20A, 89 (1938).

29. Denbigh, K. G., "The Principles of Chemical Equilibrium," University Press, Cambridge (1955).

30. Mikawa, Y., J. Chem. Soc. Japan, 73, 79 (1952).

31. Kobe, K. A., and Harrison, R. H., Petroleum Refiner, 30, No. 11, 151 (1951).

32. Perry, J. H., (editor) "Chemical Engineers' Handbook," McGraw-Hill Book Company, Inc., New York, 1950.

33. Liang, C. Y., and Nielsen, J. R., J. Chem. Phys., 22, 1293 (1954).

34. Rossini, F. D., et al, "Selected Values of Chemical Thermodynamic Properties," U. S. National Bureau of Standards Circular 500 (1952).

35. Kobe, K. A., and Harrison, R. H., Petroleum Refiner, 36, No. 10, 155 (1957).

36. Pitzer, K. S., and Li, J. C. M., J. Am. Chem. Soc., 78, 1077 (1956).

37. Smith, J. M., "Chemical Engineering Kinetics," McGraw-Hill Book Company, Inc., New York, 1956.

38. Markownikoff, W., Ann., 153, 256 (1870).

39. Hine, J., "Physical Organic Chemistry," McGraw-Hill Book Company, Inc., New York, 1956.

40. Ingold, C. K., "Structure and Mechanism in Organic Chemistry," Cornell University Press, New York, 1953.

41. Pauling, L., "The Nature of the Chemical Bond," Cornell University Press, London, 1948.

42. Raley, J. H., Rust, F. F., and Vaughn, W. E., J. Am. Chem. Soc., 70, 2767 (1948).

43. Emmett, Paul H. (editor), "Catalysis," Vol. I, Reinhold Publishing Corp., New York, 1954.

NOMENCLATURE

C = empirical, bimolecular rate constant, (lb 1,1 dichloroethane)/(hr)(lb catalyst)(atm^2).

C_c = empirical, bimolecular rate constant, (lb moles 1,1 dichloroethane)(ft^3)^2/(hr)(lb catalyst)(lb moles)^2.

C_j = concentration of component j (excluding the letters c and p) in reaction mixture, lb/ft^3.

C_p = heat capacity at constant pressure, cal/(gm mole)(°K).

F_1 = feed stream, lb/hr.

F_j = component j flow, lb/hr.

F_1 = feed stream, lb moles/hr.

F_j = component j flow, lb moles/hr.

F_o = exit stream, lb/hr.

F_f = fouling deposition on catalyst, lb/hr.

ΔH_f = enthalpy of formation, kcal/gm mole.

ΔH_v = enthalpy of vaporization, kcal/gm mole.

K_P = equilibrium constant for reaction between HCl and vinyl chloride, atm^{-1}.

K_j = adsorption equilibrium constant for component j.

k = bimolecular rate constant used in equations of Table 8A.

m = total mass in reaction mixture, lb.

M = molecular weight, lb/lb mole.

N_R = molal capacity of reactor, lb moles.

n_j = weight fraction of component j.

n_j = mole fraction of component j.

n_{j_i} = weight fraction of component j in feed stream.

n_{j_o} = weight fraction of component j in exit stream.

P = pressure, atm.

p_j = partial pressure of component j, atm.

R = gas constant, (atm)(ft^3)/(lb mole)(°R).

r_{w_j} = rate of formation of component j, lb j/(hr)(lb catalyst).

T = temperature (scale according to use).

t_r = retention time in the reactor, hr.

t_e = catalyst exposure time, hr.

V_r = volume of reaction mixture, ft^3.

W = weight of catalyst, lb.

θ = time, hr.

Values of Subscript j:

A = arbitrary product A.

HCl or a = hydrogen chloride

v.c. or b = vinyl chloride

1,1 or c = 1,1 dichloroethane

LIST OF FIGURES

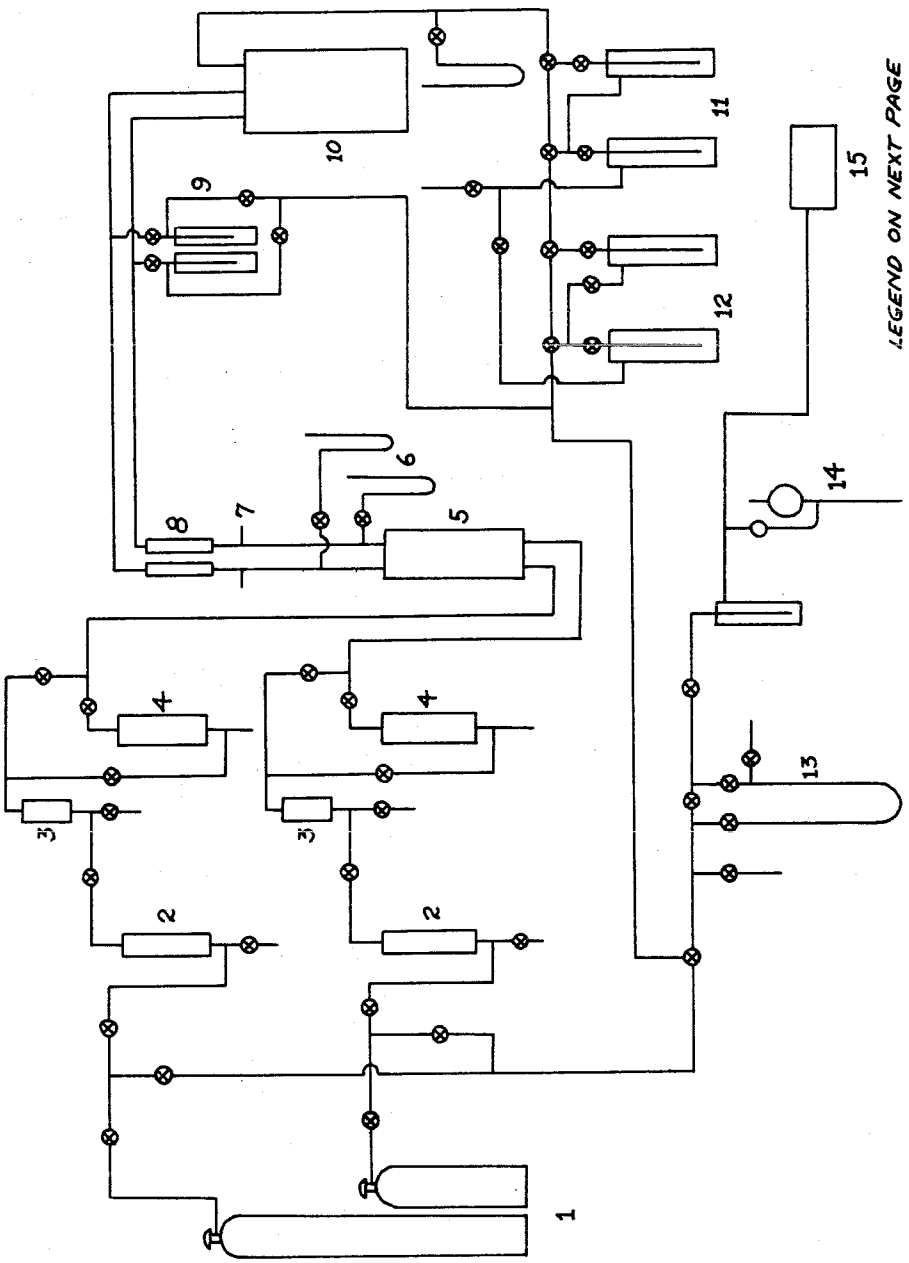

Figure 1--Flow Diagram of Stirred Reactor Apparatus.

LEGEND FOR FIGURE 1

1. Cylinders of compressed gas
2. Bubble towers
3. Expansion chambers
4. Dryers
5. Temperature-conditioning coils
6. Manometers for feed streams
7. Thermocouples for feed streams
8. Rotameters
9. Liquid-nitrogen sampling traps for feed streams
10. Stirred reactor
11. Liquid-nitrogen waste traps for product stream
12. Liquid-nitrogen sampling traps for product stream
13. Mercury manometer on vacuum line
14. McLeod gage
15. Vacuum pump

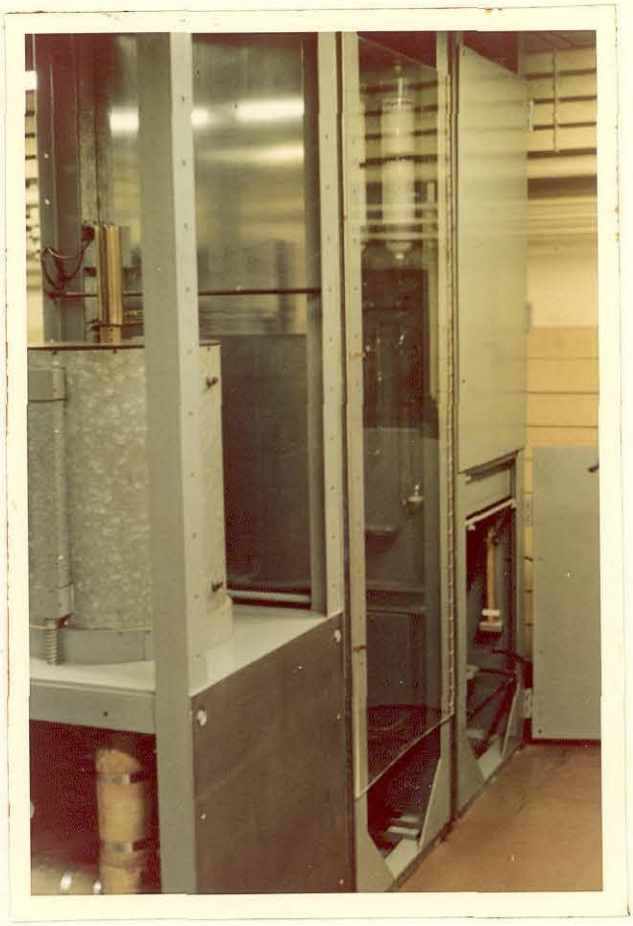

A. Compartments

B. Temperature Bench

Figure 2--Compartments for Stirred-Reactor Equipment and Measuring Equipment

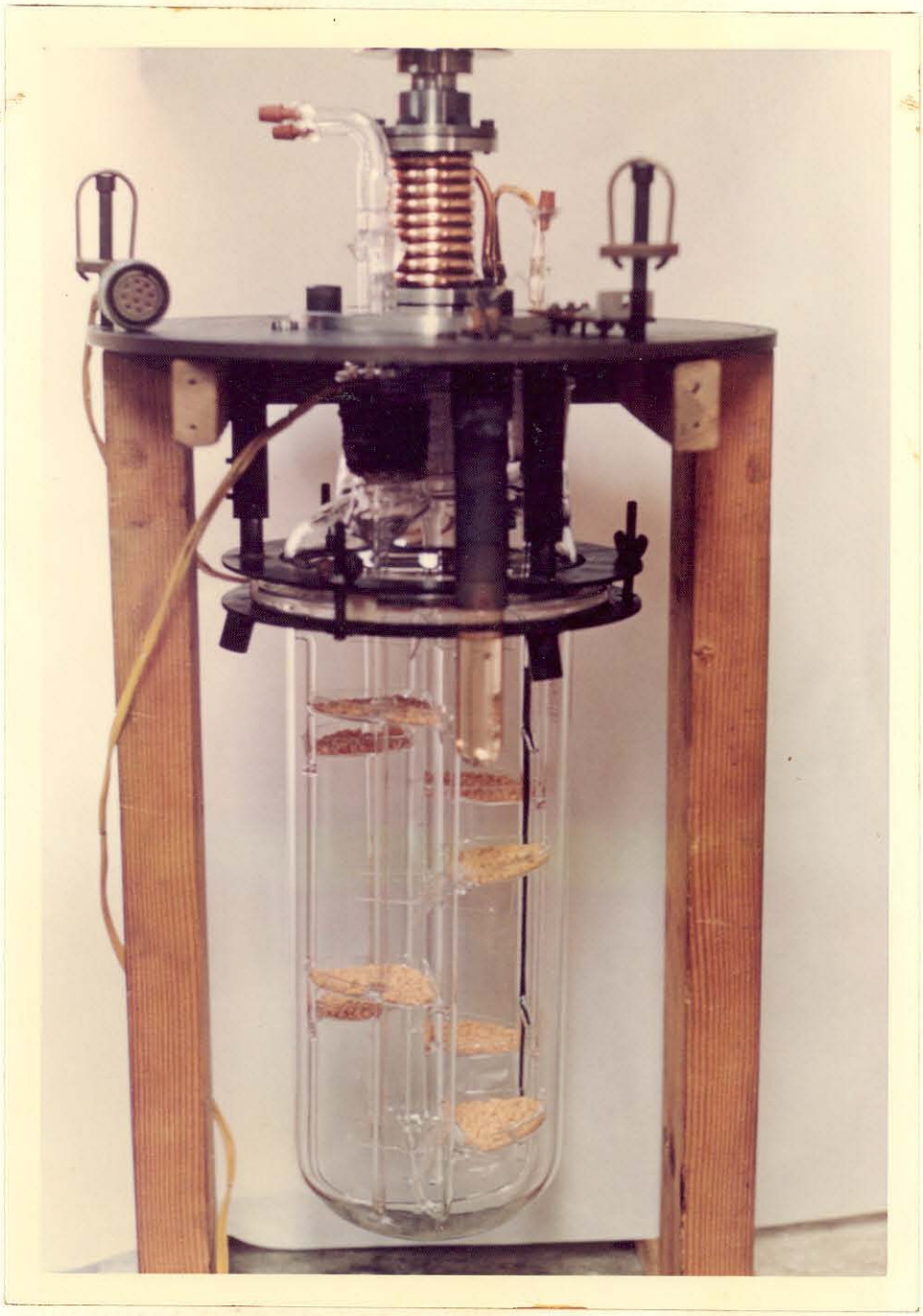

Figure 3--Complete Assembly of Stirred Reactor

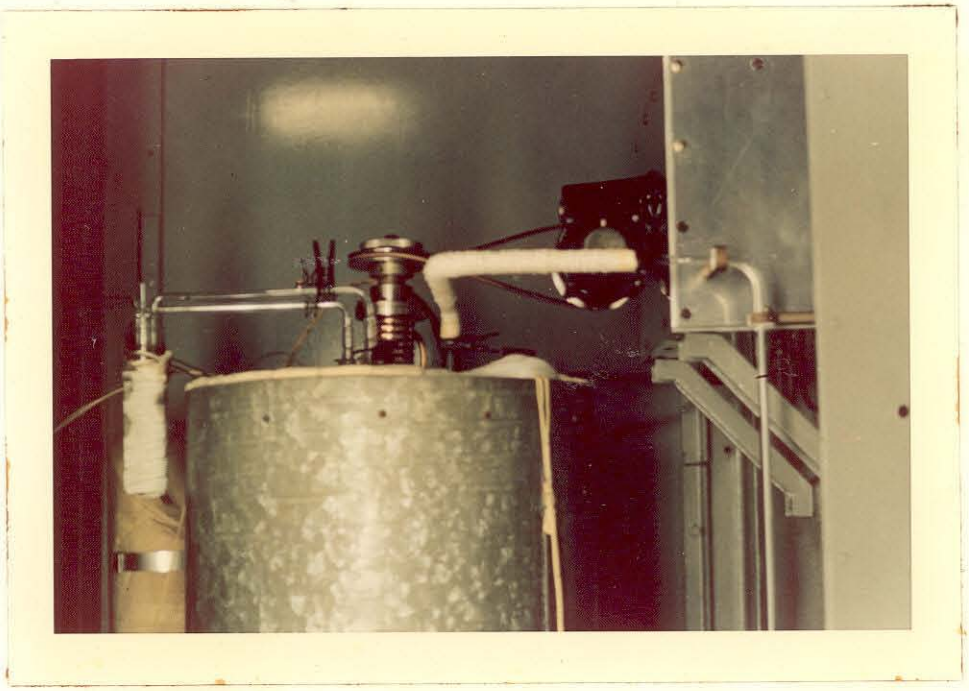

A. Oil Bath

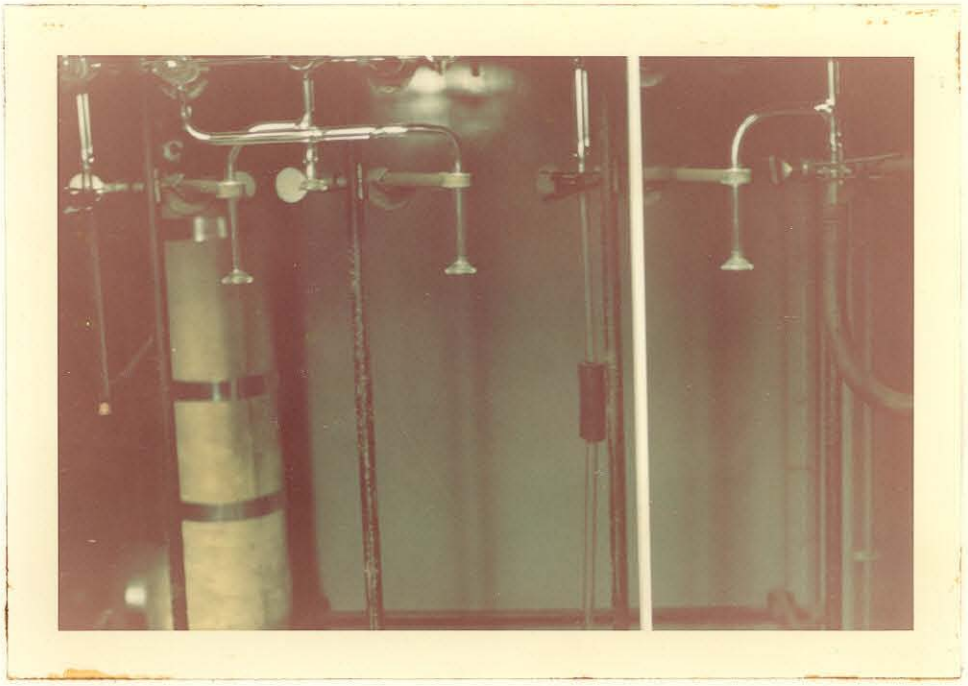

B. Product-Line Manifold

Figure 4--Reactor Oil Bath, Stirrer Motor, and Product-Line Manifold Ports

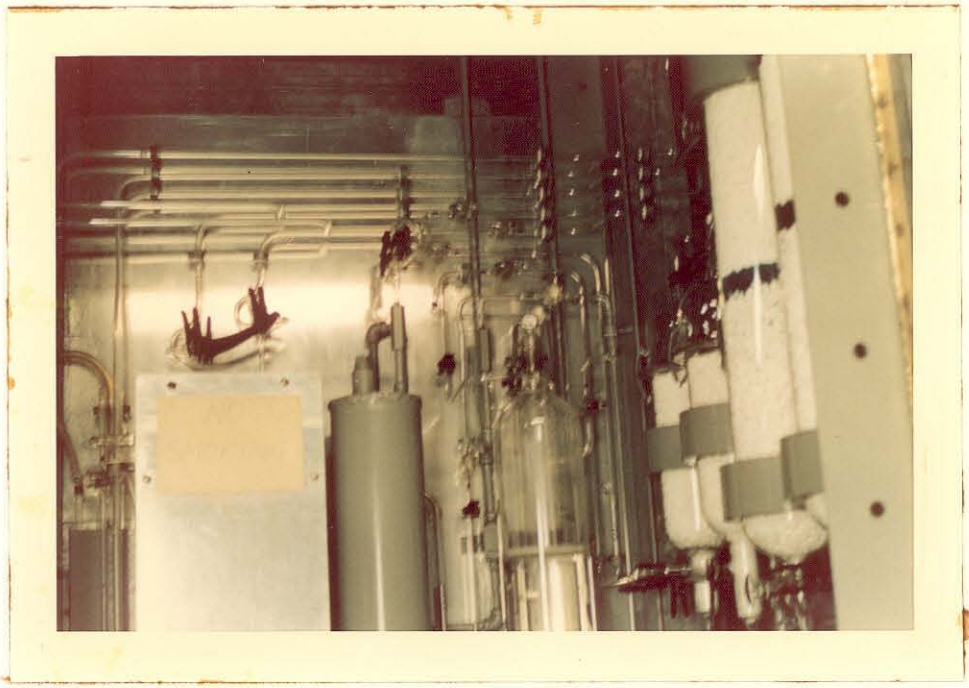

A. Upper Section

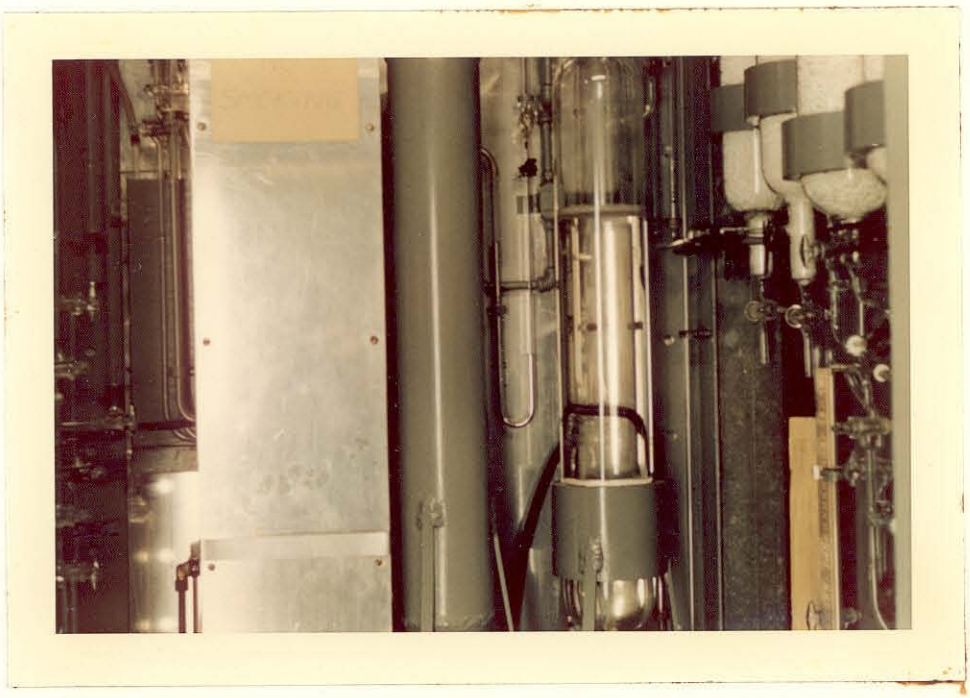

B. Lower Section

Figure 5--Feed-Conditioning Compartment

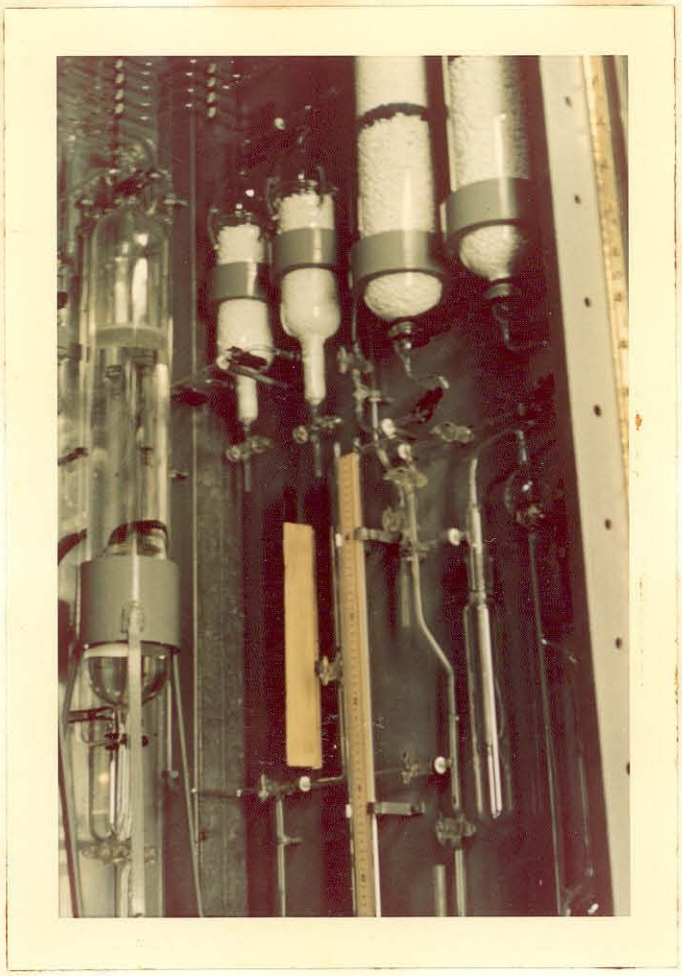

Figure 6--Vacuum-Manifold System

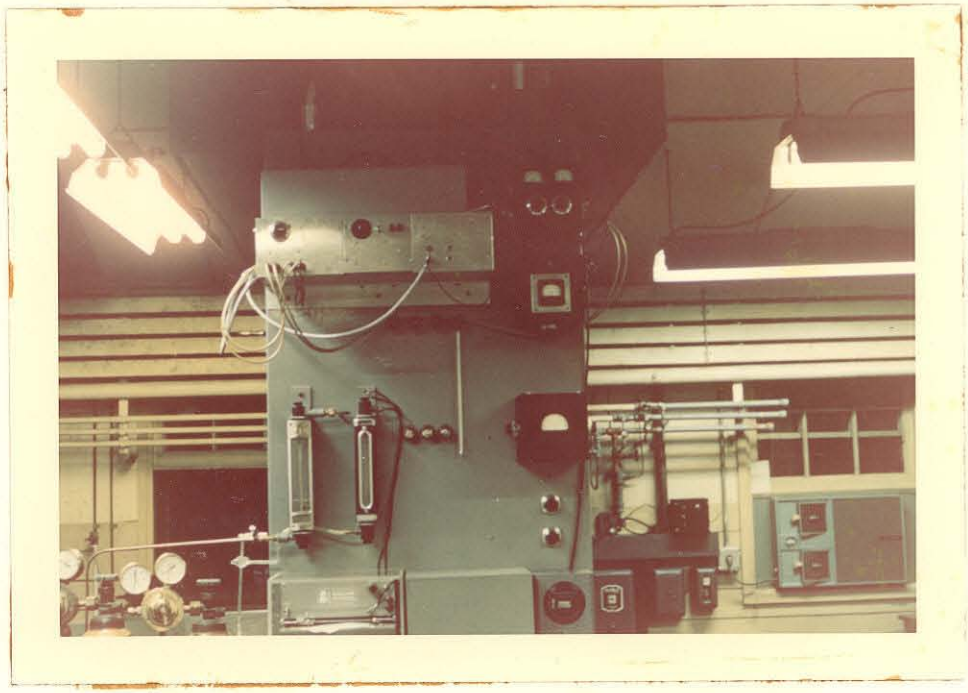

A. Upper Section

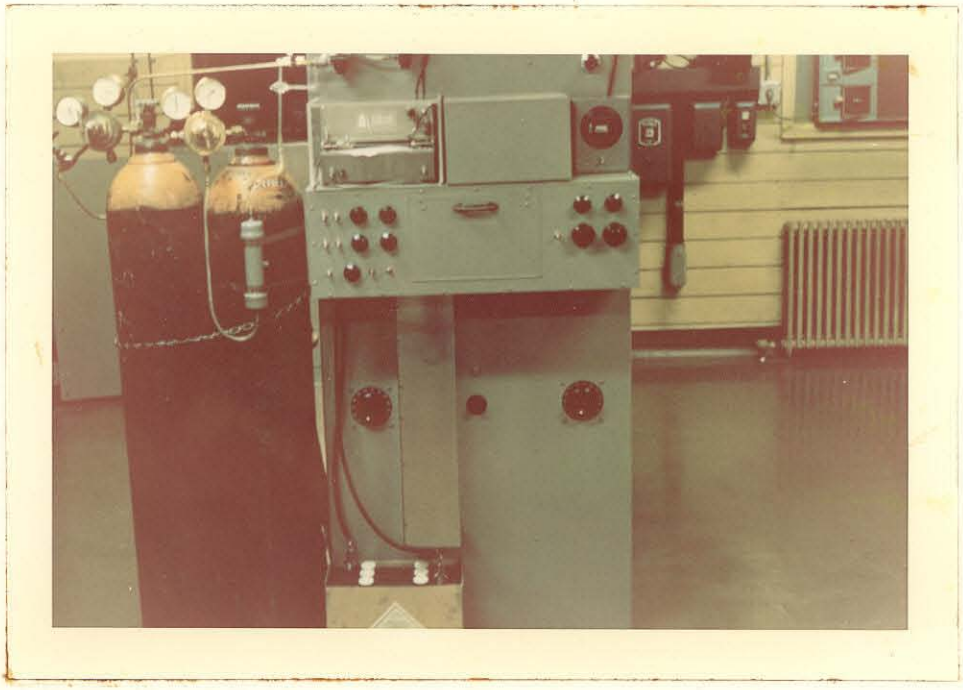

B. Lower Section

Figure 7--Exterior of Chromatography Unit

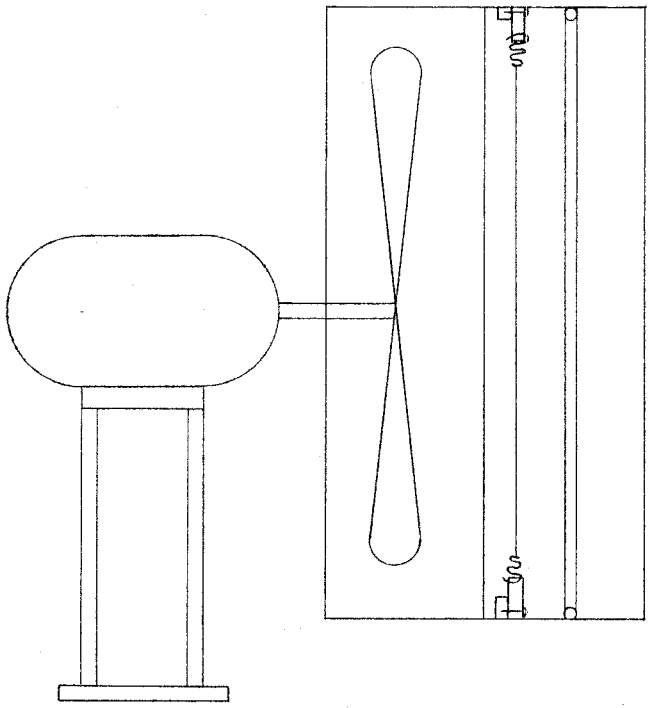

A

BLOWER - HEATER
MOUNTING

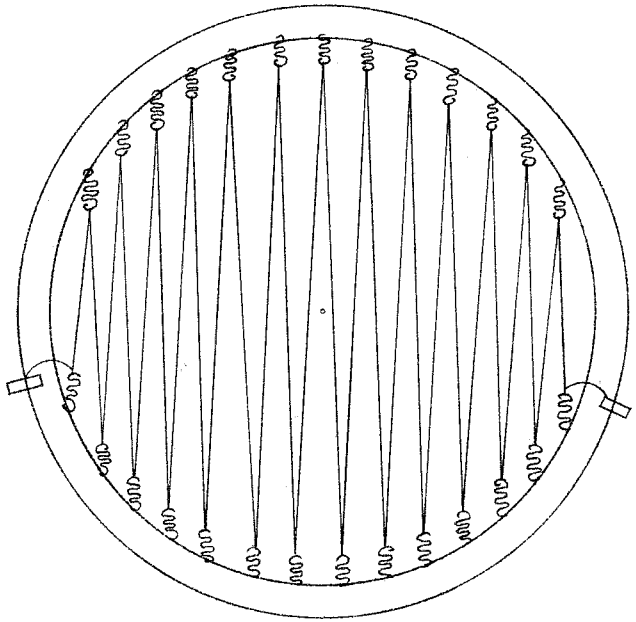

B

SPRING - MOUNTED
HEATING ELEMENT

Figure 8--Details of Chromatograph Fan and Heater System

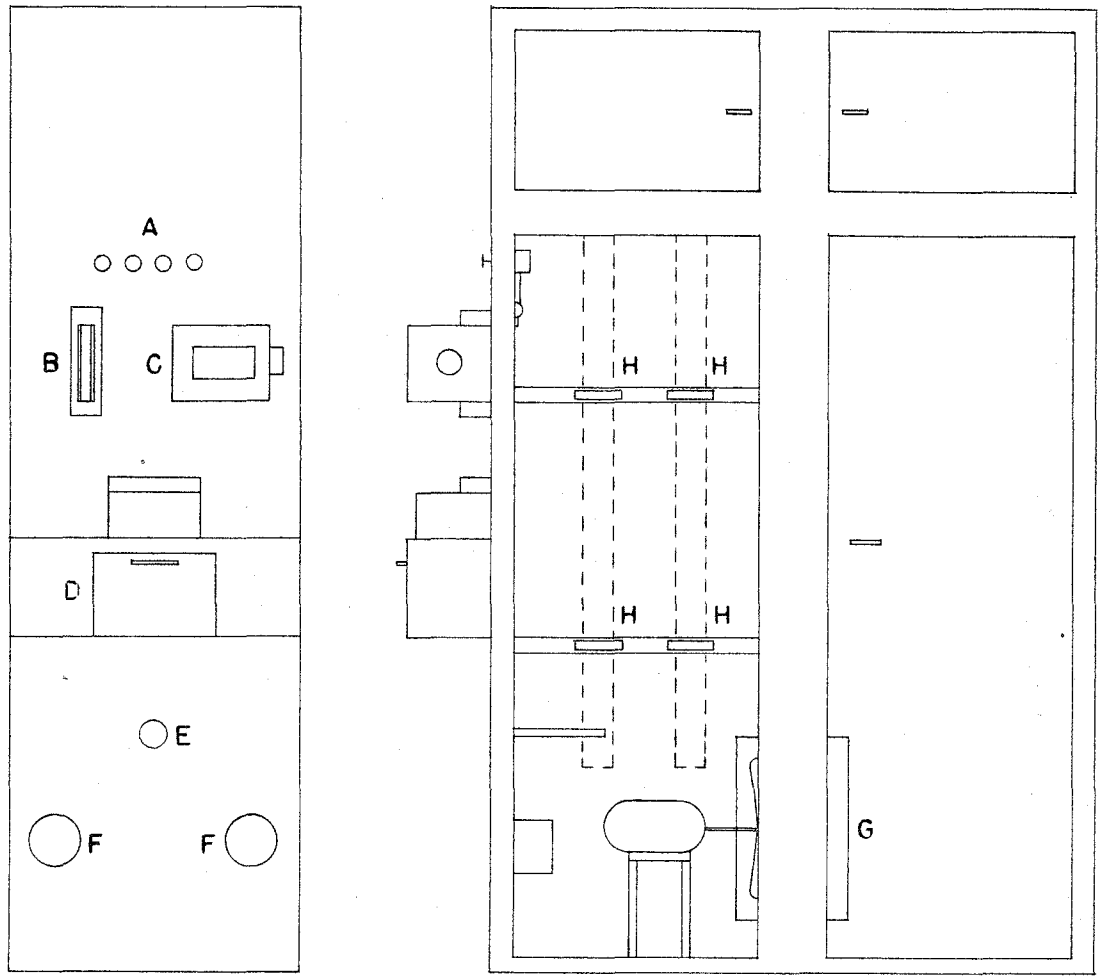

Figure 9--Diagram of Chromatograph Interior

a) Carrier-gas Distribution Valves and Manifold.

b) Carrier-gas Rotameter.

c) Balancing Bridge.

d) Battery Cabinet and Recorder Mounting Shelf.

e) Fenwal Thermostat.

f) Variac.

g) Air Heater and Circulating Fan.

h) Column Mounting Yokes.

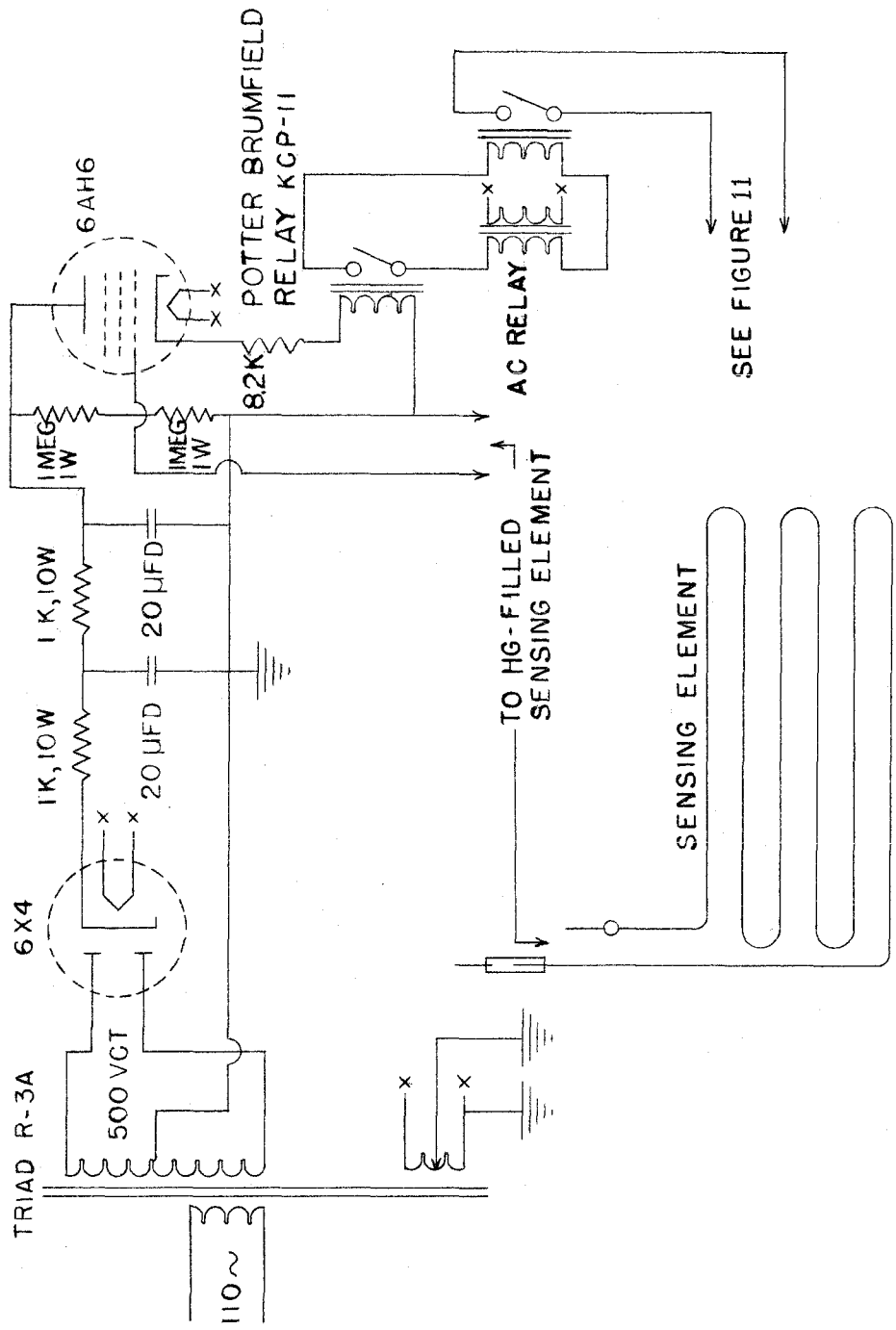

Figure 10--Circuit Details of Relay Control and Mercury-Filled Sensing Element in Chromatography Unit

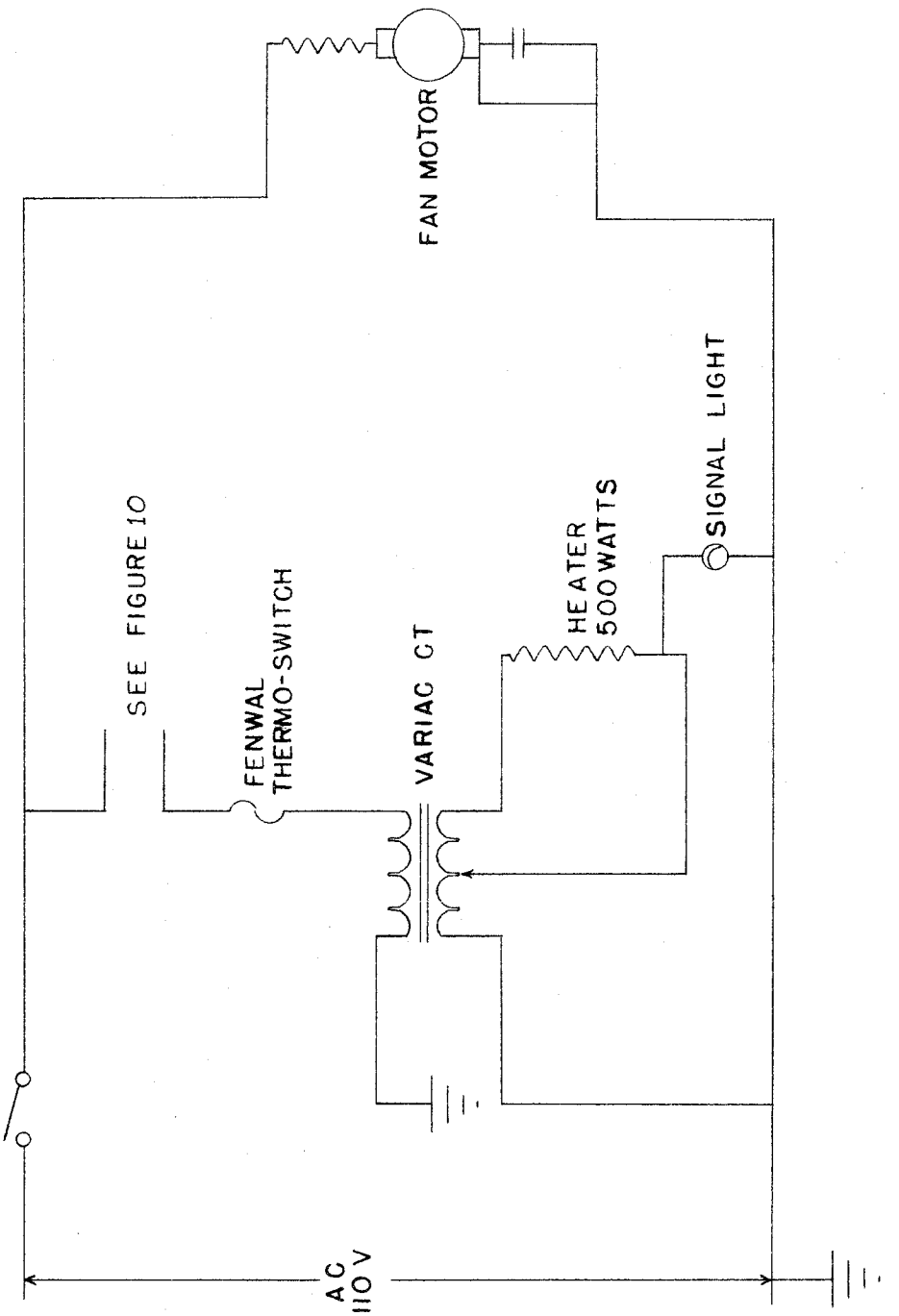

Figure 11--Circuit Details of Heater Circuit in Chromatography Unit

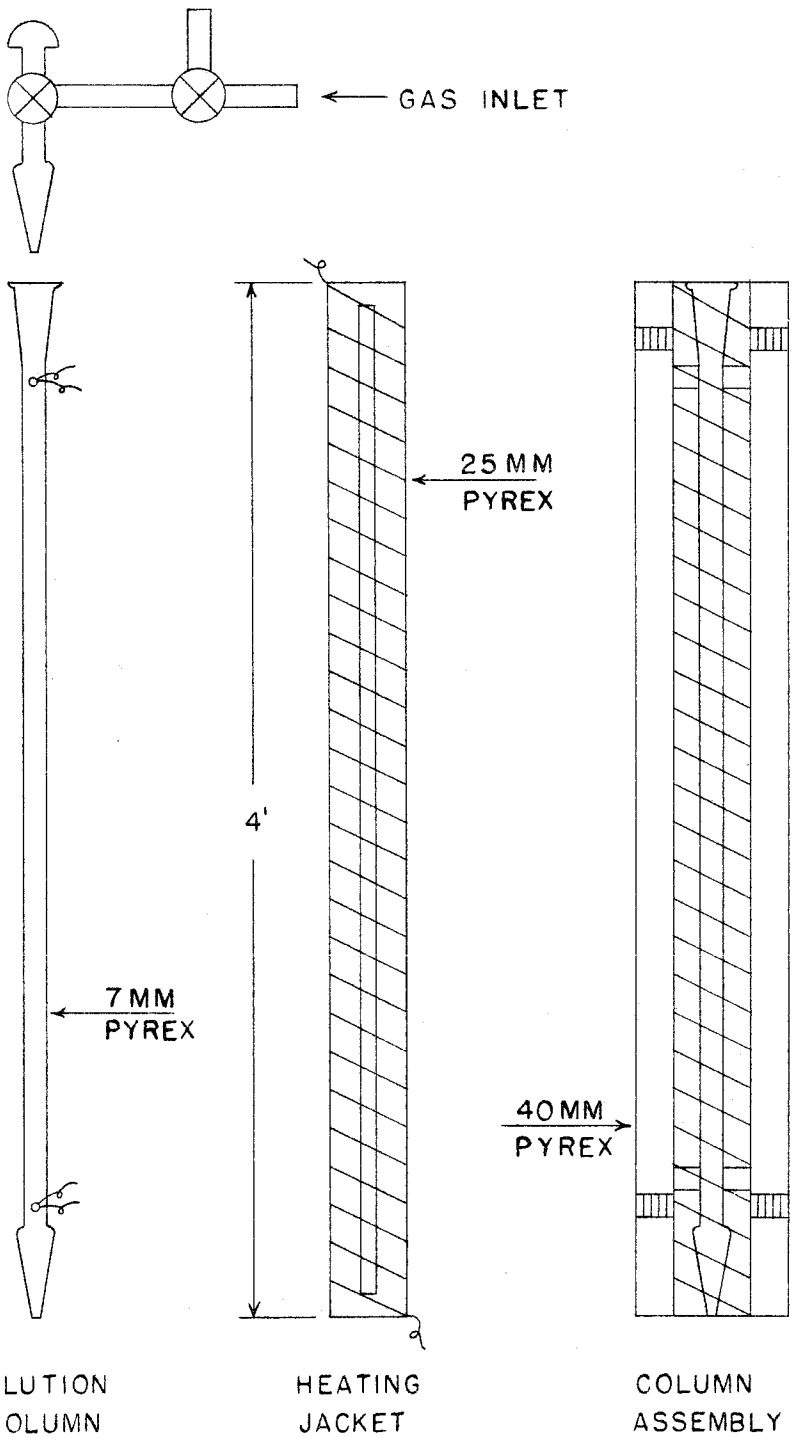

Figure 12--Details of Partition Column in Chromatography Unit

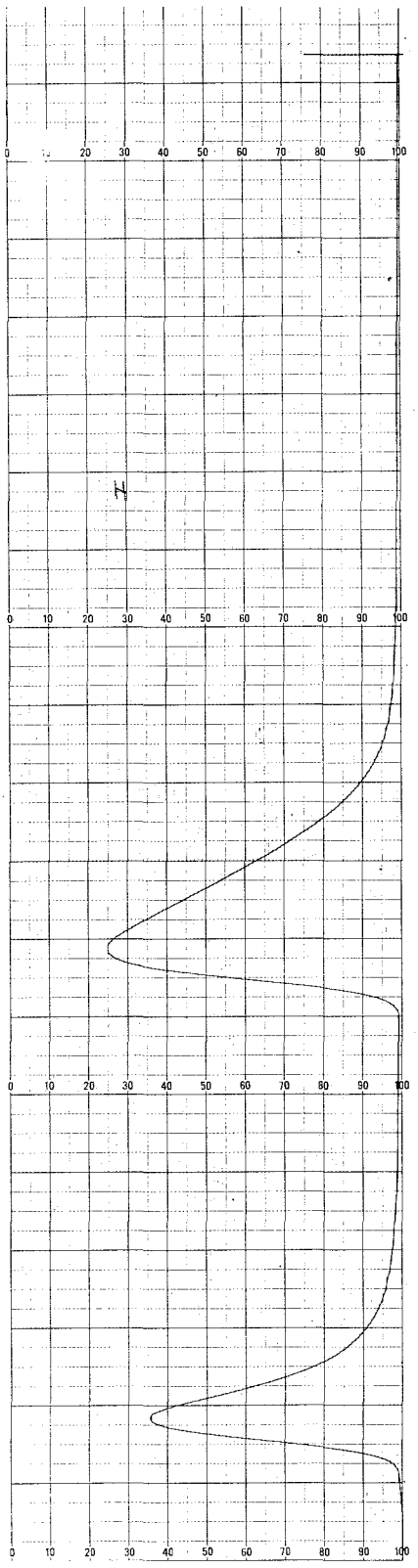

Figure 13--Elution Peaks for CO_2, Vinyl Chloride and 1,1 Dichloroethane.

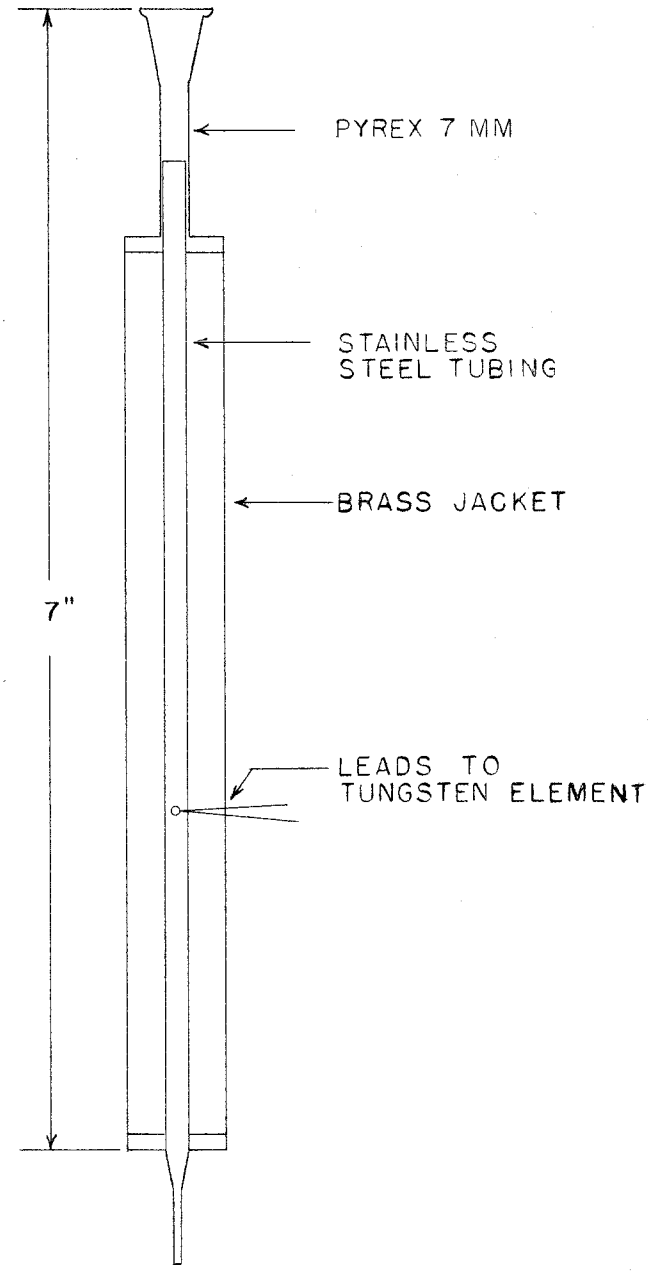

Figure 14--Details of Thermal Conductivity Cell in Chromatography Unit

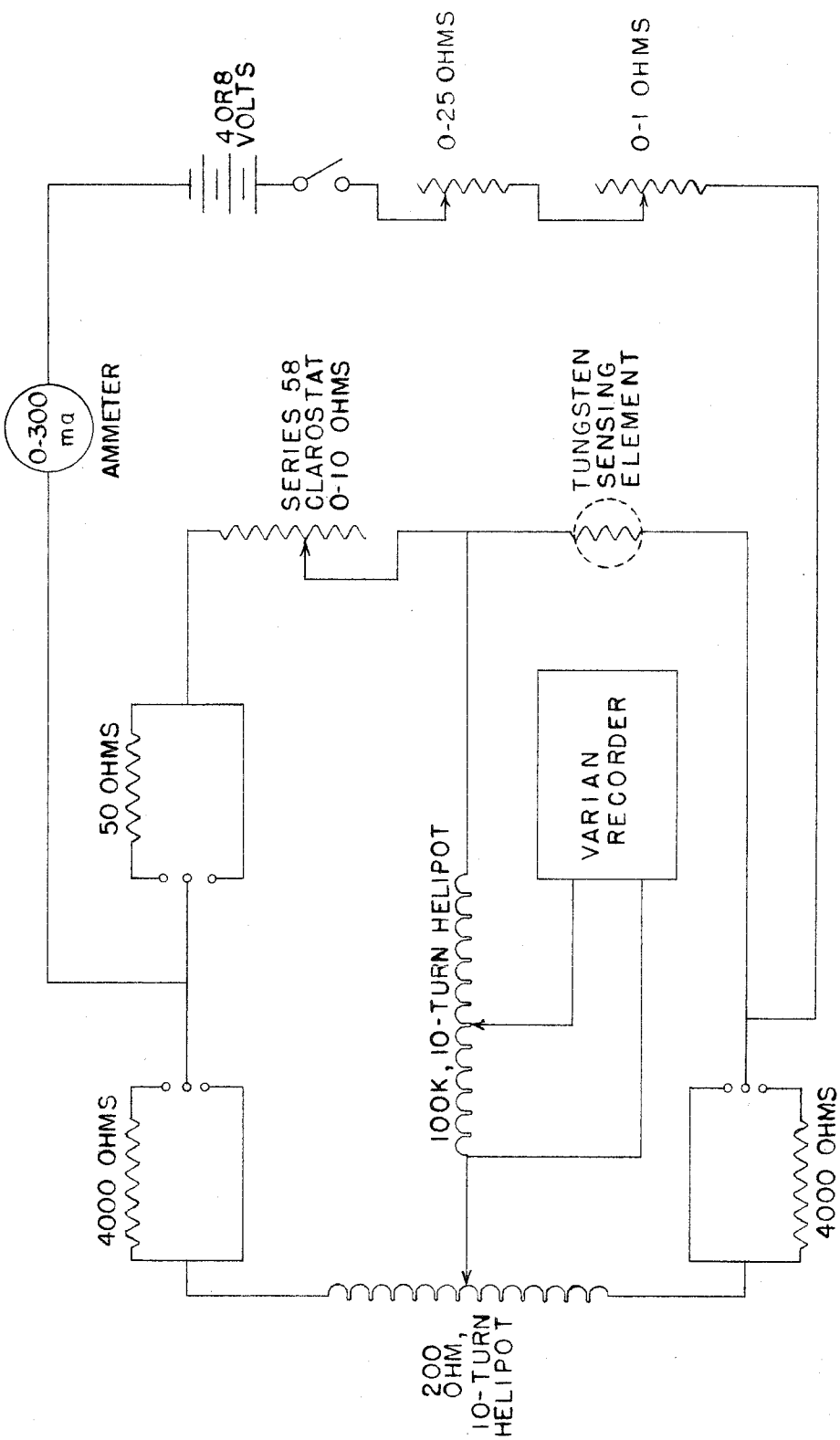

Figure 15--Detector Bridge Circuit in Chromatography Unit

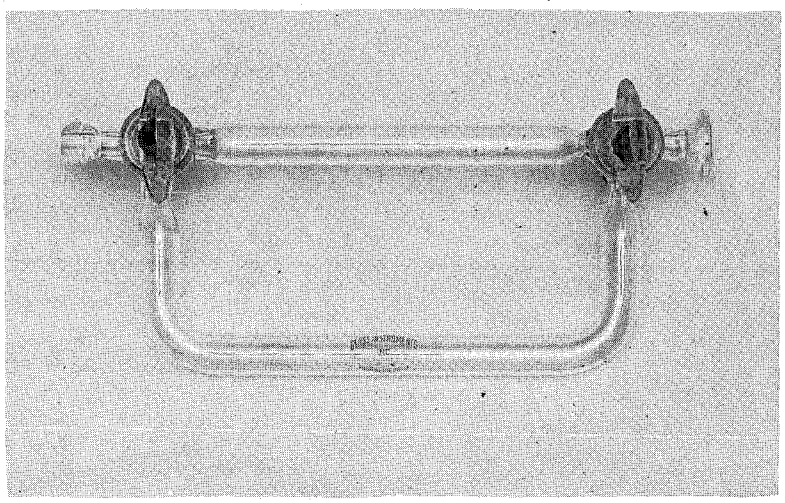

Figure 16--Portable Sampler Used with Chromatography Unit.

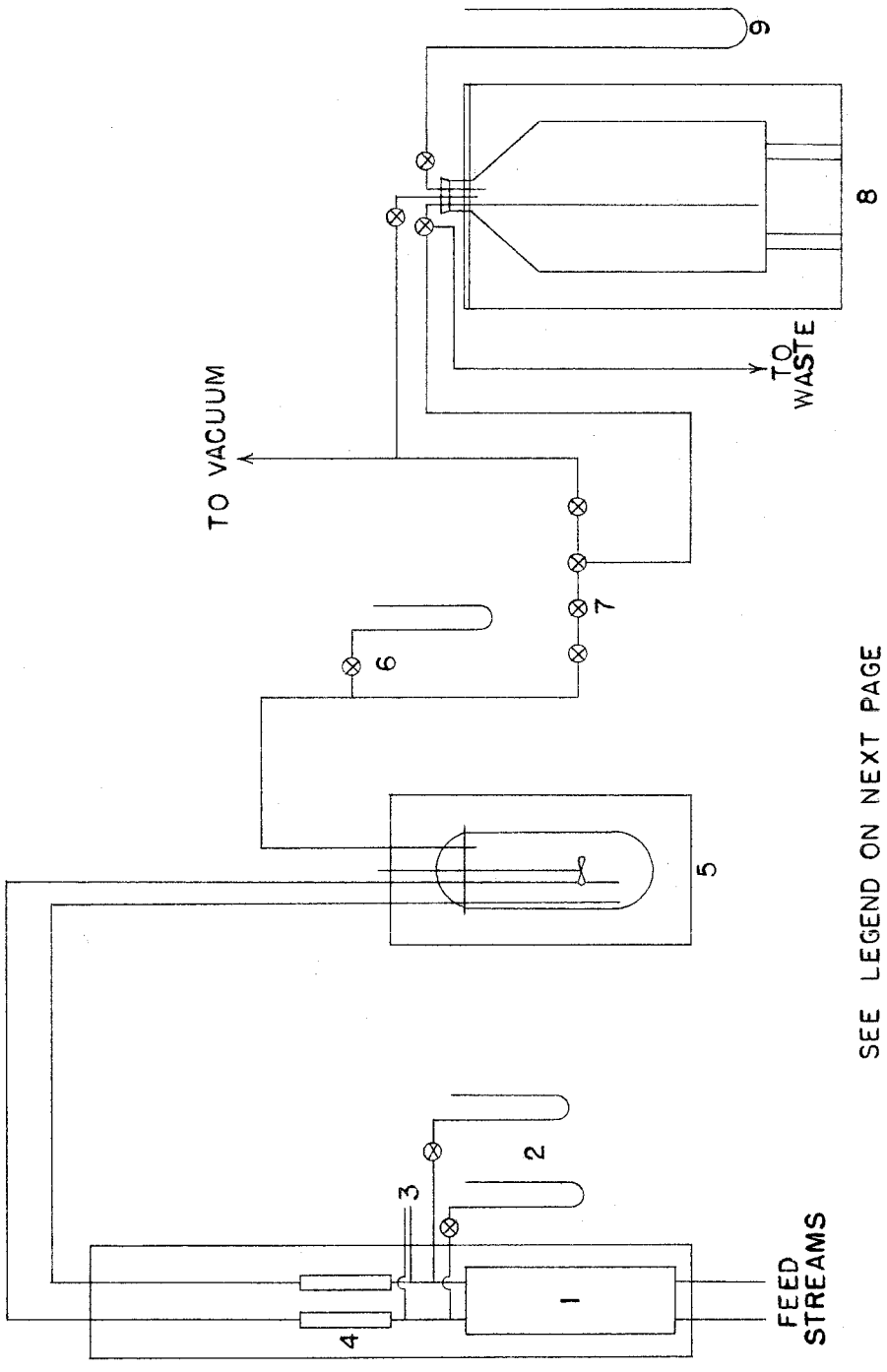

Figure 17--Flow Diagram for Rotameter Calibration Equipment

LEGEND FOR FIGURE 17

1. Temperature-conditioning coils
2. Rotameter manometers
3. Feed stream thermocouples
4. Rotameters
5. Reactor and oil bath
6. Exit stream manometer
7. Exit stream manifold
8. Carboy and water bath
9. Carboy manometer

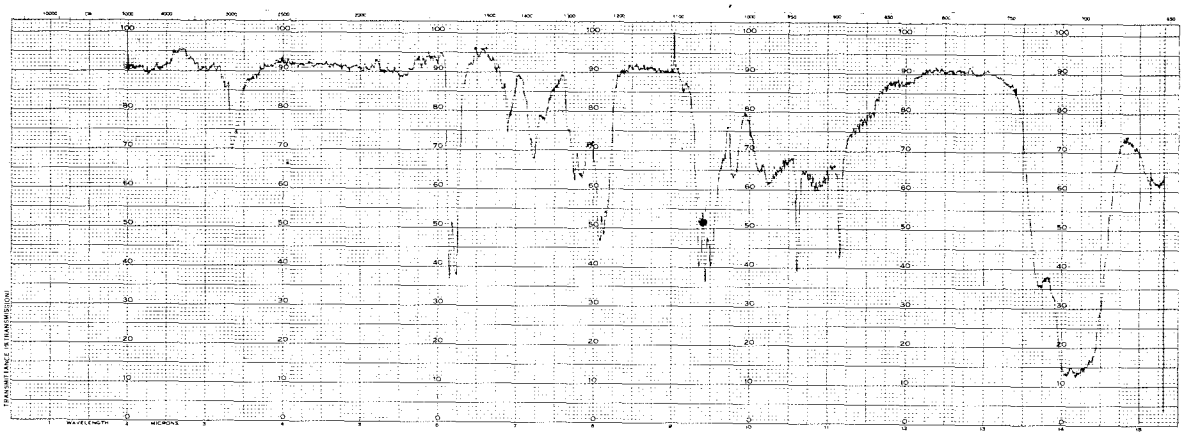

A. Sample of Reaction Mixture in Presence of $ZnCl_2$ Catalyst

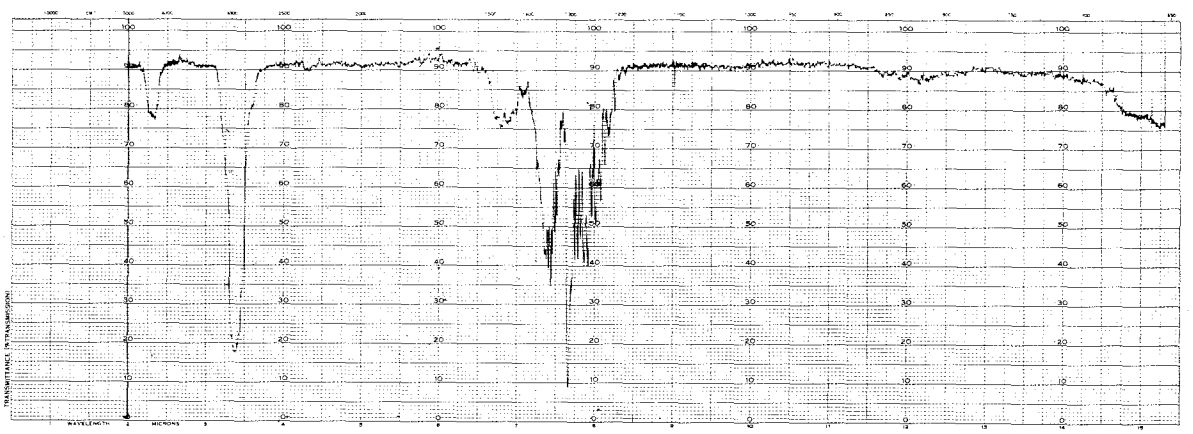

B. Natural Gas

Figure 18--Infrared Spectra of Natural Gas and Sample of Reaction Mixture from Batch Reactor.

LEGEND FOR FIGURE 18

Absorption Bands in the Infrared Region (20,21)

Methane	-	2.4 microns
		3.4
		6.5
		7.0
		7.5
		7.65
Ethane	-	2.3
		3.45
		4.25
		6.84
		12.08
Propane	-	2.39
		3.48
		6.78
		8.57
		9.36
		10.79
		13.88
Ethylene	-	2.3
		3.2
		4.8
		5.2
		5.4
		6.9
		7.1
		10.5
		12.8
HCl	-	3.41 microns
		3.60
Vinyl Chloride	-	3.20
		4.26
		5.525
		6.23
		7.24
		7.87
		9.78
		10.61
		11.155
		13.68
		14.07
1,1 Dichloro-ethane	-	9.44
		8.08
		6.88
Acetylene	-	729.1 cm^{-1}
		1328.1
		3287

Operating Conditions:

Phase - gas
Thickness - 10 cm
Pressure - 60 mm Hg
Gain - 4
Speed - 2
Suppression - 6.2

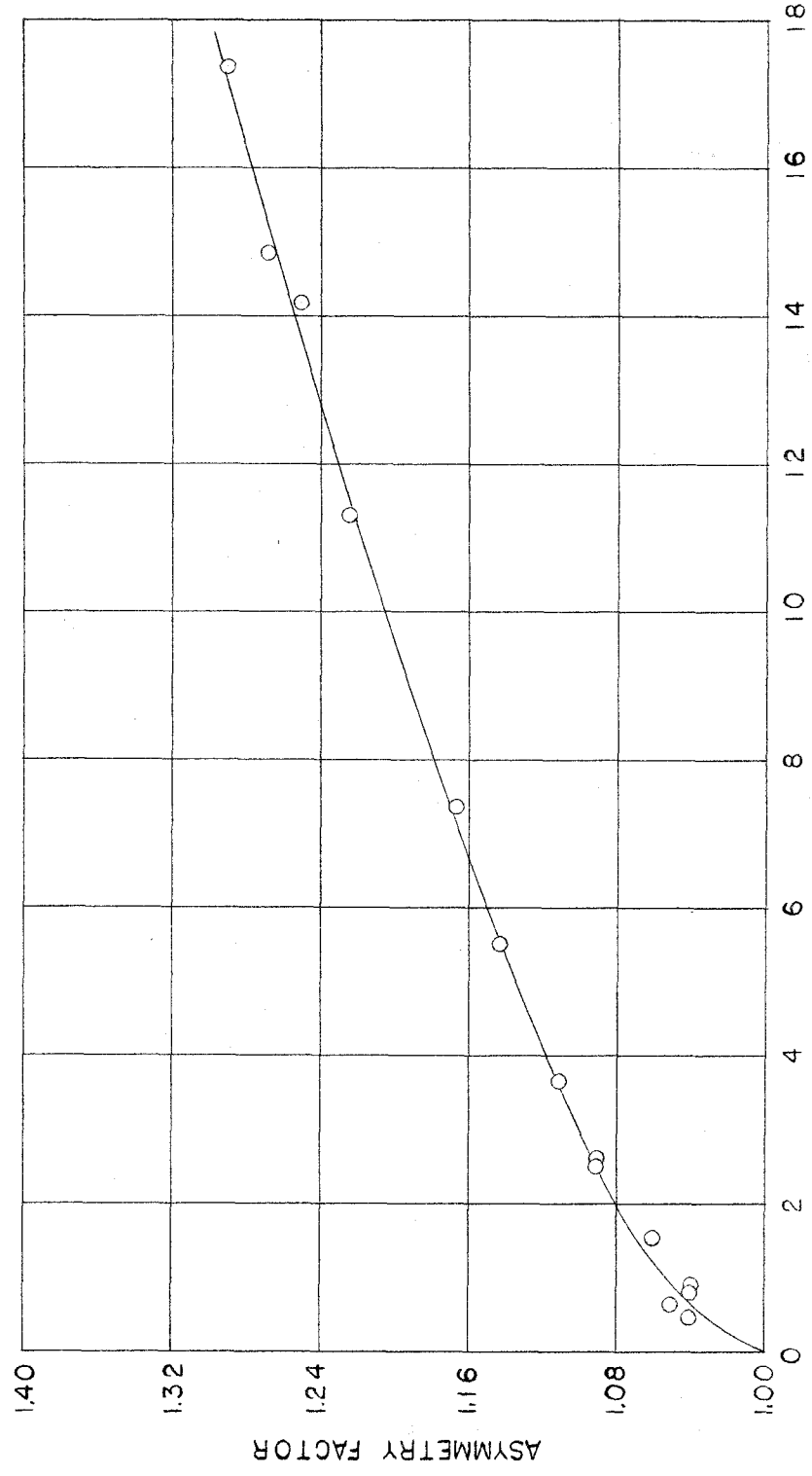

Figure 19--Asymmetry Factor for Correction of 1,1 Dichloroethane Elution Areas

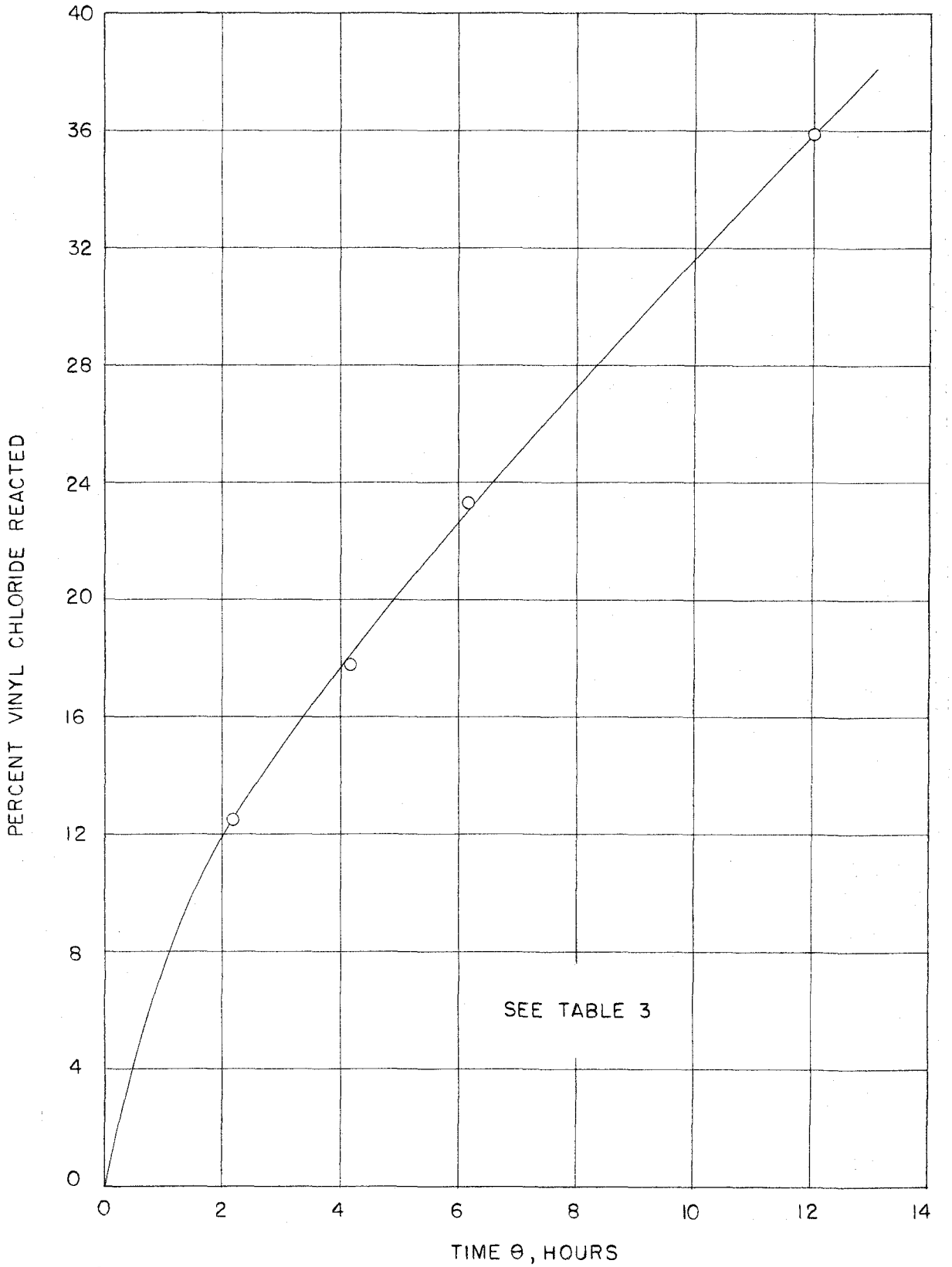

Figure 20--Percentage Vinyl Chloride Reacted vs Time in the Presence of $ZnCl_2$ Catalyst Supported on Celite. Test C in Batch Systems at 100°C

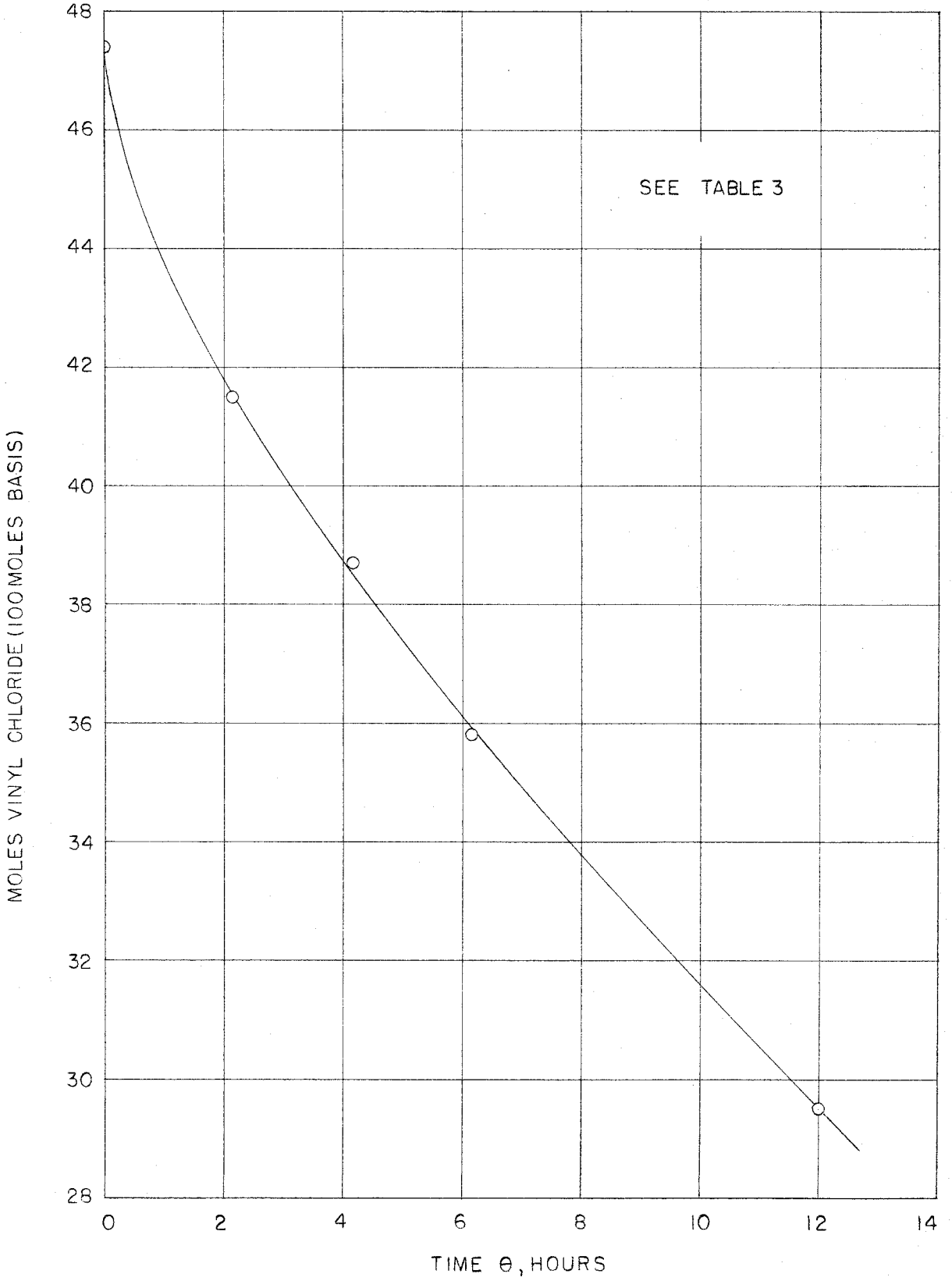

Figure 21--Moles of Vinyl Chloride Reacted vs Time in the Presence of $ZnCl_2$ Catalyst Supported on Celite. Test C in Batch Systems at 100°C

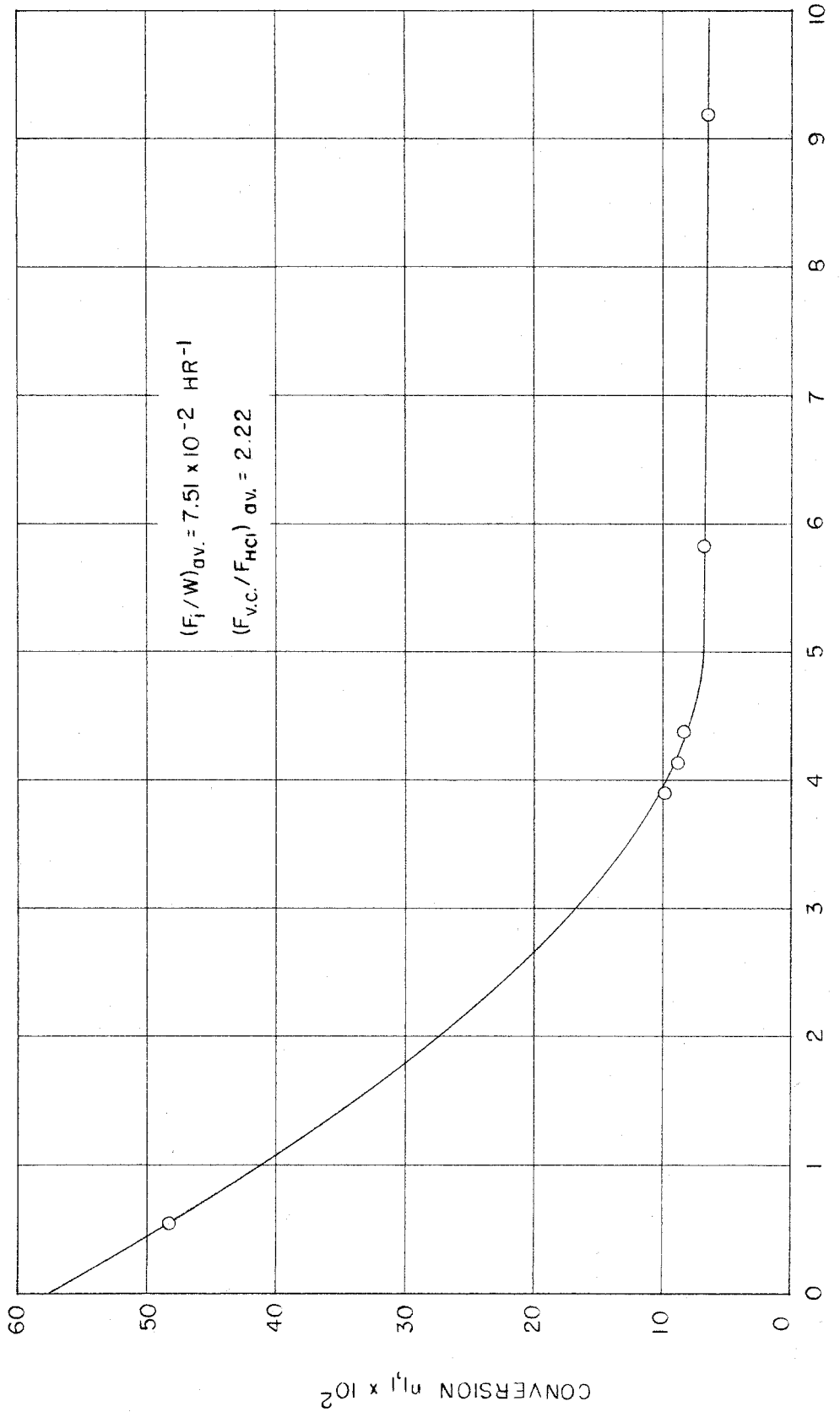

Figure 22--Conversion of 1,1 Dichloroethane vs Catalyst Exposure Time at 215°F in Stirred Reactor

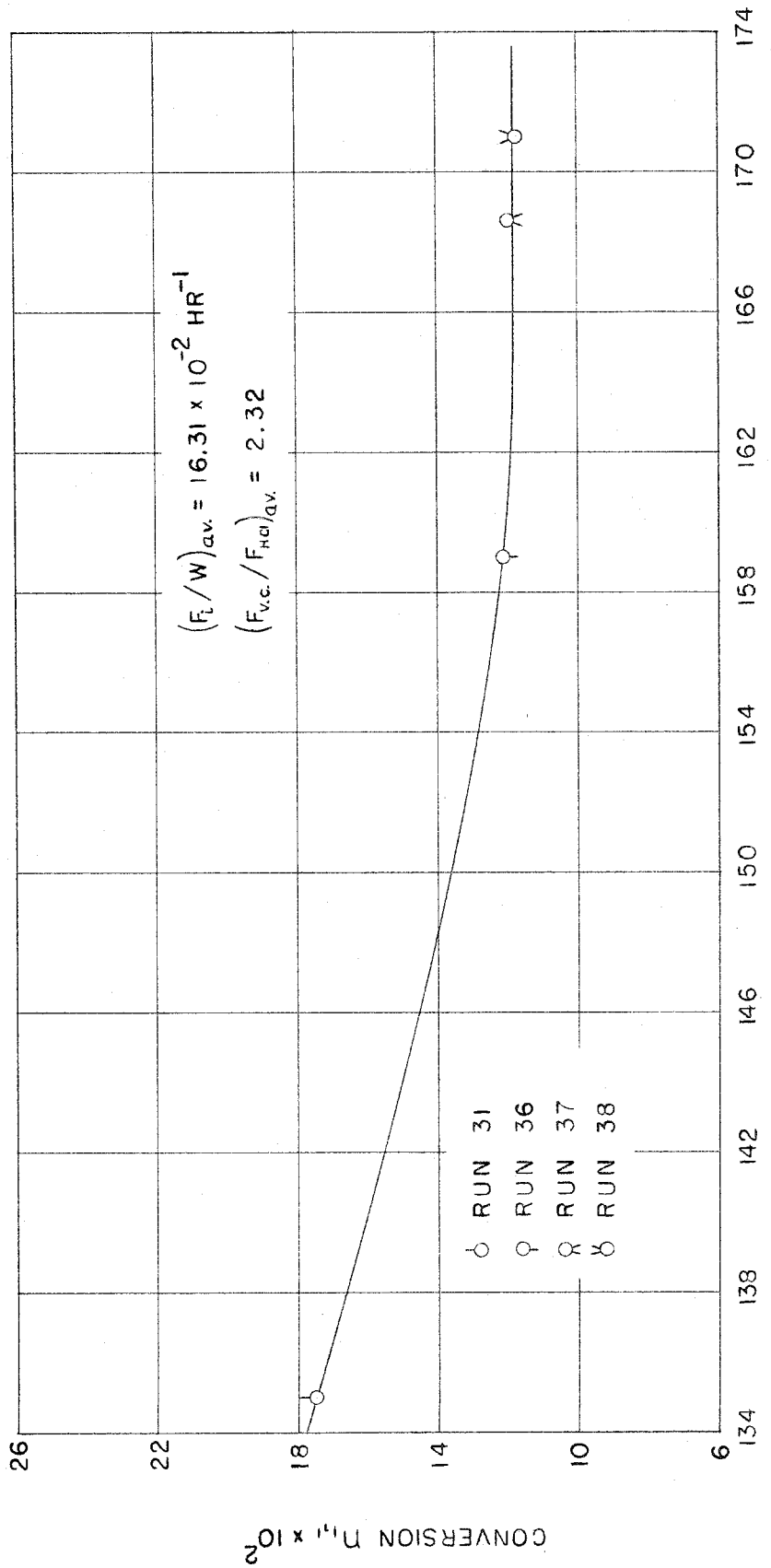

Figure 23—Conversion of 1,1 Dichloroethane vs Catalyst Exposure Time at 299°F in Stirred Reactor

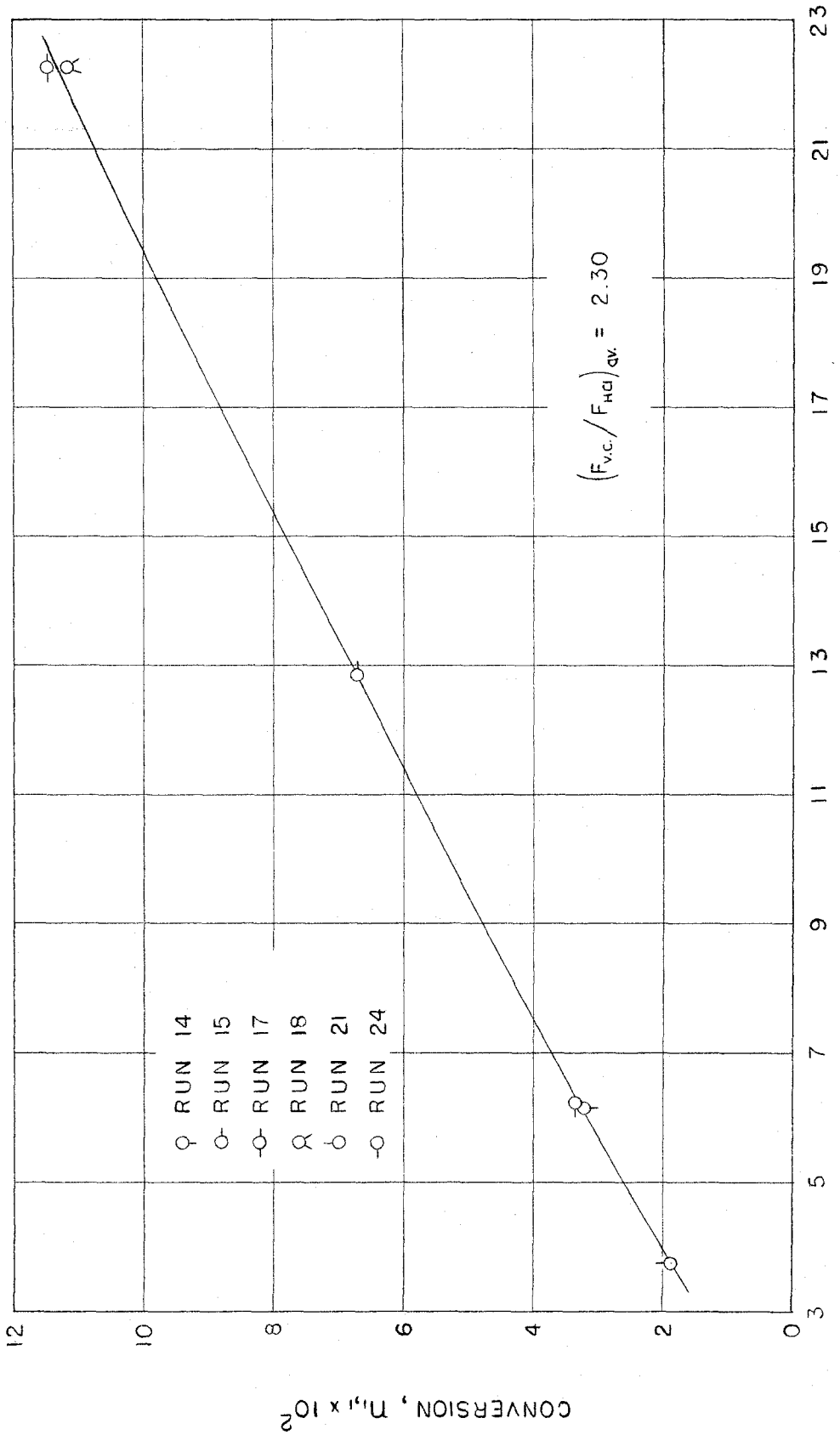

Figure 24--Conversion of 1,1 Dichloroethane vs $\frac{W}{F}$ at 215°F for a Constant Feed Ratio

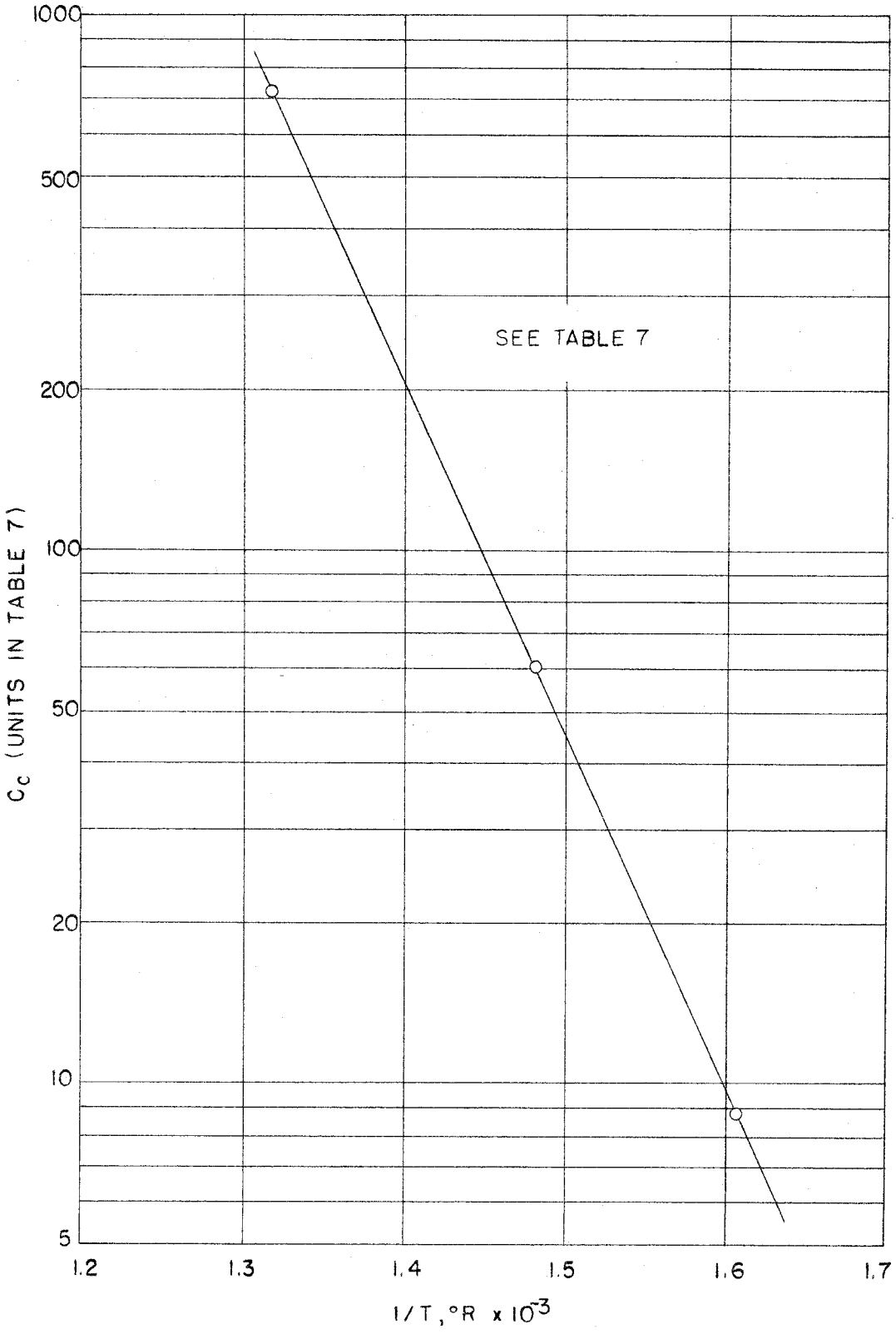

Figure 25--Arrhenius Plot of Rate Constants for a Non-Fouling Activity Level at 215°F

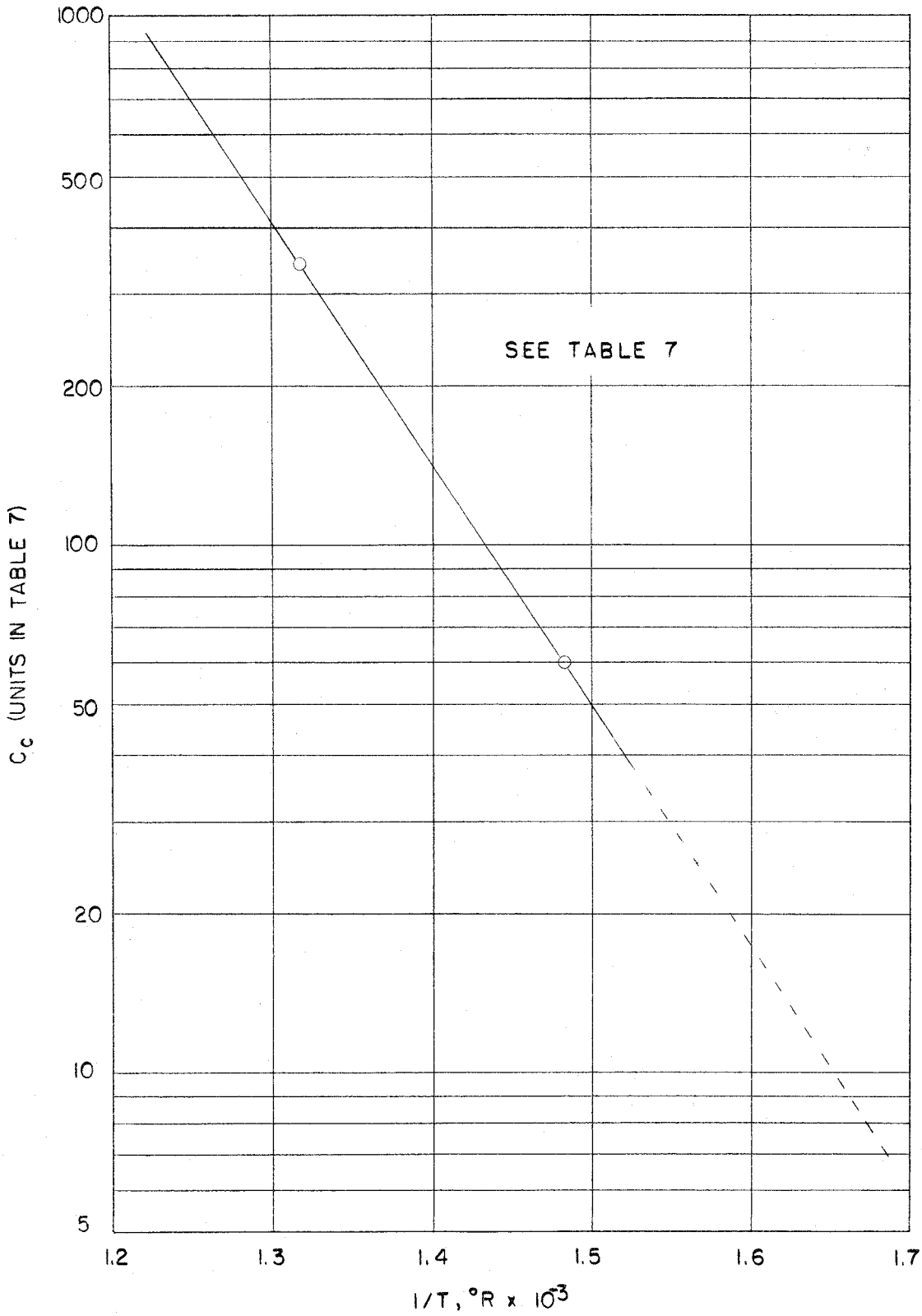

Figure 25a--Arrhenius Plot of Rate Constants for Non-Fouling Activity Levels

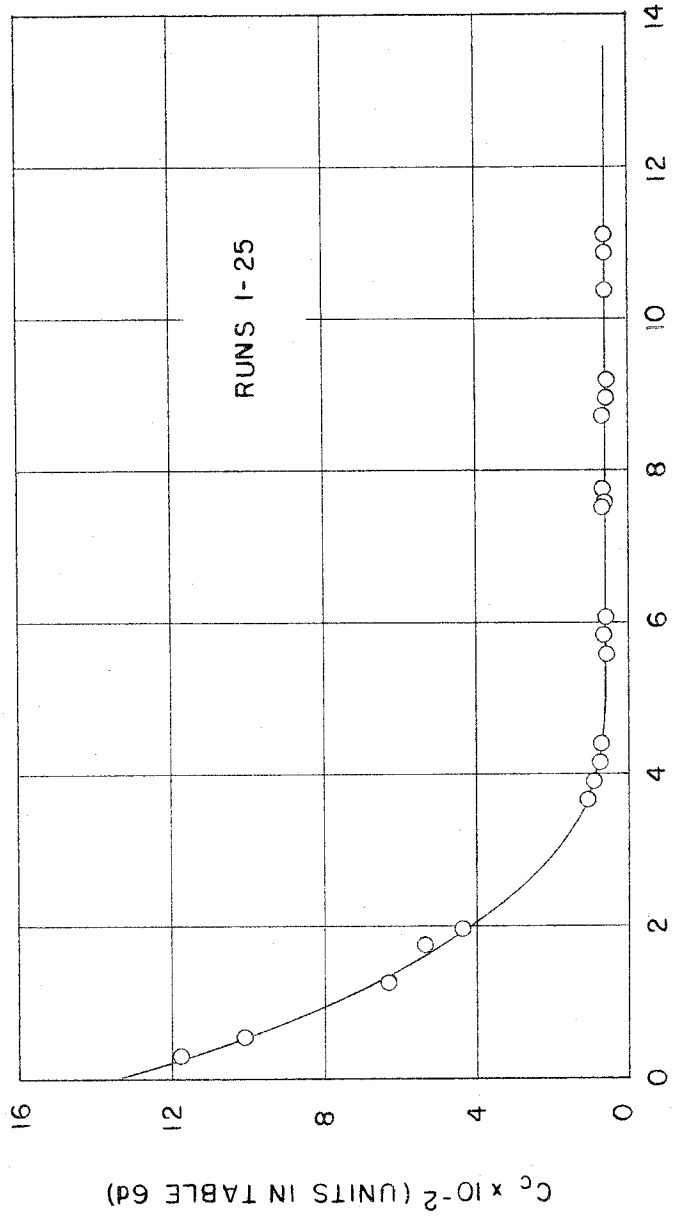

Figure 26--Rate Constant C_c vs Catalyst-Exposure Time at 215°F

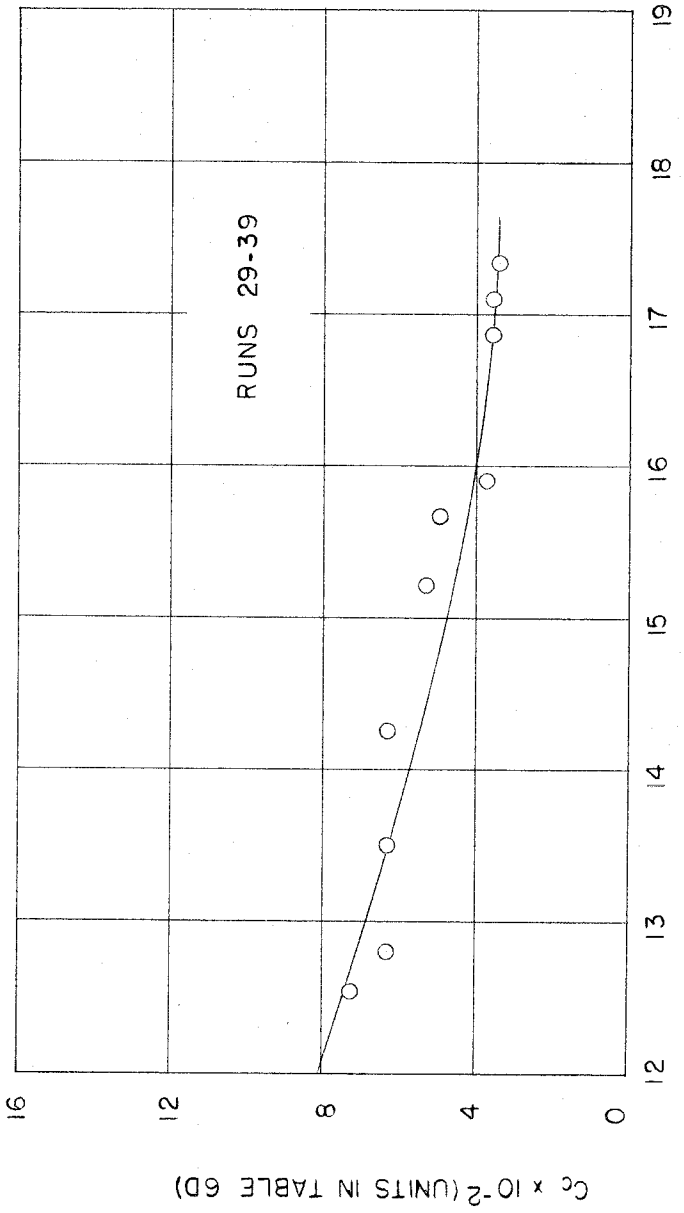

Figure 27--Rate Constant C_c vs Catalyst-Exposure Time at 299°F

LIST OF TABLES

TABLE 1

RETENTION TIMES AND VOLUMES OF REACTANTS, PRODUCTS AND CONTAMINANTS IN THE CHROMATOGRAPHIC ELUTION COLUMN

Component	Retention Time* Sec	Retention Volume** cc
Air	66	30.8***
CO_2	81	7.0
Vinyl Chloride	168	47.6
1,1 Dichloroethane	731	310.3
H_2O	905	391.5
1,2 Dichloroethane	1270	561.9

*Based on a carrier-gas flow rate of 28 cc/min corrected to 70°F and 1 atm.

**Based on corrected retention times by subtracting the retention time of air. Corrected to 70°F and 1 atm.

***Dead space in column.

TABLE 2

ASYMMETRY FACTORS FOR CORRECTION OF 1,1 DICHLOROETHANE ELUTION PEAKS

Asymmetry Area (Arbitrary Planimeter Units)	Asymmetry Factor
48	1.040
63	1.050
82	1.040
90	1.040
152	1.060
251	1.090
258	1.090
366	1.110
548	1.143
735	1.166
1130	1.224
1414	1.250
1486	1.268
1735	1.290

Table 2 (continued)

Sample calculation using the asymmetry factor:

For run 22:

Symmetry area of elution peak for 1,1 dichloroethane = 165 (arbitrary planimeter units)

From Figure 19, the asymmetry factor = 1.07

Area of 1,1 dichloroethane corrected for contamination = 165 x 2 x 1.07 = 353.1

Determination of Composition on a Weight Basis:

Peak Area		Amplification Factor	Calibration Factor	Corrected Areas	Weight Fraction
CO_2(HCl)	219.2	1.00	1.018	223.1	0.2823
Vinyl Chloride	518.2	1.00	0.996	516.1	0.6531
1,1 Dichloroethane	353.1	6.67	0.964	51.0	0.0645
	-	-	-	790.2	0.9999

TABLE 3

STUDIES OF HETEROGENEOUS CATALYSIS IN BATCH SYSTEMS.

MOLES OF REACTANTS AND PRODUCTS PER 100 MOLES OF INITIAL SYSTEM

Volume of Reaction Systems = 155 ± 4 cc

Temperature = 100.0 ± 0.5°C

Initial Pressure = 1.005 ± 0.001 atm

Test	Catalyst	Catalyst Weight gm	Contact Time hr	**HCl Initial Moles	V.C. Initial Moles	HCl Final Moles	V.C. Final Moles	1,1 Final Moles
A	$FeCl_3$	0.20	2.05	53.6	46.4	53.3	46.1	0.3
	"	"	6.08	"	"	slight decrease in vinyl chloride		no change
	"	"	12.02	"	"	"		"
B	$ZnCl_2$	0.17	2.04	53.4	46.6	53.3	46.5	0.1
	"	"	6.07	"	"	53.1	46.3	0.3
	"	"	12.01	"	"	52.9	46.1	0.5
C	*$ZnCl_2$ on 6-12 mesh Celite	1.00	2.15	52.6	47.4	46.7	41.5	5.9
	"	"	4.17	52.9	47.1	44.5	38.7	8.4
	"	"	6.17	53.3	46.7	42.4	35.8	10.9
	"	"	12.00	54.0	46.0	37.5	29.5	16.5
E	$ZnCl_2$ on 60-80 mesh dicalite	1.00	12.00	52.8	47.2	35.6	30.0	17.2
F	$ZnCl_2$ on 10-20 mesh silica gel	1.00	12.00	52.7	47.3	34.6	29.2	18.1

* Catalyst contains 1.5 millimoles of metallic halide per gram of carrier.

** Based on 100 moles of initial mixture and neglecting the fouling reaction.

TABLE 4

PERCENTAGE VINYL CHLORIDE REACTED VS TIME IN THE PRESENCE OF $ZnCl_2$ CATALYST SUPPORTED ON CELITE. TEST C IN BATCH SYSTEMS AT 100°C

% V.C. Reacted	Time, hr
12.5	2.15
17.8	4.17
23.3	6.17
35.9	12.00

TABLE 5

MOLES OF VINYL CHLORIDE REACTED VS TIME IN THE PRESENCE OF $ZnCl_2$ CATALYST SUPPORTED ON CELITE. TEST C IN BATCH SYSTEMS AT 100°C

Moles V.C. (100 Moles Basis)	Time, hr
46.7	0
41.5	2.15
38.7	4.17
35.8	6.17
29.5	12.00

TABLE 6a

COMPUTED RESULTS OF HETEROGENEOUS CATALYSIS IN THE STIRRED REACTOR

Run	T °F	*ΔT °F	P atm	ΔP lb/in^2	**R.R. V.C.	R.R. HCl	$F_{v.c.}$ lb/hr x 10^{-3}	F_{HCl} lb/hr x 10^{-3}	F_i lb/hr x 10^{-3}
1	214.86	0.19	0.971	0.0045	3.01	3.11	2.22	1.02	3.24
2	215.30	0.15	0.971	0.0044	3.15	3.18	2.49	1.08	3.57
3	215.15	0.19	0.971	0.0042	3.06	3.15	2.30	1.06	3.36
4	215.26	0.20	0.971	0.0053	5.15	5.05	8.71	3.54	12.25
5	215.13	0.22	0.971	0.0054	5.08	5.10	8.49	3.61	12.10
6	215.28	0.26	0.971	0.0060	6.06	6.08	12.60	5.45	18.05
7	215.41	0.28	0.970	0.0068	7.22	7.19	18.65	8.40	27.05
8	215.41	0.20	0.970	0.0076	7.25	7.25	18.82	8.58	27.40
9	214.85	0.23	0.970	0.0062	6.15	6.10	13.02	5.48	18.50
10	214.75	0.21	0.969	0.0047	4.03	4.07	4.92	2.12	7.04
11	214.70	0.23	0.969	0.0047	3.03	3.13	2.25	1.04	3.29
12	214.73	0.24	0.973	0.0043	3.04	3.12	2.27	1.03	3.30
13	214.80	0.21	0.973	0.0042	3.00	3.04	2.20	0.97	3.17
14	214.93	0.22	0.967	0.0049	4.06	4.13	5.00	2.21	7.21
15	215.02	0.21	0.968	0.0044	3.10	3.14	2.39	1.05	3.44
16	214.95	0.20	0.968	0.0038	2.62	2.57	1.54	0.62	2.16
17	214.98	0.21	0.971	0.0040	2.52	2.53	1.38	0.60	1.98
18	214.98	0.21	0.971	0.0040	2.52	2.53	1.38	0.60	1.98
19	214.87	0.19	0.969	0.0042	2.56	2.54	1.48	0.58	2.06
20	214.83	0.23	0.971	0.0064	6.10	6.08	12.80	5.45	18.25
21	214.86	0.22	0.971	0.0053	5.02	5.03	8.23	3.51	11.74

* ΔT is the temperature difference between the top and bottom of the reactor.

** R.R. represents Rotameter Reading (integrated average reading).
V.C. represents vinyl chloride.

TABLE 6a (continued)

Run	T °F	*ΔT °F	P atm	ΔP lb/in^2	**R.R. V.C.	R.R. HCl	$F_{v.c.}$ lb/hr x 10^{-3}	F_{HCl} lb/hr x 10^{-3}	F_1 lb/hr x 10^{-3}
22	214.83	0.22	0.973	0.0047	3.05	3.11	2.29	1.02	3.31
23	214.71	0.24	0.974	0.0040	2.55	2.47	1.44	0.55	1.99
24	214.77	0.21	0.972	0.0049	4.05	4.06	4.97	2.12	7.09
25	214.95	0.20	0.974	0.0038	2.61	2.56	1.52	0.61	2.13
26	163.88	0.16	0.974	0.0049	4.05	4.11	4.97	2.18	7.15
27	163.44	0.13	0.974	0.0042	2.99	3.00	2.19	0.93	3.12
28	163.79	0.15	0.974	0.0040	2.57	2.48	1.47	0.56	2.03
29	298.87	0.26	0.971	0.0072	6.55	6.62	15.00	6.77	21.77
30	299.01	0.29	0.973	0.0053	5.13	5.12	8.67	3.65	12.32
31	299.13	0.26	0.974	0.0049	4.09	4.10	5.10	2.17	7.27
32	299.02	0.25	0.977	0.0043	3.08	3.10	2.37	1.01	3.38
33	299.07	0.24	0.974	0.0043	3.08	3.13	2.37	1.04	3.41
34	299.15	0.25	0.973	0.0054	4.98	5.15	8.10	3.70	11.80
35	298.97	0.27	0.971	0.0055	5.09	5.15	8.50	3.70	12.20
36	299.08	0.27	0.969	0.0047	4.03	4.08	4.91	2.15	7.06
37	299.05	0.25	0.981	0.0049	4.06	4.10	5.00	2.17	7.17
38	298.95	0.23	0.976	0.0049	4.09	4.10	5.10	2.17	7.27
39	299.02	0.23	0.974	0.0053	5.03	5.10	8.28	3.61	11.89

TABLE 6b

COMPUTED RESULTS OF HETEROGENEOUS CATALYSIS IN THE STIRRED REACTOR

Run	$F_{v.c.}/F_{HCl}$ Exp.	F_1/W $hr^{-1} \times 10^{-2}$	n_{HCl}	$n_{v.c.}$	$n_{1,1}$***	n'_{HCl}	$n'_{v.c.}$	$n'_{1,1}$
1	2.18	7.35	0.1951	0.3824	0.4225	0.3398	0.3889	0.2713
2	2.31	8.10	0.1629	0.3405	0.4966	0.2990	0.3650	0.3360
3	2.17	7.62	0.1777	0.3391	0.4832	0.3208	0.3575	0.3216
4	2.46	27.78	0.2636	0.5651	0.1713	0.4014	0.5025	0.0962
5	2.35	27.44	0.2665	0.5582	0.1753	0.4056	0.4961	0.0984
6	2.31	40.94	0.2893	0.5852	0.1254	0.4271	0.5046	0.0683
7	2.22	61.35	0.3178	0.6057	0.0765	0.4542	0.5055	0.0403
8	2.19	62.15	0.3241	0.6132	0.0626	0.4595	0.5077	0.0327
9	2.38	41.96	0.3291	0.6464	0.0245	0.4599	0.5275	0.0126
10	2.32	15.97	0.2730	0.6716	0.0554	0.3982	0.5720	0.0298
11	2.16	7.46	0.2795	0.6226	0.0979	0.4115	0.5353	0.0531
12	2.20	7.48	0.2717	0.6411	0.0872	0.4006	0.5520	0.0474
13	2.27	7.19	0.2828	0.6336	0.0836	0.4137	0.5413	0.0451
14	2.26	16.35	0.3066	0.6613	0.0321	0.4351	0.5481	0.0168
15	2.28	7.80	0.2646	0.6684	0.0670	0.3893	0.5743	0.0363
16	2.48	4.90	0.2496	0.6544	0.0960	0.3741	0.5728	0.0531
17	2.30	4.49	0.2656	0.6202	0.1143	0.3965	0.5406	0.0629
18	2.30	4.49	0.2664	0.6222	0.1114	0.3971	0.5417	0.0612
19	2.55	4.67	0.2387	0.6508	0.1105	0.3619	0.5763	0.0618
20	2.35	41.39	0.3044	0.6808	0.0148	0.4303	0.5620	0.0077
21	2.34	26.63	0.2786	0.7025	0.0189	0.4004	0.5896	0.0100

*** 1,1 represents 1,1 dichloroethane.

TABLE 6b (continued)

Run	$F_{v.c.}/F_{HCl}$ Exp.	F_i/W $hr^{-1} \times 10^{-2}$	n_{HCl}	$n_{v.c.}$	$^{***}n_{l,l}$	n_{*HCl}	$n_{*v.c.}$	$n_{*l,l}$
22	2.25	7.51	0.2823	0.6531	0.0645	0.4106	0.5548	0.0346
23	2.62	4.51	0.2331	0.6639	0.1030	0.3538	0.5885	0.0576
24	2.34	16.08	0.3030	0.6636	0.0334	0.4311	0.5514	0.0175
25	2.49	4.83	0.2463	0.6547	0.0990	0.3703	0.5748	0.0549
26	2.28	16.22	0.3052	0.6888	0.0060	0.4301	0.5668	0.0031
27	2.35	7.08	0.2845	0.7017	0.0138	0.4068	0.5859	0.0073
28	2.63	4.60	0.2637	0.7171	0.0192	0.3824	0.6073	0.0103
29	2.22	49.38	0.3101	0.6003	0.0896	0.4470	0.5054	0.0476
30	2.38	27.94	0.2615	0.6163	0.1221	0.3924	0.5401	0.0675
31	2.35	16.49	0.2622	0.5629	0.1749	0.4001	0.5016	0.0984
32	2.35	7.67	0.2113	0.5305	0.2581	0.3429	0.5027	0.1544
33	2.28	7.73	0.1952	0.5652	0.2396	0.3181	0.5379	0.1440
34	2.19	26.76	0.2763	0.6128	0.1109	0.4093	0.5301	0.0606
35	2.30	27.67	0.2810	0.6166	0.1025	0.4139	0.5304	0.0557
36	2.28	16.01	0.2461	0.6329	0.1211	0.3727	0.5597	0.0676
37	2.30	16.26	0.2445	0.6359	0.1197	0.3705	0.5627	0.0669
38	2.35	16.49	0.2472	0.6356	0.1172	0.3736	0.5610	0.0653
39	2.29	26.97	0.2725	0.6498	0.0777	0.4004	0.5575	0.0421

TABLE 6c

COMPUTED RESULTS OF HETEROGENEOUS CATALYSIS IN THE STIRRED REACTOR

Run	P_{HCl} atm	$P_{v.c.}$ atm	$P_{1,1}$ atm	$r_{1,1}$ lb/(hr)(lb cat) x 10^{-2}	F_{HCl} lb moles/hr x 10^{-5}	$F_{v.c.}$ lb moles/hr x 10^{-5}	F_{i} lb moles/hr x 10^{-5}	H_R lb moles x 10^{-5}	t_r hr
1	0.3299	0.3776	0.2634	-	2.79	3.55	6.34	40.85	6.44
2	0.2903	0.3544	0.3263	4.022	2.96	3.98	6.94	40.85	5.88
3	0.3115	0.3471	0.3123	3.682	2.90	3.68	6.58	40.85	6.20
4	0.3898	0.4879	0.0934	4.759	9.70	13.94	23.64	40.85	1.73
5	0.3938	0.4817	0.0955	4.810	9.89	13.58	23.47	40.85	1.74
6	0.4147	0.4900	0.0663	5.134	14.93	20.16	35.09	40.85	1.16
7	0.4406	0.4903	0.0391	4.693	23.01	29.84	52.85	40.81	0.77
8	0.4457	0.4925	0.0317	3.891	23.51	30.11	53.62	40.81	0.76
9	0.4461	0.5117	0.0122	1.028	15.01	20.83	35.84	40.81	1.14
10	0.3859	0.5543	0.0289	0.8847	5.81	7.87	13.68	40.77	2.98
11	0.3987	0.5187	0.0515	0.7300	2.85	3.60	6.45	40.77	6.32
12	0.3898	0.5371	0.0461	0.6523	2.82	3.63	6.45	40.94	6.34
13	0.4025	0.5267	0.0439	0.6011	2.66	3.52	6.18	40.94	6.63
14	0.4207	0.5300	0.0162	0.5250	6.05	8.00	14.05	40.68	2.89
15	0.3768	0.5559	0.0351	0.5230	2.88	3.82	6.70	40.73	6.08
16	0.3621	0.5545	0.0514	0.4700	1.70	2.46	4.16	40.73	9.79
17	0.3850	0.5249	0.0611	0.5130	1.64	2.21	3.85	40.85	10.61
18	0.3856	0.5260	0.0594	0.5002	1.64	2.21	3.85	40.85	10.61
19	0.3507	0.5584	0.0599	0.5160	1.59	2.37	3.96	40.77	10.30
20	0.4178	0.5457	0.0075	0.6130	14.93	20.48	35.41	40.85	1.15
21	0.3888	0.5725	0.0097	0.5033	9.62	13.17	22.79	40.85	1.79

TABLE 6c (continued)

Run	P_{HCl} atm	$P_{v.c.}$ atm	$P_{i,l}$ atm	$r_{i,l}$ lb/(hr)(lb cat) x 10^{2}	F_{HCl} lb moles/hr x 10^{-5}	$F_{v.c.}$ lb moles/hr x 10^{-5}	F_{i} lb moles/hr x 10^{-5}	M_{R} lb moles x 10^{-5}	t_{r} hr
22	0.3995	0.5398	0.0337	0.4840	2.79	3.66	6.45	40.94	6.36
23	0.3446	0.5732	0.0561	0.4650	1.51	2.30	3.81	40.98	10.76
24	0.4190	0.5360	0.0170	0.5370	5.81	7.95	13.76	40.89	2.97
25	0.3607	0.5599	0.0535	0.4780	1.67	2.43	4.10	40.98	10.00
26	0.4189	0.5521	0.0030	0.0973	5.97	7.95	13.92	44.34	3.18
27	0.3962	0.5707	0.0071	0.0977	2.55	3.50	6.05	44.34	7.33
28	0.3725	0.5915	0.0100	0.0883	1.53	2.35	3.88	44.34	11.43
29	0.4340	0.4907	0.0462	4.424	18.55	24.00	42.55	36.33	0.85
30	0.3818	0.5255	0.0657	3.411	10.00	13.87	23.87	36.40	1.52
31	0.3897	0.4886	0.0958	2.884	5.94	8.16	14.10	36.44	2.58
32	0.3350	0.4911	0.1508	1.980	2.77	3.79	6.56	36.55	5.57
33	0.3098	0.5239	0.1403	1.852	2.85	3.79	6.64	36.44	5.49
34	0.3982	0.5158	0.0590	2.968	10.14	12.96	23.10	36.40	1.58
35	0.4019	0.5150	0.0541	2.836	10.14	13.60	23.74	36.33	1.53
36	0.3611	0.5423	0.0655	1.939	5.89	7.86	13.75	36.25	2.64
37	0.3635	0.5520	0.0656	1.946	5.94	8.00	13.94	36.70	2.63
38	0.3646	0.5475	0.0637	1.933	5.94	8.16	14.10	36.52	2.59
39	0.3900	0.5430	0.0410	2.096	9.89	13.25	23.14	36.44	1.57

TABLE 6d

COMPUTED RESULTS OF HETEROGENEOUS CATALYSIS IN THE STIRRED REACTOR

Run	$F_{v.c.}/F_{HCl}$ Calc.	% Dev. from $(F_{v.c.}/F_{HCl})$ Exp.	$P_{HCl}P_{y.c.}$ atm^2	$P_{1,1}/K_P$ atm^2	^1C x 10^2	^2C_c x 10^{-1}	t_e hr
1	1.85	-15.2	0.1246	0.0153	-	-	6
2	1.89	-18.2	0.1029	0.0190	47.94	117.5	30
3	1.81	-16.8	0.1081	0.0182	40.96	100.4	54
4	2.06	-16.2	0.1902	0.0054	25.75	63.13	78
5	2.02	-14.0	0.1897	0.0056	26.13	64.06	102
6	1.98	-14.2	0.2032	0.0039	25.76	63.15	126
7	1.89	-14.8	0.2160	0.0023	21.96	53.84	174
8	1.88	-14.2	0.2195	0.0018	17.87	43.81	198
9	1.96	-17.6	0.2283	0.0007	4.517	11.07	270
10	2.41	+3.8	0.2139	0.0017	4.169	10.22	366
11	2.17	+0.4	0.2068	0.0030	3.582	8.782	390
12	2.29	+4.2	0.2094	0.0027	3.156	7.737	414
13	2.19	-3.4	0.2120	0.0026	2.871	7.039	438
14	2.14	-5.2	0.2230	0.0009	2.364	5.796	558
15	2.46	+7.8	0.2095	0.0020	2.520	6.178	582
16	2.51	+1.2	0.2008	0.0030	2.376	5.825	606
17	2.25	-2.2	0.2021	0.0036	2.584	6.335	750
18	2.25	-2.2	0.2028	0.0035	2.510	6.154	756
19	2.58	+1.2	0.1958	0.0035	2.683	6.578	774
20	2.23	-5.2	0.2280	0.0004	2.693	6.602	870
21	2.50	+6.8	0.2226	0.0006	2.267	5.558	894

[1]Units of C are lb of 1,1 dichloroethane/(hr)(lb of catalyst)(atm)^2.

[2]Units of C_c are (lb moles 1,1 dichloroethane)(ft^3)^2/(hr)(lb of catalyst)(lb moles)^2.

TABLE 6d (continued)

Run	$F_{v.c.}/F_{HCl}$ Calc.	% Dev. from $(F_{v.c.}/F_{HCl})$ Exp.	$P_{HCl}P_{v.c.}$ atm^2	$P_{1,1}/K_P$ atm^2	^1C x 10^2	$^2C_{c^{-1}}$ x 10^{-1}	t_e hr
22	2.27	+0.8	0.2157	0.0020	2.265	5.553	918
23	2.69	+2.6	0.1975	0.0033	2.394	5.869	1038
24	2.17	-7.2	0.2246	0.0010	2.402	5.889	1086
25	2.54	+2.0	0.2020	0.0031	2.403	5.891	1110
26	2.25	-1.2	0.2313	0.0000	0.4207	0.8811	1182
27	2.45	+4.2	0.2261	0.0001	0.4323	0.9054	1206
28	2.69	+2.2	0.2203	0.0001	0.4010	0.8398	1230
29	1.91	-14.0	0.2130	0.0231	23.30	72.23	1254
30	2.26	-5.0	0.2006	0.0329	20.34	63.06	1278
31	2.06	-12.4	0.1904	0.0479	20.24	62.75	1350
32	2.26	-3.8	0.1645	0.0754	22.22	68.88	1398
33	2.53	+11.0	0.1623	0.0702	20.11	62.34	1425
34	2.15	-1.8	0.2054	0.0295	16.87	52.30	1542
35	2.14	-7.0	0.2070	0.0271	15.76	48.86	1566
36	2.44	+7.0	0.1958	0.0328	11.90	36.89	1590
37	2.35	+2.2	0.2007	0.0328	11.59	35.93	1686
38	2.44	+3.8	0.1996	0.0319	11.53	35.74	1710
39	2.32	+1.2	0.2118	0.0205	10.96	33.98	1734

TABLE 7

AVERAGE VALUES OF C_c AS A FUNCTION OF TEMPERATURE

T °F	$1/T\ ^{\circ}R^{-1} \times 10^{-3}$	$^{*}(C_c)_{av}$
163.9	1.604	8.75
215.0	1.482	60.19
299.0	1.318	722.3

*Units of C_c are (lb moles, 1,1 dichloroethane)$(ft^3)^2$/(hr)(lb catalyst)(lb moles)^2.

SECTION II

APPENDIX I

LIST OF FIGURES (APPENDIX)

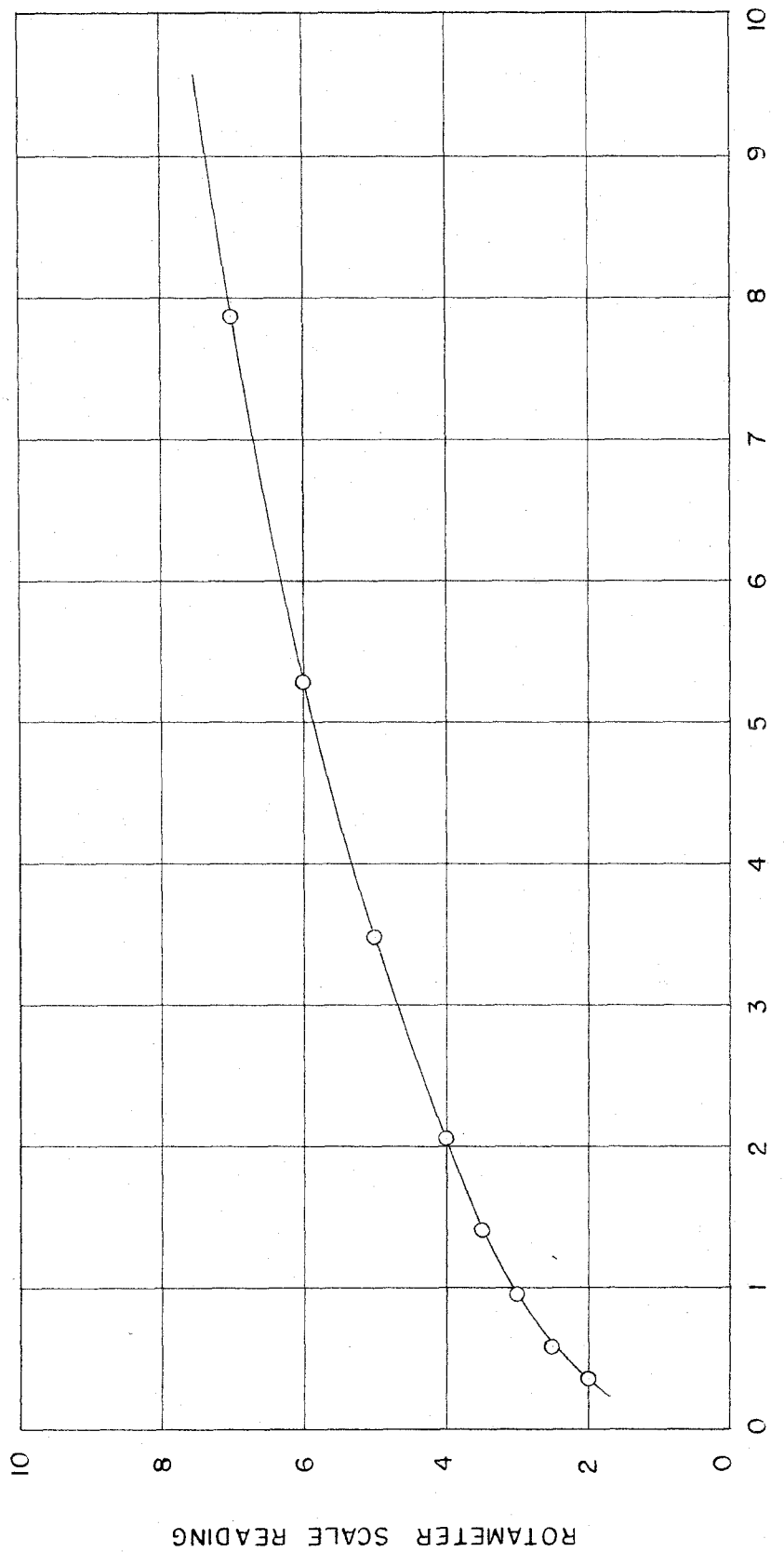

Figure 1A--Rotameter Calibration for HCl at T = 25°C and P = 1 atm

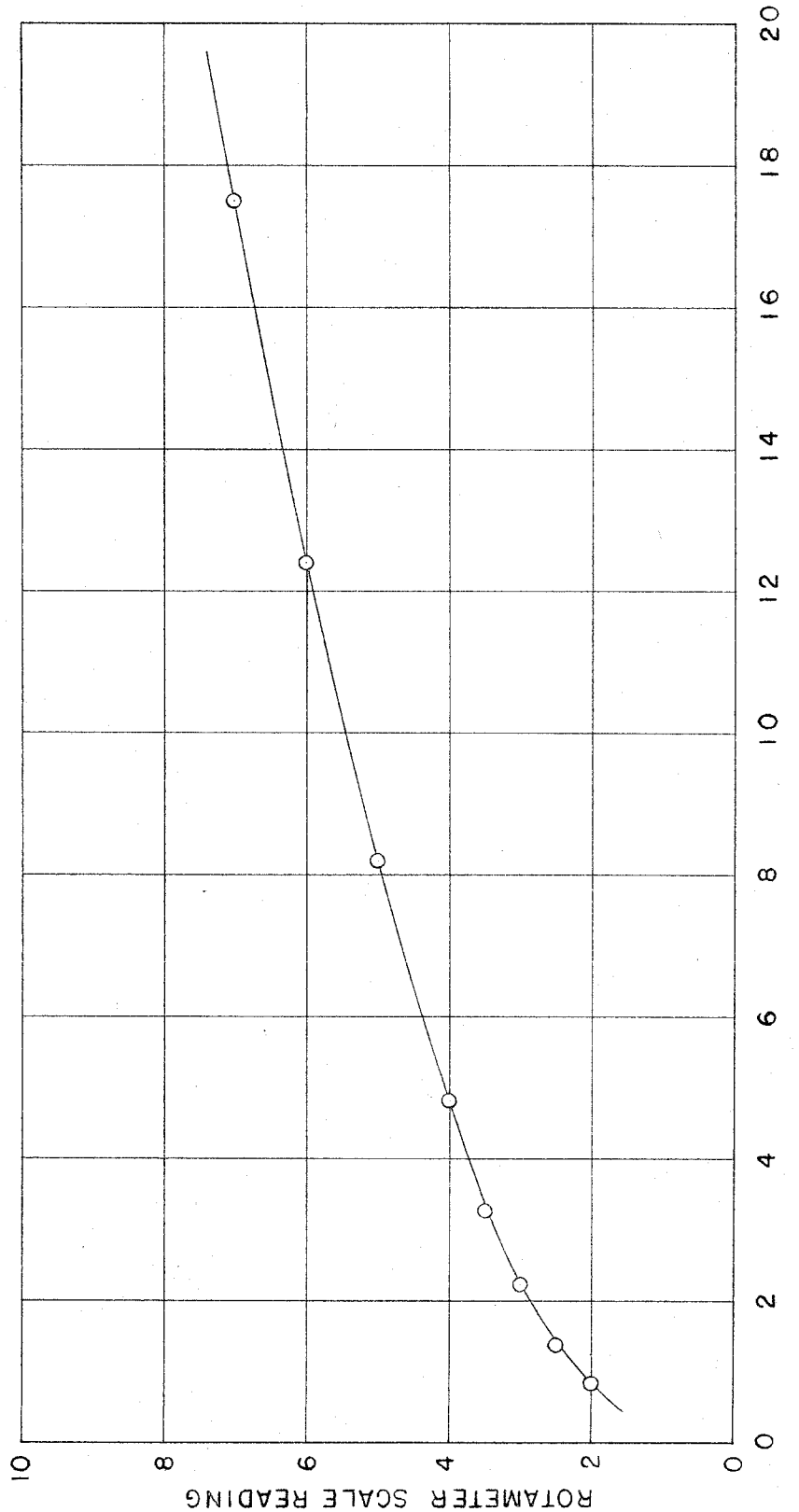

Figure 2A--Rotameter Calibration for Vinyl Chloride at T = 25°C and P = 1 atm

LIST OF TABLES (APPENDIX)

TABLE 1A

RESULTS OF EXPERIMENTAL WORK OF KHARASCH (9)

Olefin	Halogen Acid[a]	$FeCl_3$[a]	Reaction[b]		% Yield[c]		Product[d]
			Time Hrs.	Temp. °C.	Min.	Max.	(Normal)
Vinyl Bromide*	HBr, 1.6	0.019	24	25	88	—	1,1 Dibromoethane
Vinyl Bromide	HCl, 1.5	none	1296	25		10	See "e"
Vinyl Bromide	HCl, 1.5	0.001	1	25		60	See "e"
Vinyl Chloride	HBr, 1.4	0.001	24	0	77	93	1-Chloro-1-bromoethane
Vinyl Chloride	HBr, 1.4	0.001	48	25	77	93	1-Chloro-1-bromoethane
Vinyl Chloride	HBr, 1.4	0.001	48	0	86	95	1-Chloro-1-bromoethane
Vinyl Chloride	HBr, 1.4	0.001	24	25	86	95	1-Chloro-1-bromoethane
Vinyl Chloride	HCl, 1.5	none	504	25		10	1,1 Dichloroethane
Vinyl Chloride	HCl, 1.3	0.001	48	0	57	62	1,1 Dichloroethane
Vinyl Chloride	HCl, 1.3	0.001	148	25	57	62	1,1 Dichloroethane
Vinyl Chloride	HCl, 1.4	0.001	120	25	59	77	1,1 Dichloroethane
Vinyl Chloride	HCl, 1.4	0.001	72	25	71	84	1,1 Dichloroethane
Vinyl Chloride	HCl, 1.5	0.001	72	25	71	82	1,1 Dichloroethane

*Pressures of 10^{-3} to 10^{-4} mm. were used.

[a]Expressed in moles per mole of olefin.

[b]All reactions carried out in the dark.

[c]Min. yield calc. from wt. of pure dihalide isolated after the final distillation. Max. yield calc. from crude reaction product after removal of solvent, catalyst, hydrogen halide, and unchanged olefin.

[d]The products are the "normal" addition products. In those cases where percentages are given the remainder was the other possible addition product.

[e]All attempts to add HCl to vinyl bromide yielded products having no sharp boiling point, an indication that halogen exchange had taken place.

TABLE 2A

THERMOCOUPLE CALIBRATION DATA

Thermocouple emf's in Microvolts

T °F	#1	#2	#3	#4	#5	#6	#7	#8	#9	#10
32.01	0.0	0.0	0.0	0.0	0.0	0.1	0.0	0.0	0.1	0.0
175.44	3328.9	3328.0	3329.6	3329.2	3328.8					
179.13						3428.0	3426.8	3426.6	3427.3	3425.5
190.21	3703.1	3702.4	3703.8	3703.2	3703.2					
192.15						3756.5	3755.6	3755.1	3756.2	3754.0
193.96	3799.0	3798.2	3799.8	3799.0	3799.0					
196.88						3876.7	3875.5	3875.0	3876.0	3873.8
208.62						4176.8	4175.5	4175.0	4175.9	4174.0
213.42	4299.6	4298.7	4300.2	4299.5	4299.9					
216.87						4387.2	4385.9	4385.5	4386.5	4384.4
225.44						4614.8	4613.4	4612.8	4613.9	4611.8
230.89	4757.0	4756.4	4758.0	4757.4	4757.3					
234.56						4853.9	4852.6	4851.8	4853.2	4850.7
236.00	4891.2	4889.8	4891.0	4891.1	4891.6					
238.53	4956.8	4956.2	4957.9	4956.8	4057.0					
248.51						5223.2	5221.0	5220.9	5222.2	5229.1
262.64						5600.0	5598.1	5597.8	5598.8	5596.6
278.14						6019.0	6018.2	6017.9	6018.6	6016.7
279.02	6044.0	6042.5	6045.2	6043.6	6044.0					
298.95	6619.2	6617.0	6620.1	6618.5	6619.6					
299.07						6623.0	6621.3	6620.1	6621.8	6619.7

Thermocouples #1 - #5 used in reactor probe.
#6 and #7 used in feed streams.
#8 - #10 used in reactor oil bath.

TABLE 3A

ROTAMETER CALIBRATION DATA

Rotameter Scale Reading*	Mass Rate HCl lbs/hr x 10^{-3}	Mass Rate Vinyl Chloride lbs/hr x 10^{-3}
2.0	0.3450	0.8106
2.5	0.5730	1.338
3.0	0.9414	2.196
3.5	1.378	3.231
4.0	2.044	4.812
5.0	3.463	8.160
6.0	5.259	12.33
7.0	7.854	17.41
8.0	10.92	23.13

*For T = 25°C and P = 1 atm.

TABLE 4A

CHROMATOGRAPH CALIBRATION DATA

Sample	Actual Weight %			Calculated Weight %			Correction Factor		
	HCl	Vinyl chloride	1,1 Dichloro-ethane	HCl	Vinyl chloride	1,1 Dichloro-ethane	HCl	Vinyl chloride	1,1 Dichloro-ethane
1	0.2481	0.6863	0.0656	0.2456	0.6868	0.0676	1.010	0.999	0.970
2	0.2777	0.7038	0.0185	0.2696	0.7111	0.0193	1.030	0.990	0.961
3	0.2454	0.6741	0.0805	0.2452	0.6715	0.0833	1.001	1.004	0.966
4	0.3101	0.6591	0.0308	0.3008	0.6671	0.0321	1.031	0.988	0.959
5	0.3708	0.6138	0.0154	0.3586	0.6257	0.0157	1.034	0.981	0.983
6	0.2570	0.5701	0.1729	0.2565	0.5605	0.1830	1.002	1.017	0.945

Average Values of Correction Factors

Component	Correction Factor
HCl	1.018
Vinyl Chloride	0.996
1,1 Dichloroethane	0.964

TABLE 5A

WEIGHT OF CATALYST IN REACTOR TRAYS

Tray Number*	Catalyst Weight, gm
1	14.9954
2	15.0211
3	15.0169
4	15.0031
5	14.9779
6	15.0154
7	14.9774
8	14.9928

Weight of Catalyst after 1734 hr = 130.4502 gm

Weight of Fouling Deposit = 10.4502 gm

*Trays were numbered in descending order from the top of the reactor to the bottom.

TABLE 6A

LEAST-SQUARES ANALYSIS OF RUNS 14 to 25

FOR DETERMINING K_p

Run	$r_{1,1}$ x 10^2 *	p_a **	p_b	p_c	$\frac{p_a p_b}{r}$	$\frac{p_a^2 p_b}{r}$
14	0.5250	0.4207	0.5300	0.0162	42.4706666	17.86740944
15	0.5230	0.3768	0.5559	0.0351	40.0503097	15.09095669
16	0.4700	0.3621	0.5545	0.0514	42.7200957	15.46894665
17	0.5130	0.3850	0.5249	0.0611	39.3930799	15.16633576
18	0.5002	0.3856	0.5260	0.0594	40.5489004	15.63565599
19	0.5160	0.3507	0.5584	0.0599	37.9517209	13.30966852
20	0.6130	0.4178	0.5457	0.0075	37.1930603	15.53926059
21	0.5033	0.3888	0.5725	0.0097	44.2257103	17.19495616
22	0.4840	0.3995	0.5398	0.0337	44.5558057	17.80004438
23	0.4650	0.3446	0.5732	0.0561	42.4784344	14.63806849
24	0.5370	0.4190	0.5360	0.0170	41.8219739	17.52340706
25	0.4780	0.3607	0.5599	0.0535	42.2501945	15.23964516
Σ	6.1275	4.6113	6.5768	0.4606	495.6599523	190.47435489

*Units are given under NOMENCLATURE.

**Subscripts a, b, and c on p represent HCl, vinyl chloride, and 1,1 dichloroethane, respectively.

TABLE 6A (continued)

Run	$\frac{p_a p_b^2}{r}$	$\frac{p_a p_b p_c}{r}$	$\frac{p_c}{r}$	$\frac{p_a p_c}{r}$	$\frac{p_b p_c}{r}$
14	22.50945330	0.688024799	3.0857142	1.298159964	1.635428526
15	22.26396716	1.405765870	6.7112810	2.528810681	3.730801108
16	23.68829307	2.195812919	10.9361702	3.959987229	6.064106376
17	20.67742764	2.406917182	11.9103313	4.585477551	6.251732899
18	21.32872161	2.408604684	11.8752499	4.579096361	6.246381447
19	21.19224095	2.273308082	11.6085271	4.071110454	6.482201533
20	20.29625301	0.278947952	1.2234910	0.511174540	0.667659039
21	25.31921915	0.428989390	1.9272799	0.749326425	1.103367743
22	24.05122392	1.501530652	6.9628099	2.781642555	3.758524784
23	24.34863860	2.383040170	12.0645161	4.157432248	6.915380629
24	22.41657801	0.710973556	3.1657355	1.326443175	1.696834228
25	23.65588390	2.260385406	11.1924686	4.037123424	6.266663169
$\sum$	271.74790032	18.942300662	92.6635747	34.585784607	50.819081481

$$C\sum\frac{p_a^2 p_b}{r}-\frac{C}{K_p}\sum\frac{p_a p_c}{r}=\sum p_a \qquad (1\text{-}6A)$$

$$C\sum\frac{p_a p_b^2}{r}-\frac{C}{K_p}\sum\frac{p_b p_c}{r}=\sum p_b \qquad (2\text{-}6A)$$

$$K_p = 17.2 \text{ and } k_c = 0.0245 \qquad (3\text{-}6A)$$

TABLE 7A

DETERMINATION OF K_p AS A FUNCTION OF TEMPERATURE

The Van't Hoff equation is given by,

$$\frac{d(\ln K)}{dT} = \frac{\Delta H_f}{RT^2} \qquad (1\text{-}7A)$$

where:

$$\Delta H_f = \Delta H_{25^oC} + \int_{25}^{T} \Delta C_p dT \qquad (2\text{-}7A)$$

Published Data:

Component	*Thermodynamic Quantity	Value	State	Source
HCl	$\Delta H_{f\ 25^oC}$	-22.063 kcal/gm mole	g	32
HCl	C_p	6.70 + 0.00084T cal/gm mole ^oK	g	32
Vinyl Chloride	$\Delta H_{f\ 25^oC}$	+7.500 kcal/gm mole	g	31
Vinyl Chloride	C_p	5.5 + 0.0244T cal/gm mole ^oK	g	31
1,1 Dichloroethane	$\Delta H_{f\ 25^oC}$	-36.4 kcal/gm mole	l	34
1,1 Dichloroethane	$\Delta H_{v\ 57.4^oC}$	+7.3 kcal/gm mole	-	34
1,1 Dichloroethane	C_p	7.3 + 0.0359T cal/gm mole ^oK	g	33

Calculated Data:

$\Delta H_{f\ 25^oC}$ = -36.4 + 7.3 = -29.1 kcal/gm mole for gaseous 1,1 dichloroethane, assuming that $\frac{d(\Delta H_v)}{dT}$ is negligible between 57.4°C and 25°C.

* Definition of symbols given under NOMENCLATURE.

TABLE 7A (continued)

$$\Delta C_p = -4.9 + 0.0107\ T \text{ cal/gm mole } {}^{o}K$$

$$\int_{298.17}^{T} \Delta C_p\, dT = -4.9\ T + \frac{0.0107\ T^2}{2}\Bigg|_{298.17}^{T} \qquad (3\text{-}7A)$$

$$= 981 - 4.9\ T + 0.0054\ T^2$$

$$\Delta H_{25^o} = -29.1 - (-22.063 + 7.5) = -14.54 \text{ kcal/gm mole.}$$

$$\Delta H_T = -14,540 + 981 - 4.9\ T + 0.0054\ T^2$$

$$= -13,559 - 4.9\ T + 0.0054\ T^2 \qquad (4\text{-}7A)$$

$$d(\ln K_p) = \frac{1}{R}\left(\frac{-13,559}{T^2} - \frac{4.9}{T} + 0.0054\right) dT \qquad (5\text{-}7A)$$

$$\ln K_p = \ln K_{25^o} + \frac{1}{R}\left(\frac{13,559}{T} - 4.9 \ln T + 0.0054\ T - 19.15\right) \qquad (6\text{-}7A)$$

Using $K_p = 17.2$ atm^{-1} at 215^{o}F and solving for $\ln K_{25^o}$ from Equation 6-7A, the value is 7.889.

$$\ln K_p = 7.889 + \frac{1}{1.987}\left(\frac{13,559}{T} - 4.9 \ln T + 0.0054\ T - 19.15\right) \qquad (7\text{-}7A)$$

From Equation 7-7A, $K_p = 86.2$ atm^{-1} at 163.9^{o}F and

$K_p = 2.0$ atm^{-1} at 299.0^{o}F

TABLE 8A

RATE-CONTROLLING MECHANISMS FOR A BIMOLECULAR REACTION IN HETEROGENEOUS CATALYSIS

Case I:

Assume activity coefficients are unity.

Assume HCl, vinyl chloride and 1,1 dichloroethane are adsorbed on the surface of the catalyst and that reaction occurs between adsorbed molecules.

Assume only one kind of active site available.

A. *Surface reaction controlling.

$$r = \frac{k_1 K_a K_b \left(p_a p_b - \frac{p_c}{K_p}\right)}{(1 + K_a p_a + K_b p_b + K_c p_c)^2} \qquad (1\text{-}8A)$$

B. Adsorption of HCl controlling.

$$r = \frac{k_2 \left(p_a - \frac{p_c}{K_p p_b}\right)}{1 + K_b p_b + \left(\frac{K_a}{K_p}\right)\left(\frac{p_c}{p_c}\right) + K_c p_c} \qquad (2\text{-}8A)$$

C. Adsorption of vinyl chloride controlling.

$$r = \frac{k_3 \left(p_b - \frac{p_c}{K_p p_a}\right)}{1 + K_a p_a + \left(\frac{K_b}{K_p}\right)\left(\frac{p_c}{p_a}\right) + K_c p_c} \qquad (3\text{-}8A)$$

TABLE 8A (continued)

D. Desorption of 1,1 dichloroethane controlling.

$$r = \frac{k_4 K_p \left(p_a p_b - \frac{p_c}{K_p}\right)}{1 + K_a p_a + K_b p_b + K_c K_p p_a p_b} \qquad (4\text{-}8A)$$

E. HCl very weakly adsorbed.

$$r = \frac{k_5 K_a K_b \left(p_a p_b - \frac{p_c}{K_p}\right)}{\left(1 + K_b p_b + K_c p_c\right)^2} \qquad (5\text{-}8A)$$

F. Vinyl chloride very weakly adsorbed.

$$r = \frac{k_6 K_a K_b \left(p_a p_b - \frac{p_c}{K_p}\right)}{\left(1 + K_a p_a + K_c p_c\right)^2} \qquad (6\text{-}8A)$$

Case II:

Assume activity coefficients are unity.

Assume reaction occurs between a gas molecule and an adsorbed molecule

Assume only one kind of active site available.

A. HCl and vinyl chloride both adsorbed.

Reaction between adsorbed vinyl chloride and gaseous HCl.

$$r = \frac{k_7 K_b \left(p_a p_b - \frac{p_c}{K_p}\right)}{1 + K_a p_a + K_b p_b + K_c p_c} \qquad (7\text{-}8A)$$

TABLE 8A (continued)

B. HCl and vinyl chloride both adsorbed.

Reaction between adsorbed HCl and gaseous vinyl chloride.

$$r = \frac{k_8 K_a \left(p_a p_b - \frac{p_c}{K_p}\right)}{1 + K_a p_a + K_b p_b + K_c p_c} \qquad (8\text{-}8A)$$

C. Vinyl chloride adsorbed but HCl not adsorbed.

Reaction between adsorbed vinyl chloride and gaseous HCl.

$$r = \frac{k_9 K_b \left(p_a p_b - \frac{p_c}{K_p}\right)}{1 + K_b p_b + K_c p_c} \qquad (9\text{-}8A)$$

Case III:

Assume activity coefficients are unity.

Assume HCl, vinyl chloride and 1,1 dichloroethane are adsorbed on the surface of the catalyst and that reaction occurs between adsorbed molecules.

Assume two kinds of active sites available.

A. Surface reaction controlling.

$$r = \frac{k_{10} K_a K_b \left(p_a p_b - \frac{p_c}{K_p}\right)}{(1 + K_a p_a + K_c p_c)(1 + K_b p_b + K_c p_c)} \qquad (10\text{-}8A)$$

TABLE 8A (continued)

Results of Simultaneous Solution of Equation 1-8A for runs 14 through 25 at 215°F.

Runs Combined .	K_a	K_b	K_c	k_1
19, 16, 15, 14	1.83	0.216	3.05	0.223
22, 19, 15, 14	6.09	0.830	12.7	0.083
25, 19, 15, 14	1.33	0.144	1.92	0.342
23, 19, 15, 14	2.26	0.277	4.00	0.176

Omitting the combination (22,19,15,14), the average values of K_i and k_1 are:

$$K_a = 1.81 \; ; \; K_b = 0.212 \; ; \; K_c = 2.99 \; ; \; k_1 = 0.247$$

---

*Definitions of symbols are given under NOMENCLATURE.

PROPOSITIONS

1. a. Two of the many constituents found in the polluted air of Los Angeles County are NO and NO_2. The trace analysis (1) of these components by the APCD is based upon a color change in the reaction between NO_2 and Saltzman reagent. In analyzing for NO, the air is first passed through an ozone chamber or an aqueous solution of potassium permanganate which presumably oxidizes the NO to NO_2. Some difficulty is encountered in this process because of over-oxidation of the NO_2 to higher oxides. Hence, the analysis for NO is highly unreliable. It is proposed that oxidation of NO by N_2O_5, preceded by freezing out other oxidizable materials, would improve the analysis considerably.

b. The analysis for NO and NO_2 is performed on a continuous 24-hour basis. Assuming that these concentrations could be obtained accurately, their simultaneous values at fixed times would be useful in studying the mechanisms of the reactions which form smog. The continuous analyzer used by the APCD often does not obtain simultaneous concentrations because of differences in retention times of the two gas streams. A method for automatically checking and adjusting the retention times is proposed.

2. Upon determining the temperature and pressure characteristics of violent weather disturbances, such as tornadoes, difficulty is encountered in placing the measuring instruments in

the disturbance. This problem is practically eliminated if a weather balloon can be filled after it is placed in the disturbance. For example, it may be dropped from an airplane flying above the disturbance. A portable reactor which is used to fill the balloon with relatively dry hydrogen is proposed.

3. In the Chemical Engineering Laboratory at Caltech, the material and energy transport from steady-state liquid drops has been studied (2). A somewhat similar experiment for determining the overall heat transfer coefficients of steady-state bubbles is proposed.

4. The results obtained from aqueous thermal decomposition studies of sodium dithionite could be explained by two alternative mechanisms for the rate-determining step. These are:

Initial Step: $S_2O_4^{=} \rightleftharpoons 2SO_2^{-}$

Alternative Rate-Determining Steps:

$$S_2O_4^{=} + HSO_2 \longrightarrow S_2O_3^{=} + HSO_3$$

or $$HS_2O_4^{-} + SO_2^{-} \longrightarrow S_2O_3^{=} + HSO_3$$

An experiment which is based upon the Brönsted effect and which would have some value in determining the prevailing mechanism is proposed.

5. The Stokes solution for viscous flow around a sphere is well known. A more difficult problem, however, is the case in which the approaching liquid has a uniform velocity gradient. It would be of interest to measure the forces on a sphere suspended in this type of a flow system. Such a measurement would be of value in estimating the transport of sediment from stream beds.

6. a. The addition reaction between HCl and vinyl chloride in the presence of $ZnCl_2$ could be conveniently studied in a differential reactor which is in series with a chromatograph column. At steady flow of the reactants, periodic sampling through the chromatograph column would give directly the differential rate of reaction. The change in conversion as a function of catalyst fouling could also be obtained.

b. The addition of a strong Lewis acid such as BF_3 to the reactants would be of interest in determining the possibility of forming 1,2 dichloroethane.

7. a. The ozone content of polluted air in Los Angeles County is determined quantitatively by three independent tests (1), i.e.,

A) Rate of cracking produced in a standard sample of natural rubber.

B) Ultraviolet spectrophotometry.

C) Oxidation of KI to give I_2.

It has been observed by the writer that within the limits of

accuracy, these tests do not always give consistent values for the O_3 concentration. For example, on days having a low inversion layer and bright sunshine, the ozone content observed by rubber cracking is slightly lower than either of the other two methods. On days having hazy sunshine, the ozone content observed by the UV spectrophotometric analysis is lower than the values observed by rubber cracking or KI oxidation. It is proposed that an explanation for this inconsistency may be obtained by analyzing the air for organic peroxides.

b. Unusually strong eye irritation is often observed on days in which the ozone concentration is normal but in which the terrain is blanketed with a fog-like haze. County Pollution authorities attribute the irritating effect to sulfur trioxide in the presence of the ultrafine droplets of moisture. It is proposed that aerosol samples of the air be analyzed carefully for constituents dissolved in the droplets. The presence of the oxides of both nitrogen and sulfur may indicate that initially NO_2 and SO_2, which are well known contaminants, dissolve in the droplets and then react according to the equation,

$$NO_2 + SO_2 \longrightarrow NO + SO_3$$

which occurs in the liquid phase. Also, the presence of organic peroxides would add to the irritating effect.

8. It is well known that in condensation processes, dropwise condensation is more efficient than film condensation (3). The critical film thickness for transition from dropwise to film condensation and vice-versa depends upon the surface tension of the condensed vapor and the wetability of the condensation surface. An experiment is proposed to determine the minimum film thickness of a liquid on a metal surface, which is required for the transition.

9. a. In the thermal decomposition of aqueous sodium dithionite, the net rate of reaction showed half-order dependence on the H^+ concentration in the pH range of 4.8 to 7.0. There is reason to believe that outside of this range the order may change significantly. Hence, a careful study of the H^+ effect over a wide range of pH would help to establish the relationship of H^+ to the mechanism of decomposition.

b. Similarly, the effect of H^+ on the formation of the sulfoxylate ion $SO_2^=$ in dithionite solutions should be studied. Here, an additional problem of analyzing for $SO_2^=$ in the presence of SO_2^- and $S_2O_4^=$ presents difficulties requiring further investigation.

10. The existence of a free-radical chain reaction in the thermal decomposition of sodium dithionite may possibly be determined by two experiments, namely,

A) Measurement of the quantum yield in the photochemical decomposition.

B) The measurement of the effects of adding a free-radical trap such as phenol or hydroquinone.

REFERENCES

1. Handbook of Manual Air Sampling, Air Pollution Control District, County of Los Angeles.

2. Hsu, N.T., Reamer, H. H. and Sage, B. H., "Experimental Methods for Measurement of the Evaporation of Drops," Document No. 4219, American Documentation Institute, Library of Congress, Washington, D.C., 1954.

3. Walker, William H., et al, "Principles of Chemical Engineering," McGraw-Hill Book Company, Inc., New York, 1937.